HIGH ENERGY DENSITY BATTERIES

A STUDY OF ALUMINIUM–AIR BATTERY

A THESIS SUBMITTED FOR THE DEGREE

OF

DOCTOR OF PHILOSOPHY

OF

THE CITY UNIVERSITY

BY

ROBERT LOVEJOY QUARSHIE

CHEMICAL ENERGY RESEARCH CENTRE
THE DEPARTMENT OF CHEMISTRY

THIS WORK WAS CARRIED OUT UNDER THE SUPERVISION OF PROFESSOR A.C.C. TSEUNG AND FINANCED BY THE SCIENCE AND ENGINEERING RESEARCH COUNCIL

DECEMBER, 1985.

PAGE NUMBERS ARE CUT OFF IN THE ORIGINAL

...In thankfulness to God and all those whose love for me has been my fountain of inspiration...

ACKNOWLEDGEMENT

I wish to express my sincere gratitude to my supervisor, Prof. Tseung, for his advice, help and encouragement throughout the period of this research work. And above all, for creating an amiable atmosphere to work in.

I also wish to thank [redacted], for his guidance and useful comments during the initial stages of this research.

My thanks are also due to my colleagues in the Chemical Energy Research Centre, for their readiness to help and participate in discussions. I also wish to thank [redacted] of the Physics Department for his help with the SEM work and to [redacted] for his help with the X-ray diffraction analyses. And I duly acknowledge the cooperation of the Technical Staff of the Chemistry Department for their assistance in various ways.

Finally, I wish to render my sincere gratitude [redacted].

R.L. QUARSHIE

DECEMBER, 1985.

CITY UNIVERSITY

LONDON

ABSTRACT

The performance of the Al anode is optimised by destabilising the resistive oxide film on the surface of the metal without increasing the rate of corrosion, and by using a suitable electrolyte in which the Al reaction products are readily soluble.

The destabilisation of the resistive oxide layer is done by alloying the Al metal with alloying elements of high hydrogen overpotential. Elements such as, Zn, Ga, In, Pb, Bi and Sn are found to be highly indispensible. Whereas, Fe and Cu are found to have deleterious effect on the self-discharge characteristics of the anode, resulting in a high rate of hydrogen evolution on the metal. The hydrogen evolved is suppressed by the addition of inhibitors to the electrolyte, to reduce the anodic sites of the Fe and Cu atoms on the surface of the Al metal. Trace amounts of mercuric oxide (HgO) is found to be the best inhibitor. It does not only reduce the rate of hydrogen evolution on the Al surface, it also couples with the atoms on the metal surface to produce an anodic shift in potential.

The low solubility of Al reaction products in the conventional electrolytes gives rise to the problem of cell clogging, which at the moment characterises the

state-of-art in the development of Al-air batteries. This problem is alleviated by using an electrolyte mixture in which the solubility of Al is increased by as much as 140% . The higher solubility obtained for the electrolyte mixture means that its use in aluminium cells, results in a reduction in the amount of reaction product precipitated and thus reduces the tendency of cell clogging. Moreover, the precipitate formed in the electrolyte is granular and can therefore be easily pumped or cleaned away.

One other problem encountered, in the use of existing Al-air batteries, is the the storage capability of the Al anodes. This problem is dealt with, in this work, by finding an alloy that is electrochemically active in the operating medium but behaves like the bare metal, aluminium, under atmospheric conditions. Alloy Q4 is found to possess these qualities. The alloy can be stored openly and infinitely, and can be handled anyhow without any damaging effect. The system, using this anode, can therefore be recharged conveniently and safely. For applications that demand long time use with minimal supervision, an automatic means of recharging has been validated. The anode material is fabricated into shot , to enable a continuous automatic feeding of the active anode material into the cell.

As part of the optimisation of the Al anode performance, temperatures between 40 and 45°C are

found to be the optimum operating temperature range for Al cells.

Full cell discharge characteristics of the improved cell show that the aluminium anode material used in the cell has a high limiting current density and thus, allows high currents to be drawn from the cell. Also, since aluminium is comparatively more soluble in the electrolyte used, the cell can operate at a longer discharge time, than normal, without getting clogged up. A typical cell containing about 57 g of electrolyte, is discharged at 3A for over 48 hours without any serious problems; e.g the problem of cell clogging. The energy density of the cell is calculated for, a 24 hour operation time, to be nearly 400 Wh/Kg; 3,714 Wh/Kg of Al. The cell can be operated from as low as $-20^{o}C$ without the use of an external heater to warm it up.

The commercial viability of the cell is highlighted. The cell, so-improved, can be used to provide power for applications both onshore and offshore. It can be used as the main power source in submersibles, life-boats, military field equipment and reconnaissance vehicles. It can also be used as emergency power source for lighting, burglar and fire alarms, computer memory banks, as starters for car engines and as back-ups for generators.

CONTENTS

PART 3: ELECTROCHEMICAL AND PHYSICAL PROPERTIES OF SELECTED ELECTROLYTE MIXTURES

LIST OF FIGURES

LIST OF TABLES

1 INTRODUCTION

The need for portable energy has seen an upward trend over the past decade. As technology gets sophisticated so does the type of energy required. Energy requirements range from high energy outputs for vehicles, both manned and unmanned, to low energy outputs for consumer products.

Although, there are several ways of tapping energy from the vast amount of energy resources providence offers, preference for electrochemical energy conversion is substantial. Suffice it to say, that, because of the increasing pollution caused by the use of fossil fuels to produce energy it may well be that the continuation of an affluent civilisation into the next century will require a change to clean energy conversion technology. Electrochemical energy conversion is a way forward in this direction.

Over the years a large variety of batteries has been produced, both converters and accumulators, to exploit their suitability for deemed purposes [1-5]. Most of these batteries are not without drawbacks.

For high energy uses, where weight and volume limitations apply, a battery that has a high energy

density (high energy to weight ratio) is desirable. Aluminium, when used as the anode material in batteries, can enable such high energy densities to be realised; owing to a lower specific consumption and a high negative thermodynamic value of the standard electrode potential E^o (in aqueous akaline):

	E^o (V)	(g/Ah)
Magnesium	-2.69	0.454
Aluminium	-2.35	0.336
Zinc	-1.25	1.220

It has a relatively low atomic weight of 26.98 along with a trivalent oxidation state, resulting in a gram-equivalent weight of 9.00. From a volume standpoint, aluminium should yield 8.04 Ah/cm^3, as compared with 5.85 for zinc and 3.83 for magnesium. Additionally, in common with zinc but not with magnesium, the hydroxide of aluminium is amphoteric in nature so that an aluminium cell should operate over a wide pH range. Also, world resources of the metal are large. It is produced in large quantities and, in terms of Ah capacity, is cheaper than zinc.

These properties of aluminium has attracted numerous research efforts and has been the subject of many patents [6-22]. The metal has been considered as a battery electrode, though originally as cathode rather than anode, since the 1850s when Hulot [23] described the zinc

(mercury)/aluminium cell, with dilute sulphuric acid as electrolyte. According to Cazin [24], this cell, at the start, delivered current ''at least comparable to that of the zinc/platinum element''.

Aluminium, as anode, was used in the buff cell of 1857 [25]; a two-fluid battery:

Al/dil. acid in porous pot/nitric acid/C

with an EMF of 1.377 V. The Mennons patent of 1859 [6] and the Eager and Milburn patent of 1891 [7] cover essentially the same system. The latter also mentions a single-fluid cell and a subsequent patent [8] suggests sodium bichromate as cathodic reactant, claiming that (when used) with 'electric glow lamps', the resulting cell gave better and steadier light than cells of their other patent. In 1893, Brown was granted a patent [9] which describes a cell with an anode of an amalgamated aluminium-zinc alloy and a carbon cathode. A 1902 patent granted to Anderson [10] claims a cell with aluminium anode, carbon cathode, and an electrolyte of dilute nitric acid, potassium bichromate and calcium fluoride; the latter purported to reduce wasteful corrosion. The addition of zinc chloride to the electrolyte was recommended for stronger currents in closed-circuit work. In 1904, Noble and Anderson [11] patented a cell with aluminium and carbon electrodes and an electrolyte of dilute nitric acid kept at a temperature of 150°F

or higher. They reported an EMF of 1.5 V with low internal resistance. Vince's patent of 1933 [12] reported a cell with concentric spirals of aluminium and copper, separated by a spacer material; the latter also serving as an absorbent for the sodium hydroxide electrolyte. In 1935, Pennock and Lee patented a cell with a liquid aluminium amalgam anode, a carbon cathode, and a sodium hydroxide electrolyte [13]. The cell was constructed in such a way to enable the anode to be replenished with aluminium powder, shots, or filings during service. The inventors claimed a 1.3 V EMF and a steady and constant current for this cell.

In 1948, Heise, Schumacher, and Cahoon reported the use of aluminium or amalgamated aluminium as an anode in heavy-duty chlorine-depolarised batteries [14]. With amalgamated aluminium, open circuit voltage was as high as 2.45 V, but wasteful corrosion limited the use of these cells to short-time operation, well below that with zinc. In 1951, an early reference was made to an aluminium analog of a Leclanche-type cell in Sargent's patent [15] covering the system:

$$Al/aq.\ NaOH+ZnO/porous\ membrane/MnO_2(C)$$

The inventor suggested that aluminium precipitates zinc from the caustic-alkali zincate solution, to form a protective coating on the anode, at least while the cell is not in operation. Ruben's patent of 1953 [16]

disclosed the use of manganous chloride tetrahydrate as the electrolyte salt in an aluminium/manganese dioxide cell. An EMF of 1.56 V, with relative freedom from wasteful anode corrosion and correspondingly low gas production, was reported. These were further improved by Stokes [26-28]. In 1956, Lozier, Glicksman, and Morehouse patented aluminium anode cells with cathodes of positive halogen organic compounds, such as N,N-dichloro-p-toluene sulphonamide or N,N-dichlorodimethylhydantoin [17]. These cells were shown to have high capacities on continuous drain (4-ohm), but other properties such as shelf life or capacity on intermittent drain were not disclosed.

To exploit, fully, the higher energy density attributes of aluminium, the metal is coupled with oxygen (from air) to form an Al-air cell. The Al-air cell belongs to a category of cells known as Metal-air cells, the concept of which is based primarily on a notion procured as far back as 1868 when Leclanché publicly described his now famous cell. That cell [29] consisted of an amalgamated zinc negative electrode, an ammonium chloride electrolyte, and a positive electrode made from a mixture of manganese dioxide and carbon powder. Leclanché observed that when the cell container was only half-filled with electrolyte, and the upper portion of the manganese dioxide/carbon mixture was only moist rather than immersed in the electrolyte, the performance of the cell was improved. It became clear from that

observation that atmospheric air was playing part in the improved performance of the cell through its action at the porous carbon electrode.

Maiche followed up this observation, in 1879, by omitting the manganese dioxide and, instead, adding platinum to the carbon powder. He retained the zinc and ammonium chloride of the Leclanche cell, demonstrating the first true zinc-air cell [29]. In 1932, Heise and Schumacher described an air-depolarised zinc battery with an alkali electrolyte [29]. That battery used a porous carbon black electrode, which was prevented from becoming completely flooded with the electrolyte by impregnation with paraffin wax. The type of cell was subsequently commercialised by the Union Carbide Company in the United States of America. The cell, produced and used for railway signalling, could be obtained in a 'renewable' form. A new electrode assembly and calcium hydroxide regenerative material were provided. The calcium hydroxide precipitated the zinc in solution, regenerating the electrolyte, and the zinc anodes were replaced with new ones. That was probably the first instance of a 'mechanically rechargeable' metal-air cell.

In about 1950, the National Carbon Company of the U.S.A., developed a small air deplorised hearing-aid cell. The unit contained a perforated zinc electrode and two thin wet-proofed carbon air elctrodes; one on each side of the zinc. The electrolyte was immobilised, as in

all 'dry' cells. Thus the subsequent battery, which had a capacity of about 0.4 A-hr [30], was the first commercial 'dry-cell' primary metal-air battery. After about 1960, with the development programmes for fuel cells having gained impetus towards the end of the 1950s, a great deal of research and development was carried out on air elactrode structures for room-temperature alkaline electrolyte cells. As a 'fall-out' from that work, high current density air electrodes became available, and they were incorporated in metal-air cells.

Though the potentials of aluminium as anode material in metal-air batteries have been recognised over decades ago [31]. It was not until 1967 that a successful Al-air battery capable of producing at least 70 W of power was reported [18].

Since then islands of research work have been carried out on the system. Tseung *et al* investigated the potentials of the system as a pacemaker [32]. And in Yugoslavia continuous mechanical recharging was achieved by spring loading wedge-shaped aluminium plates [33]. In 1976, Despic *et al* examined the effect of alloying aluminium with small amounts of gallium and indium, on the open circuit potential of a typical aluminium anode battery [34]. Cooper *et al* [35] considered the use of the system for automotive propulsion, in 1978.

At the First International Workshop on Reactive

Metal-air Batteries, in 1979, it was suggested that attempts should be made to replace zinc anodes in primary or mechanically rechargeable metal-air batteries [36]. Following that Despic *et al* investigated the behaviour of aluminium and its alloys at high current densities of anodic dissolution [37]. The observation generated the idea that the application of pulsating current to discharging aluminium anodes in a battery may have a beneficial effect on the performance of the latter. They therefore investigated the effect of pulsalting current on the anode polarisation of a typical aluminium anode battery [38]. At the 12th International Power sources Symposium, in 1980, Torstein Valand [39] described the potentials of Al-air cells as small electric generators for field use. The cell described had a total cell efficiency of approximately 40% and a current efficiency of 100% with respect to Al. However, there were still problems to be solved before the cell was to be put into any use. The major problems identified were the tendency of aluminium to passivate and the voluminous reaction products which clogged up the cell. Similar problems were faced by those who tried to develop the system.

The standard electrochemical potential of aluminium of -2.35 V is not achieved, in practice. Potentials far below the theoretical value are observed; this may be due to the formation of thin oxide film on the surface of the metal, partially passivating the metal [40]. The

passivating oxide film on the surface of pure aluminium was reduced by alloying [41,42]. But in most cases, though higher potentials were achieved, the efficiencies obtained were short of 100%. Furthermore, the alloys produced gave off a lot of hydrogen at open circuit. Attempts to inhibit the hydrogen evolution by alloying the aluminium with indium, mercury or gallium [43], gave rise to problems with the mechanical recharging of the system since the alloys so-produced, were highly activated and had to be stored and handled under stringent conditions [39].

Also, when aluminium dissolves, a large quantity of reaction products in the form of hydrated aluminium oxides are formed, which tend to clog up the cell in a short time if not removed [39]. Many of the researchers used NaOH as the electrolyte and as such were faced with a large volume of reaction products and subsequently, a large build up of reaction heat within the system. Hydrocyclones have been used to remove the finely dispersed reaction products [39] but, even though they were effective, some of the reaction products by-passed them and circulated in the system; increasing the tendency of clogging in the cell.

The above problems, pertaining to the operation of the Al-air cell, are recognised and the possible solutions form the basis of this research work. To achieve the ultimate aim, the problems were critically analysed and

attempts were made to resolve each problem on its own merit; but bearing in mind the objective. The objective being, the production of a steady high current for a consumed electrode that is capable of recharging whilst the battery is in service.

2 CONCEPTS AND PRINCIPLES OF CELL OPERATION

2.1 INTRODUCTION

A power cell, or an electrochemical power source, is a device which enables the energy liberated in a chemical reaction to be converted directly into electricity.

Many chemical substances are able to exist in more than one oxidation state. Thus, they can donate or accept electrons from other species. A net transfer of electrons may occur spontaneously whenever the free energy of the whole system is reduced by such a process. An electron transfer between an electronic conductor and some species in an electrolytic phase is known as an electrochemical reaction or electrode process. For such a transfer to proceed on a continuous basis, the principle of electroneutrality requires the presence of a second electrode process in which electron transfer takes place in the opposite direction. Hence, a cell basically consists of two electrodes, anode and cathode, and an electrolyte.

If the two electrodes are placed apart in a vessel containing the electrolyte and then connected through a

resistor, the connection will permit charge flow round the circuit and hence formation of ions in solution. As charge transfer (in the appropriate direction) at the interfaces produces exactly the same result as the homogeneous electron exchange, the whole cell process including the electron flow through the load resistor will also be spontaneous; driven by the net free energy change associated with the cell reaction.

The quantity of a chemical species reduced or oxidised during a cell reaction is related, by Faraday's laws, to the total electric charge transferred across the metal-solution interfaces. A current I amps flowing in the circuit for a time of t seconds is equivalent to the transfer of It coulombs of charge across any interface in the cell. Consider the general electrode process:

$$M^{x+}(aq) - ne \rightarrow M^{(x+n)+}(aq)$$

Now if the oxidation of each $M^{x+}(aq)$ ion involves the transfer of n electrons to the external circuit, then the passage of It coulombs must correspond to the oxidation of

$$It/nF \qquad (2.1)$$

moles of $M^{x+}(aq)$, N_M, where F is the Faraday's constant which has a value of 96,490 C mol^{-1}. If

N_{TM} represents the total number of moles of $M^{x+}(aq)$ present, then the maximum capacity of the cell, that is, the total number of charge that could be supplied to the external circuit is given by

$$Q_T = It = nF.N_{TM} \qquad (2.2)$$

Recalling that current can only flow in a cell if there are two electrodes, the transfer of It coulombs in the appropriate direction at the second electrode brings about the reduction of $P^{y+}(aq)$ ions, the second electrode process being:

$$P^{y+}(aq) + ne \longrightarrow P^{(y-n)+}(aq)$$

2.2 BASIC PRINCIPLES

2.2.1 THE CATHODE

Conventionally, a battery positive electrode contains a metallic oxide component, which is reduced to a lower oxidation state when the battery operates. In practice, however, metal oxides are not the only reducible materials which have been used in positive electrodes; oxygen itself is employed as the oxidising agent. It is

reduced electrochemically to form hydroxyl ions, as follows:

$$4e + O_2 + 2H_2O \longrightarrow 4OH^- \qquad (2.3)$$

The reaction takes place readily, provided the electrode is provided with an adequate amount of active catalyst to promote the required reaction. The electrode must be electronically conducting and resistant to corrosion or poisoning.

The oxygen used is in the gas phase, the electrolyte usually in the liquid phase, whilst the catalyst, needed to complete the reaction, is normally in the solid phase. The reaction, therefore, occurs in the vicinity of three adjacent phases. As such, the design of the electrode must be such as to stabilise the interfaces between the three phases and to maximise the overall area of contact.

Oxygen, or air, electrodes are usually in the form of a porous, conducting solid, into which can penetrate both the electrolyte and the gas. There are several methods of stabilising the gas-liquid interface within the pores, and they depend upon capillary action. By wet-proofing some of the pores, the contact angle is raised, and electrolyte cannot penetrate. The wet-proofing is effected by polytetrafluoroethylene (PTFE) or by paraffin wax. Alternatively, if two distinctly different pore sizes are employed, it is possible to arrange the

conditions so that the electrolyte floods the fine pores, but is kept out of the coarse pores by a positive gas pressure. Also, as a means of preventing the electrolyte from leaking out through the electrode pores, a wet-proof technique is used. The oxygen side of the electrode is cladded with a thin layer of porous water-repellent plastic, such as a mixture of PTFE and acetylene black.

The thermodynamic reversible potential of the oxygen reduction reaction (2.3) is given as 1.23 V positive to a hydrogen electrode in the same electrolyte [44]. In practice however, potentials less than the thermodynamic value are observed. When current is drawn, further loss of potential (or polarisation) occurs, so that a plot of electrode potential versus current would appear as in Fig. 2.1.

2.2.2 THE ELECTROLYTE

The function of the electrolyte, in metal-air cells, is to act as an ionic conductor, enabling the ionic species produced at the air electrode to travel to the metal electrode, where they are consumed. Water is also involved in the electrode reactions and this, too, is carried across the cell by the electrolyte. Because the electrolyte is not an electronic conductor, it prevents the passage of electronic current between the two electrodes.

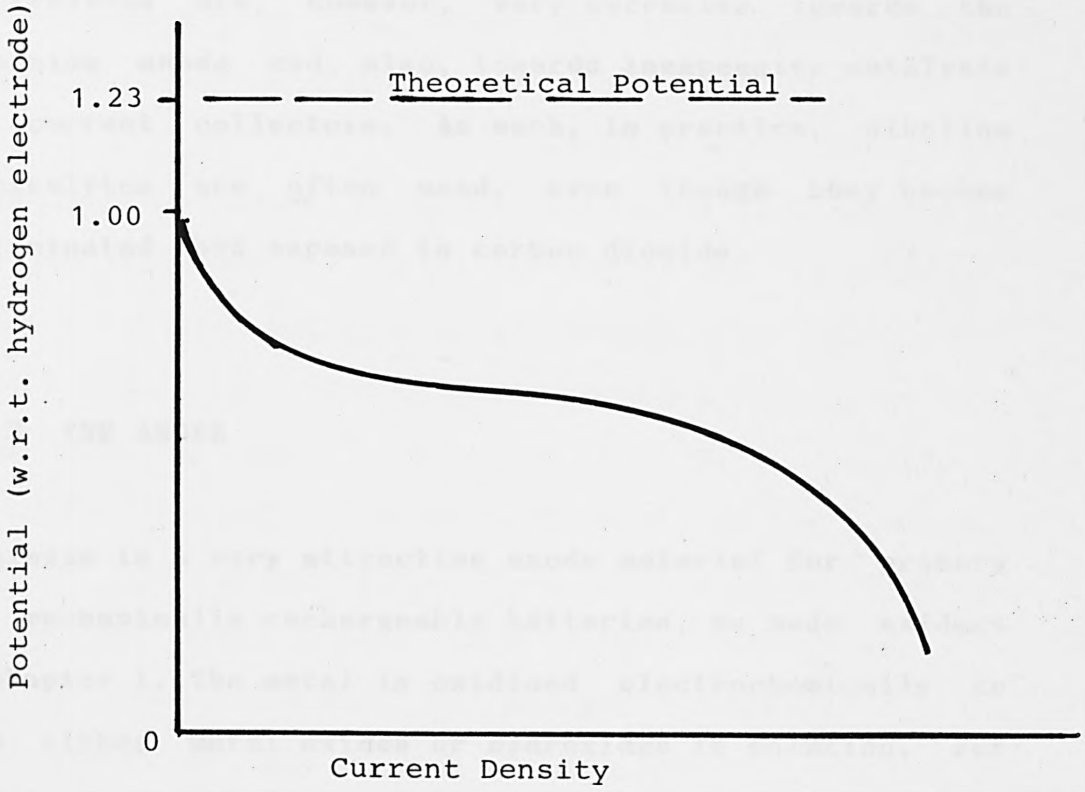

FIG. 2.1 TYPICAL CURRENT-POTENTIAL CURVE FOR AN OXYGEN ELECTRODE

The Aluminium anode does not require a highly alkaline electrolyte and will discharge satisfactorily in neutral electrolytes such as potassium chloride, ammonium chloride, and sodium chloride, but the air electrode requires a highly acidic or alkaline electrolyte in order to achieve high current densities [45]. Highly acidic electrolytes are, however, very corrosive towards the aluminium anode and, also, towards inexpensive catalysts and current collectors. As such, in practice, alkaline electrolytes are often used, even though they become contaminated when exposed to carbon dioxide.

2.2.3 THE ANODE

Aluminium is a very attractive anode material for primary and mechanically rechargeable batteries, as made evident in chapter 1. The metal is oxidised electrochemically to form either metal oxides or hydroxides in solution. For example, in alkaline solutions, trihydrated alumina is produced

$$Al + 3OH^- \longrightarrow Al(OH)_3 + 3e \qquad (2.4)$$

$$3e + 3H_2O \longrightarrow 3OH^- + 1.5H_2 \qquad (2.5)$$

the product so-formed is soluble in excess alkali. Simultaneous to this reaction (current producing) is the corrosion reaction (2.5), with the evolution of hydrogen.

Since aluminium is an electronic conductor, and since most electrochemical oxidation reactions of metals are fast, catalysts are not needed in the fabrication of the electrode. During the reaction, however, the anode is dissolved, and the quantity of electricity that can pass (the 'capacity' of the electrode) is determined by the amount of aluminium present.

The standard electrochemical potential of aluminium in alkaline solution is given as -2.35 V. In practice, however, anodic potentials far below the theoretical value are observed, probably due to the formation of thin oxide film on the surface of the metal, partially passivating the metal [9,16,17,26,40,46] or the corrosion reaction (self-discharge), that occurs even when no current is being passed (2.5). Lower potentials are produced when current is passed; resulting in a polarisation of the nature as shown in Fig. 2.2. This polarisation is attributable mainly to the electronic resistance of the electrode, and to the slowness of diffusion of reactants and products in the electrolyte. Since the electrode geometry changes radically during polarisation, the factors contributing to polarisation change with time. In general, polarisation tends to increase with time.

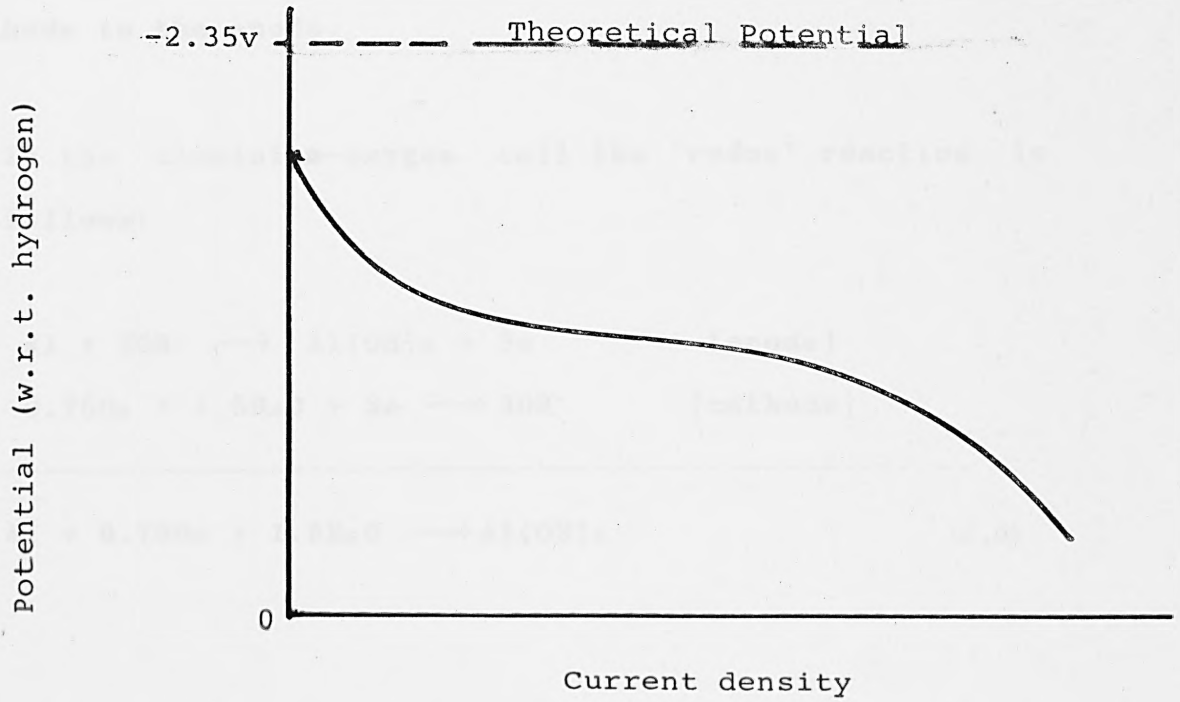

FIG. 2.2 TYPICAL CURRENT-POTENTIAL CURVE FOR ALUMINIUM ELECTRODE

2.2.4 THE FULL-CELL

When the anode, cathode and electrolyte are brought together to form the three major components of the full-cell, the cell potential is equal to the difference between the potentials of the cathode and anode (Fig. 2.3). A combination of the reduction-oxidation reactions of the cathode and anode takes place during the discharge of a cell. The cathode is reduced by the absorption of electrons released in the oxidation of the anode. Electric current flows in the external circuit from the cathode to the anode.

In the aluminium-oxygen cell the 'redox' reaction is as follows:

$$Al + 3OH^- \longrightarrow Al(OH)_3 + 3e \qquad \text{[anode]}$$

$$0.75O_2 + 1.5H_2O + 3e \longrightarrow 3OH^- \qquad \text{[cathode]}$$

$$Al + 0.75O_2 + 1.5H_2O \longrightarrow Al(OH)_3 \qquad (2.6)$$

The theoretical potential and energy density being 2.7 V and 2980 Ah/kg Al respectively [47].

Aluminium-air cells are divided into two principal

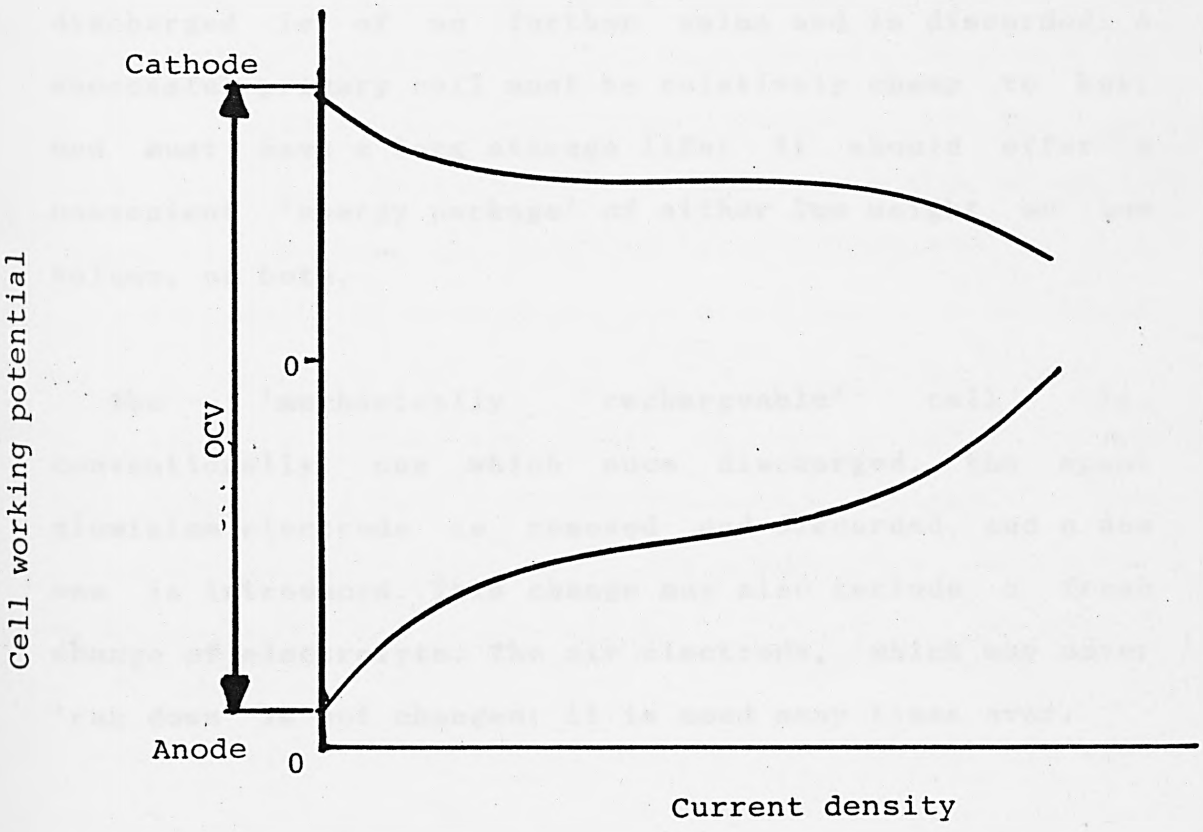

FIG. 2.3 CURRENT-POTENTIAL CURVE FOR A FULL CELL

classes depending on their design characteristics:

(i) primary cells

and (ii) mechanically rechargeable cells.

The primary cell is, basically, one which once discharged is of no further value and is discarded. A successful primary cell must be relatively cheap to buy, and must have a long storage life; it should offer a convenient 'energy package' of either low weight or low volume, or both.

The 'mechanically rechargeable' cell is, conventionally, one which once discharged, the spent aluminium electrode is removed and discarded, and a new one is introduced. This change may also include a fresh change of electrolyte. The air electrode, which may never 'run down' is not changed; it is used many times over.

2.3 THERMODYNAMICS AND KINETICS OF CELL REACTIONS

2.3.1 ENERGETICS

If thermodynamic properties of the reactants and products of the overall cell reaction are known, thermodynamics permits the calculation of the open-circuit cell

potential or electromotive force (EMF) provided competing reactions are not involved. The thermodynamic calculation is not depedent on a knowledge of the mechanism or steps involved in the overall cell reaction. In practice, considerable difficulty is often encountered because of uncertainty of the nature and thermodynamic properties of the species involved in the overall cell reaction at various stages of discharge. Nevertheless, even when the data for the thermodynamic properties of the chemical components within the cell are insufficient for precise calculations, thermodynamics may still permit predictions of cell potential to within 0.1 V [48]. When extraneous competing reactions are known or suspected to cause difficulty under open-circuit conditions, the thermodynamically calculated EMF represents an upper limit.

The application of thermodynamics to battery systems, though important, has a limited role [49]. As such, a detailed development of the thermodynamics of electrochemical cells is considered to be beyond the scope of this chapter. These details can be found elsewhere [50-52]. However, aspects of the subject of direct importance in batteries will be considered. The limitations of the application of thermodynamics, follow from two very important factors [53]. First, it is the kinetics and problems of mass transfer which limit battery performance and these are not predictable by thermodynamics. Secondly, many important battery systems

utilise chemical constituents which are not well defined and for which there is no appropriate thermodynamic data.

The limited role can be little more than, possibly with some intelligent guesses, a figure for the Gibbs free energy of systems that can be estimated and perhaps confirmed by measurement of an open-circuit potential. It is hazardous to go further to deduce mechanisms of reactions without kinetic investigation [53]. The exercise does, however, identify the basic feasibility of the chosen system as a potential source of electrical work.

To apply thermodynamics to a battery system, it is assumed that the cell operates at a constant temperature and pressure. Consider for example a cell:

Electrode (1)/Electrolyte/Electrode (2)

I S I'

and let the electrode reactions be:

$$M \longrightarrow M^{n+} + ne$$

$$P^{n+} + ne \longrightarrow P$$

Then, summing,

$$M + P^{n+} \longrightarrow M^{n+} + P \qquad (2.7)$$

The thermodynamics of the redox couple can be described in terms of the free energy change in the overall electrochemical reaction (2.7). Thus,

$$\Delta G = \Delta G^{\circ} + RT\ln\left((a_{m^{n+}}\, a_{p}) \,/\, (a_{m}\, a_{p^{n+}})\right) \qquad (2.8)$$

where ΔG^{o} is the standard free energy change.

Suppose now that the electrical resistance of the external load is very great so that the cell is passing a very small current. It can then be said that the cell is operating at a nearly-equilibrium condition, because a negligible current across the electrode means a negligible overpotential at the electrodes. Hence, the Nernst equation can be applied to calculate the potential differences at the two interfaces.

The Nernst equation is given as [53]:

$$E = E^{o} + (RT/nF)\ln\left((a_{m^{n+}})/a_{m}\right) \qquad (2.9)$$

where $a_{m^{n+}}$, a_{m} are the activities of the electron acceptor and electron donor respectively. The equation, first derived by Nernst, tells how the potential of an interface varies with the activity (roughly, the concentration) of ions in solution. In dilute solution,

the activities can be replaced by concentrations. It is worth pointing out that the Nernst equation can be applied only rarely to the study of electrodes in solution, because it is quite difficult to find interfaces which do exhibit the simple kind of equilibrium (i.e. just one reaction, such as $Ag^{+} + e \longrightarrow Ag$) in control. More often, several reactions determine the behaviour of an electrode when no current passes across it. However, Nernst's equation is of immense basic significance because it tells, in terms of basic thermodynamic quantities (standard free energies of the ions etc. which take part in the reaction), what the potential of an electrode at equilibrium ought to be. It gives the potential to which the overpotential in kinetics can be referred.

Now, applying the Nernst equation to the cell reaction in question, we have,

$$\begin{aligned} E_{I'} &= E^{\circ}_{(2)} + (RT/nF)\ln(a_{p^{n+}}/a_{p}) \\ E_{I} &= E^{\circ}_{(1)} + (RT/nF)\ln(a_{m^{n+}}/a_{m}) \end{aligned} \qquad (2.10)$$

But:

$$E_{cell} = E_{I'} - E_{I} \qquad (2.11)$$

is the reversible potential of the cell, and therefore (from equation (2.10)

$$nFE_{cell} = nFE^{\circ}_{cell} - RT\ln((a_{m^{n+}} a_{p})/(a_{m} \quad a_{p^{n+}})) \qquad (2.12)$$

By comparing equations (2.8) and (2.11):

$$nFE \quad = - \Delta G \qquad (2.13)$$

This relation is the most fundamental one in the study of the energy relations of electrochemical cells and, therefore, is the basic equation in electrochemical energy conversion [54-58]. It tells that the potential developed by a cell at equilibrium depends only on the free energy change in the chemical reaction which occurs in the cell. No properties of the substrates come into the discussion at all. Thus, the free energy change in the reaction in the electrochemical cell is only that of the overall chemical reaction, and not a function of the energy of the electrons in the metal concerned (for no term for that energy appear in 2.8 or 2.12).

The heat effect of a cell reaction is equal to the decrease in the total enthalpy H of the reaction. This quantity is not the same as the decrease in free energy. Therefore, even when a cell is operated under optimal conditions and its potential is very close to EMF, not all of the reaction energy is transformed into electrical energy; some part of it is always released as heat [54]. The unavailable energy is determined by the change in the reaction entropy:

$$- \Delta H = nFE - T \Delta S \qquad (2.14)$$

where T is the absolute temperature. The heat effect can be conveniently expressed in electrical units, that is referred to unit charge passed through a cell:

$$E' = - \Delta H/nF \qquad (2.15)$$

By convention, E' is called the thermoneutral voltage [54]. The unavailable energy can then be expressed in the form:

$$- T \Delta S = nF (E' - E) \qquad (2.16)$$

If a cell is operated at a potential, V, below the EMF, the difference $\Delta H_{\Delta v} = nF(E - V)$ is also released as thermal energy. The total heat released in discharging a cell is found as the sum of these two components:

$$- \Delta H_{cell} = - T\Delta S + (- \Delta H_{\Delta V}) = nF (E' - V) \qquad (2.17)$$

The Gibbs-Helmholtz equation [59], one of the most important equations in chemical thermodynamics, can be presented here in the following form (in electrical units):

$$E = E' + T (dE/dT) \qquad (2.18)$$

The above equation clearly shows that for systems with $E < E'$ the slope dE/dT is negative, so that the EMF falls off as temperature increases. For systems with $E > E'$, the EMF rises as temperature increases.

2.3.2 METAL-SOLUTION INTERFACE [60]

IONS IN SOLUTION

The chemical reactions that produce electrochemical power within a battery for the most part are heterogeneous processes occuring at the electrode surface rather than at a distance from the electrode surface [61]. To understand the factors controlling these heterogeneous processes, it is necessary to consider the structure of the interface. Both the electrolyte and the electrode sides of the interface differ substantially from the bulk phases in their electrical properties. However, electrochemical reactions cannot continuously occur at an electrified surface in contact with a solution without a corresponding reservoir of ions in solution [62]. The demand for electric charge at the interface cannot be met by ions which remains stationary in the solution, or just move about at random. There is a logistic part in electrochemistry. The ions and the particles have each to move up (at a calculable rate) to the interphase

between solution and electrode to receive an electron from the electrode, or to give up an electron to it.

Ionic solutions are the media in which the ions exist. These ions are the reservoir of charges for electrodes, and thus for processes in which substances directly produce electricity. Knowledge of the energy of ions in solution is important. For example, the depth of the energy well occupied by an ion in solution determines the difficulty of transferring an electron to the ion [63]. It is easy to understand that, if an ion is tightly bonded to the solvent it will not be as easy for an electron to neutralise it as when it is less tightly bound. Solvation energy therefore influences overpotential. As the concentration of solution rises (and therefore the average distance between particles decreases), so the energy of interaction between cations and anions increases, as a consequence of Coulomb's law [64].

It follows, qualitatively, that the properties of ionic solutions (essentially dependent upon the mean energy of the ions) will depend upon the concentration of the ions. Consider the equation [65]:

$$\mu_i = \mu_{0i} + RT \ln f_i C_i = \mu_{0i} + RT \ln a_i \qquad (2.19)$$

where a_i is called the activity of the ionic species i and c_i is the concentration of an ion in solution. Here, the activity of an ionic species is the product of the concentration of the ion in the solution and a term f_i; RT In f_i is the ionic attraction energy between a mole of positive and a mole of negative ions, at a concentration c. When the solution is very dilute, the ions will be so far apart that the energy of their interactions will be negligible. If this is so, then the 'energy of unideality' (which is the ions' energy of interaction with each other) must tend to zero. Hence, RT Inf must tend to zero, and it then follows that f tends to 1 (and In f to 0) as the concentration of ions in the solution diminishes. An ideal solution (no interaction energy), therefore, has an activity coefficient of 1.

Ionic solvation had to be considered because it is part of understanding the stability of an ion in solution, and how solvation influences solubility. Also, the energy which ions get by interacting together in solution had to be considered since calculations on electrode processes cannot be accurately done unless something about the energies of the ions in solution, from which the electrodes will enable energy to be extracted, is known. Another reason for knowing something about these activity coefficients is that when the potential of an electrode in solution is to be calculated as a function of the concentration of the ions present, in the special case when the exchange of electric charges

between the ion and solution has an equal rate in both directions, this electrode potential, E , can be shown to be given by

$$E = E^{\circ} + (RT/F)\ln c_i + (RT/F)\ln f_i \qquad (2.20)$$

Thus, the most convenient calculation in the theory of electrode processes (which always involves E) cannot be done without knowing the activity coefficient of the electrolyte.

The above description of a solution deals with the sorting and distribution of ions with respect to each other, how they join up and interact with solvent molecules, and how they interact with each other and affect the energy (and thereby the properties) of the solution. Ions collide in solution, but they rebound, and concern has been with the time-average situation among many thousands of millions of collisions. It could be that ions do not immediately bounce off each other but stay 'stuck' together temporarily ('ionic dipoles'), or, in a more extreme sense, that some cation will bond with one or more anions. Then, complex ions (two or more ions associated together for time exceeding say 1 s) may exist in solution. Temporary association into ionic dipoles will mean that a fraction of ions, at any moment, will not be available to function as ions. The associated ion-pairs could be treated as being in equilibrium with

the corresponding free ions: $C^+ + A^- \dashrightarrow C^+A^-$; if the law of mass action is applied to this equilibrium,

$$K_{assoc} = a_{(C^+A^-)} / a_{(C^+)} a_{(A^-)} \qquad (2.21)$$

where a represents the activity of the corresponding species and is a constant at a given temperature and pressure. $K_{assoc.}$, is called 'the association constant', and its value expresses the tendency of the free ions to associate temporarily together into pairs.

There are three ways in which ions reach the electrode, and then withdraw from it.

(i) Diffusion is the easiest to understand. If an electrode is giving electrons to metal cations, there will be a concentration gradient towards the electrode; the concentration of the metal ions will get less as the electrode is approached, because the electrode is removing a lot from the solution. Diffusion occurs down the concentration gradient towards the electrode. The equation is

$$i_{diff} = - DFn(dC / dx) \qquad (2.22)$$

Where i_{diff} is the rate of diffusion of ions to the electrode expressed in $Cm^{-2}S^{-1}$; D is the diffusion coeffient; F the Faraday constant; and dc/dx is the concentration gradient near the electrode.

This equation enables the understanding of how an electrode reaction can occur. Suppose a small current is passing through the electrode. Then the concentration gradient needed to make -DF(dc/dx) equal to this small current (i.e. to make the ions diffuse up at a rate equal to the rate at which their partner electrons are arriving at the surface) will itself be correspondingly small. Thus, the concentration at the electrode surface will be scarcely different from that in the bulk. However, as the current density increases dc/dx must increase. The maximum concentration gradient will be (see Fig 2.4):

$$\frac{dC}{dX} = \frac{C_{bulk} - C_{electrode}}{\delta} = \frac{C_{bulk}}{\delta} \qquad (2.23)$$

and that a limiting current (cf. 2.22), the highest which can exist in a given electrolyte for the deposition of a given species, will be observed for $c_{electrode} = 0$.

(ii) Another mode of transport of ions in solution is

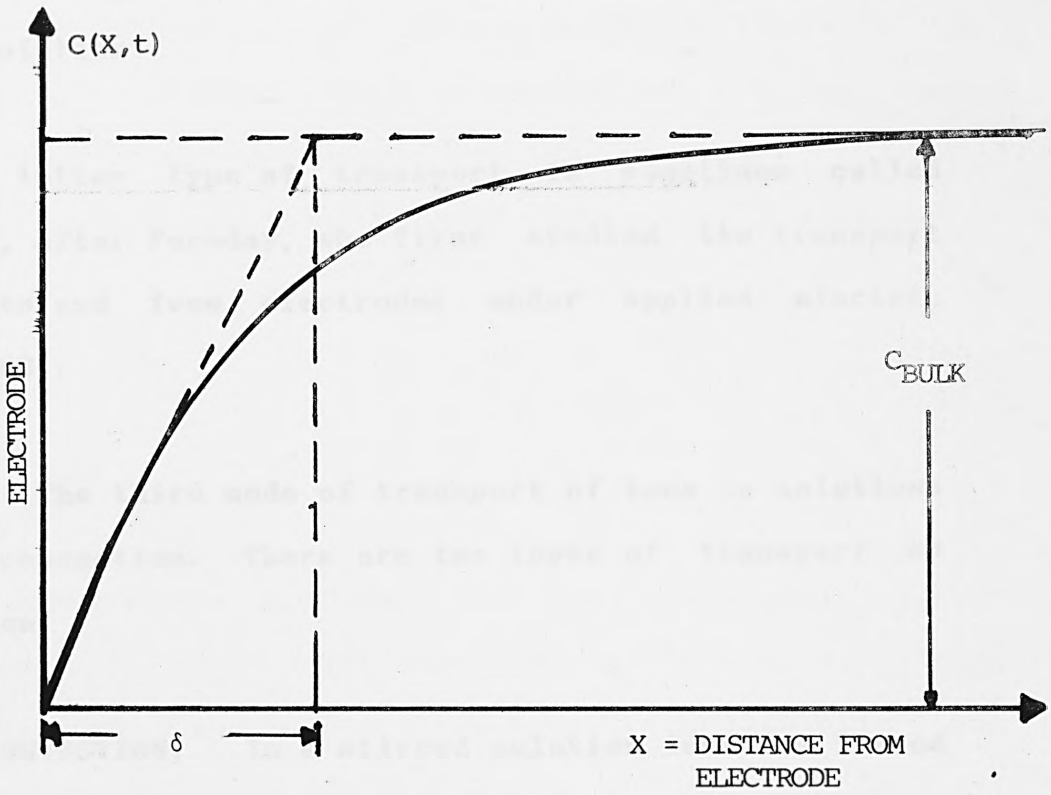

FIG. 2.4 DIFFUSION PATH OF IONS IN SOLUTION

one in which the electric field produced between the electrodes pulls the ions through the solution towards the electrodes. The field accelerates the ions, pulling the anions towards the negative electrode (anode, in a battery system) and the cations towards the positive one (cathode). Thus, the total rate of arrival of ions at an electrode will depend on the concentration gradient and also on those ions brought up independently of the concentration gradient, as a result of the electric field in the solution.

This latter type of transport is sometimes called Faradaic, after Faraday, who first studied the transport of ions to and from electrodes under applied electric fields [66].

(iii) The third mode of transport of ions in solutions is by convection. There are two types of transport by convection.

FORCED CONVECTION: In a stirred solution ions are forced to the electrode interface.

NATURAL CONVECTION: During deposition at an electrode, ions are removed from the solution to become atoms on the electrode. The layer of solution near to the electrode becomes depleted of ions, so causing density differences and hence convection 'stirring' in the vicinity of the electrode.

Apart from the situation very near the electrodes, where diffusion is helping the transport of ions to and from the interfaces, there is an intermediate region, between the electrodes, where only the electric field makes the ions move. This is because far away from the electrodes there are no concentration gradients. Here, a strange thing happens: the ions do not move at equal rates, in fact anions (−) often move faster that cations (+) [67]. If the total current density carried is i, it is divided into two parts, i_+ and i_-. A quantity called transport numbers [68] can be defined as:

$$t_+ = i_+ / i \; ; \; t_- = i_- / i \qquad (2.24)$$

The concentration gradients at the electrodes adjust themselves, in such a way that the rate of arrival of the ions due to the Faradaic transport, together with ions arriving by diffusion and convection, equals the current at each electrode.

The potential difference across a metal-solution interface disturbs the ionic distribution within the solution in the vicinity of the interface and an ionic double-layer results (see Fig. 2.5). Immediately adjacent to the electrode surface there exists a compact layer of ions of charge predominantly opposite to that of

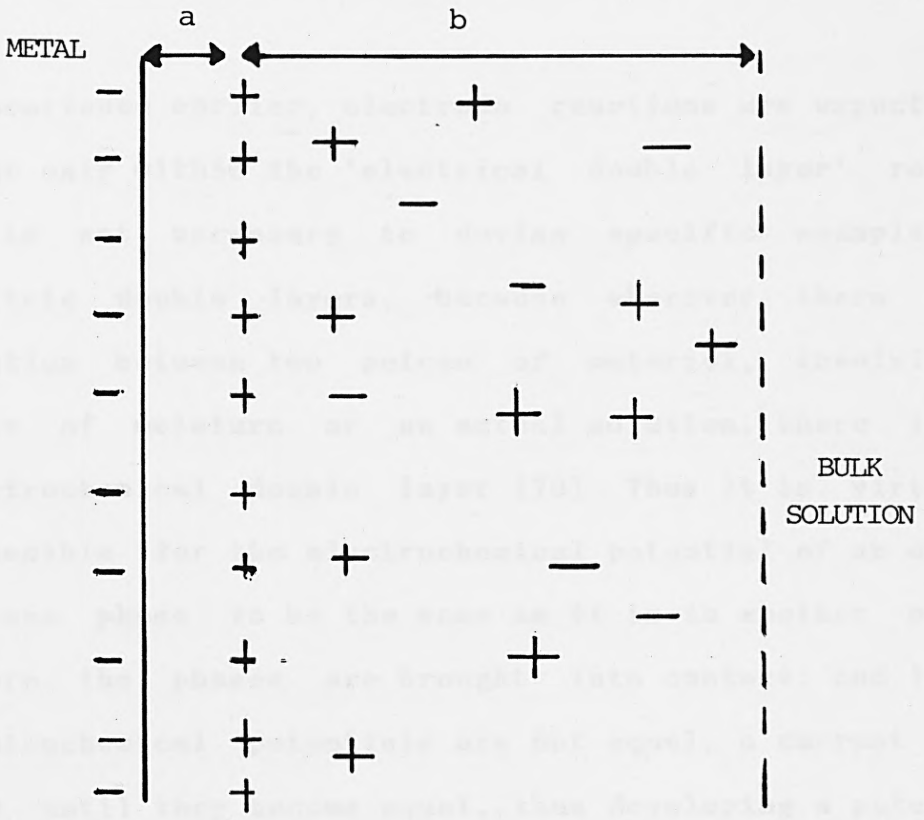

FIG. 2.5 THE HELMHOLTZ DOUBLE LAYER MODEL

the electrode. This layer is called the Helmholtz layer and the plane through the electrical centres of the ions is referred to as the Helmholtz plane. This plane corresponds to the distance of closest approach of the ions to the electrode surface for the particular type of ions which predominate in the Helmholtz layer.

NATURE OF THE ELECTRIC DOUBLE LAYER [69]

As mentioned earlier, electrode reactions are expected to occur only within the 'electrical double layer' region. It is not necessary to devise specific examples of electric double layers, because wherever there is a junction between two peices of material, involving a layer of moisture or an actual solution, there is an electrochemical double layer [70]. Thus it is virtually impossible for the electrochemical potential of an entity in one phase to be the same as it is in another phase, before the phases are brought into contact; and if the electrochemical potentials are not equal, a current will flow until they become equal, thus developing a potential difference.

If the number of electric charges which flow per unit time onto a metal surface from an outside source of power is changed, two things can happen. First, these charges can easily leave the surface of a metal in contact with a solution and neutralise protons in the adjacent solution,

forming adsorbed atoms of hydrogen on the metal. If there really is no difficult in this, the only effect of attempting to change the surface charge on the metal (by, say, increasing the flow of electrons from an outside source) will be the formation of more hydrogen atoms at the interface, and nothing else. There would be no change in net charge on the surface, and hence no change in potential between the metal and the solution. The electrons flow in, and the charges on the surface never increases in concentration because the electrons jump across the double layer and form H from the H^+ ions in the solution. The interface is then termed 'non-polarisable'. On the other hand, there are interfaces which are 'polarisable'. In the ideal polarisable interface, when charge flows in from outside it doesn't flow out on to entities in the solution. In such cases there is difficulty in the transfer of an electron across an interface to H^+ in solution. The electric double layer then acts like a capacitor. One plate is the electrode and the other plate is the layer of charges on the solution. For a real capacitor the relation of the potential difference V between its plates to the charge on its plates is given by:

$$V = (d / \varepsilon_r \varepsilon_0)q \qquad (2.25)$$

where q is the charge per unit area, d is the distance

between the plates, ε_0 is the permittivity of a vacuum, and ε_r the relative permittivity of the material between the plates.

It follows that for types of surface in solution which are 'polarisable', if the electric charge is made to increase on one side of the plate and does not leak away into the solution, the potential difference across the double layer will increase or decrease as the charge on the plate increases or decreases. Both types of interface discussed here are idealized extremes, and in reality there are no completely polarisable interfaces nor are there any interfaces which are completely non-polarisable. However, some interfaces are much more polarisable than others, and to simplify some of them are called 'polarisable' (though a little charge leaks across them) and some 'non-polarisable' (though there is a slight build-up of charge and potential across the interface).

A key to understanding the part played by electrochemistry in so many phenomena is to appreciate the considerable electric field strength in the interphase double layer. By taking an approximate value of the potential difference within the double layer to be 1 V, and an approximate value of the distance between the layers of charges in the double layer to be about 0.3 nm, the electric field strength can be found to be (cf.2.25):

$1/(0.3 * 10^{-9}) = 3 * 10^{9}$ V m^{-1}

An electric field strength as high as this is not obtainable except in electrochemical interphases [71]. It is this strong field acting upon molecules and ions during their electrochemical reaction which so greatly affects their reaction rates, the rates of processes at electrodes.

Historically, the first model describing the structure of the electrode-solution interface was that of Helmholtz and Perrin [69]. It regards the double layer simply as a plane layer of charges of opposite sign on the electrode. The Helmholtz model is considered to be much oversimplifield. It is argued that a strict and rigid distribution of ions on a simple plane seems unlikely. There must be thermal agitation of the ions on the solution side and they are not confined to one single sheet at 0.5 nm or so from the metal, but distributed over a much greater distance into the bulk of the solution [72]. This idea of the distribution of charge on the solution side was the main point of another theory, the Gouy-Chapman theory of the diffuse layer [73]. It resembles, in respect of this distribution, the Debye-Huckel theory of the ionic atmosphere [74], which it preceded historically. The interplay of thermal and electrical forces near a charged electrode builds up an ionic cloud of effective thickness k^{-1} where

k^{-1} in the case of a 1,1-valent electrolyte is given by

$$K^{-1} = 1 / B\sqrt{C} \qquad (2.26)$$

which becomes, when B is written out explicitly:

$$K^{-1} = 1 / B\sqrt{C} = 1 / ((N_A e_0^2 / 500\, \varepsilon_r\, \varepsilon_0\, KT)^{0.5}\sqrt{C}) \qquad (2.27)$$

In this relation, c is the bulk concentration of the 1,1-valent electrolyte in mol/dm^3, and k the Boltzman constant (1.38 x 10^{-23} J K^{-1}).

The Gouy-Chapman theory gives an overestimate, with too much stress on distribution, which means physical (coulombic) adsorption, and not enough stress upon the sticking of the ions on to the electrode on the solution side [72]. A third model of the situation in the double layer is that of Stern, in which the ideas of Helmholtz and of Gouy-Chapman were combined. According to Stern, some of the charge on the solution lies in a plane called 'the plane of closest approach', and the remainder is spread out in the solution (in Gouy-Chapman style). The

plane of closest approach of the ions to the electrode divides the solution side into two regions: a Helmholtz-Perrin region, and a Gouy-Chapman region. Each of these two regions can be simulated by a parallel-plate capacitor (see Fig. 2.6), and therefore the double layer is equivalent to two capacitors in series. The variation of potential with distance is linear in the first region and exponential in the second region. The total capacitance of the double layer is therefore given by:

$$\frac{1}{C} = \frac{1}{C_H} + \frac{1}{C_G} \qquad (2.28)$$

where C_H and C_G are the capacitances of the two equivalent capacitors.

2.3.3 ELECTROCHEMICAL KINETIC PARAMETERS [75]

PICTURE OF ELECTRONIC CHARGE TRANSFER

Consider an electron emitted from a metal into a vacuum. As the electron tries to enter the vacuum a positive image charge is induced on the metal, and the electrons experience a force pulling it back. Thus, the electron encounters an energy barrier of finite height and width.

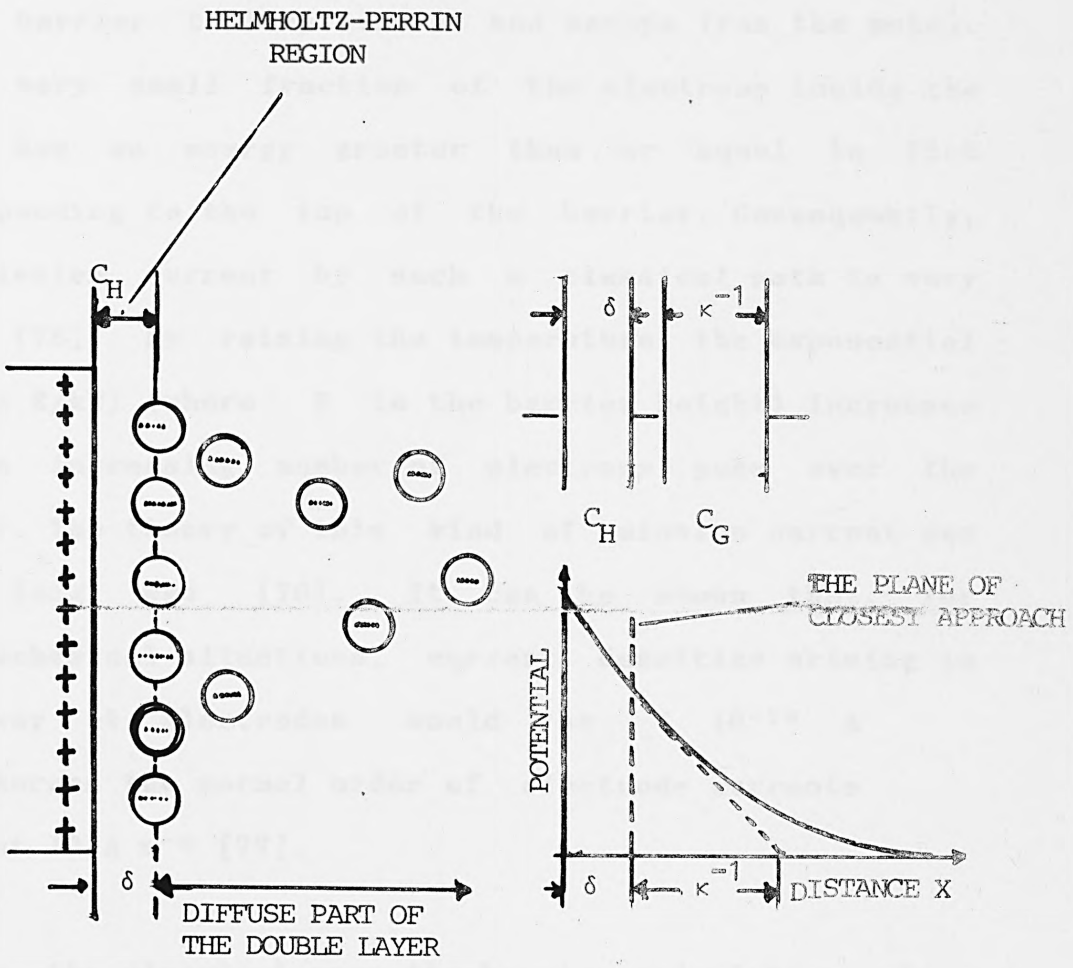

FIG. 2.6 THE STERN DOUBLE LAYER MODEL

It can be expected, using classical mechanics, that the electron would have to have an energy greater than the energy barrier to leap over it and escape from the metal. Only a very small fraction of the electrons inside the metal has an energy greater than or equal to that corresponding to the top of the barrier. Consequently, the emission current by such a classical path is very small [76]. By raising the temperature, the exponential $\exp(-\Delta E/kT)$ (where E is the barrier height) increases and an increasing number of electrons pass over the barrier. The theory of this kind of emission current was given long ago [76]. It can be shown that, for electrochemical situations, current densities arising in this way at electrodes would be $< 10^{-16}$ A m^{-2}, whereas the normal order of electrode currents is about 10 A m^{-2} [77].

Thus, the classical over the barrier calculation gives results quite remote from currents observed experimentally, and may therefore be concluded that classical mechanics cannnot apply to the transfer of electrons from a metal in solution to neighbouring ions. The law of quantum-mechanical 'tunnelling ' governs when an electron leaves a metal and goes into solution [78]. Quantum-mechanical tunnelling will determine the probability that an electron can leave solution and enter the metal. Fig. 2.7 illustrates quantum-mechanical tunnel transfer through a barrier. According to classical

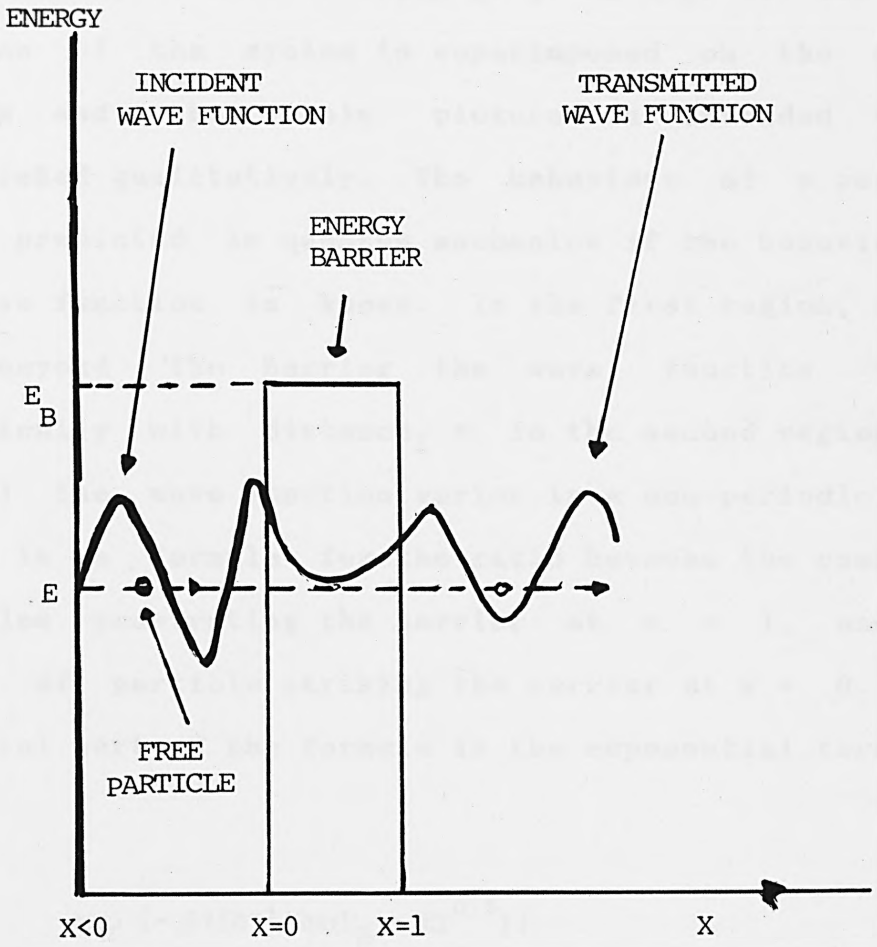

FIG. 2.7 QUANTUM-MECHANICAL TUNNELLING OF A FREE PARTICLE THROUGH A RECTANGULAR ENERGY BARRIER IN A VACUUM

mechanics, a free particle of energy E smaller than the energy E_B of the barrier could never escape to the region $x > 1$. In quantum mechanics, there is some probability that the particle will get to the other side of the barrier, because the behaviour of the particle is described by a wave-function [77]. In Fig. 2.7 the wave function of the system is superimposed on the energy diagram and the whole picture is intended to be interpreted qualitatively. The behaviour of a particle can be predicted in quantum mechanics if the behaviour of the wave function is known. In the first region, $x < 0$, and beyond the barrier the wave function varies periodically with distance, x. In the second region ($0 < x < 1$) the wave function varies in a non-periodic way. There is a formula for the ratio between the number of particles penetrating the barrier at $x = 1$, and the number of particle striking the barrier at $x = 0$. The essential part of the formula is the exponential term:

$$\exp \{-.4\P 1h^{-1}(2m(E_B - E)^{0.5})\} \qquad (2.29)$$

where m is the mass of the particle. Hence, the transmission coefficient will not be zero unless at least one of the quantities E_B, 1 or m has the value of infinity. For a given $(E_B - E)$ and 1, the transmission coefficient increases as the mass of the particle

decreases. Thus, electrons tunnel more easily than atoms. But it is electrons which have to cross the barrier. It can be shown, using the Fermi-Dirac distribution function [77]

$$P_E = \frac{1}{\exp (E - E_f) / KT) + 1}$$

where E_f is known as the Fermi energy,

that if E is about 0.1 eV above the Fermi energy the probability (at 298 K) of the level containing an electron is < 0.01, and if it is 0.1 eV below the Fermi level, the probability that the level will be full is 0.99. Thus, for energy levels around the Fermi level, there are many electrons available to react with materials in solution. For levels below the Fermi level, there are no empty states and no mobility, so that electron transfer is not possible. It can therefore be assumed (as a reasonable approximation) that all the electrons involved in the electric current do have energies of E_f.

Figure 2.8 illustrates tunnelling at a metal-electrolyte interface. The shape of the barrier varies with distance in a smooth fashion. The tunnelling of an electron (of energy E_f) from a metal to a particle (e.g. a cation) in the solution takes place only if another energy condition is fulfilled. There must be a level in that particle which is available (empty) and

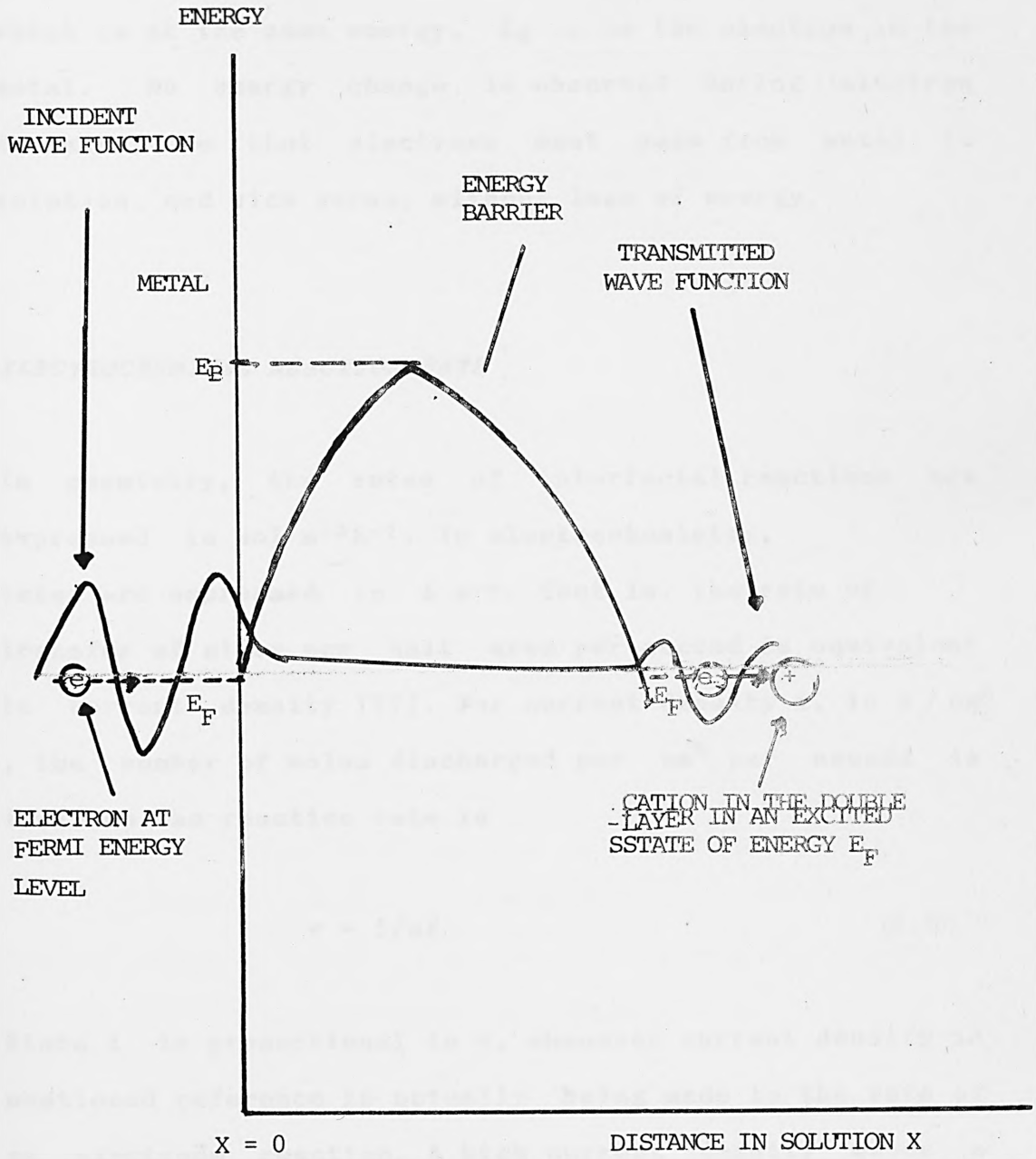

FIG. 2.8 QUANTUM-MECHANICAL TUNNELLING OF AN ELECTRON THROUGH A METAL-SOLUTION INTERFACE

which is at the same energy, E_f , as the electron in the metal. No energy change is observed during electron transfer, so that electrons must pass from metal to solution, and vice versa, without loss of energy.

ELECTROCHEMICAL REACTION RATE

In chemistry, the rates of interfacial reactions are expressed in mol $m^{-2}S^{-1}$. In electrochemistry, rates are expressed in A m^{-2}. That is, the rate of transfer of atoms per unit area per second is equivalent to current density [77]. For current density i, in A/cm^2 , the number of moles discharged per cm^2 per second is i/nF. so the reaction rate is

$$v = i/nF \qquad (2.30)$$

Since i is proportional to v, whenever current density is mentioned reference is actually being made to the rate of an electrode reaction. A high current density means a high electrochemical reaction rate.

EXCHANGE CURRENT DENSITY AND TRANSFER COEFFICIENT

When the electrode is made more negative, electrons are expelled to the solution; and when it is made more

positive, they are attracted. However, at any conditions of the electrode, there is some emission of electrons and some acceptance of them. It depends upon whether the electron-ejecting or the electron-accepting current is greater. A net electrochemical reaction rate can therefore be written as:

$$i_{net,\ cathode} = i_- - i_+ \qquad (2.31)$$

This equation means: 'the net cathode current density observed in an outside circuit is the difference of the cathodic (electron emitting) current density and the anodic (electron accepting) current density. There must be an analogous equation for the net anode current (when the electrode is positive enough to make the partial anodic current predominate), and this will be:

$$i_{net,\ anode} = i_- - i_+ \qquad (2.32)$$

This equation would read: 'the net anode current density is the difference of the actual anodic current density, and the corresponding cathodic current density'. Figure 2.9 illustrates the physical meaning of these two current densities. When the cathodic current is greater than the

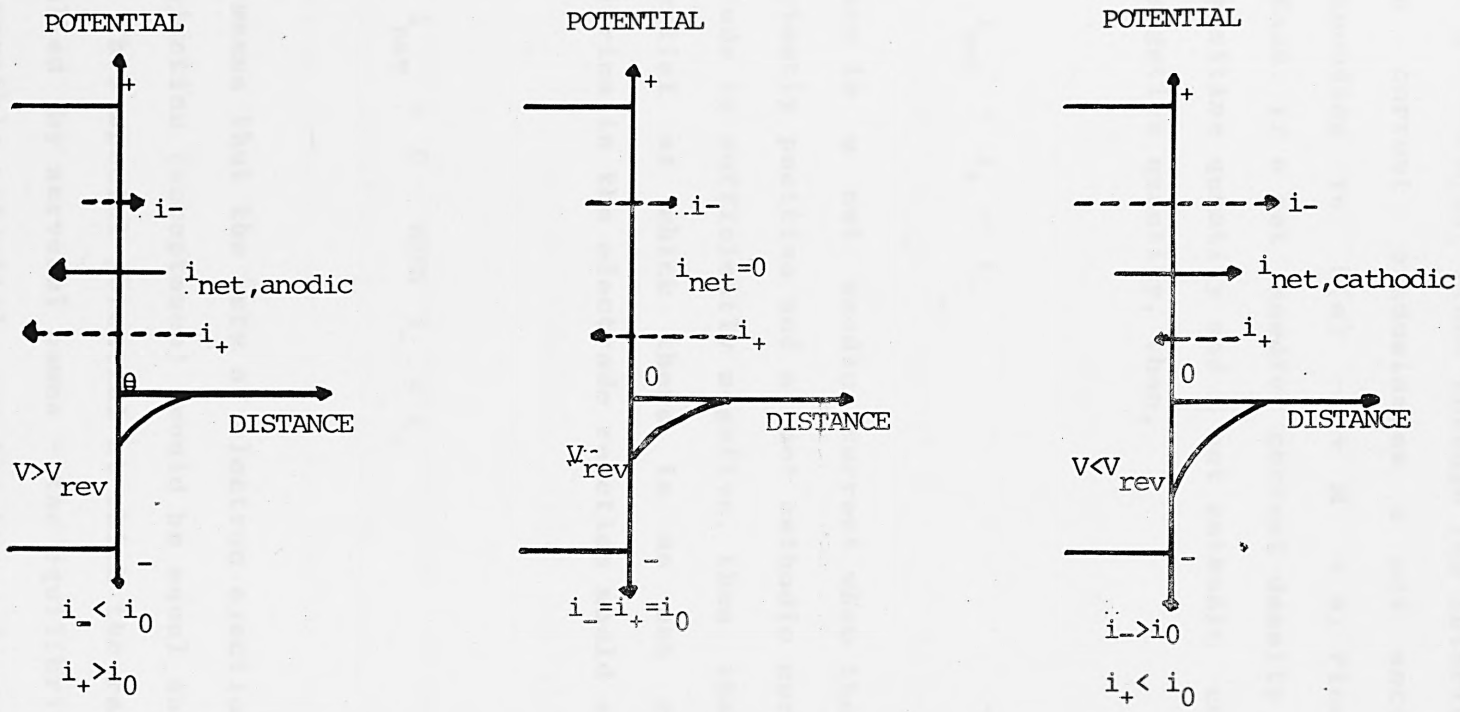

FIG. 2.9 THE MEANING OF EXCHANGE CURRENT DENSITY

anodic current a net cathodic current, corresponding to M + e ----> M(e), flows through the interface; when the anodic current predominates a net anodic current, corresponding to M(e) ----> M + e, flows through the interface. If a net anodic current density is considered as a positive quantity and a net cathodic current density as a negative quantity, then,

$$i_{net} = i_{+} - i_{-} \tag{2.33}$$

If there is a net anodic current when the electrode is sufficiently positive and a net cathodic current when the electrode is sufficiently negative, then there must exist a potential at which there is no net current, i.e. equilibrium in the electrode reaction would exist. Hence:

$$i_{net} = 0 \quad \text{WHEN} \quad i_{-} = i_{+} \tag{2.34}$$

This means that the rate of electron ejection (emission) and injection (acceptance) would be equal and the current zero. This special potential at which the rates are equal is called by serveral names - the equilibrium potential, the reversible potential, or the thermodynamic potential. It is often denoted as E. Thus,

$$i_{net} = 0 \quad \text{when } V = E \tag{2.35}$$

The relation between net current density and potential difference V is given by [79]

$$i_{net} = (i_+)_{V=0} \exp((1-\alpha)FV / RT) - (i_-)_{V=0} \exp(-\alpha FV/RT) \tag{2.36}$$

From equations (2.35)and (2.36), it follows that:

$$i_0 = (i_+)_{V=0} \exp((1-\alpha)FE / RT) = (i_-)_{V=0} \exp(-\alpha FE/RT) \tag{2.37}$$

where i_o is the EXCHANGE CURRENT DENSITY.

Figure 2.9 illustrates also the meaning of exchange current density. At equilibrium (i.e., when V = E), the partial anodic and cathodic current densities (positive equilibrium) are equal and $i_0 = i_+ + i_-$. When V is more positive than E, $i_+ > i_0$, $i_+ < i$, and a net anodic current (electrons from solution to metal) flows through the interface. When V is more negative than E, $i_- > i_0$, $i_+ < i$, and a net cathodic current flows through the interface.

The difference between V and E is known as OVERPOTENTIAL, . That is,

$$\eta = V - E \tag{2.38}$$

Combining equations (2.35-2.38):

$$i = i_0(((\exp((1 - \alpha)\, F\eta / RT) - \exp(-\alpha F\eta/RT)) \tag{2.39}$$

This is the Butler-volmer equation [79], and it relates the net current density of the electrochemical reaction to the overpotential. Suppose that the electrochemical reaction occurs at large anodic overpotentials, i.e. at $\eta >> RT/F$, it can be seen from the form of the equation that the second term in the equation can be neglected, so that:

$$i = i_0 \exp((1 - \alpha)\, F\eta / RT) \tag{2.40}$$

If the electrochemical reaction occurs at large cathodic overpotentials, i.e. at $\eta << RT/F$, it is the first term in the equation that can be neglected, and the Butler-Volmer equation reduces to:

$$i = -i_0 \exp(-\alpha F\eta / RT) \tag{2.41}$$

Equations (2.40) and (2.41) can be rewritten as:

$$\eta = -\frac{RT}{(1-\alpha)F}\ln i_0 + \frac{RT}{(1-\alpha)F}\ln i \; ; \qquad (\eta >> RT/F) \tag{2.42}$$

$$-\eta = -\frac{RT}{\alpha F}\ln i_0 + \frac{RT}{\alpha F}\ln(-i) \; ; \qquad (\eta << -RT/F) \tag{2.43}$$

Equations (2.42) and (2.43) are known as Tafel equations [80].

Consider now an experiment performed at large anodic overpotentials. Equation (2.42) shows that the plot η against ln i should be a straight line with the slope given by $RT/(1-\alpha)F$ (see also Fig. 2.10); RT/F is a known quantity, and α, the transfer coefficient can be derived from the experimental value of this slope. Equation (2.42) also shows that η is zero for ln i = ln i_o ; extrapolation to $\eta = 0$ (the dotted line in Fig. 2.10), gives the value of i_o. Fig. 2.11 shows how the values of α and i_o can be obtained from experiments performed at large cathodic overpotentials, when equation (2.43) applies.

Consider very small anodic or cathodic overpotentials, i.e. $|\eta| << -RT/F$. Then, the exponentials in the

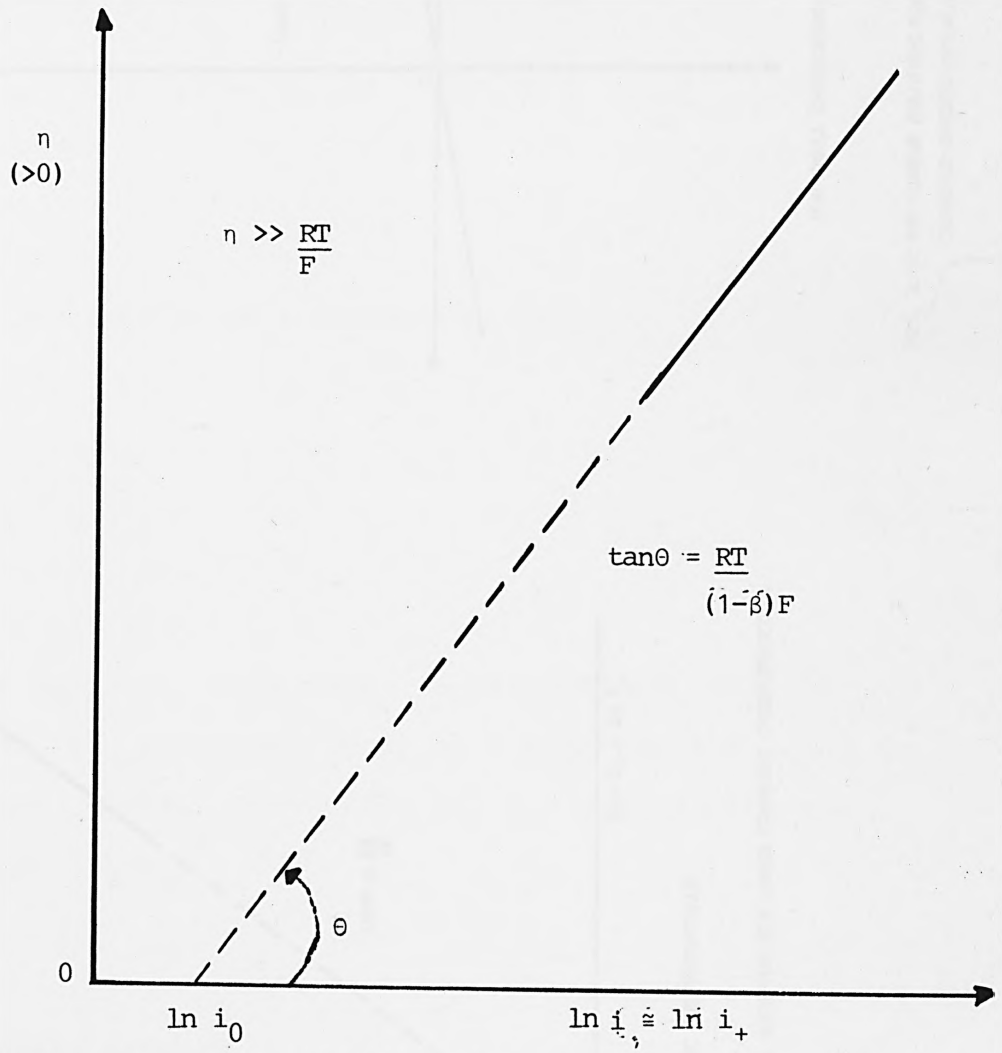

FOR LARGE ANODIC OVERPOTENTIALS

FIG. 2.10 THE TAFEL EQUATION FOR LARGE ANODIC OVERPOTENTIALS

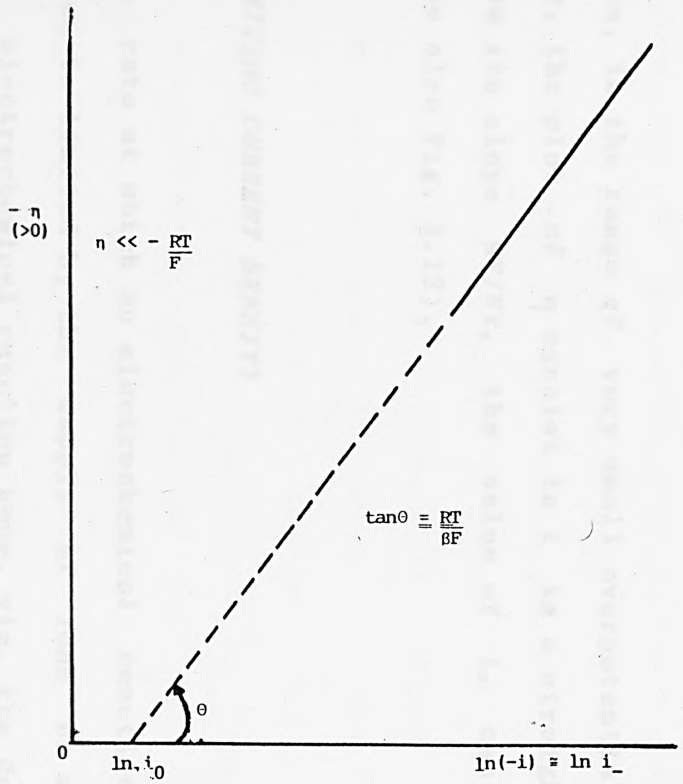

FOR LARGE CATHODIC OVERPOTENTIALS

FIG. 2.11 THE TAFEL EQUATION FOR LARGE CATHODIC OVERPOTENTIALS

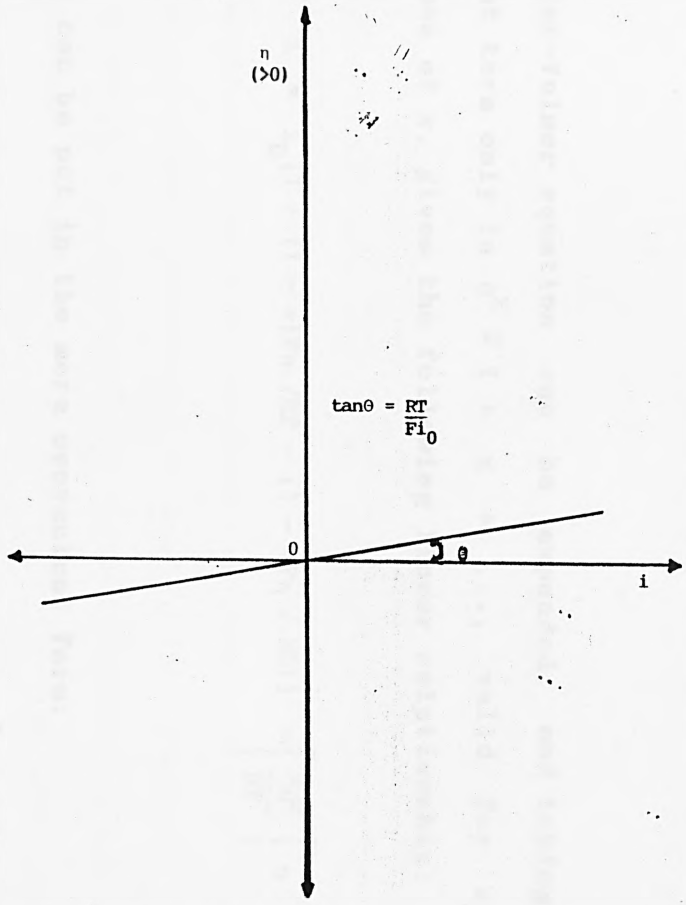

FOR SMALL OVERPOTENTIALS

FIG. 2.12 THE LINEAR RELATION FOR SMALL ANODIC OR CATHODIC OVERPOTENTIALS

Butler-Volmer equation can be expanded, and taking the first term only in $e^x \cong 1 + x + \ldots$, valid for small values of x, gives the following linear relationship:

$$i = i_0(1 + (1 - \alpha)F\eta /RT - (1 - \alpha F\eta / RT)) = \left[\frac{i_0 F}{RT} \right] \eta \qquad (2.44)$$

This can be put in the more convenient form:

$$\eta = \frac{RT}{F} i/i_0 \qquad (2.45)$$

Thus, in the range of very small overpotentials, < 10 mV, say, the plot of η agnaist ln i is a straight line, and from its slope RT/Fi, the value of i_o can be obtained (see also Fig. 2.12).

LIMITING CURRENT DENSITY

The rate at which an electrochemical reaction can take place is limited by the supply of ions or molecules to the electrochemical reaction zone, viz. the double layer, from the bulk of the solution. If diffusion, convection, stirring, etc, cannot supply the ions fast enough, then the current will be limited by one of these processes

which transport the ions to the surface.

Consider the case in which the charge-transfer limitations are small or negligible compared to the transport limitations. This would happen if the charge-transfer overpotential (the type dealt with in the Butler-Volmer equation) is negligible compared to the overpotential produced by concentration change at the interface. Thus, if transport of ions to and from the interface is easy, the concentration at the interface is virtually that obtaining in the bulk. But if transport is relatively poor, the ionic concentration at an interface between metal and solution will be less than that obtaining in the bulk. The transport of ions to the electrode would not have kept up with the demand of the electron flow. The overpotential caused by this concentration change is known as the concentration overpotential, η_c . The Butler-Volmer equation shows that when η tends to zero, i_o must tend to infinity for i to remain finite; the charge-transfer overpotential can be neglected by comparison with the concentration overpotential when the exchange-current density of the charge transfer reaction is sufficiently great.

Consider such a situation in which the charge-transfer overpotential can be neglected. The charge transfer reaction is assumed to be near equilibrium, and

therefore, the Nernst equation can be used to express the potential difference across the interface. Thus, when the current is zero:

$$E = E^{\circ} + \frac{RT}{F} \ln C_{bulk} \qquad (2.46)$$

because the concentration at the electrode surface is equal to the bulk concentration. When a current density i passes through the interface, $c_{electrode}$ (c_e) $\neq$ c_{bulk}, and:

$$V = E^{\circ} + \frac{RT}{F} \ln C_e \qquad (2.47)$$

Thus:

$$\eta_c = V - E = \frac{RT}{F} \ln (C_e / C_{bulk}) \qquad (2.48)$$

The rate (expressed as current density) of passage of material down a concentration gradient is given as [81]:

$$i = - DF\eta(dC / dx) \qquad (2.22)$$

The Nernst model (Fig.2.4) [82] can be used to express the concentration gradient, i.e using equation 2.23,

$$i = n\,DF\,\frac{C_{bulk} - C_e}{\delta} \qquad (2.49)$$

When c_e becomes zero, i has its greatest value, the limiting current density, i_L:

$$i_L = n\,DF\,(C_{bulk} / \delta) \qquad (2.50)$$

From equations (2.49) and (2.50) it follows that

$$C_e / C_{bulk} = 1 - (i / i_L) \qquad (2.51)$$

and thus:

$$\eta_c = \frac{RT}{F} \ln(i - i/i_L) \qquad (2.52)$$

or:

$$i = i_L(1 - \exp(F\eta_c / RT)) \qquad (2.53)$$

Equation (2.53) gives the relation between the current density and the concentration overpotential when the electrochemical reaction is restricted only by transport limitation (Fig. 2.13).

In an unstirred solution, the value of δ is the order of 5×10^{-4} m [83]. In a stirred solution it may be decreased with rapid stirring to $< 10^{-6}$ m, so i_L may be increased some 500 times by stirring.

2.4 BATTERY CHARACTERISTICS AND PERFORMANCE CRITERIA

A cell may be characterised in terms of:

(i) its available capacity,
(ii) its available energy, and
(iii) the power it can deliver.

It is not very useful to consider efficiency in the sense used to assess heat engines since batteries cannot be regarded as thermal converters. Rather, the efficiency of an electrochemical power source can be expressed in terms of capacity or of energy delivered.

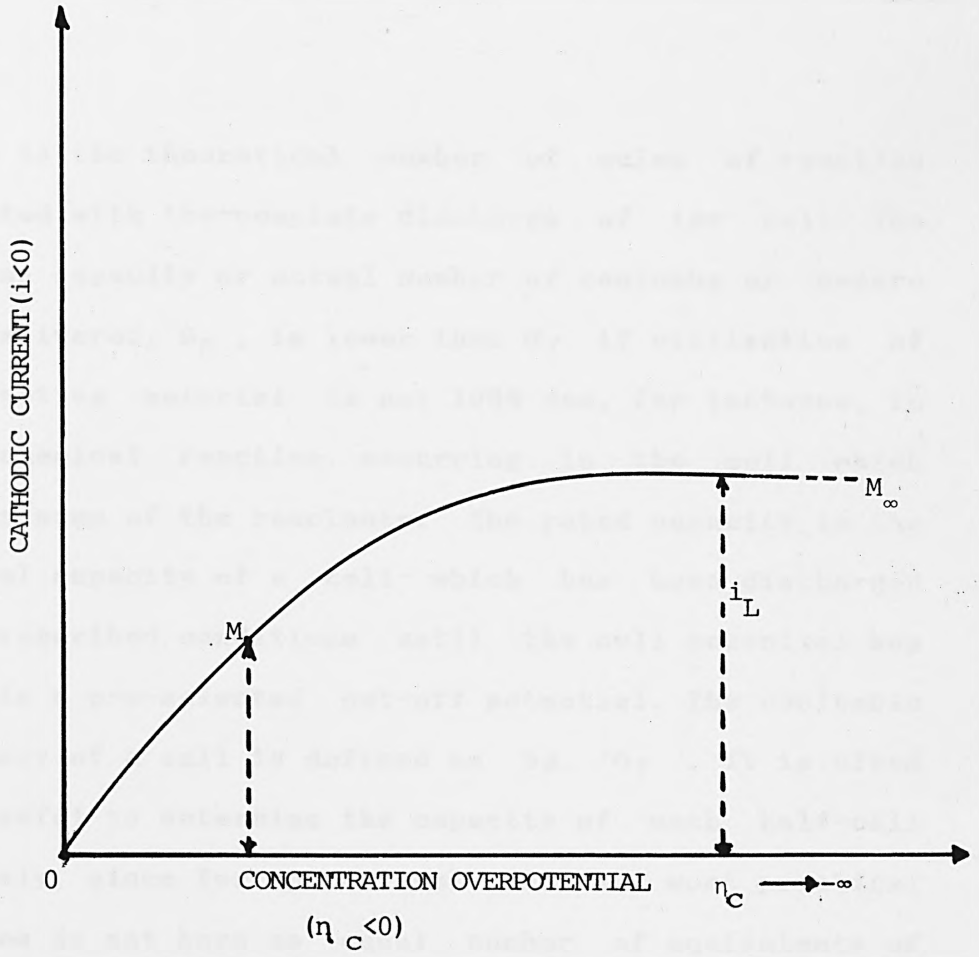

FIG. 2.13 THE RELATION BETWEEN CURRENT DENSITY AND CONCENTRATION OVERPOTENTIAL

2.4.1 CAPACITY

The theoretical capacity of a cell or half-cell may be calculated as

$$Q_T = x\ (nF) \qquad (2.54)$$

where x is the theoretical number of moles of reaction associated with the complete discharge of the cell. The practical capacity or actual number of coulombs or ampere hours delivered, Q_p , is lower than Q_T if utilisation of electroactive material is not 100% due, for instance, to some chemical reaction occurring in the cell which consumes some of the reactants. The rated capacity is the practical capacity of a cell which has been discharged under prescribed conditions until the cell potential has fallen to a pre-selected cut-off potential. The coulombic efficiency of a cell is defined as Q_p / Q_T . It is often more useful to determine the capacity of each half-cell separately, since for operational reasons, most practical batteries do not have an equal number of equivalents of anodic and cathodic reactants.

For purposes of comparison, it is convenient to calculate the specific capacity, defined as the capacity divided by the mass of the cell or half-cell, and usually

given in units of Ah/kg. In some cases a volume-basis specific capacity is preferred (e.g., Ah/dm^3).

2.4.2 ENERGY

The theoretical available energy for one mole of reaction (not for complete discharge) is given by

$$E_T = -\Delta G = nFE \tag{2.13}$$

where E is the cell EMF. The actual amount of energy delivered for one mole of reaction, or practical available energy is

$$E_P = \int_0^{nF} V.dq = \int_0^t V(i)dt \tag{2.55}$$

and is dependent on the manner in which the cell is discharged. The units of energy are either joules (i.e. watt seconds) or more commonly watt hours. (1 Wh = 3600 J). The total energy of a cell is sometimes termed the 'watt hour capacity'. As mentioned earlier the cell potential, V, deviates progressively from its (maximum) thermodynamic value as the rate of discharge increases. Hence the energetic efficiency is a variable quantity,

which must be associated with closely defined discharge conditions if it is to be meaningful.

Theoretical and practical energies can also be expressed in terms of the complete discharge of a particular cell:

$$E'_T = x(nFE) \qquad (2.70)$$

and

$$E'_P = \int_0^{xnF} V.dq \qquad (2.71)$$

where x is again the number of moles of reaction and q is the charge associated with a complete discharge.

The energy density (also known as specific energy) is the parameter used when assessing relative cell performance. Thus a small battery, weighing 25 g, and capable of delivering 10 Wh or 36 KJ at a particular discharge current, would be said to have an energy density of 400 Wh/Kg. Again it is sometimes more useful to consider a volume based specific energy (e.g. Wh/dm^3).

2.4.3 POWER

The level of discharge current drawn from a cell is detemined principally by the external load resistance.

The power delivered, P, is given by the product of the current flowing and the associated cell potential:

$$P = IV \tag{2.72}$$

The power rating of a battery specifies whether or not it is capable of substaining a large current drain without undue polarisation. As more and more current is drawn from a cell, the power initially rises; it reaches a maximum and then drops as the cell potential falls away due to polarisation effects. The maximum power point is best determined experimentally by measuring V as a function of I. In certain circumstances it it possible to calculate the maximum power point, e.g. if electrode polarisation is small and the internal resistance of the cell is known. The rated power of a battery is the power delivered (in watts) under stated discharge conditions.

The rated power density (or specific rated power) is again the most convenient parameter for comparing different battery systems, and is generally quoted in W/kg or W/dm^3. The rated power density and rated energy density are both critical factors when assessing batteries for applications such as motor traction where the battery itself has to be transported. A cell generally has a maximum permitted continuous power level; prolonged discharge above this value is liable to cause overheating and a consequent degradation of the cell. On the other hand, a cell may be capable of a much higher

rated instantaneous power. For short discharges the battery does not reach a thermal stationary state and its thermal capacity may be able to accommodate the heat generated if the thermal conductivities of its constituents are sufficiently high. Further mass transport polarisation effects are of less significance for short discharges. Certain batteries, such as those used for starting large diesel engines, depend specifically on their high instantaneous power capabilities.

2.4.4 POLARISATION AND DISCHARGE CURVES

More detailed information on the characteristic behaviour of cells under load and at various stages of discharge can be conveyed by graphs. Plots of cell potential against current are usually referred to as polarisation (or performance) curves; graphs of cell potential as a function of the fraction of discharge completed are known as discharge curves. A typical cell polarisation curve (Fig. 2.14) has three regions. Initially there is a rapid fall in cell potential at low current drain, due to ACTIVATION POLARISATION, usually associated to a large extent with one of the two electrode processes. Activation polarisation originates when reactions of high activation energy (electron transfer, adsorption, surface reaction (see section 2.3)) are slow and rate-controlling. It is affected by the chemical nature

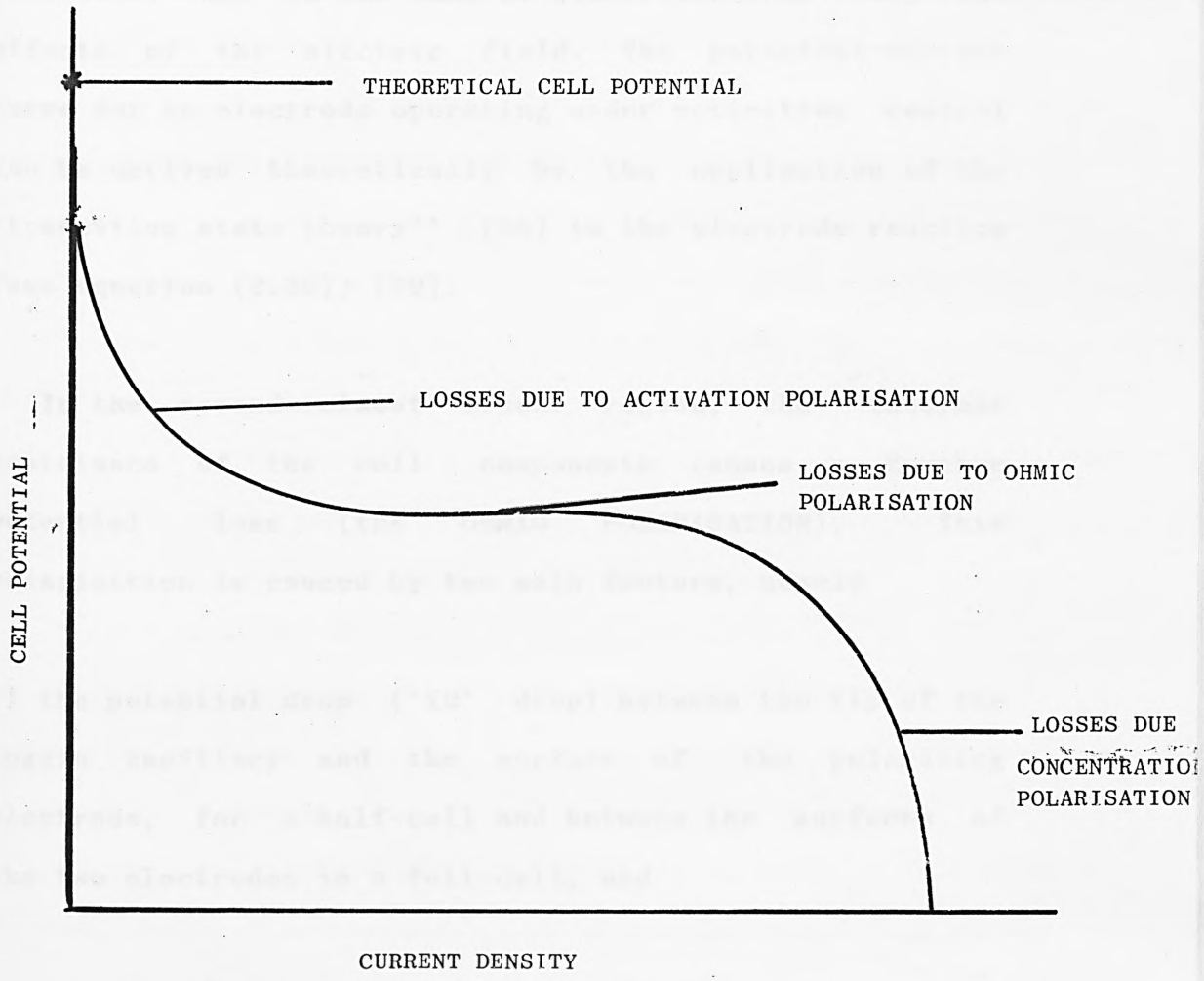

FIG. 2.14 POLARISATION CURVE FOR A TYPICAL CELL SHOWING THE DIFFERENT TYPES OF POLARISATION OVERPOTENTIALS

of the electrode surface. The magnitudes of the energies depend on the properties of the reactants, products and intermediates, as for most other physical and chemical reactions, and in the case of electrochemical step the effects of the electric field. The potential-current curve for an electrode operating under activation control can be derived theoretically by the application of the 'transition state theory'' [84] to the electrode reaction (see equation (2.39)) [79].

In the second almost linear region, the internal resistance of the cell components causes a further potential loss (the OHMIC POLARISATION). This polarisation is caused by two main factors, namely

i) the potential drop ('IR' drop) between the tip of the luggin capillary and the surface of the polarising electrode, for a half-cell and between the surfaces of the two electrodes in a full-cell, and

ii) the resistance caused by any products accompanying either the discharge or dissolution of electrode material.

The second factor may produce a very high polarisation value where the product forms an adherent and continuous surface layer as, for example, an oxide film possessing a very high electrical resistance. The same effect is obtained when gaseous products are occluded on the

electrode.

In the region at relatively high current drain, the ohmic polarisation is combined with further electrode polarisation, CONCENTRATION POLARISATION, caused by the concentration gradient which develops under irreversible conditions between the electrolyte immediately in contact with the electrode and the bulk of the electrolyte, thereby generating mass transfer problems (see section 2.3).

While such curves provide much useful information, they must be interpreted with some care. First, it is often necessary to examine polarisation curves at various stages of discharge since both electrode and electrolyte characteristics can alter considerably as discharge products build up. Second, polarisation curves are usually time dependent, so that the details of how they have been determined must be examined; e.g. has there been a relatively fast sweep of potential or current through the requisite values, or has a slow, pseudo-steady state approach been taken?

Discharge curves show either the open circuit potential of a cell or half-cell as a function of the fraction of discharge completed, or much more commonly, the cell potential during a deep discharge, usually under a fixed load or at constant current. The abscissa may be calibrated in terms of the quantity of electricity passed

(Ah) or as a percentage of the theorectical capacity or as a fuction of time. A useful method of characterising the discharge (or charge) rates used either in recording discharge curves or for determining practical capacities, is to standardise the current in terms of the nominal cell capacity. A C-rate of $\mathcal{T}$ implies that the nominal capacity of the cell (measured in Ah) is delivered in $1/\mathcal{T}$ hours: e.g. for a 2 Ah cell, discharge at C/5 signifies a current drain of 0.4 A.

2.4.5 SELF-DISCHARGE CHARACTERISTICS

Self-discharge of a battery amounts simply to the capacity loss under open circuit conditions and the rate at which this occurs is termed self-discharge rate. A contributing factor to the self-discharge of a battery is the instability of a battery electrode material in the electrolyte medium under shelf conditions. The self-discharge of a battery is therefore related to the shelf-life of the battery, in the majority of cases where all the battery active constituents are contained in the same unit and in contact.

3 PREPARATION, MEASUREMENT AND ANALYTICAL TECHNIQUES

This chapter describes the experimental techniques that had been employed, in the course of the research, for more than one topical investigation. Where a technique was exclusively used for only one topical investigation, the details of that technique are included in the chapter detailing the investigation.

3.1 HALF-CELL TESTING

Current density - Potential relationships are very important in electrode-performance testings, as indicated in the preceding chapter. To obtain such characteristics for each electrode (anode & cathode), a third supplementary electrode, the reference electrode, must be introduced. The reference electrode has a constant potential to which each working potential may be referred. If only one electrode (say, the anode) is of interest, the other (the cathode) can be dispensed with and replaced by a counter electrode together with an external power source so that the reaction of interest can be monitored under a wide range of conditions.

Although the system wil be 'driven' rather than 'self-driving', the behaviour of the test electrode, nevertheless, represents an exact picture of the contribution such an electrode would make to a full cell.

PROCEDURE

The TEST ELECTRODE (working electrode) was immersed in the test electrolyte along with the two electrodes, the nonpolarisable REFERENCE ELECTRODE and the COUNTER ELECTRODE (Fig. 3.1). The potential of the test electrode relative to that of the reference electrode was held at a preselected value by an electronic device known as the POTENTIOSTAT. This instrument - one of the benefits acquired by electrodics from electronics consists of a source of potential, an electronic voltmeter and a current source all organised in a particular way. The potentiostat measures the potential V of the test electrode and compares this with a preselected value V* from the potential source (in the potentiostat). If there is a difference $dV = dV^* - V$ between the measured potential and the chosen potential, the potentiostat tells its current source to send a current I between the reference electrode and the test electrode. The direction and magnitude of this current is electronically chosen to keep the potential of the electrode at the desired value, i.e., to make $dV = V^* - V = 0$. In effect, the potentiostat controls the

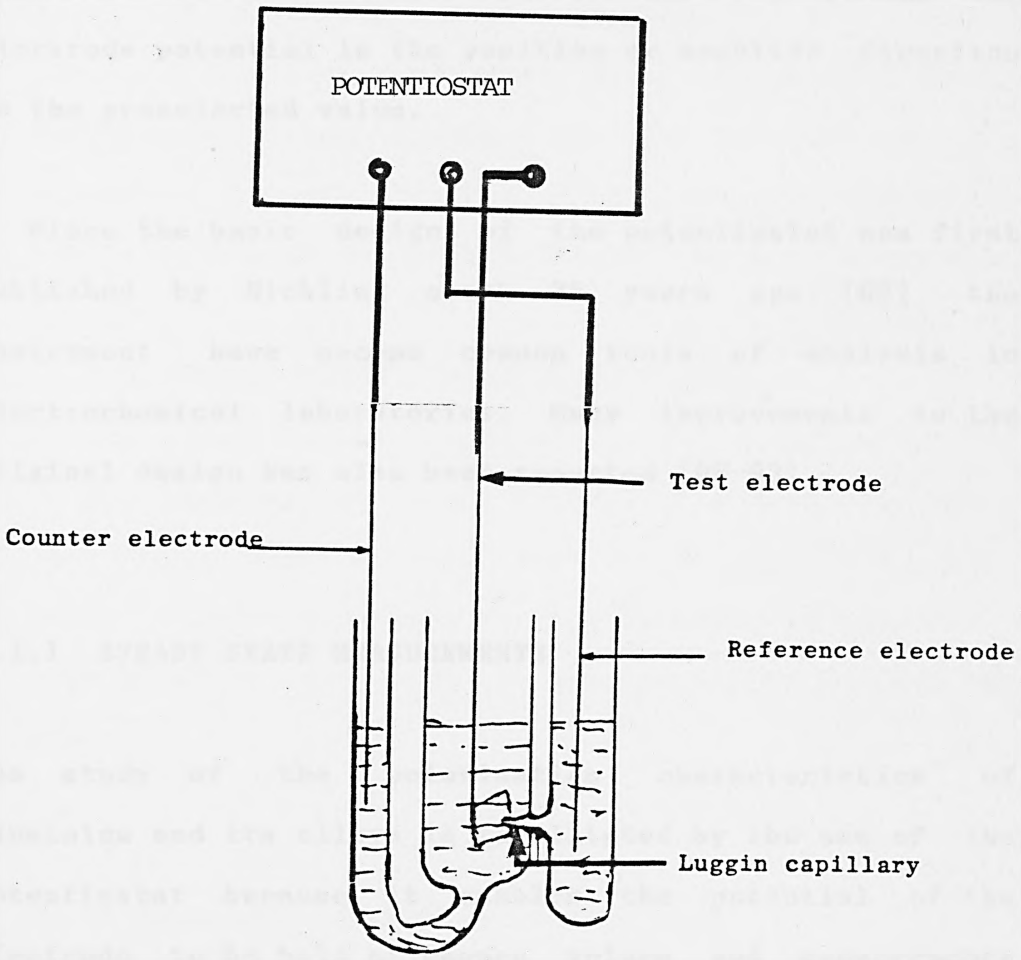

FIG. 3.1 HALF-CELL TESTING

rate of the charge-transfer reactions at the metal-solution interface and, by increasing the de-electronation or electronation current, pushes the electrode potential in the positive or negative direction to the preselected value.

Since the basic design of the potentiostat was first published by Hickling about 35 years ago [85] the instrument have become common tools of analysis in electrochemical laboratories. Many improvements to the original design has also been reported [86-93].

3.1.1 STEADY STATE MEASUREMENTS

The study of the polarisation characteristics of aluminium and its alloys is facilitated by the use of the potentiostat because it enables the potential of the electrode to be held at chosen values and measurements made, e.g. of the steady-state current density at each value of the potential, or vice-versa. Plots of Potential versus Current density are then made from the data recorded. Steady state polarisation characteristics may also be determined in two other ways:

i) GALVANOSTATIC POLARISATION [94]

The working electrode potential is measured against the reference electrode, whilst passing a constant

current between the working and counter electrodes (Fig. 3.2) for a lengthy period of time. Plots of Potential versus Time are then made from the data obtained. Galvanostatic measurements can also be made using the schematic circuit in Fig. 3.3. Constant current is supplied from an adjustable, stabilised D.C. power supply.

ii) POTENTIOSTATIC POLARISATION [95]

The working electrode potential is held constant and the steady state current flowing through the cell is noted. A potentiostatic circuit is shown in Fig. 3.4. The data obtained are used to make a plot of Current versus Time.

3.1.2 TRANSIENT STATE MEASUREMENTS [96]

It is often necessary to make measurements over times of the order of milliseconds, sometimes microseconds, and occasionally nanoseconds. One reason for this is that quick measurements means less chance of the reaction surface changing during measurement, which would otherwise lead to difficulties in interpretation. Also, in steady state current-potential measurements, mass transfer effects are nearly always present often in a form which makes correction and allowance for the effects difficult to perform quantitatively. Fast reactions, in particular, (large i_0) give pure concentration

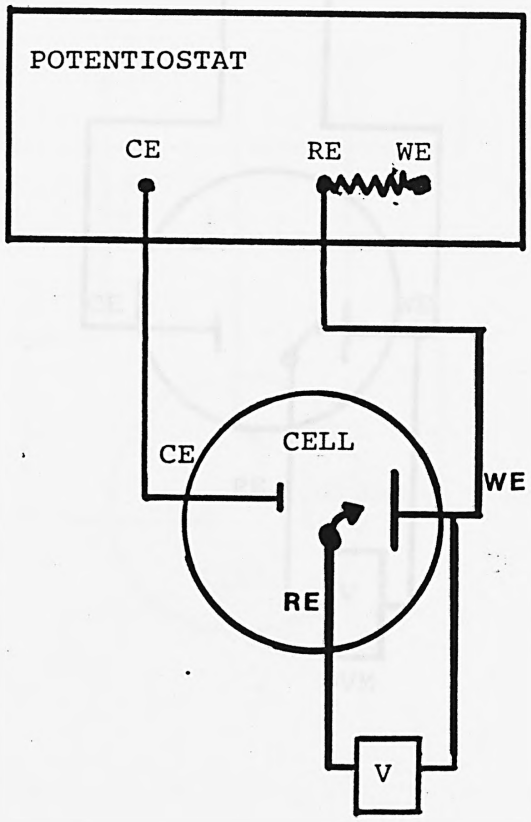

FIG. 3.2 SCHEMATIC CIRCUIT DIAGRAM FOR STEADY-STATE GALVANOSTATIC MEASUREMENTS USING A POTENTIOSTAT

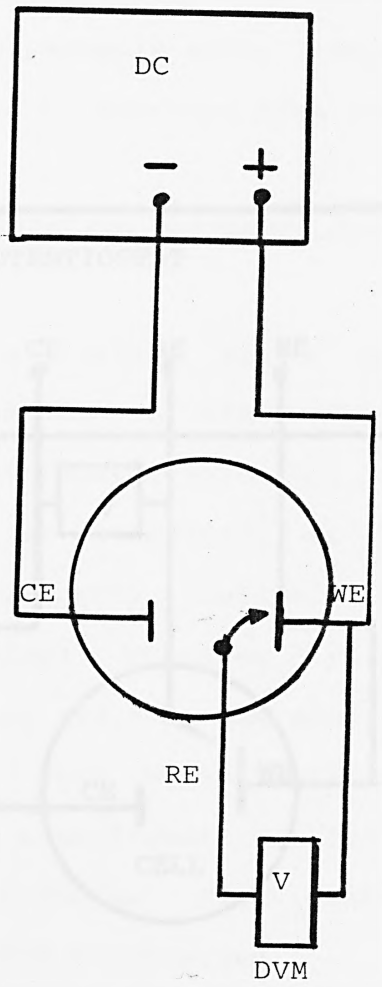

FIG. 3.3 SCHEMATIC CIRCUIT DIAGRAM FOR STEADY-STATE GALVANOSTATIC MEASUREMENTS USING A DC POWER SOURCE

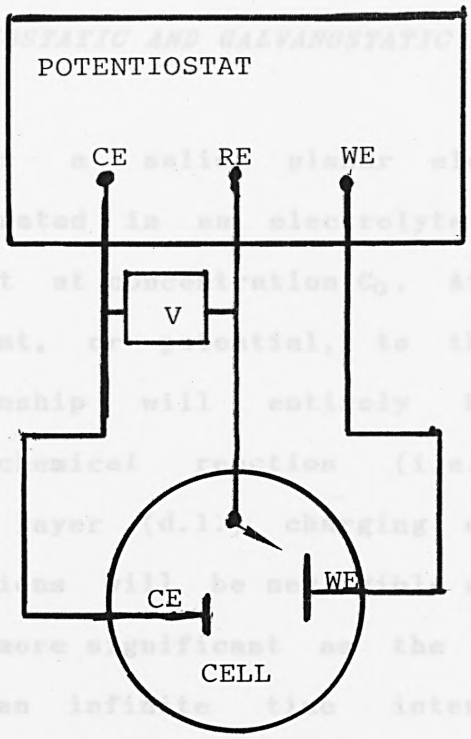

FIG. 3.4 SCHEMATIC CIRCUIT DIAGRAM FOR STEADY-STATE POTENTIOSTATIC MEASUREMENTS

polarisation curves, from which it is not possible to derive any valuable data. Thus, making it necessary to use a method to overcome mass transfer effects.

POTENTIOSTATIC AND GALVANOSTATIC POLARISATION [97]

Consider a solid, planar electrode, immersed and equilibrated in an electrolyte solution containing a reactant at concentration C_O. At the instant of applying a current, or potential, to this electrode the $i - \eta$ relationship will entirely be governed by the electrochemical reaction (i.e. neglecting ohmic and double layer (d.l.) charging effects). Mass transfer limitations will be negligible at this instant, but will become more significant as the reaction time increases. After an infinite time interval the steady state condition will be attained.

In principle the TRANSIENT behaviour of an electrode (either at constant i or V), under 'mass-transfer free' conditions at zero time, can be measured using an oscilloscope. However, it is not possible to make measurements at exactly zero time due to double layer charging effects; every electrode behaves as a leaky condenser and at the instant of applying a potential, or current, a very small, but finite, time is required to charge the electrode. This time interval depends on the CAPACITY of the electrode double layer and therefore the

electrode surface area and can be as long as several microseconds. At the instant of polarisation then, the electrode current is non-faradaic. For very fast electrochemical reactions, even this short time can result in some mass transfer effects and in such studies the electrode area is kept small to minimise the double layer effects.

Two procedures may be used to interpret electrode transients. One is to take measurements at the shortest time interval at which d.l. charging is complete and accept a certain amount of mass transfer polarisation. The double layer charging time can be measured from the electrode transient in the absence of reactant. Alternatively, measurements can be obtained from the mathematical relationship for the transient.

It is shown that, for a stationary electrode, at constant overpotential, whereby the reactant arrives solely by diffusion from the bulk electrolyte, which extends to infinity in a perpendicular direction to the electrode surface, i.e. Semi-infinite Linear Diffusion [98], the current transient is given by [99,100]:

$$i = i_0(\exp(-\alpha nFn/RT) - \exp((1-\alpha)nFn/RT) \times \exp(\lambda_t^2)\operatorname{erfc}(\lambda\sqrt{t}) \qquad (3.1)$$

The first two terms are identical to equation 2.39 for a reaction controlled solely by electron transfer and are independent of time (t). The last two terms correct this expression for mass transfer where

$$\lambda = \frac{i_o}{nF}\left[\frac{\exp(-\alpha nF\eta)}{C_O\sqrt{D_O}} + \frac{\exp(-(1-\alpha)nF\eta)}{C_O^o\sqrt{D_R}}\right] \qquad (3.2)$$

where i_0, n, F, α, η, are as defined in chapter 2; C_O^o and C_R^o are the bulk concentrations of reactants and products respectively. D_O and D_R are the diffusion coefficients of reactants and products respectively. At t = 0 the function exp(y). erfc(y) is unity and mass transfer effects are absent. As t increases the function continuously decreases [100] and mass transfer becomes more evident. Assuming diffusion is the sole method of transfer, at $t \longrightarrow \infty$, $i \longrightarrow 0$.

For short time intervals, when $(\lambda\sqrt{t}) << 1$, the term erfc $(\lambda\sqrt{t})$ can be expanded, i.e. a plot of i vs. $\sqrt{t}$ is linear. If this plot is extrapolated to $\sqrt{t} = 0$, then the i-intercept is the current density at zero time. Since the term $(\lambda\sqrt{t})$ also relies on the exchange current density equation (3.2) and i_0 is a measure of the reaction rate, then for very fast reactions the time interval at which $(\lambda\sqrt{t})$ is much less than unity may be

too short to make reliable measurements. A similar $\eta - \sqrt{t}$ relationship can be derived when a constant current pulse is applied and the overpotential transient is measured [97,101]. For fast electron transfer reactions, the GALVANOSTATIC DOUBLE PULSE is used. This is because during the initial moments following the application of the current step, for such reactions, the current is primarily nonfaradaic and contributes to charging the double layer. Gerischer and Krause [102] developed the double pulse method in which two constant currents are applied to the electrode. The first large pulse mainly serves to charge the double layer to a potential that corresponds to the value, at the instant of application of a smaller pulse.

The above relationships are derived under the simplest possible diffusion conditions, viz. semi-infinite linear diffusion at plane electrodes. With more complex geometries, the derivations become increasingly difficult [101] and may even become impossible, e.g. porous electrodes. Also, the equations do not apply when other forms of mass transfer are possible and measurements should be confined to short time intervals in order to minimise transport by convection, vibration, etc..

Apart from the application of potential or current pulses, methods are available in which an alternating component of overpotential (usually sinusoidal) is superimposed on a steady state condition. By postulating

an 'equivalent circuit' for the electrode reaction and measuring the impedance and phase shifts between i and η, kinetic data can be obtained for the process [103,104]. These methods are very useful techniques but the analysis of data becomes increasingly involved as the complexity of the reaction increases.

3.1.3 FABRICATION AND PRE-TREATMENT OF TEST ELECTRODE

Aluminium plates of negligible thickness, 0.4 mm, were used as the electrode material. For each test electrode a strip was cut off the plate in an 'L' shape (Fig. 3.5) such that when connected to the test instruments, the test area was directly centred towards the luggin capillary within the test cell. Apart from the test area, the part of the strip that was inevitably immersed in the test solution, was covered with a teflon tape to prevent contact between the electrolyte and the 'unaccountable' area of the metal. Care was taken to ensure that electrolyte was not trapped under the tape. The test area of the electrode was made up by the two sides of the exposed part of the strip, having a One by four centimetre perimeter, with a total surface area of two square centimetre.

The electrode was degreased, usually in acetone, and washed with a suface active detergent and then rinsed in distilled water, prior to test runs.

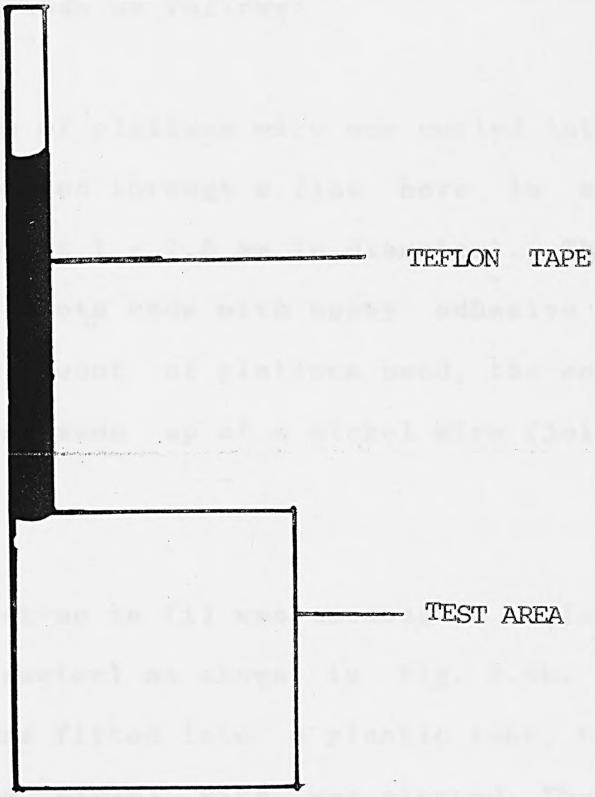

FIG. 3.5 TEST (WORKING) ELECTRODE

3.1.4 FABRICATION OF REFERENCE ELECTRODE

The $Hg/HgO.OH^-$ electrode system was used as the reference electrode in the half-cell testing. The electrode was made as follows:

i) A piece of platinum wire was curled into a hook at one end and passed through a fine bore in a tiny hollow glass tube (about 1 - 1.5 mm in diameter). The bore was then sealed at both ends with epoxy adhesive (Fig. 3.6a). To reduce the amount of platinum used, the encased end of the wire was made up of a nickel wire (joined to the platinum hook).

ii) The set-up in (i) was encased in a glass tube (of a suitable diameter) as shown in Fig. 3.6b. The open end of the tube was fitted into a plastic tube, through which the protruding nickel wire was pierced. The arrangement was ensured to be completely sealed at both ends.

iii) An opening was bored on the lower end of one facade of the outer tube (see Fig. 3.6b). Through the opening, globules of mercury was introduced into the outer tube. The amount of mercury was such that it covered completely the exposed platinum hook. 'Red' mercuric oxide was next introduced into the tube and spread evenly over the top of the mercury. Care was taken to ensure that there was no exposed platinum in contact

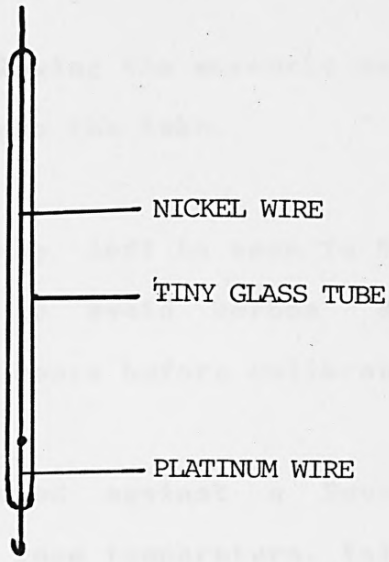

FIG.3.6a FIRST STAGE OF REFERENCE ELECTRODE FABRICATION

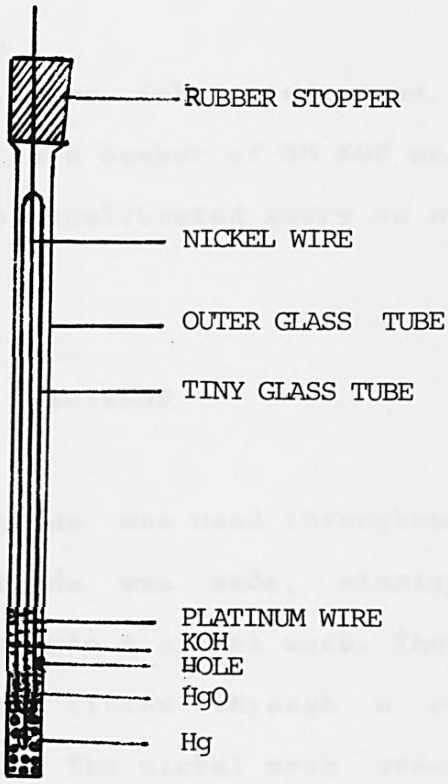

FIG. 3.6b REFERENCE ELECTRODE ($Hg/HgO.OH^-$)

with the mercuric oxide. Following the mercuric oxide, a 5M KOH solution was syringed into the tube.

iv) The whole arrangement was left to soak in 5M KOH, stored in a dessicator to avoid carbon dioxide contamination, for at least 24 hours before calibration.

v) The electrode was calibrated against a Reversible Hydrogen Electrode (RHE), at room temperature. Values of 927-930 mV should be obtained [105]. If the electrode gave a value outside this range, it should be discarded and a fresh one made.

The reference electrode, once fabricated, was used many times over, storing it in a beaker of 5M KOH under a dessicator. The electrode was recalibrated every so often.

3.1.5 FABRICATION OF COUNTER ELECTRODE

The nickel mesh counter electrode was used throughout the half-cell testings. The electrode was made, simply, by spot welding a nickel wire onto a nickel mesh. The free end of the nickel wire was fitted through a rubber stopper as shown in Fig. 3.7. The nickel mesh used was scrubbed thorougly with a detergent and degreased in acetone before welding the wire onto it.

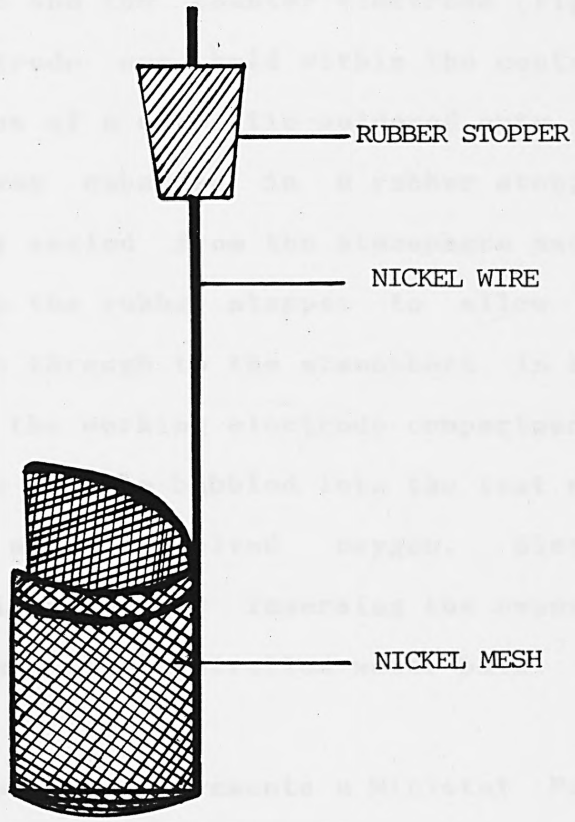

FIG. 3.7 COUNTER ELECTRODE

3.1.6 EXPERIMENTAL SET-UP

A three-compartmental glass cell was purposely designed and constructed, to contain the working electrode, the reference electrode and the counter electrode (Fig. 3.8). The working electrode was held within the central cell compartment by means of a clip, tin-soldered onto a tiny copper rod which was embedded in a rubber stopper. The cell was completely sealed from the atmosphere except for a tiny bore-hole in the rubber stopper to allow any gas evolved to escape through to the atmosphere. In Fig. 3.8 the inlet tube to the working electrode compartment is to enable nitrogen gas to be bubbled into the test solution to strip off any dissolved oxygen. Electrolyte temperature was maintained by immersing the experimental cell in a thermostatically controlled water bath.

For the steady state measurements a Ministat Precision potentiostat was used. The magnititude of current or potential applied to the test cell was read off using a Thandar TM 355 Digital multimeter. The potential or current response respectively, was measured in the same manner and for galvanostatic experiments, recorded onto a JJ CR 600 chart recorder.

For transient state measurements, a Chemical Electronics Type RB1 waveform generator and a DM 64 Telequipment oscilloscope were used in addition to the

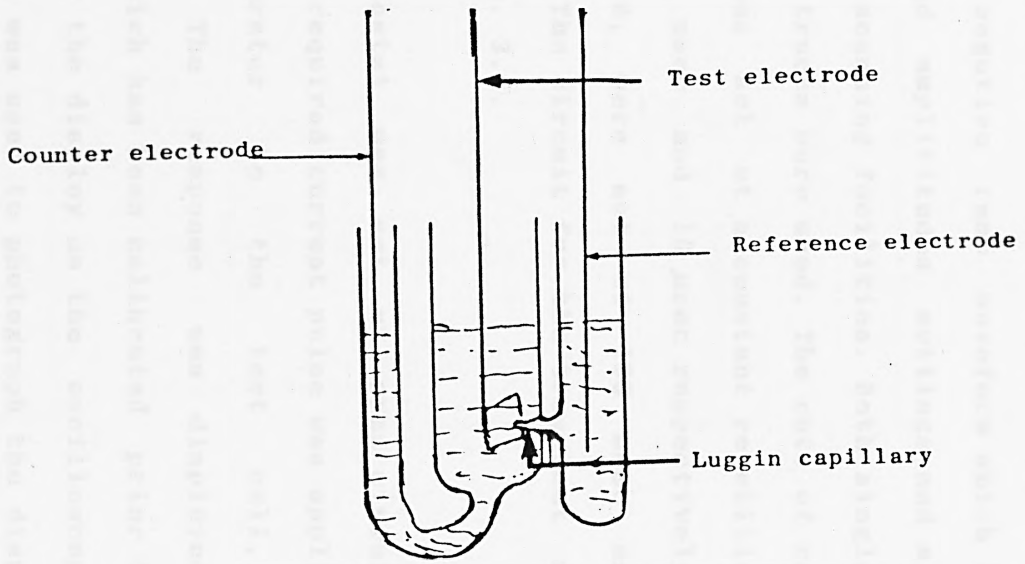

FIG. 3.8 A THREE COMPARTMENTAL TEST-CELL

instrumentations for steady state measurements. Pulsed currents were obtained using the waveform generator in conjunction with the potentiostat. The waveform generator has two main outputs, a double rectangular pulse and, a positive and negative ramp waveform which has variable sweep rates and amplititudes settings and allows single scan or cyclic scanning facilities. Both single pulse and double pulse traces were used. The rate of repetition of a pulse train was set at a constant repetition and delay periods of 30 msec and 10 μsec respectively. The pulse rates, A and B, were set at 100 msec and 30 msec respectively. The circuit for the transient measurements is shown in Fig. 3.9.

The potentiostat was set at open-circuit potential (OCV) and the required current pulse was applied from the waveform generator to the test cell, via the potentiostat. The response was displayed on the oscilloscope which has been calibrated prior to the test. To read clearly the display on the oscilloscope screen, a polaroid camera was used to photograph the display.

3.1.7 THE DETERMINATION OF INTERNAL RESISTANCE (IR DROP)

Ohmic polarisation appears as a component in a half-cell polarisation curve, mainly due to the working-to-reference electrolyte gap. The magnitude of

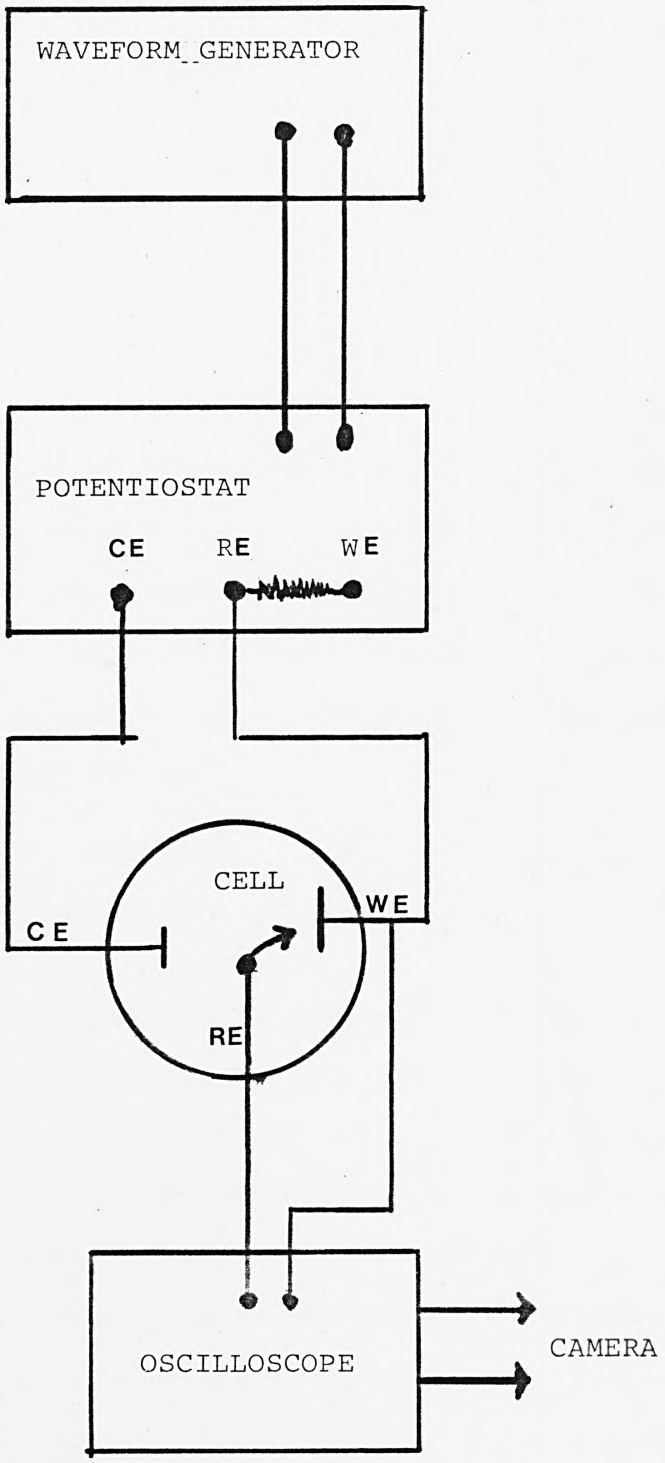

FIG. 3.9 SCHEMATIC CIRCUIT DIAGRAM FOR TRANSIENT STATE GALVANOSTATIC MEASUREMENTS

this 'IR' also depends on electrolyte concentration and temperature. The IR drop can be measured using the interruptor method.

In this method, a steady D.C. polarising current is interrupted at high frequency (50 Hz is convenient) by means of a fast-acting mercury-wetted relay, producing a train of square-waves through the cell. Ohmic polarisation is instantaneous, and can be measured instantly on an oscilloscope; the magnitude of the IR drop can be assessed, using Ohm's Law, for any selected current through the cell

PROCEDURE

The test and reference electrodes, during a half-cell testing, were connected to the oscilloscope. A separate power source was used to provide the steady current needed for the IR measurements. During the measurements, the potentiostat was put to standby and the test electrode was connected to the positive terminal of the power source. The negative terminal was linked to the mercury interruptor which was in turn linked to the counter electrode in the test-cell. A current was passed through the cell and the resulting potential was read from the square waves formed on the oscilloscope.

Ohm's law was used to calculate the potential drop for

the current being used to polarise the test electrode at the time of taking the IR measurements. The resulting potential was substracted from the main potential reading for the test electrode, at the time, to give the polarisation potential of the electrode at the particular current density.

3.1.8 DATA ANALYSIS

The data obtained from the half-cell testings were used to plot respective polarisation and discharge curves to assist in the interpretation of the test electrode polarisation phenomena.

The Visicalc electronic worksheet was used in conjuction with an HI-80 plotter [106] on an Apple computer to produce the necessary graphs. An example of the commands sent via the Visicalc program to the HI-80 plotter for a typical polarisation curve is shown in the Appendix; A1.

3.2 HYDROGEN EVOLUTION MEASUREMENTS

The hydrogen evolved at the electrode was collected over water in a graduated glass tube. The volume of water pushed out of the tube was taken as the volume of gas evolved.

For the purpose, the special apparatus shown in Fig. 3.10 was constructed and used. The apparatus was made up of a burette, filled with water, inverted in a large glass tube filled with a thermostatic water. A rubber tubing was fitted to the tip of the burette and connected to the test cell. The pressure in the whole system was equated to one atmosphere by means of a hook-shaped adjoint fitted to the bottom of the large glass tube.

PROCEDURE

The rubber tubing at the tip of the burette was connected to the test cell (Fig. 3.10). The test cell was filled with the electrolyte and the test electrode and counter electrode (in the case where current is applied) were immersed into the electrolyte. Care was taken to ensure that the cell was completely sealed and airtight.

The gas evolved was collected by means of the apparatus described above. The nature of the gas evolved was established, by means of gas chromatography, to be predominantly hydrogen gas.

The amount of gas collected at the operating cell temperature was obtained by taking the temperature of the collecting vessel and using the gas equation to correct for volume of gas at the operating temperature. That is,

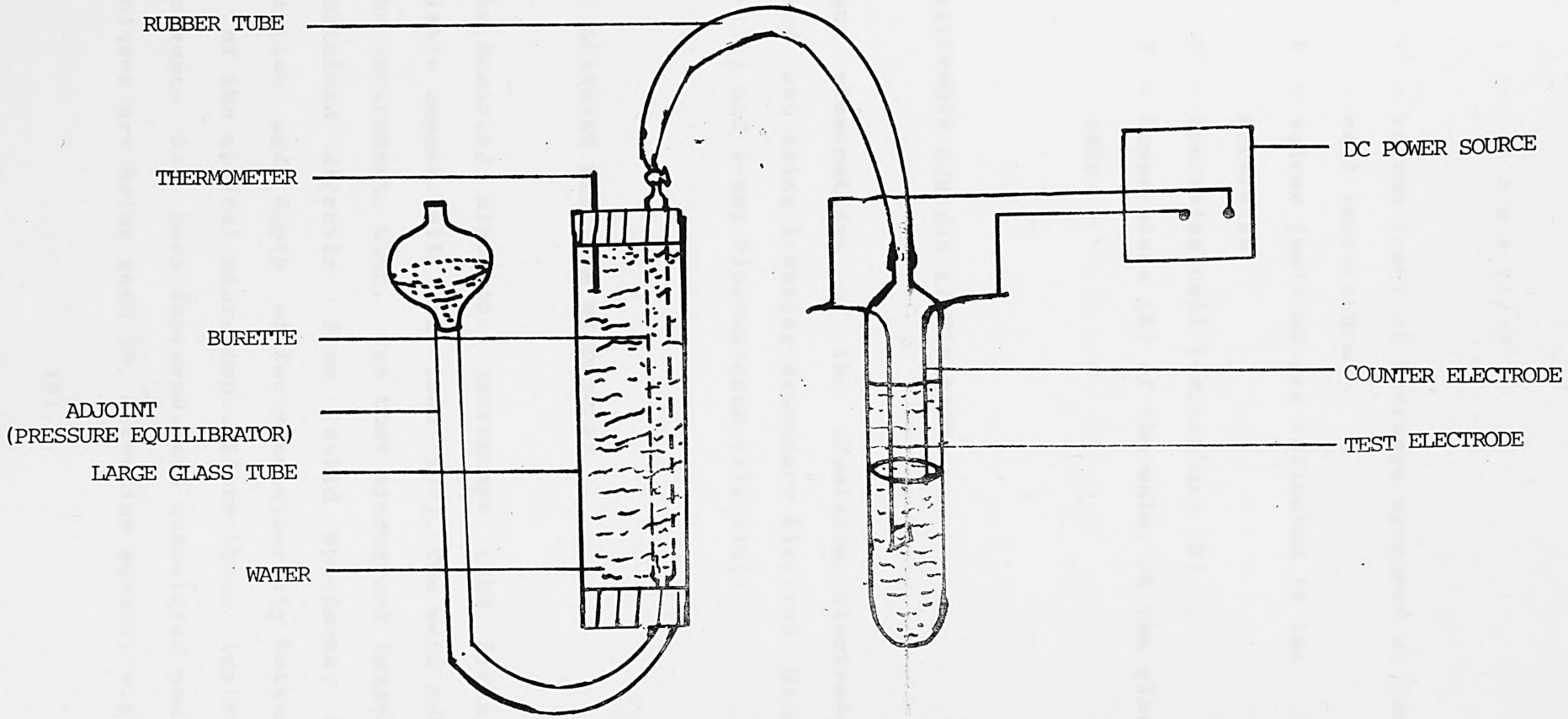

FIG. 3.10 HYDROGEN EVOLUTION MEASUREMENTS

$$V' = V * T'/ T \quad (3.3)$$

where V' = volume (cm^3) of hydrogen measured at the cell temperature

V = volume (cm^3) of gas collected in the apparatus

T' = operating cell temperature (K)

and T = temperature (K) of the water in the glass tube.

3.3 ELECTRODE SURFACE EXAMINATION

Surface examinations of the aluminium electrodes were carried out using Scanning Secondary Electron Microscopy [107-111] and X-Ray Flourescence [112-114].

3.3.1 SCANNING ELECTRON MICROSCOPY

The Scanning Electron Microscope (SEM) first became available commercially in 1965 [107]. The main advantage of the instrument, then, was that micrograph images could be obtained directly from solid specimens, with a resolution and depth of focus considerably better than that of the optical microscope. Since then, instrumental performance has been improved, and associated analytical techniques are being used in a routine manner, e.g. X-ray

methods to determine chemical elements and electron channelling patterns to determine crystallography. The instrument is being operated increasingly in the transmission mode to examine thin foil specimens. More effort is being made to use the SEM for obtaining quantitative results, and the range of its applications has widened. Consequently, although the SEM was initially seen as complementary to other types of electron-optical instrument, it is now competing with them.

The principle of the SEM in its most common form is illustrated schematically in Fig. 3.11. Electrons from a heated filament F are accelerated by a high voltage, usually in the range 5 - 50 kV, and then passed down the centre of an electron optical column. The electrons are formed into a probe by three magnetic lenses L_1, L_2, and L_3, and focused onto the surface of a solid specimen S. The probe is made to scan the specimen in the form of a square raster, in the same way as the spot scans a commerical television screen. The scanning is achieved by passing a current from a sawtooth generator G through the scan coils, which are generally located between lenses L_2 and L_3. The same sawtooth current also passes through the corresponding coils of a cathode-ray tube CRT so as to produce an identical but larger raster on the viewing screen. The probe, incident on the specimen surface, causes electrons to leave the surface. The electrons strike a collector C, and the resulting electron current signal, amplified by an amplifier, is used to control the

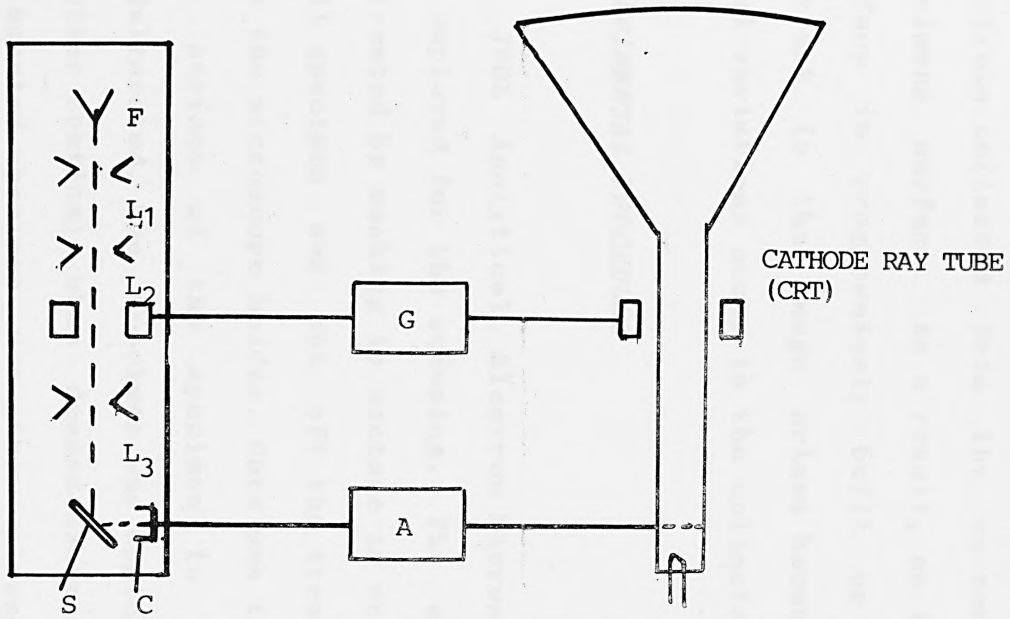

FIG. 3.11 SCHEMATIC DIAGRAM OF A SCANNING ELECTRON MICROSCOPE

intensity of the CRT. There is an exact point-to-point correspondence between the raster on the specimen surface and the raster on the CRT screen; the intensity of each point on the latter is a direct measure of the number of electrons collected from the corresponding point of the specimens surface. As a result, an image of the specimen surface is progressively built up on the CRT screen. Contrast in the image arises because, during scanning, local variations occur in the collected signal.

EXPERIMENTAL PROCEDURE

The JEOL Analytical Electron Microscope model JEM 100B was employed for the scanning. The aluminium sample was pretreated by washing in acetone in an ultrasonic bath. A small specimen was cut off the treated sample and fixed onto the microscope holder. Care was taken to ensure that the surface of the specimen to be examined was unadulterated. The specimen was coated with 10 nm of gold (sputter coating) when deemed necessary. The holder with the mounted specimen was then placed in the scanning instrument, ready for scanning.

A scanning mode at 40 keV Beam was used for all the samples. At the first instance, the specimens were roughly examined at long depth of field (LDF) and then after the gain settings have been correctly adjusted, the high resolution marking was used as the depth of focus

for the specimen.

Micrographs were obtained from the the scans. And to help understand, comprehensively, the surface morphorlogy, the surface composition of the specimens were analysed using the X-ray flourescence facility associated with the electron microscope.

3.3.2 X-RAY FLOURESCENCE

X-ray spectrometry [112-114] as an analytical method involves photons derived from those electronic transitions which are more energetic than those observed in the far ultraviolet spectrum. This sets a lower limit of about 30 eV to the energy range; the upper limit is set by the binding energy of the K electrons in plutonium, about 120 keV.

The first consideration in spectrometric methods is the accurate measurement of wavelength and intensity. X-ray spectrometers can be built to measure these quantities with the necessary resolution, accuracy, and sensitivity. The wavelengths (or energies) immediately identify the elements in the sample, but the intensity data can be reduced to accurate weight fractions or concentrations only if allowance can be made for variations from one sample to another in the absorption of X-rays, or if these variations can be nullified in the

sample preparation. A proper appreciation of the details of instrumentation and applications depends upon an understanding of the basic principles of X-ray spectrometry and of X-ray fluorescence in particular.

The use of electrons to generate X-ray lines directly from a sample acting as the target is known as X-ray emission spectrometry; a familiar example is electron microprobe analysis. In the sealed X-ray tube used for spectrometry powerful beams (up to 50 mA), accelerated by voltages of up to 100 keV, strike water-cooled targets to give an X-ray output consisting of the characteristic lines of the target (20-60 per cent of the total) superimposed on a continuum. The continuum begins at an energy corresponding to the accelerating voltage, has a maximum at two-thirds of this energy, and tails off at low energies. The tubes can be used as X-ray sources in the generation of secondary fluorescence, as in X-ray fluorescence spectrometry.

The main features of X-ray spectrometry can be either advantages or disadvantages according to the circumstances and no balance sheet will therefore be attempted. The main points to be considered are that

i) Information is given on the elemental composition only, except in the case of the low atomic number (Z) elements.

ii) Detection limits of better than 20 ppm. can be

achieved from Mg (Z = 12) to Bi (Z = 83).

iii) The smallest amount of material that can be measured is in the range 10^{-8} - 10^{-6} g.

iv) The sampling depth is small 2 - 100 μm.

v) Thin films, filters, and liquids are measured most easily; metals can be measured rapidly if standards are available; rocks and insoluble powders cause more difficulty.

EXPERIMENTAL PROCEDURE

The EDAX 9100/60 system (manufactured by Philips) was used for the X-ray flourescence work. The specimen was prepared as for the scanning work described above. After scanning, the specimen holder was tilted to allow the X-rays emitted from the surface of the specimen to be collected in the EDAX system and analysed. The EDAX 'SQ' program was used for analysis.

3.4 CHEMICAL ANALYSIS OF TEST MATERIAL

Apart from sodium, potassium, which were determined by flame photometry [115,116], and low concentrations of lead, which was determined by polarography [117,118], all other elements were determined either by atomic absorption spectrophotometry [119-121] or by 'wet' chemical analysis [122-124].

PROCEDURE

A) ATOMIC ABSORPTION

For the analyses by atomic absorption spectrophotometry, the samples were dissolved in concentrated acid solution and diluted by a suitable factor, so as to obtain absorbances within the linear range given by the standard concentrations.

Prior to carrying out the analyses, the spectrophotometer (Fig. 3.12) was switched on and left for a few minutes to allow the hollow cathode lamp to warm up. The few minutes was adequate since it was a double beam instrument that was used. An air-acetylene flame was used with a pre-mix burner. The fuel and support gas pressures were adjusted until a slight yellow colour was added to the flame. The fuel pressure was turned up to impart a strong yellow glow.

A standard sample solution was then aspirated and its absorbance reading was noted at the required wavelength for the element being determined. The gain correction for the wavelength was adjusted to obtain a maximum absorbance. The monochromator was at this point exactly on the required line. With the burner height adjusting knob, the burner was raised so that the light beam just passed over the tip of it (base of the flame). De-ionised

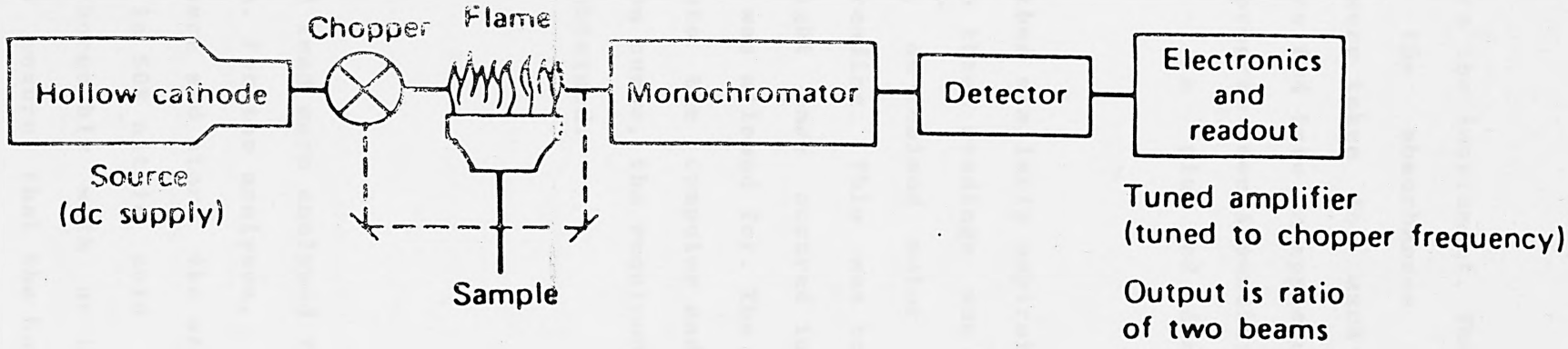

FIG. 3.12 Schematic diagram of an atomic absorption instrument

water was used to zero the instrument. The standards were next aspirated and the absorbances recorded. Three absorbance readings were taken for each standard and the averages obtained were fed into an apple computer using a specially written program (see Appendix; A2) to obtain a calibration curve - a plot of Absorbance against Concentration.

Each sample was then similarly aspirated three times. The average of the three readings was then recorded. After each reading, de-ionised water was aspirated to give a zero base-reading. This was to ensure that any fluctuation that might have occured in the instrument during each reading was allowed for. The average readings obtained were fed into the computer and, in combination with the calibration curve, the required concentrations of the samples were obtained.

B) POLAROGRAPHY

Low concentrations of lead were analysed for using a PAR model 264 polarograph. For the analyses, all bottles and flasks needed to prepare and store the standards (conc. < 1 ppm) were soaked in 50% nitric acid overnight. they were then washed thoroughly with de-ionised/distilled water. This was to ensure that the bottles and flasks were free of even traces of lead and other contaminants.

25 ml of 20 ppm Pb solution was put into a 500 ml graduated flask and made up to the mark with 0.1 M sodium nitrate solution (background solution) to prepare a 1 ppm Pb solution. Out of the 1 ppm stock solution, 250 ppb, 500 ppb and 750 ppb standard solutions were prepared.

The standards were immediately run on the polarograph (traces of Pb ions tend to cleave to the walls of the container. Thus if left standing for a considerable length time, there will be reduction in Pb concentration which may be significant at such low concentrations). Three runs were made for each sample. For each run the solutions were purged by bubbling nitrogen gas through to remove all dissolved oxygen present. The samples were purged for 4 minutes for the first runs and 2 minutes each for the next two runs. After the differential pulse polarograms (Fig. 3.13) were obtained for 250 ppb, 500 pp, 750 ppb and 1000 ppb (1 ppm) lead standards, the peak height of each polarogram was noted and the average for each run was fed into the computer, using the same program as for the atomic absorption, along with the concentration for the run to produce a plot of Peak height against Concentration. The test samples were then analysed in the same way as described for the standards and the peak heights fed into the computer to obtain the corresponding concentration from the calibration plot produced earlier.

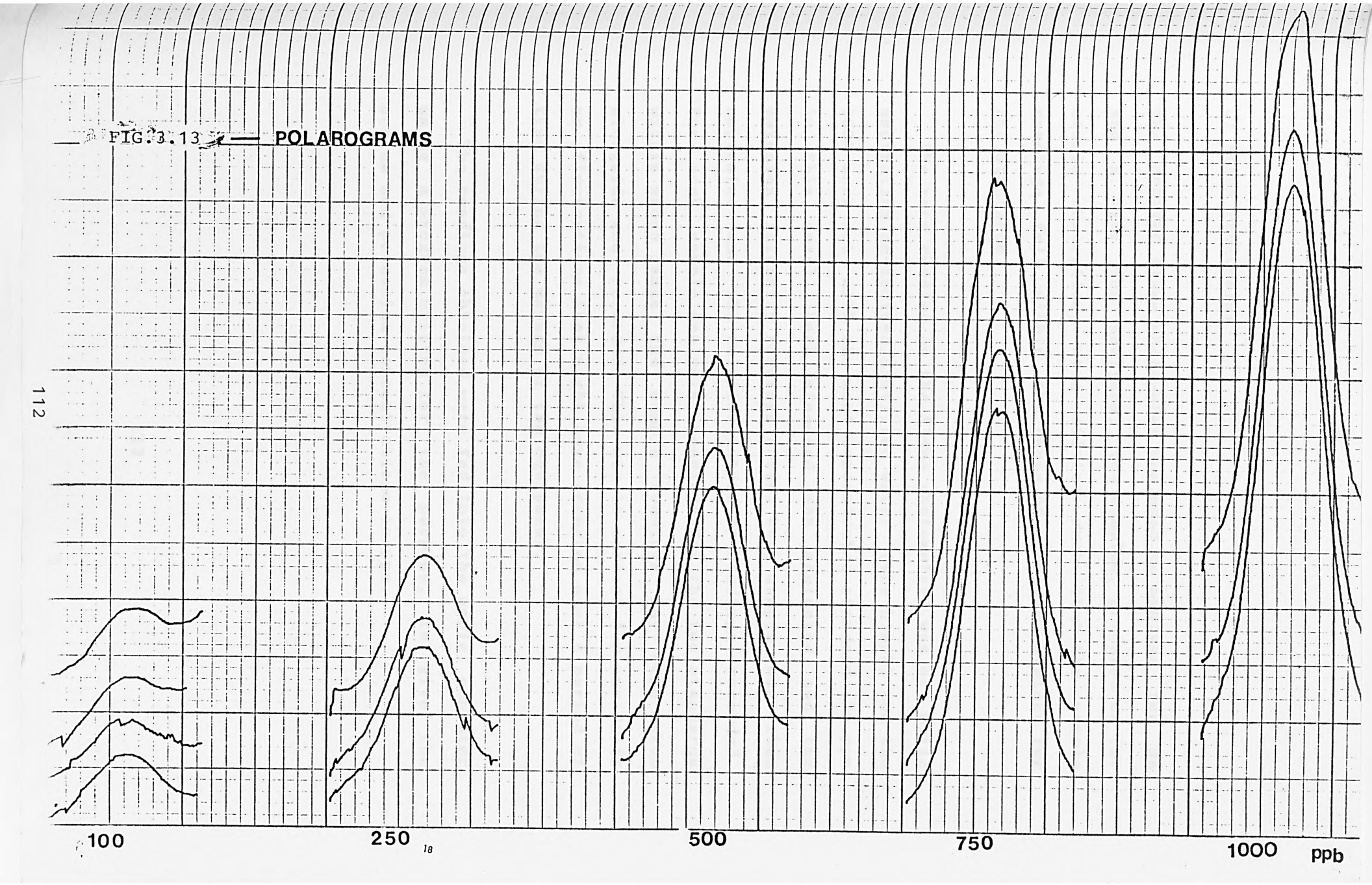

FIG. 3.13 — POLAROGRAMS

C) FLAME PHOTOMETRY

The CORNING flame photometer was used to analyse for Na and K. For the analyses, the samples, prepared as for atomic absorption, were diluted such that the sample readings fell within the range of readings obtained for the standards.

The zero reading on the flame photometer was set while aspirating de-ionised/distilled water (the blank) and the 100% mark set with the most concentrated standard (25 ppm in this case). Each standard was aspirated and the emission intensity readings noted. Each sample was then aspirated and the emission intensity readings recorded. For each sample analysis, readings for the two standards within whose range the sample readings lay were taken alongside and recorded. This was to correct for any drift or fluctuations that might have occurred over a period of time during the usuage of the equipment.

The readings obtained were fed into the apple computer using a program written for the purpose, to give the sodium and potassium concentrations in ppm.

4. THE USE OF ALUMINIUM AS BATTERY ANODE MATERIAL

4.1 INTRODUCTION

The use of aluminium as anode material in primary batteries depends largely on adequate corrosion control. The large amount of research carried out on the subject of aluminium corrosion has, however, been on reactions central to such phenomena as pitting, stress cracking, localised corrosion, and so on [125-132]. Very much less has been done on the controlled corrosion of high purity aluminium. Of the few investigations that have been carried out [9,15-17,26,40,46,133-137], most indicated that pure aluminium is a poor anode for use in a power source; inspite of the highly attractive anode characteristics. The reasons given by these workers were that:

i) the protective oxide film on the surface of the metal prevents the high theoretical reversible potentials of aluminium to be achieved [133]. The passivating, resistive oxide layers being reinforced when aluminium is dissolved in electrolytes in which aluminium oxides are not readily soluble [9,16,17,26,40,46,134-136].

ii) high rates of corrosion are found in those electrolytes in which the oxide layers are dissolved [15,137].

Thus, to successfully use aluminium as a galvanic anode,

i) the protective layer on the surface of the metal must be destabilised without increasing the rate of corrosion.

ii) And also, a suitable electrolyte in which the aluminium oxides are readily soluble must be used.

This chapter is devoted to the optimisation of the anodic performance of aluminium through the destabilisation of the protective oxide layer on the surface of the metal. The optimisation of the anodic performance of the metal through the use of a suitable electrolyte will be discussed in a subsequent chapter.

OPTIMISATION OF ALUMINIUM AS BATTERY ANODE MATERIAL

Since the poor performance of aluminium as battery anode material is attributed, to a large extent, to the oxide layer on the surface of the pure metal, one way of reducing the passivity is by breaking down the resistivity of this oxide layer. This can be done by

alloying the metal with other suitable metals [31,34,37,38,41-43,138]. A good way of finding the metals suitable for alloying with aluminium is by considering the place occupied by aluminium in the Periodic Table relative to the useful additions, tramp elements and impurities found in commercial alloys. Typical elements are shown in Table 4.1

The vast majority of commercial aluminium alloys contain additions taken from the sodium period (e.g. Al-Mg, Al-Si, Al-SiMg), the copper sub-period (e.g. Al-Cu) or both (e.g. Al-CuMg, Al-CuMgSi) [139]. This technological fact stems from the crystallographic properties of aluminium [139-141].

An important criterion for selecting a suitable element for alloying is that the element must be soluble in the solid solution of aluminium, at equilibrium.

Aluminium crystallizes with a face-centred cubic lattice structure (f.c.c.) and undergoes no allotropic transformations. Consequently, the phase equilibrium diagrams are quite simple, in that there are no equilibrium curves starting from a transformation point. The lattice constant of a face-centred cubic aluminium (a_o) is 4.014 Å at 25 °C. Thus the smallest distance between two adjacent aluminium atoms will be 2.8577 A at 25°C ($d = a_o / \sqrt{2}$). This value is important in the systematic study of aluminium alloys, since the size factor (SF),

Table 4.1 Typical alloying elements (p.117) has been removed for copyright reasons

defined as the ratio of atomic diameters of the solute (d_{Mg} for instance) and the solvent (d_{Al}) is a criterion that gorverns the behaviour of the dissolved element in the alloys (142). If a size factor lies between 0.85 and 1.15 (range +/- 15%), this size factor favours solubility of the element concerned in solid aluminium, if equilibrium is reached.

$$\text{SF of Al-Mg} = (d_{Mg} / d_{Al}) = (3.1906 / 2.8577) = 1.12$$

and (4.1)

$$\text{SF of Al-Si} = (d_{Si} / d_{Al}) = (2.3458 / 2.8577) = 0.823$$

Table 4.2 gives the atomic diameters of the various elements found in aluminium alloys.

Other conditions must also be satisfied. That is, neither the crystallographic structures nor the valencies of the two elements, Al and the alloying element, must differ excessively. Magnesium, for example, has a hexagonal structure and silicon a diamond-type structure, while the valency differences (w.r.t. Al) are -1 and +1 respectively. The co-ordination number, i.e. the number of equidistant atoms surrounding a given aluminium atom is equal to 12 for the f.c.c. aluminium lattice [139]. This number is useful in interpreting plastic deformation behaviour. The theoretical co-ordination number for

TABLE 4.2 ATOMIC DIAMETER OF TYPICAL ALLOYING ELEMENTS

ELEMENT	ATOMIC DIAMETER (A)
Be	2.221
B	1.760
C	1.540
N	1.400
O	1.320
F	1.280
Na	3.708
Mg	3.191
Al	2.857
Si	2.345
P	2.200
Ti	2.910
Cr	2.490
Mn	2.240
Fe	2.520
Co	2.507
Ni	2.490
Cu	2.551
Zn	2.659
Zr	3.120
Sn	3.010
Pb	3.490
U	3.000

magnesium is 12 and that for silicon is 4, since the diamond-type structure of silicon involves four homopolar bonds. A 'covalent diamond-type' lattice is less easily dissolved than a hexagonal lattice [139]. In a perfect f.c.c. crystal of aluminium, there are interstices between the atoms. These can accommodate atoms of very small diameter, forming interstitial solid solutions [143,144].

If a dissolved atom is placed between two aluminium atoms at a distance a = 4.04 Å apart, i.e. half-way along the unit cell edge, it can be calculated that its diameter would have to be

$$(\sqrt{2} - 1).d = 0.41 * 2.857 \text{ Å} = 1.17 \text{ Å} \qquad (4.2)$$

if it just touched both the aluminium atoms. Each interstitial atom would have six nearest neighbours (Al) at a distance of 2.02 Å. On the other hand, if the interstitial atom is placed at the centre of a sub-cell representing 1/8 of the unit cell, there will be four nearest neighbours (Al) at a distance of [146]

$$(\sqrt{3/4}).a = 0.433 * 4.04 \text{ Å} = 1.75 \text{ Å} \qquad (4.3)$$

Atoms of small diameter such as carbon (d_C = 1.54 Å) can thus occupy interstitial positions by distorting the lattice. The same is true of nitrogen, boron and

hydrogen. but the effects of the free energy of compound formation may intervene.

It can be deduced from the discussion of interstices that additional atoms of atomic diameter exceeding 1.17 Å will form not interstitial solid solutions in aluminium but substitutional solutions [143,144], in which the aluminium atom is replaced by the solute atom. Moreover, provided the free energy of compound formation with aluminium is high, atoms of quite small diameter can form compounds even in the liquid state (molten alloy). These compounds are neither interstitial nor substitutional but have a well-defined crystallographic structure [139].

In addition to the interstices in the f.c.c. aluminium lattice and the local distortions produced by the substitution of alloy atoms for aluminium atoms, there are other lattice defects which participate actively in the movement of atoms through the lattice under the influence of concentration gradients. For a lattice atom Al_1 to migrate to an adjacent site Al_2 and remain there with the original potential energy E_p it must be supplied with additional energy E_a (activation energy). The curve of potential energy against position in the lattice is sinusoidal, with a minimum E at positions Al_1 and Al_2 and a maximum (E_p + E_a) half-way between the two sites. To migrate from equilibrium position Al_1 to equilibrium position Al_2 the atom must therefore overcome a potential energy barrier, and its ability to do so depends on its

temperature.

If an atom is removed from the lattice a vacancy is formed. These vacancies themselves migrate. When an atom enters a vacant site it leaves behind another vacancy which can be occupied by another atom; thus the vacancies can move in different directions in the aluminium lattice, a phenomenon known as vacancy diffusion. If the atom, removed to form a vacancy, is replaced in an interstitial position a so-called Frenkel defect is formed. If on the other hand the aluminium atom is replaced on the free crystal surface, a so-called Schottky defect is formed.

4.2 EXPERIMENTAL

4.2.1 PREPARATION OF ALLOYS

On a laboratory scale, alloy specimens can be prepared by melting a considerable amount of high purity aluminium and the useful additions in a carbon crucible. The solid solution is then poured into a thick iron mold. The surfaces of the alloy ingots are scraped and the ingots themselves rolled to a manageable thickness and then homogenized by heating at 350 - 400 ^{o}C for 4 hours. The ingots are then cooled down to ambient temperature in the furnace. They are then rolled to the desired electrode

thickness (i.e. 0.4 mm). The rolled specimens are then heated up to 400 ^{o}C again for another 4 hours and then cooled down to 100 ^{o}C and quenched in water. The heat treatment needs to be closely controlled, since it affects the properties of the alloy prepared, and can therefore be varied.

The alloying elements must be of high hydrogen ovepotential, to minimise hydrogen evolution. The subject of effective alloying elements has been studied closely by numerous workers and has been the subject of some patents [18,147-152] According to Reding and Newport [147] the effective elements for alloying are Hg, Ga, In, Sn, Bi, Mg, Ba, Zn, and Cd. Murai et al [148] studied the anodic behaviour of an aluminium alloy. They prepared the alloy by adding 6% Zn, 0.1% Sn, 0.1% Bi and 0.01% Ga to 99.84% aluminium. They showed that the presence of small amounts of Cu, Si and Fe (<0.1%) has a deleterious effect on the anode efficiency and electrode potential.

Heterogeneity in alloy matrix such as precipitation, will raise the rate of corrosion, as such the concentration of the alloying elements must be kept within the solubility of aluminium. Regard must also be given to environmental pollution, by used batteries, by using alloying elements of low toxicity.

Several alloys were prepared for the purpose of

optimising the performance of aluminium as a galvanic anode.

4.2.2 CHEMICAL ANALYSIS of ALLOYS

The alloys studied were prepared by British Aluminium Company Ltd.. The compositions of the alloying elements in the specimens were verified by the analytical techniques described in section 3.4. The results from the analyses are listed in Table 4.3.

4.2.3 POLARISATION OF ALUMINIUM AND ITS ALLOYS

Electrochemical studies were carried out to investigate the effectiveness of the alloys prepared as possible anode material. 5M KOH, prepared from a laboratory reagent grade material and de-ionised/distilled water, was used as the test electrolyte. Nitrogen gas was bubbled through the solution to remove any dissolved oxygen.

Each working electrode was prepared, as described in section 3.1.3, from a 0.4 mm thick aluminium alloy plates. The electrode was pretreated and immersed in the test electrolyte solution held in the three compartmental cell confiquration described. The half-cell testing

TABLE 4.3 ANALYSIS OF TEST ALLOYS (% W/W)

ELEMENTS:	ZN	CU	MG	SI	FE	MN	TI	GA	PB	BI	SN	IN
ALLOYS												
Q4	0.005	0.010	<0.005	<0.010	0.020	0.002	0.001	0.027	0.160	0.160		
Z1	4.400	<0.010	<0.001	<0.010	0.010	<0.010	0.011					0.020
Z2	2.010	<0.010	<0.001	<0.010	0.010	<0.010	0.013					
Z3	4.470	<0.010	<0.001	<0.010	0.010	<0.010	0.013					
ZS1	4.570	<0.010	<0.001	<0.010	0.010	<0.010	0.020				0.120	

procedure (see section 3.1) was carried out under steady state polarisation conditions. The IR drop at each selected current density was measured and used to correct for the potential reading at the current density. The experiment was carried out three times for each test alloy using fresh working electrode and electrolyte solution each time. The polarisation characteristics of aluminium and its alloys were recorded and plots of potential against current density made.

The entire experimental procedure was repeated for half-cell testing under steady state and transient state galvanostatic and transient state potentiodynamic conditions. The galvanostatic measurements were carried out for a constant current density of 100 mA cm^{-2}.
Fresh working electrodes and test electrolyte solutions were employed for tests carried out under each condition. The polarisation characteristics of the working electrode, under each testing condition, were recorded and plots of potential against time and potential against current density were respectively made.

4.2.4 ANODIC EFFICIENCY

Electrode utilisation tests were carried out by preparing the test electrodes as for half-cell testing. Each electrode was weighed and then immersed in the test

electrolyte whilst passing through a steady current of 200 mA. The time for immersion was noted and after a considerable discharge period, the electrode was retrieved and weighed. The weight loss was noted alongside the period of discharge. The experiment was repeated three times for each electrode material.

4.2.5 SELF-DISCHARGE CHARACTERISTICS OF ALUMINIUM AND ITS ALLOYS

The test solution was poured into the special test tube shown in Fig. 4.1 the test tube was immersed into a water bath at 25°C. A test electrode was freshly prepared, as relayed above, and weighed and then placed into the solution in the test tube. The time was noted concurrently. The test tube was completely sealed and the gas evolved was collected over water according to the procedure described in section 3.2. After a noted time period, the amount of gas evolved was recorded.

The electrode was removed from solution, washed in acetone under ultrasonic vibration, and wiped dry with a soft tissue and weighed again. The difference in weight was recorded, alongside the period of time the electrode had been in solution. The experiment was repeated, in triplicates, for each electrode material.

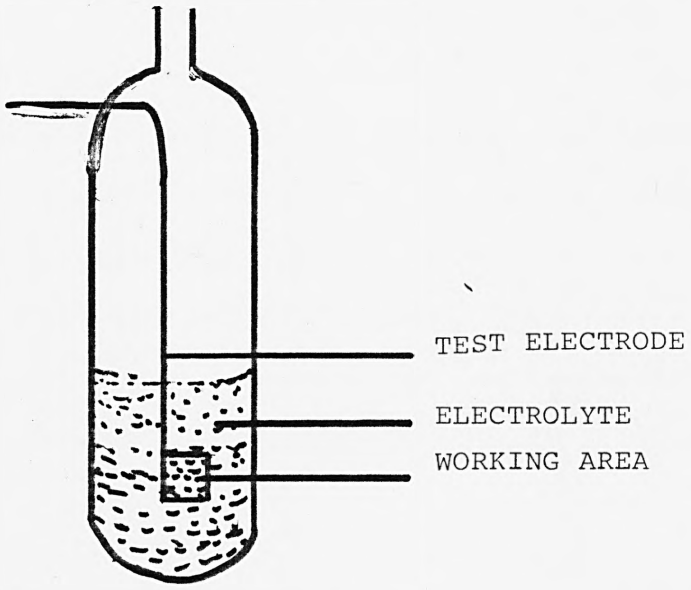

FIG. 4.1 SPECIAL TEST CELL FOR SELF-DISCHARGE MEASUREMENTS

All the above experiments were carried out at 25°C. The temperature being maintained and ensured by performing the experiments in the thermostatically controlled water bath mentioned in section 3.1.6.

4.2.6 SURFACE EXAMINATION

The surfaces of the test electrodes, polarised in the half-cell testings, were examined using the scanning electron microscopy and X-ray flourescence techniques described in section 3.3. The electrodes were pretreated for the purpose according to the procedure relayed in that section. Both the surface of each electrode before polarisation and after polarisation were examined. The change in the surface morphology was then ascertained.

4.3 RESULTS AND DISCUSSION

4.3.1 POLARISATION PERFORMANCE

The results obtained from the polarisation measurements are shown in Appendix B. The mean of the three runs for each electrode in each experiment was taken and used to plot respective graphs of potential versus current density and potential versus time.

The data shown in Tables B1-B12 were used to plot graphs of potential versus current density. The plots are shown as Figs. 4.2, 4.9-4.14. Figure 4.2 shows the steady state measurements. It can be seen from the curves that at open-circuit, the potentials (rest potentials) for the alloys are higher than that for pure Al. Thus, the alloying elements can be said to destabilise the resistive oxide film on the surface of aluminium. The rest potentials for alloys Z1, Z2, Z3 and ZS1 are almost the same and higher than that for alloy Q4. This is due to the differences in alloy composition. As can be seen in Table 4.3, alloys Z1, Z2, Z3 and ZS1 are predominately Al-Zn alloys, differing only in the concentration of Zn and the other types of elements added, whereas Q4 is predominately bare Al with very low concentrations of several additives.

Because alloys Z1, Z2, Z3,and ZS1 contain a higher proportion of Zn than Q4 has, the higher rest potentials observed for these alloys can be attributed to the concentration of Zn in the lattice structure. It can be argued that the presence of Zn greatly enhances the breakdown of the resistivity of the oxide layer on aluminium and thus, charge-transfer across the metal-solution interface becomes less inhibited enabling higher negative potentials to be realised.

As current density is increased, however, the

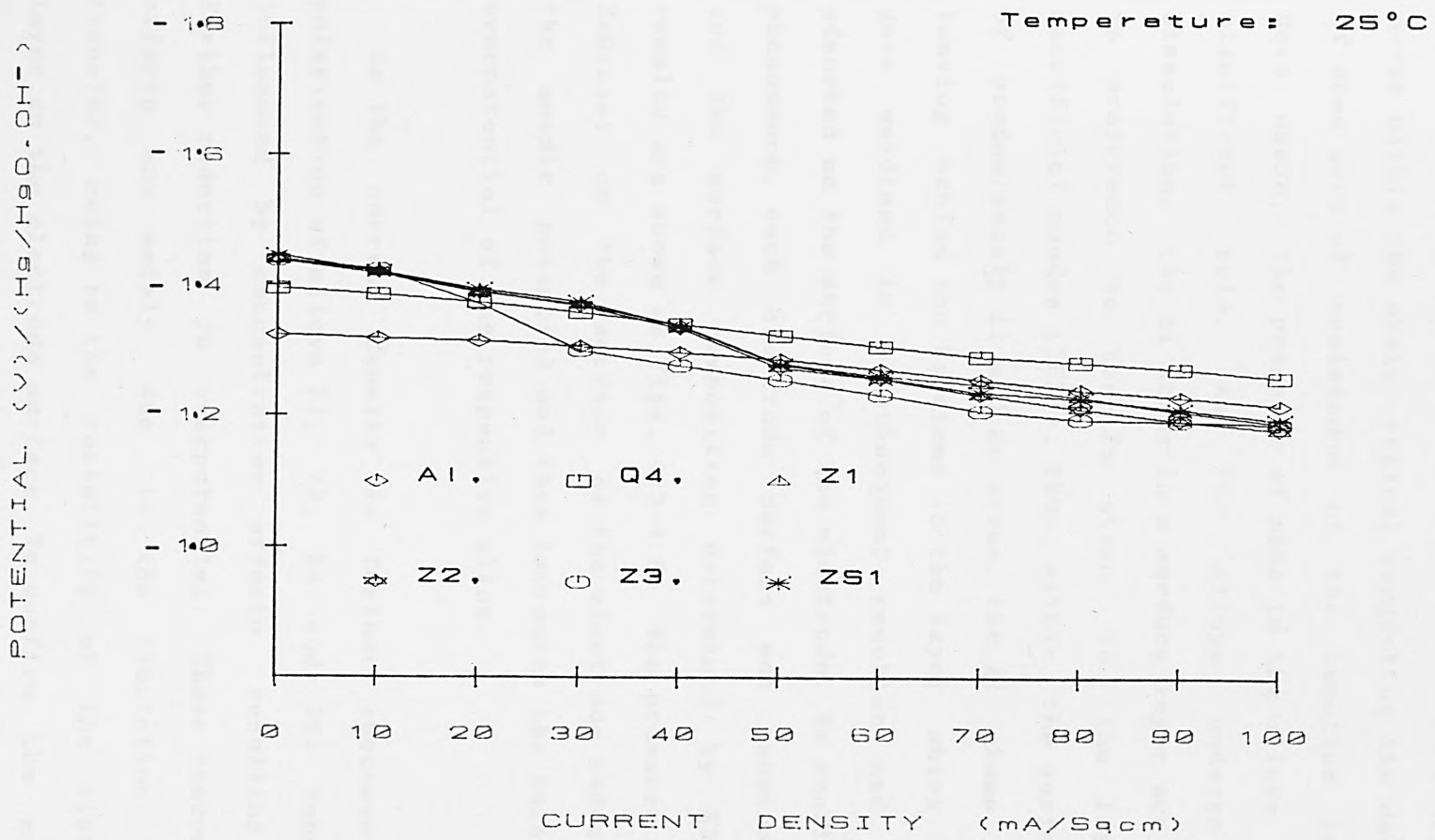

FIG. 4.2 STEADY STATE POLARISATION OF Al AND ITS ALLOYS

performances of these alloys become greatly reduced as compared to that of Q4. This increases in overpotential occur within the ohmic region, suggesting the development of some sort of resistance at the reaction interface. Here again, the presence of zinc in the alloys plays a significant role. As the alloys undergo anodic dissolution, the Al atoms in a surface layer are consumed in preference to the Zn atoms in the layer (see sacrificial anodes [153]). Thus, within the surface layer of predominately Al and Zn atoms, the Al atoms dissolve leaving behind the Zn atoms in the layer which in turn gets oxidised in a subsequent reaction and remains adsorbed on the surface of the electrode. To confirm this phenomenon, each electrode surface was examined by SEM and the surface composition determined by EDAX. The results are shown as Figs. 4.3-4.8. The presence of Zn as $ZnO_{(ads)}$ on the surface of the electrode reduces the anodic potential and thus increases the polarisation overpotential of the respective alloy.

As the current density is further increased, the polarisation of alloys Z1, Z2, Z3 and ZS1 tends to be influenced by concentration effects resulting in a further reduction in overpotential. These concentration effects are mainly due to the limitation in mass transfer, owing to the resistivity of the zinc oxide layer on the electrode surface. To confirm the existence of mass transfer limitation, all the electrodes were

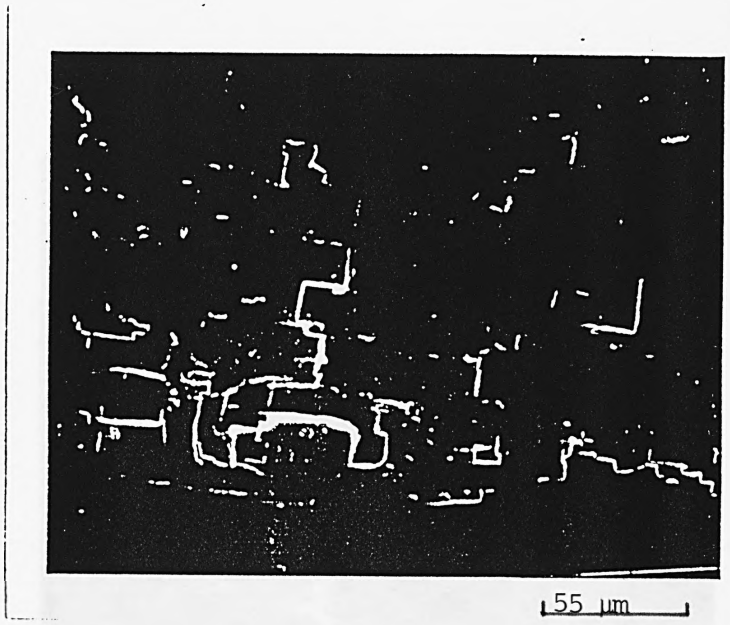

FIG. 4.3a SURFACE MORPHOLOGY OF PURE Al BEFORE POLARISATION

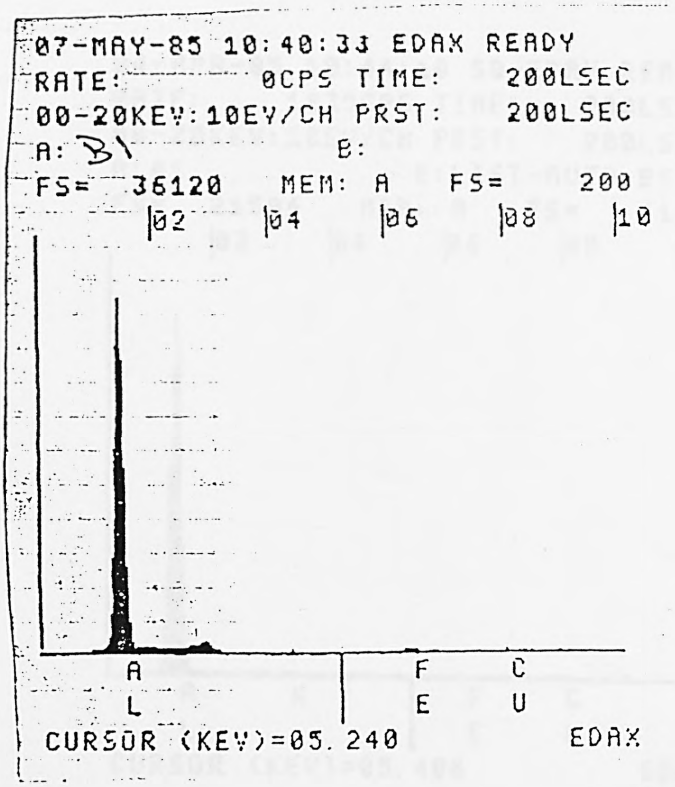

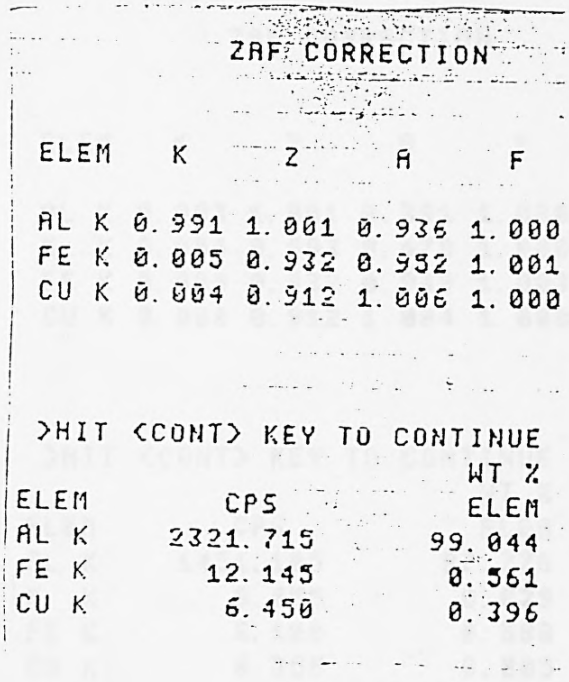

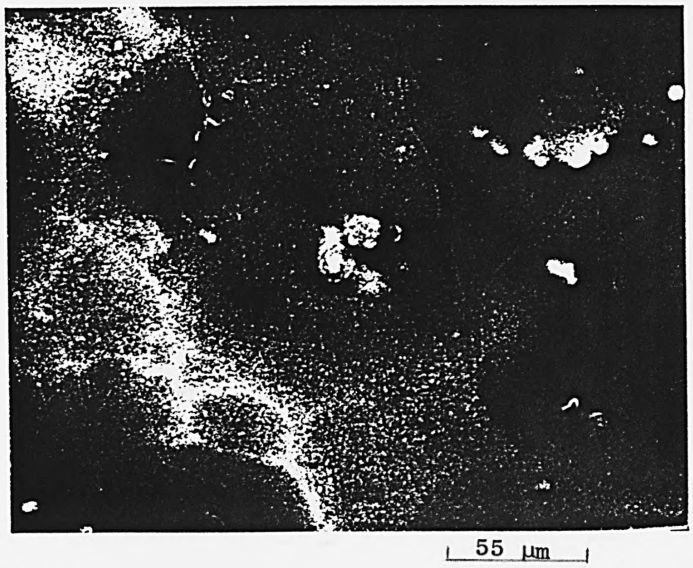

FIG. 4.3b SURFACE MORPHOLOGY OF PURE Al AFTER POLARISATION

```
24-APR-85 10:44:10 SQ-EDAX READY
RATE:     1835CPS TIME:    200LSEC
00-20KEV:10EV/CH PRST:    200LSEC
A:#1              B:LIST-AUTO BKG
FS=   21594    MEM: A    FS=   4159
      |02     |04     |06     |08     |10
```

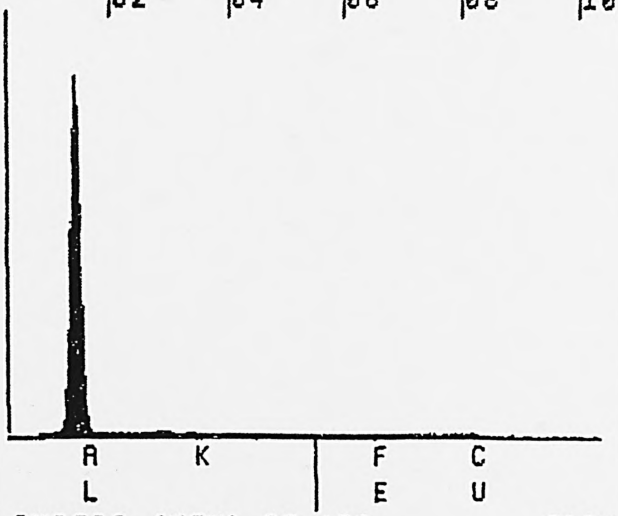


```
CURSOR (KEV)=05.480          EDAX
```

ZAF CORRECTION

ELEM	K	Z	A	F
AL K	0.983	1.001	0.891	1.000
K K	0.004	0.993	0.478	1.000
FE K	0.005	0.932	0.949	1.003
CU K	0.008	0.912	1.004	1.000

>HIT <CONT> KEY TO CONTINUE

ELEM	CPS	WT % ELEM
AL K	1451.105	97.778
K K	8.655	0.829
FE K	8.100	0.588
CU K	8.355	0.805

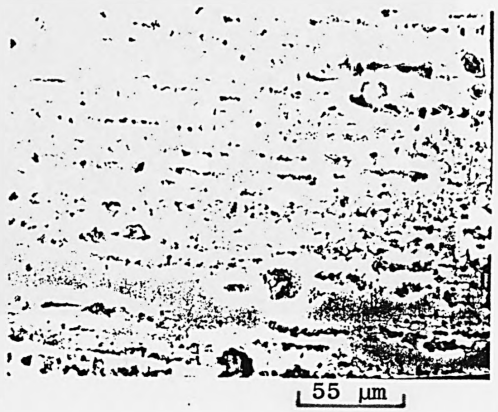

BEFORE

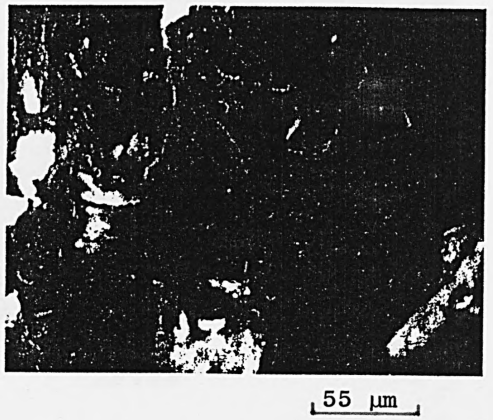

AFTER

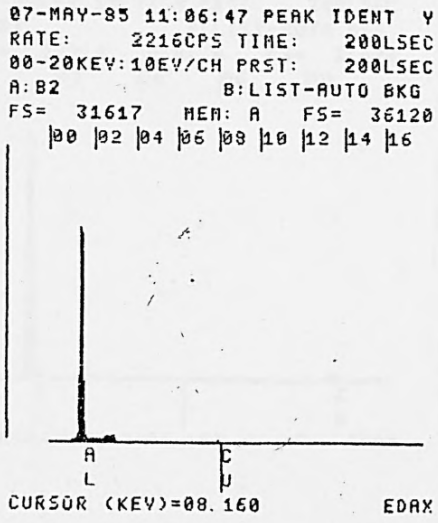

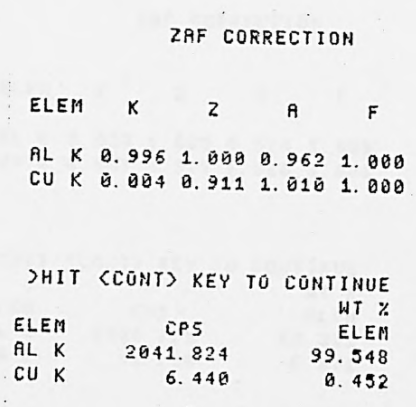

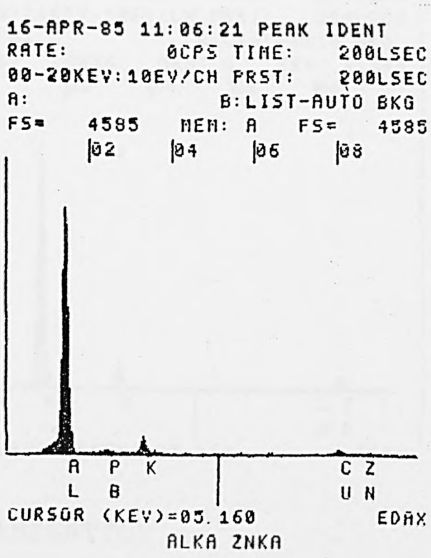

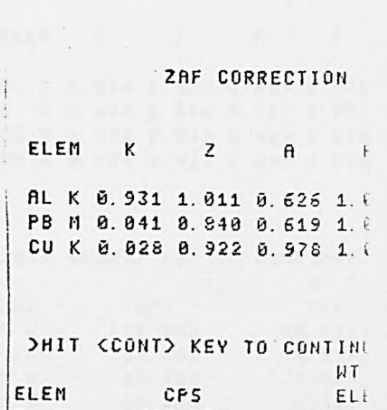

FIG. 4.4 SURFACE MORPHOLOGY OF ALLOY Q4 BEFORE AND AFTER POLARISATION

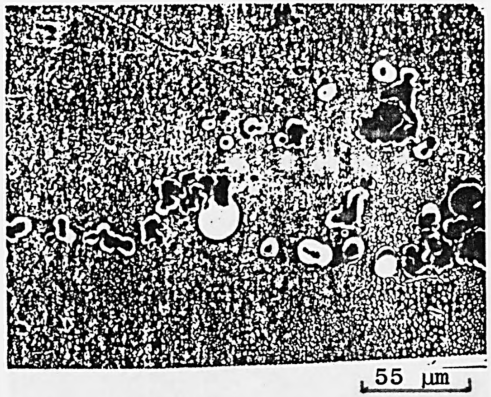

BEFORE

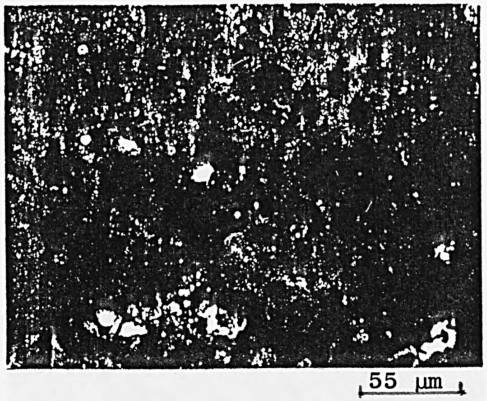

AFTER

07-MAY-85 11:39:14 SQ-EDAX READY
RATE: 2919CPS TIME: 200LSEC
00-20KEV:10EV/CH PRST: 200LSEC
A:B3 B:LIST-AUTO BKG
FS= 29914 MEM: A FS= 31690

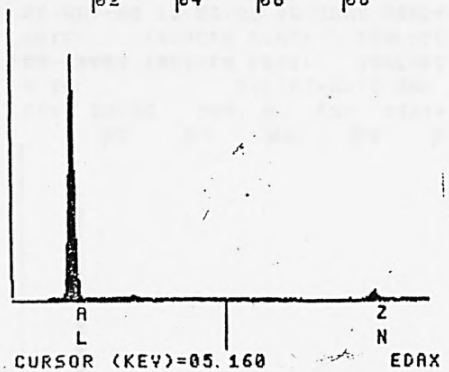

ZAF CORRECTION

ELEM	K	Z	A	F
AL K	0.933	1.005	0.574	1.000
ZN K	0.067	0.919	1.018	1.000

>HIT <CONT> KEY TO CONTINUE

ELEM	CPS	WT % ELEM
AL K	1924.775	93.329
ZN K	93.120	6.671

24-APR-85 11:13:27 SQ-EDAX READY
RATE: 2CPS TIME: 200LSEC
00-20KEV:10EV/CH PRST: 200LSEC
A:B3 B:LIST-AUTO BKG
FS= 10836 MEM: A FS= 21594

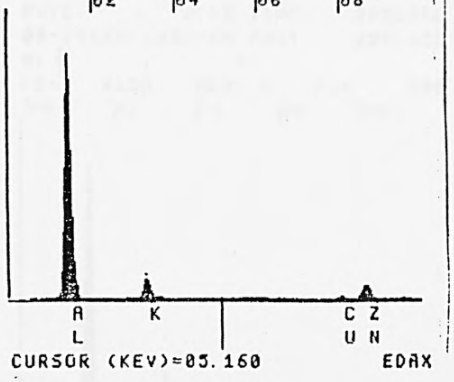

ZAF CORRECTION

ELEM	K	Z	A	F
AL K	0.830	1.008	0.409	1.001
K K	0.055	1.000	0.497	1.000
CU K	0.021	0.919	0.989	1.000
ZN K	0.094	0.923	1.002	1.000

>HIT <CONT> KEY TO CONTINUE

ELEM	CPS	WT % ELEM
AL K	716.509	80.696
K K	68.865	8.997
CU K	13.425	1.879
ZN K	55.345	8.429

FIG. 4.5 SURFACE MORPHOLOGY OF ALLOY Z1 BEFORE AND AFTER POLARISATION

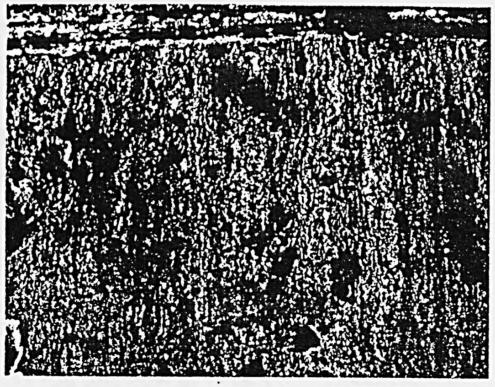

BEFORE

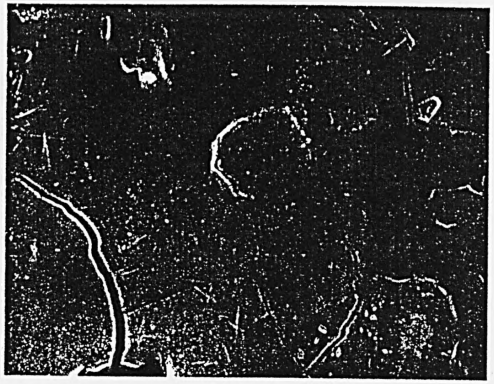

AFTER

```
07-MAY-85 12:56:26 SQ-EDAX READY
RATE:     1925CPS TIME:    200LSEC
00-20KEV:10EV/CH PRST:     200LSEC
A:86              B:LIST-AUTO BKG
FS=  23292   MEM: A   FS=  14244
      |02    |04    |06    |08    |10
```


```
CURSOR (KEV)=05.240          EDAX
```

ZAF CORRECTION

ELEM	K	Z	A	F
AL K	0.929	1.005	0.557	1.000
CU K	0.003	0.916	1.008	1.000
ZN K	0.068	0.919	1.018	1.000

>HIT <CONT> KEY TO CONTINUE

ELEM	CPS	WT % ELEM
AL K	1491.471	92.889
CU K	4.175	0.350
ZN K	73.840	6.761

```
24-APR-85 10:13:55 EDAX READY
RATE:        0CPS TIME:    200LSEC
00-20KEV:10EV/CH PRST:     200LSEC
A: 6              B:
FS=   4159   MEM: A   FS=     200
      |00    |02    |04    |06    |08
```

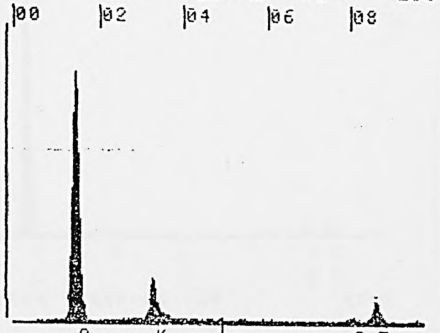


```
CURSOR (KEV)=04.960          EDAX
```

ZAF CORRECTION

ELEM	K	Z	A	
AL K	0.773	1.009	0.362	1.
K K	0.092	1.001	0.511	1.
CU K	0.018	0.921	0.979	1.
ZN K	0.117	0.924	0.994	1.

>HIT <CONT> KEY TO CONTIN

ELEM	CPS	WT ELE
AL K	276.265	74.9
K K	47.910	13.6
CU K	4.855	1.3
ZN K	28.465	9.8

FIG. 4.6 SURFACE MORPHOLOGY OF ALLOY Z2 BEFORE AND AFTER POLARISATION

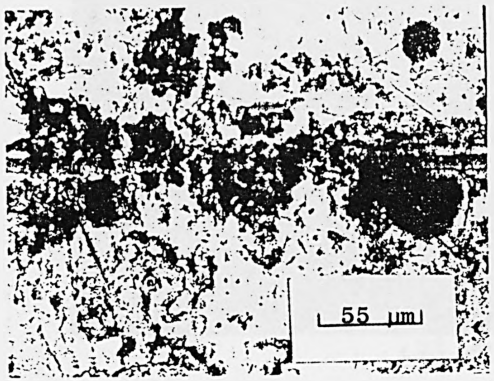

BEFORE

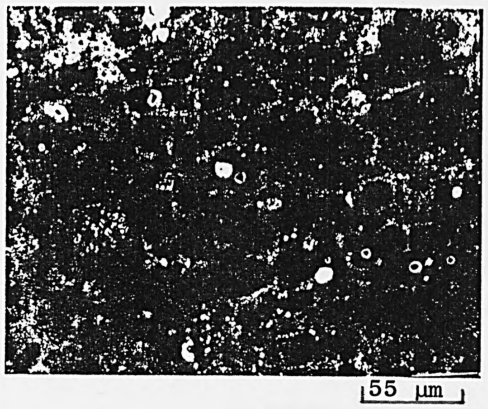

AFTER

```
07-MAY-85 11:57:36 SQ-EDAX READY
RATE:        0CPS TIME:    142LSEC
00-20KEV:10EV/CH PRST:    200LSEC
A:B4              B:LIST-AUTO BKG
FS=   23140    MEM: A    FS=   29952
      |02     |04     |06     |08     |10
```

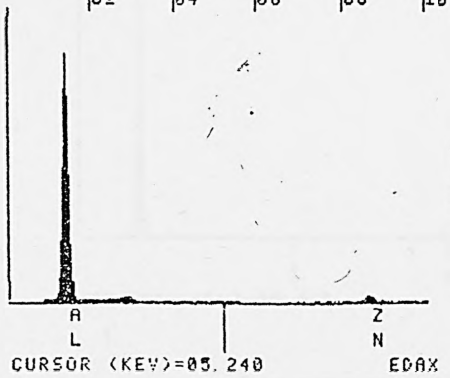

ZAF CORRECTION

ELEM	K	Z	A	F
AL K	0.938	1.004	0.594	1.000
ZN K	0.062	0.919	1.018	1.000

>HIT <CONT> KEY TO CONTINUE

ELEM	CPS	WT % ELEM
AL K	2064.824	93.796
ZN K	91.962	6.204

```
24-APR-85 11:46:49 SQ-EDAX READY
RATE:     3635CPS TIME:    156LSEC
00-20KEV:10EV/CH PRST:    200LSEC
A:#4              B:LIST-AUTO BKG
FS=   13799    MEM: A    FS=   10836
00      |02     |04     |06     |08
```

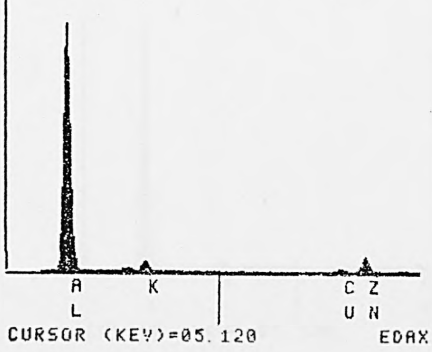

ZAF CORRECTION

ELEM	K	Z	A	F
AL K	0.855	1.008	0.415	1.000
K K	0.028	1.000	0.485	1.000
CU K	0.022	0.919	0.997	1.000
ZN K	0.095	0.923	1.009	1.000

>HIT <CONT> KEY TO CONTINUE

ELEM	CPS	WT % ELEM
AL K	1188.074	84.224
K K	57.343	4.977
CU K	22.896	2.045
ZN K	89.881	8.754

FIG. 4.7 SURFACE MORPHOLOGY OF ALLOY Z3 BEFORE AND AFTER POLARISATION

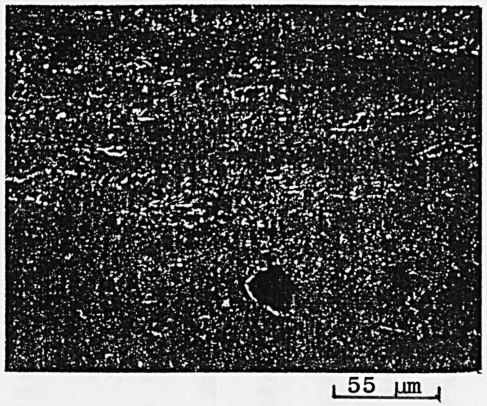

BEFORE

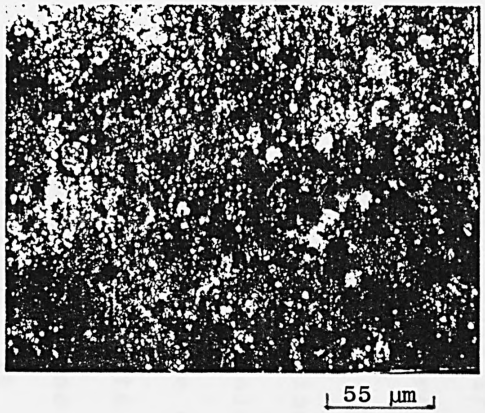

AFTER

```
07-MAY-85 12:32:54 SQ-EDAX READY
RATE:     2653CPS TIME:     96LSEC
00-20KEV:10EV/CH PRST:    200LSEC
A:B5              B:
FS=   14228   MEM: A   FS=  23140
      |02     |04     |06     |08
```

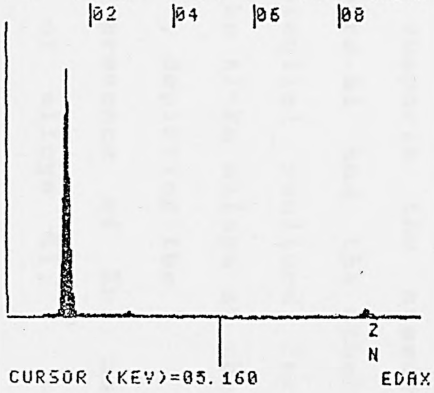


```
CURSOR (KEY)=05.160          EDAX
```

```
                ZAF CORRECTION

ELEM    K      Z      A      F

AL K  0.936  1.004  0.584  1.000
ZN K  0.064  0.919  1.018  1.000


 >HIT <CONT> KEY TO CONTINUE
                                WT %
ELEM        CPS                ELEM
AL K     1901.263             93.583
ZN K       87.987              6.417
```

```
24-APR-85 12:11:30 SQ-EDAX READY
RATE:     2815CPS TIME:    111LSEC
00-20KEV:10EV/CH PRST:    200LSEC
A:#5              B:
FS=    9024   MEM: A   FS=  13801
|00     |02     |04     |06     |08
```

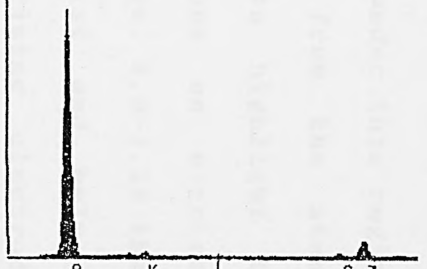


```
CURSOR (KEY)=05.120          EDAX
```

```
                ZAF CORRECTION

ELEM    K      Z      A      F

AL K  0.861  1.009  0.398  1.0
K  K  0.010  1.000  0.474  1.0
CU K  0.018  0.920  1.003  1.0
ZN K  0.111  0.923  1.014  1.0


 >HIT <CONT> KEY TO CONTINU
                                WT
ELEM        CPS                ELE
AL K     1089.144             86.1
K  K       17.870              1.7
CU K       16.699              1.6
ZN K       95.590             10.3
```

FIG. 4.8 SURFACE MORPHOLOGY OF ALLOY ZS1 BEFORE AND AFTER POLARISATION

polarised under transient conditions (see section 3.1). The results from the transient state measurements represent what happens in the absence of mass transfer limitations, since mass transfer effects, due to concentration polarisation, are absent under this regime. These results are compared to results from the steady state measurements (see Figs. 4.9-4.14) to highlight the effect of mass transfer limitations on electrode polarisation. It can be seen from Figs. 4.9-4.14 that, overall, mass transfer limitations exist and help to increase the overpotential of the polarising electrode. The effect is, however, greater for the Al-Zn alloys.

The data obtained from the galvanostatic polarisation of the alloys (Tables B13-B24) were used to plot discharge curves (plots of potential versus time). These curves are shown in Figs. 4.15-4.21. Figure 4.15 shows steady state measurements, from which it can be seen that all the electrodes were able to hold a steady current at a constant potential, in excess electrolyte. The potential at which the steady current is held differs for each electrode-type. Overall, Q4 supports the steady current at a higher potential than pure Al and the other alloys. It can be seen that the potential realised for pure Al is higher than that for the Al-Zn alloys at the high current density of 100 mA cm^{-2}, depicting the extent of the resistivity due to the presence of Zn, as $ZnO_{(ads)}$, on the polarising surface of alloys Z1,

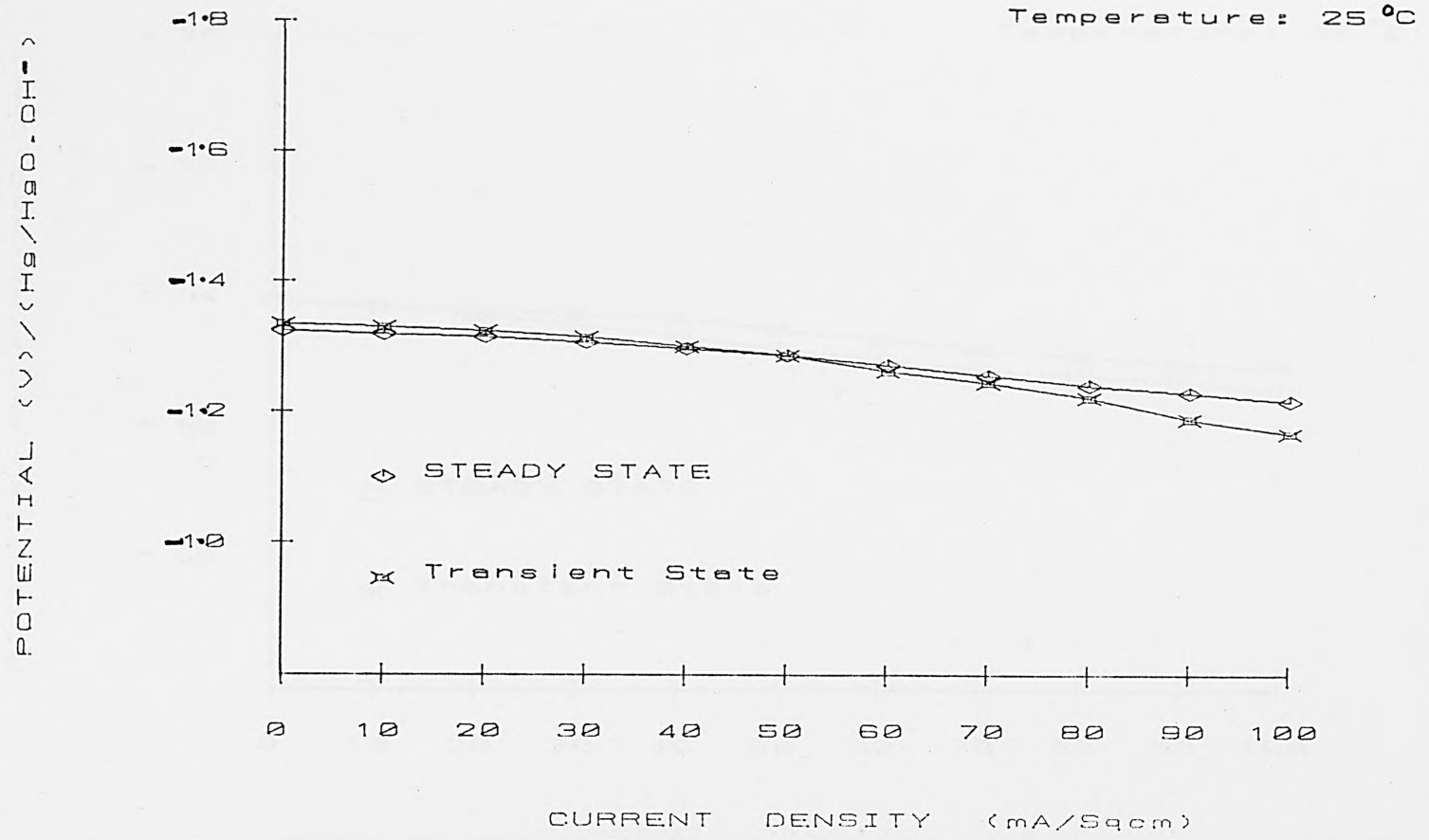

FIG. 4.9 TRANSIENT/STEADY STATE POLARISATION OF Al IN 5M KOH

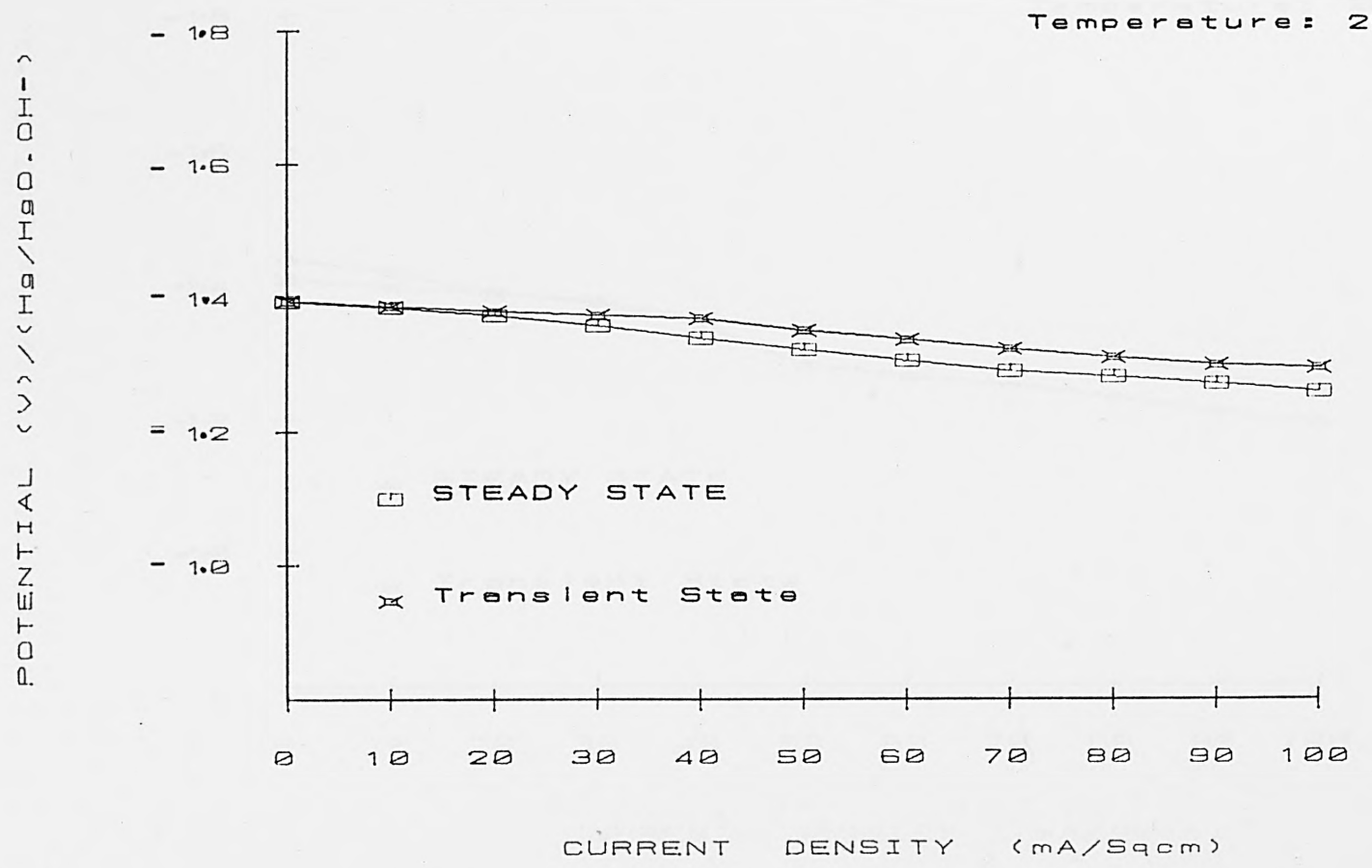

FIG. 4.10 TRANSIENT/STEADY STATE POLARISATION OF Q4 IN 5M KOH

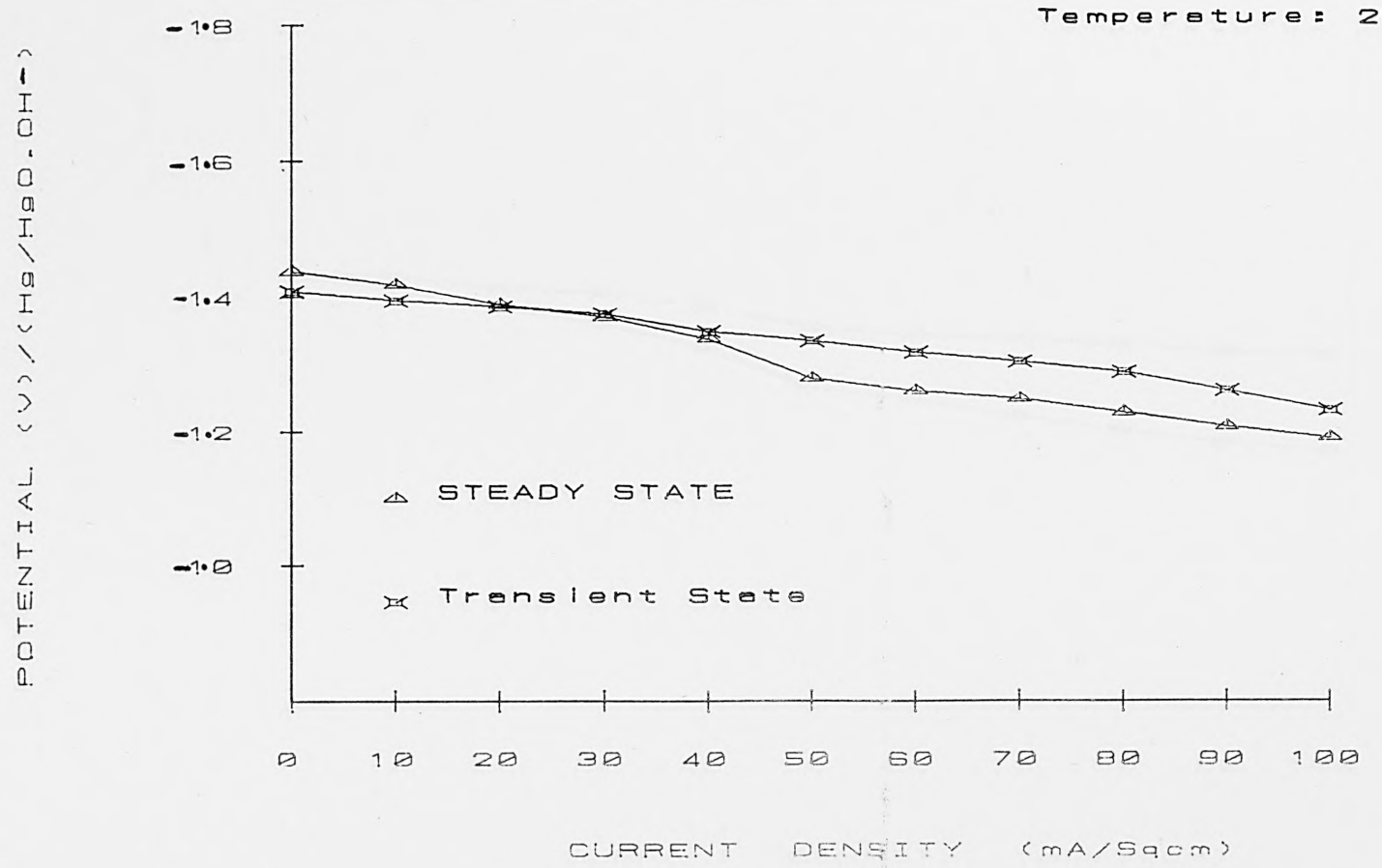

FIG. 4.11 TRANSIENT/STEADY STATE POLARISATION OF Z1 IN 5M KOH

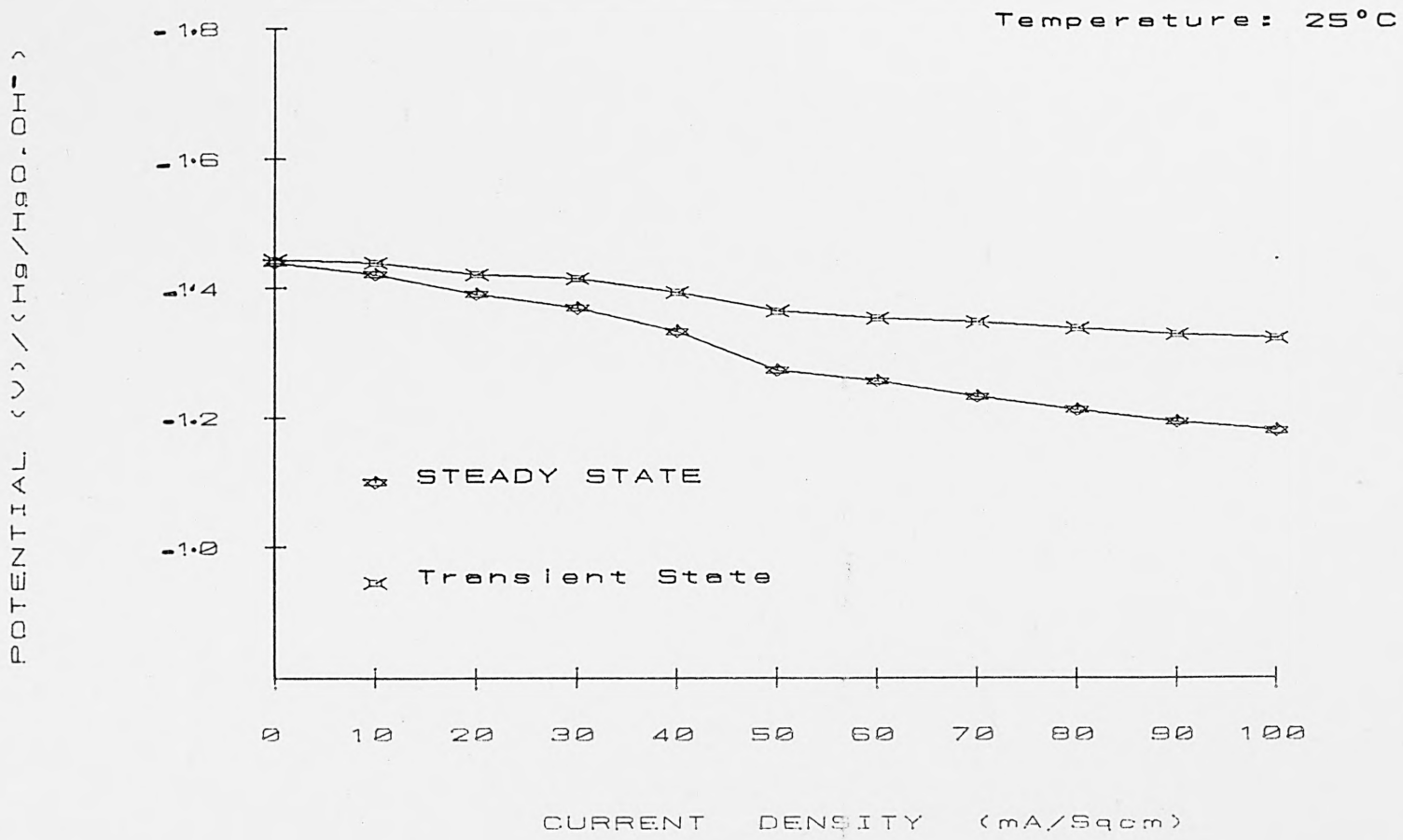

FIG. 4.12 TRANSIENT/STEADY STATE POLARISATION OF Z2 IN 5M KOH

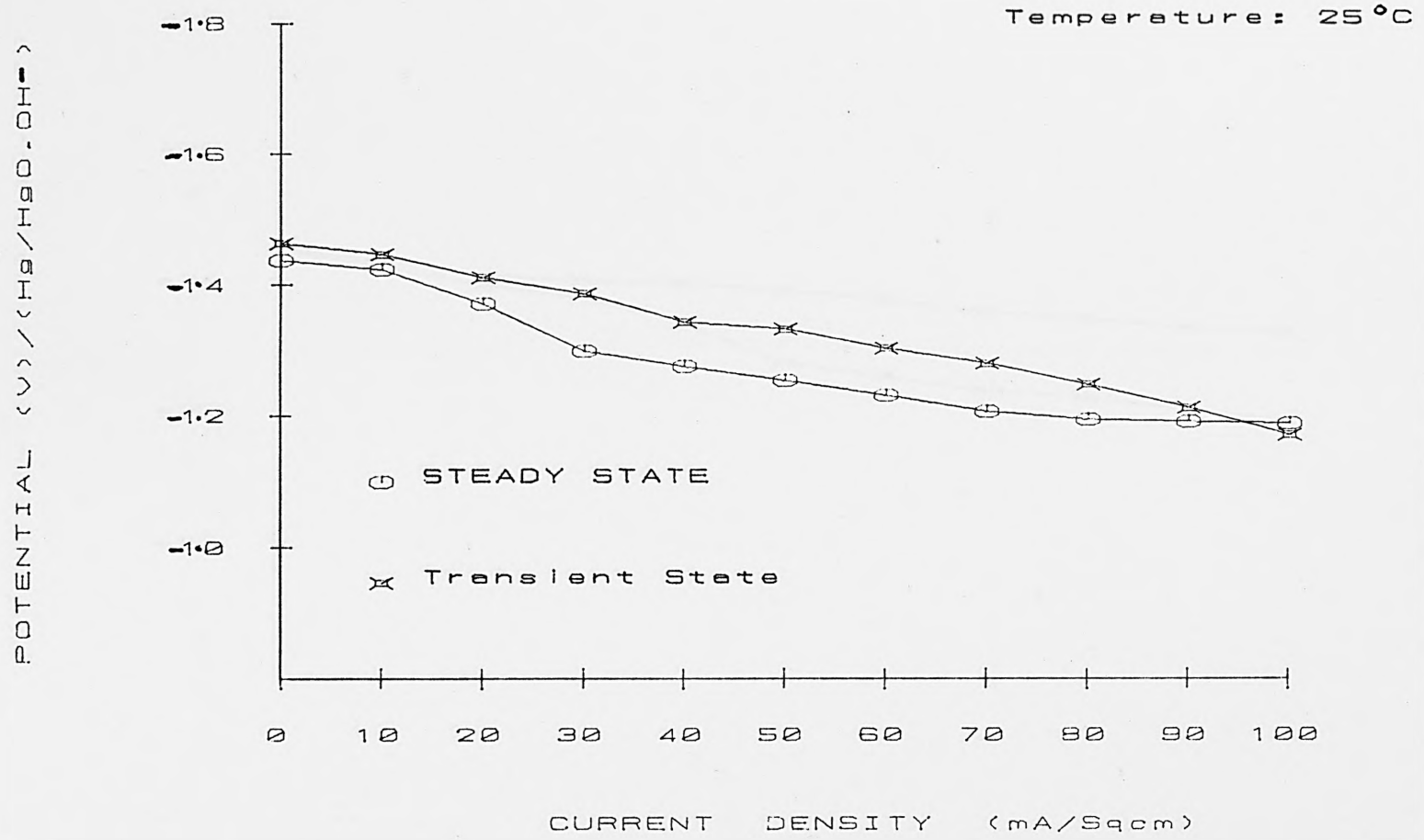

FIG. 4.13 TRANSIENT/STEADY STATE POLARISATION OF Z3 IN 5M KOH

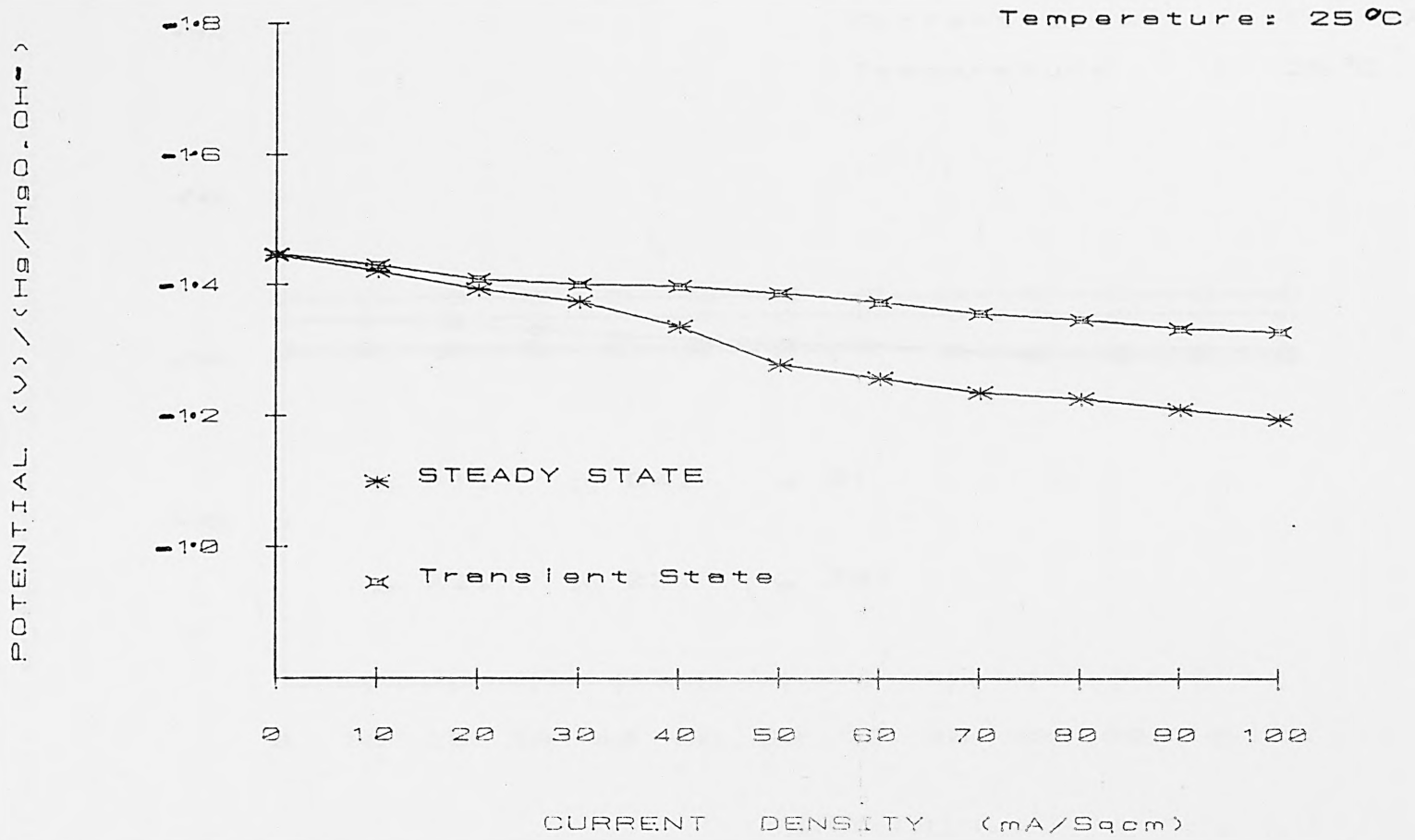

FIG. 4.14 TRANSIENT/STEADY STATE POLARISATION OF ZS1 IN 5M KOH

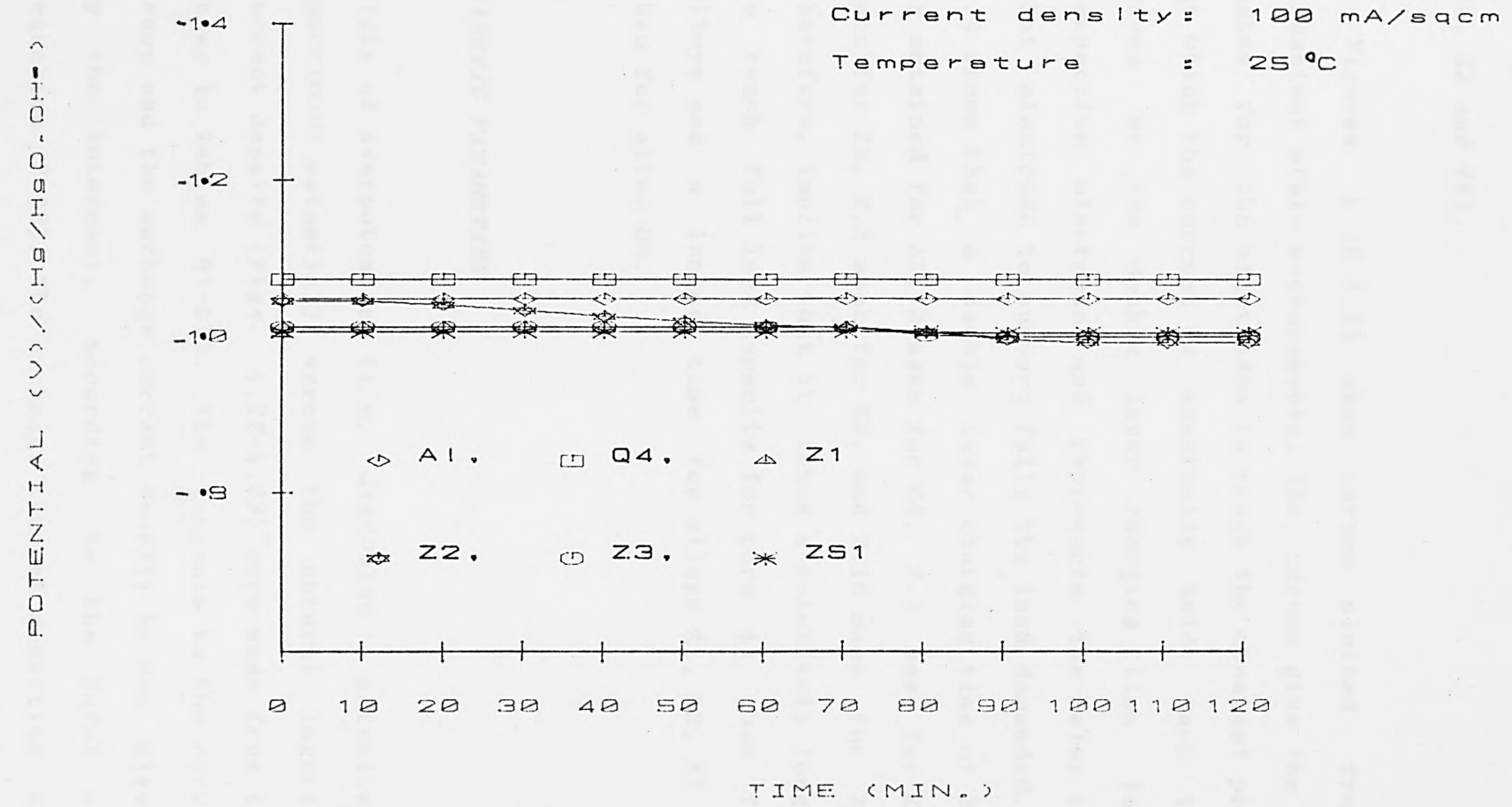

FIG.4.15 STEADY STATE GALVANOSTATIC POLARISATION OF Al AND ITS ALLOYS IN 5M KOH

Z2, Z3 and ZS1.

Figures 4.16-4.21 show curves plotted from the transient state measurements. The curves give the time it takes for the electrodes to reach the constant potential at which the current is eventually held. Each time is given as the double layer charging time for the respective electrode and represents the delay time for that electrode to support fully the load demanded. Table 4.4 shows that a double layer charging time of 2.3 msec is obtained for A1, 2 msec for Q4, 2.1 msec for Z1, 2.25 msec for Z2, 2.2 msec for Z3, and 2.15 msec for ZS1. It therefore, implies that it takes a relatively longer time to reach full load capacity for pure Al than for its alloys and a longer time for alloys Z1, Z2, Z3 and ZS1 than for alloy Q4.

KINETIC PARAMETERS

Plots of overpotential (i.e. discharge potential minus open-circuit potential) versus the natural logarithm of current density (Figs. 4.22-4.33) were made from the data shown in Tables B1-B12. The tangents to the curves were drawn and the exchange current density i_o was given by the intercept, according to the Tafel equation (equation 2.42). The exchange current densities obtained for the electrode reactions are presented in Table 4.5.

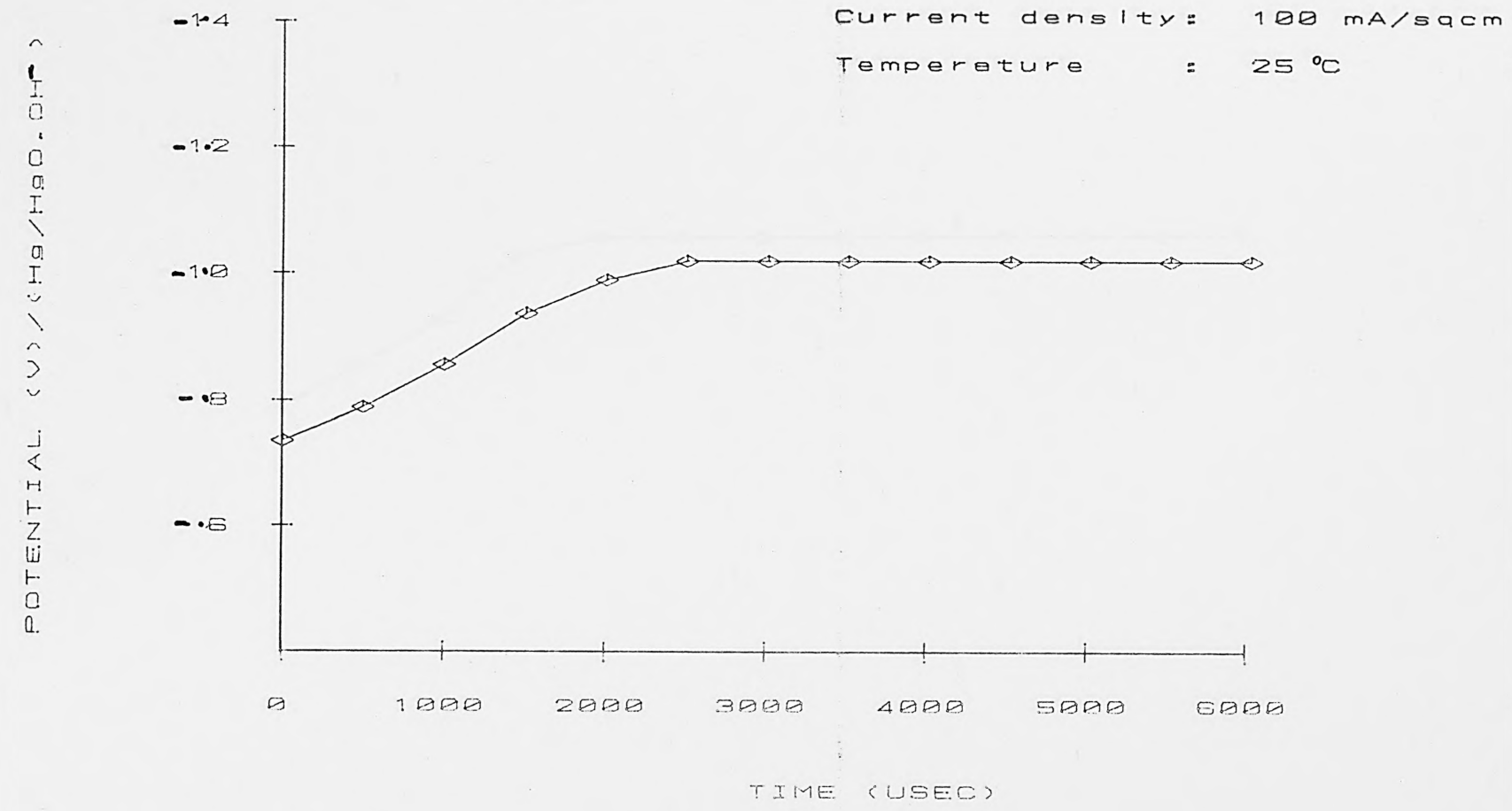

FIG.4.16 TRANSIENT STATE GALVANOSTATIC POLARISATION OF Al IN 5M KOH

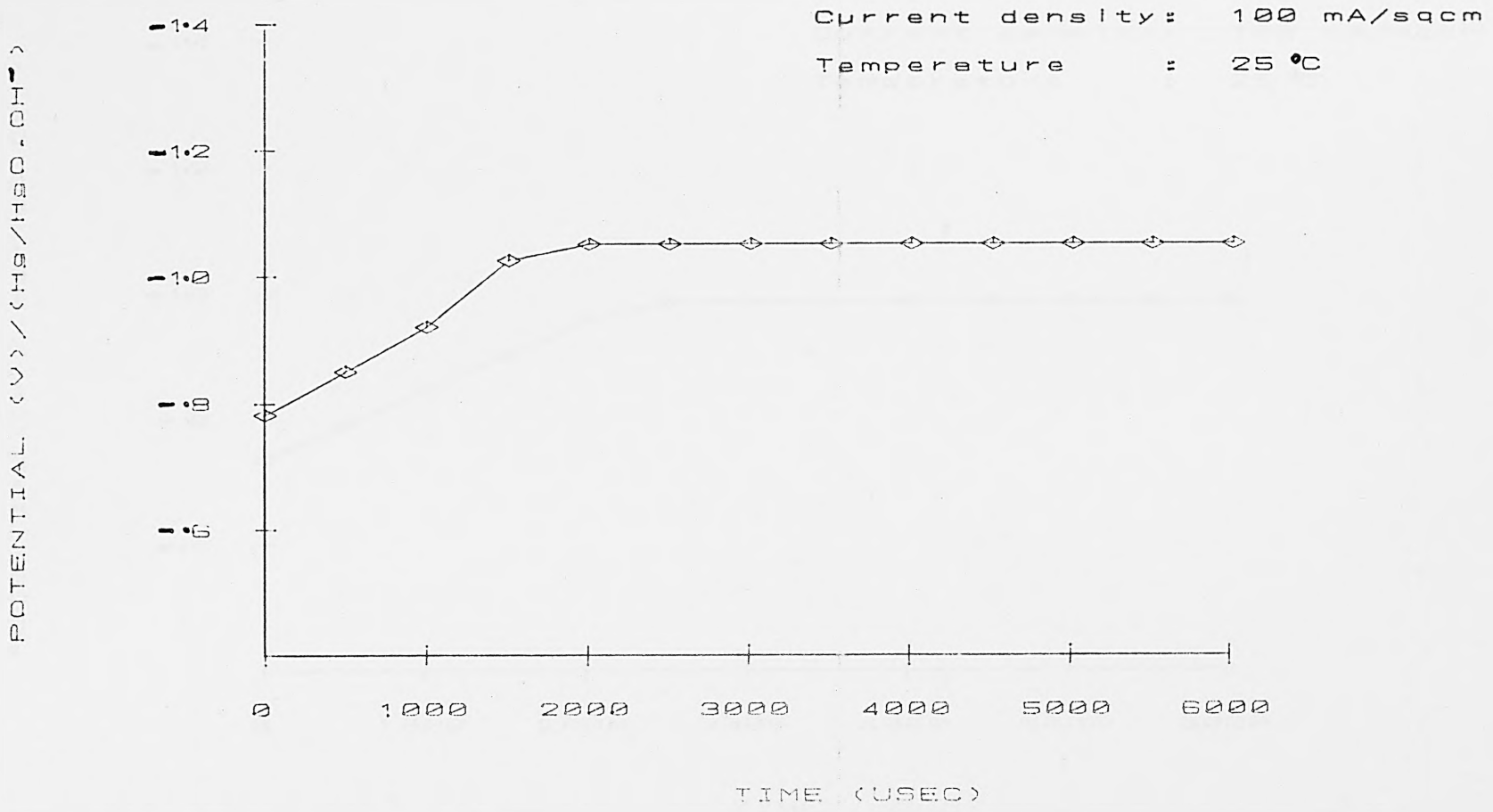

FIG. 4.17 TRANSIENT STATE GALVANOSTATIC POLARISATION OF Q4 IN 5M KOH

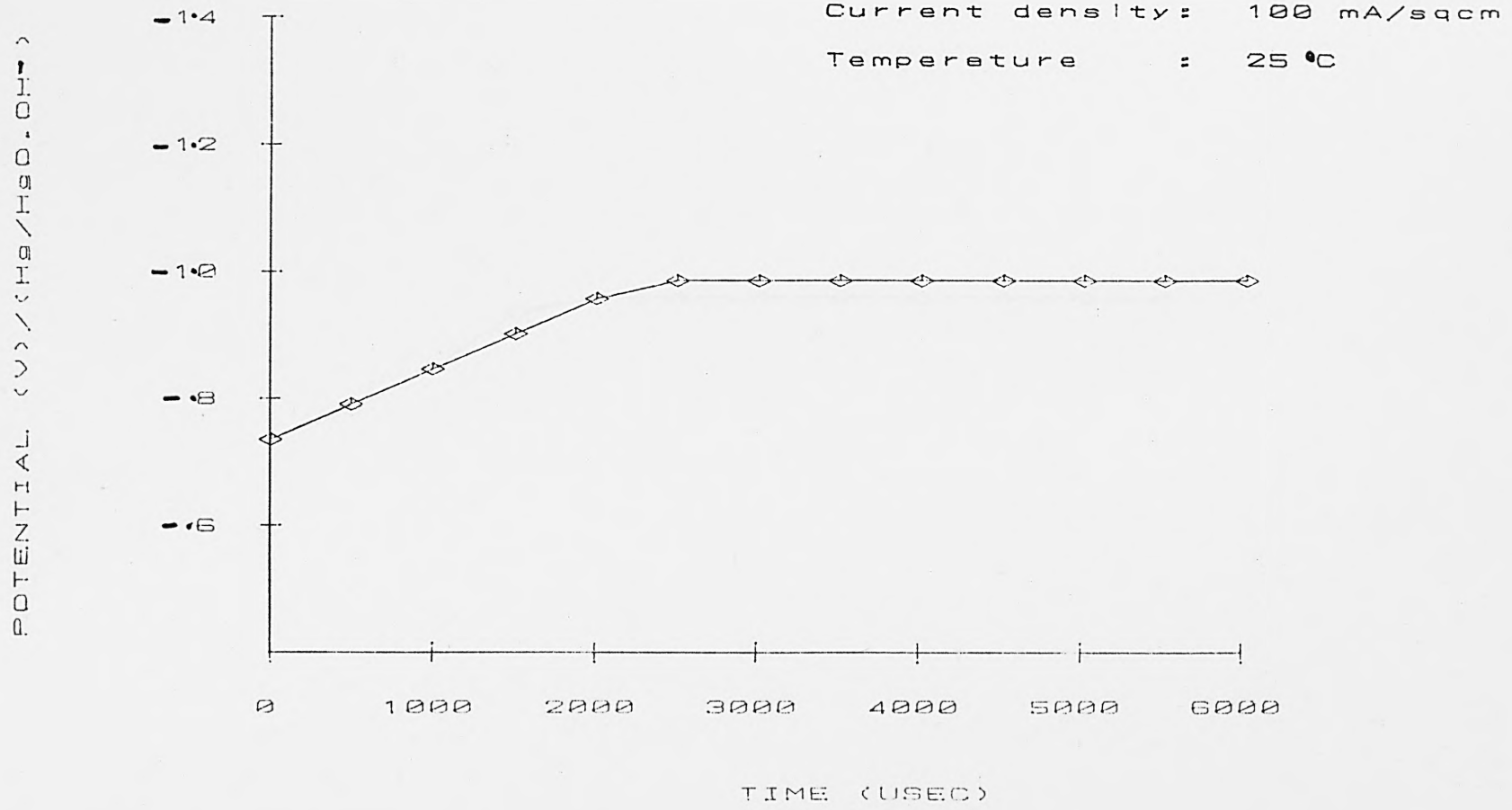

FIG. 4.18 TRANSIENT STATE GALVANOSTATIC POLARISATION OF Z1 IN 5M KOH

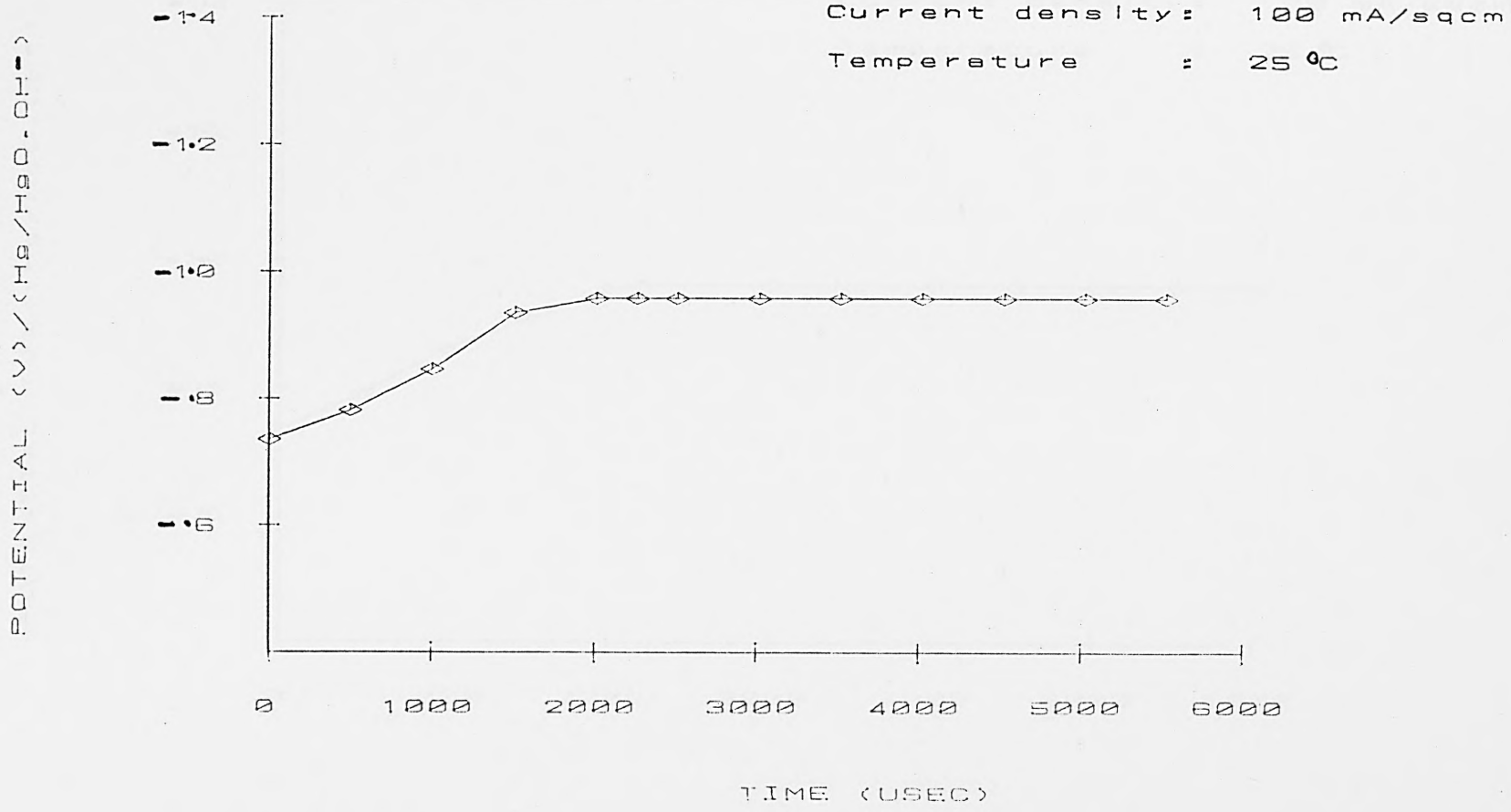

FIG. 4.19 TRANSIENT STATE GALVANOSTATIC POLARISATION OF Z2 IN 5M KOH

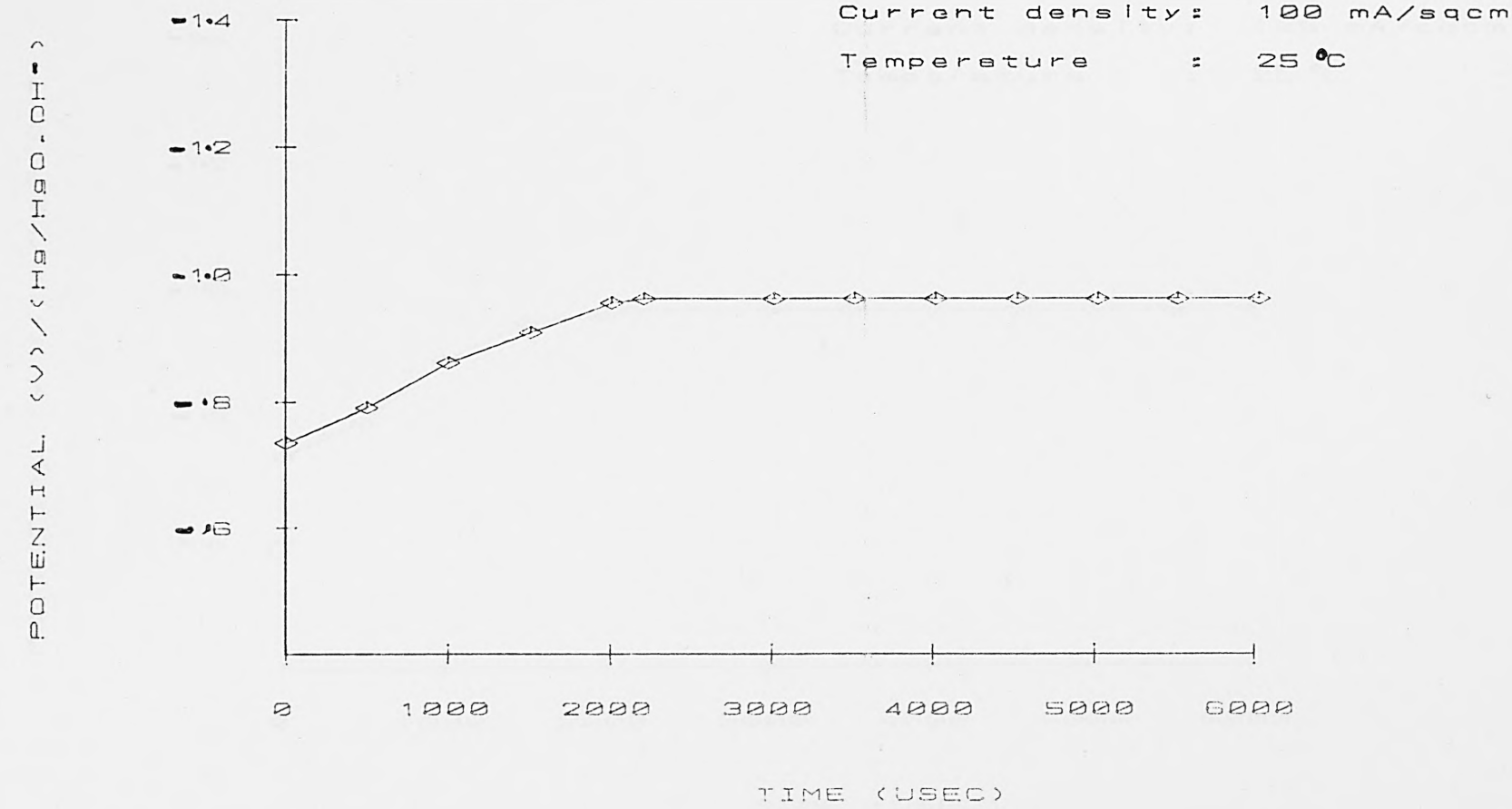

FIG. 4.20 TRANSIENT STATE GALVANOSTATIC POLARISATION OF Z3 IN 5M KOH

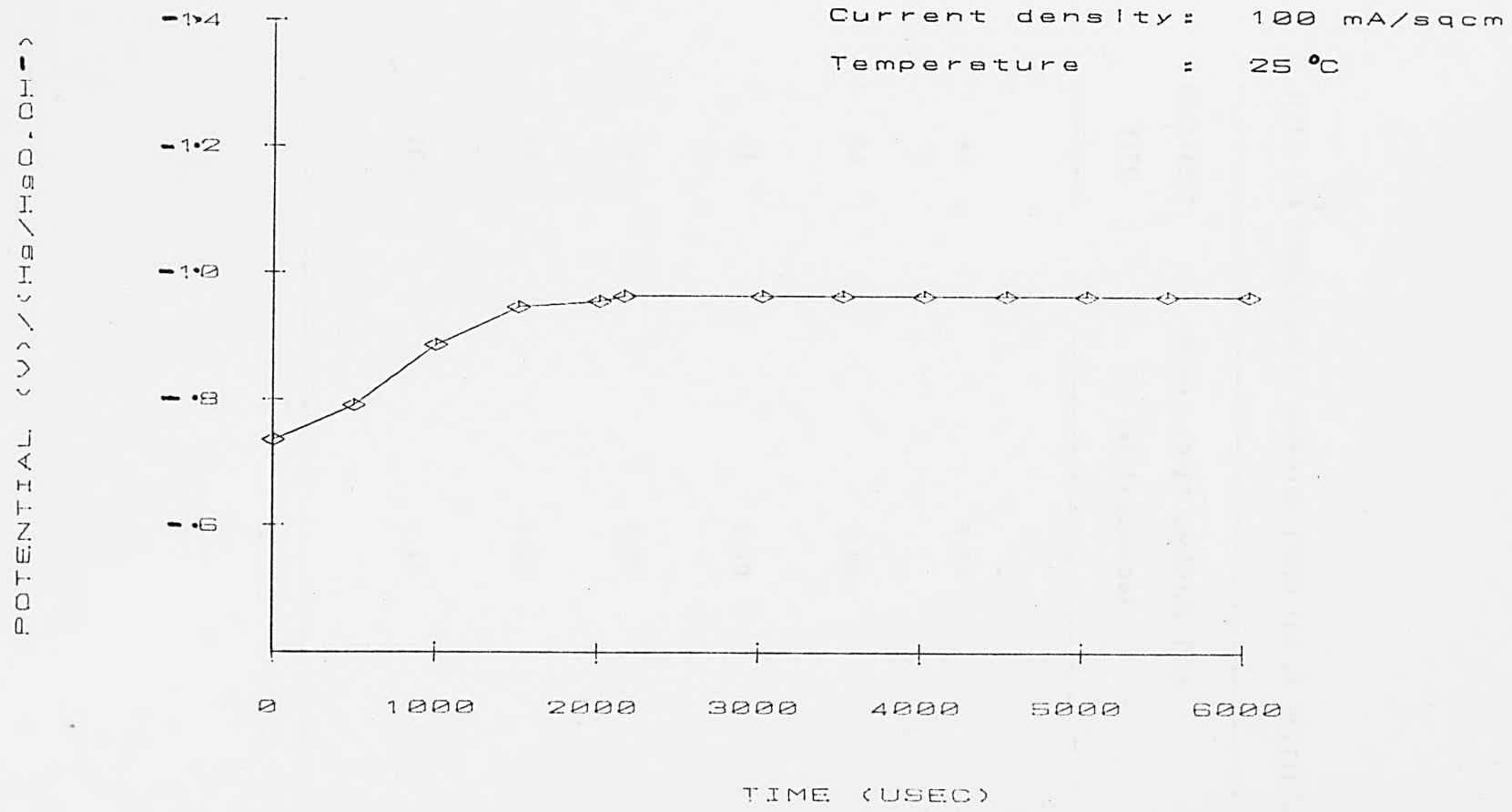

FIG. 4.21 TRANSIENT STATE GALVANOSTATIC POLARISATION OF ZS1

TABLE 4.4 DOUBLE LAYER CHARGING TIMES FOR A1 ELECTRODES

ELECTRODE TYPE	DOUBLE LAYER CHARGING TIME (milliseconds)
A1	2.30
Q4	2.00
Z1	2.10
Z2	2.25
Z3	2.20
ZS1	2.15

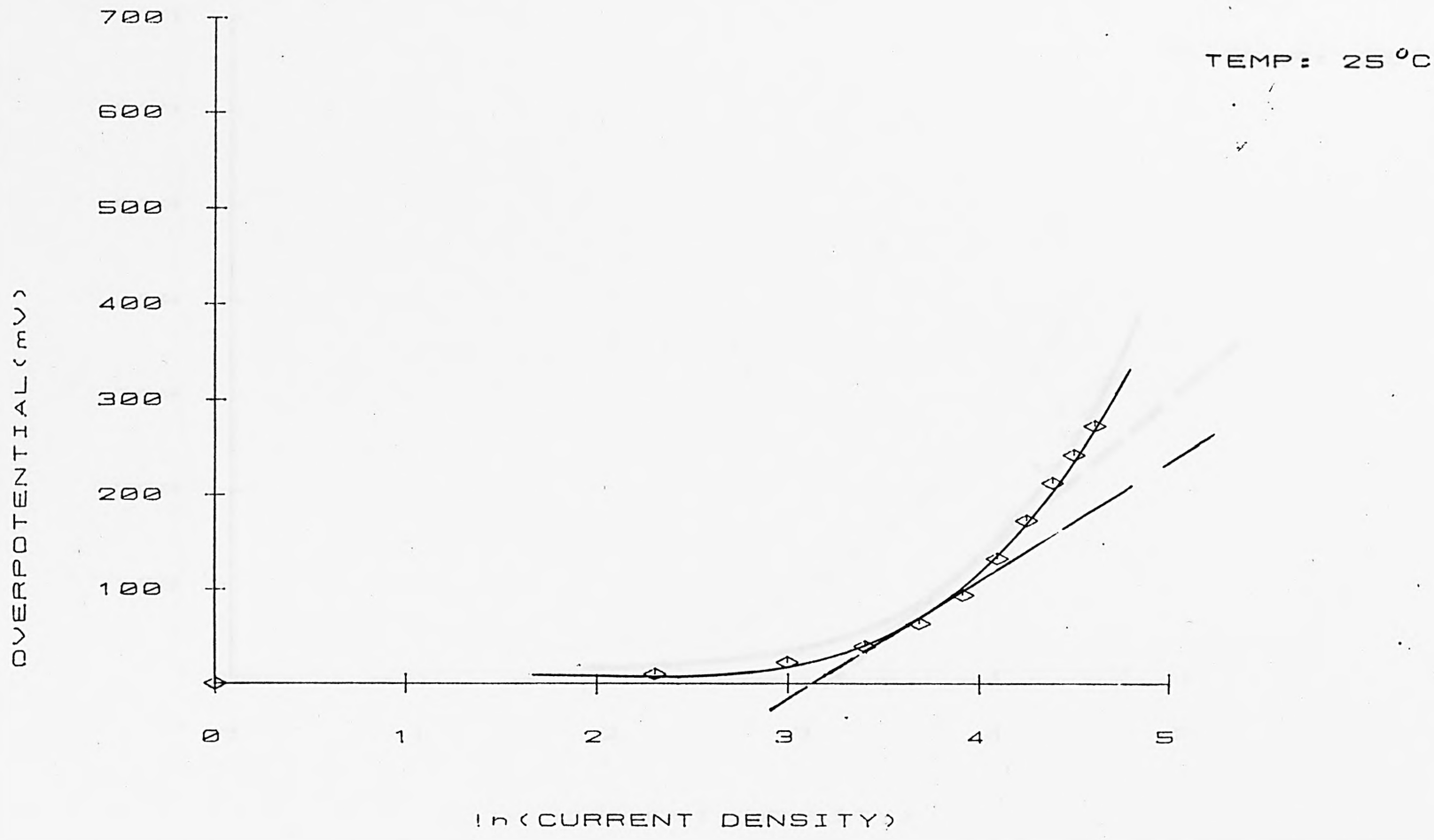

FIG. 4.22 TAFEL PLOT OF STEADY STATE POLARISATION OF Al

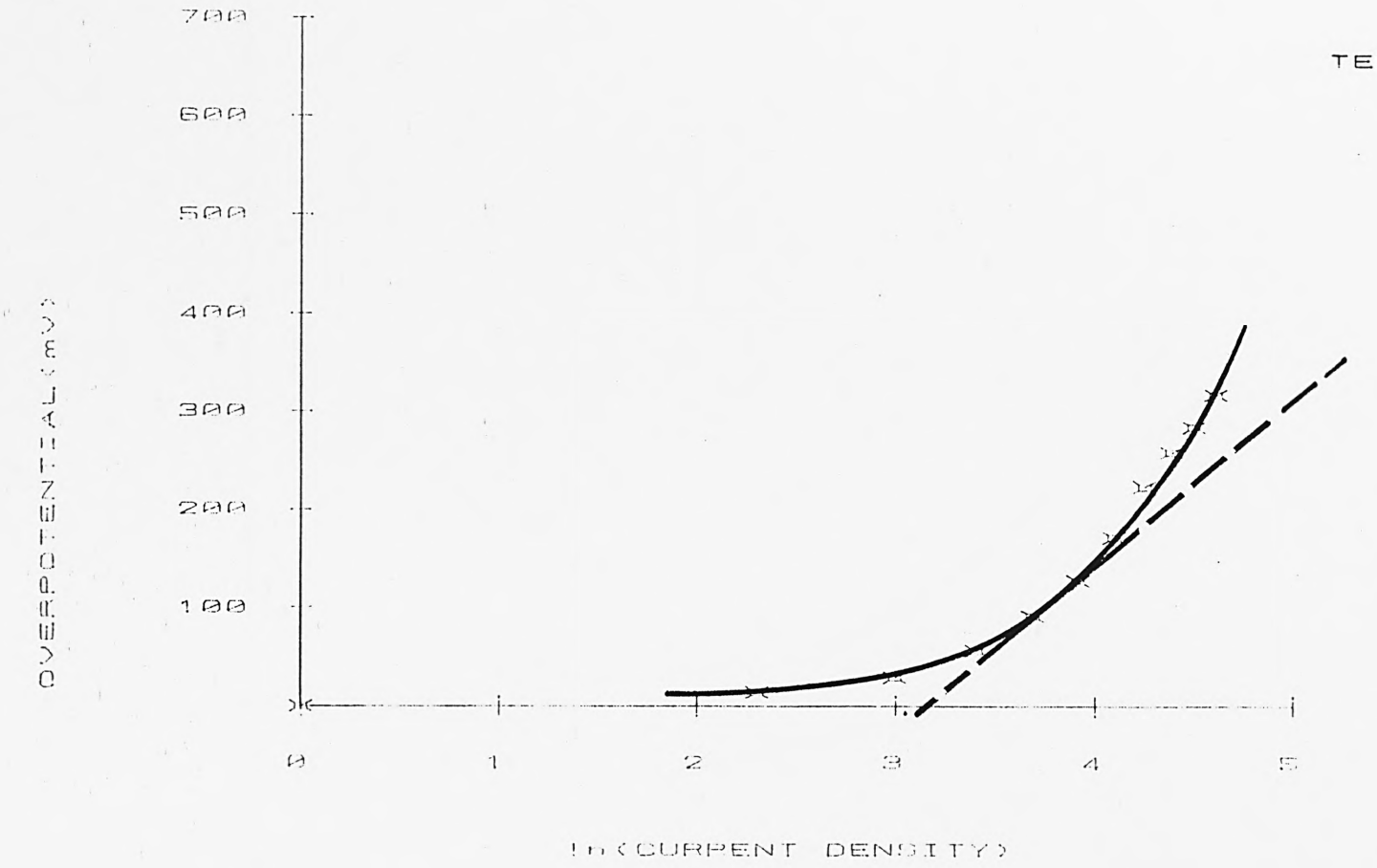

FIG. 4.23 TAFEL PLOT OF THE TRANSIENT STATE POLARISATION OF Al

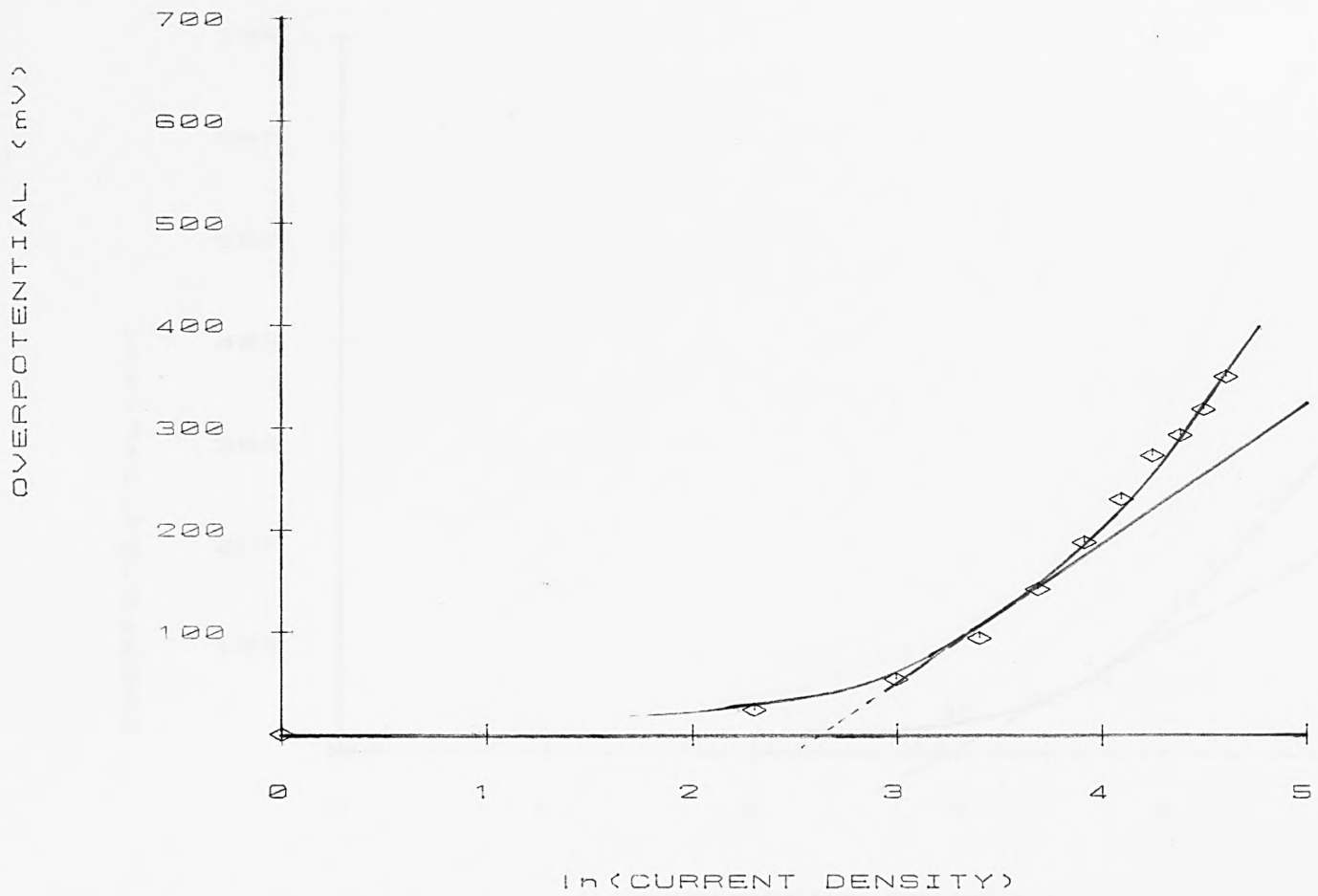

FIG. 4.24 TAFEL PLOT OF THE STEADY STATE POLARISATION OF Q4

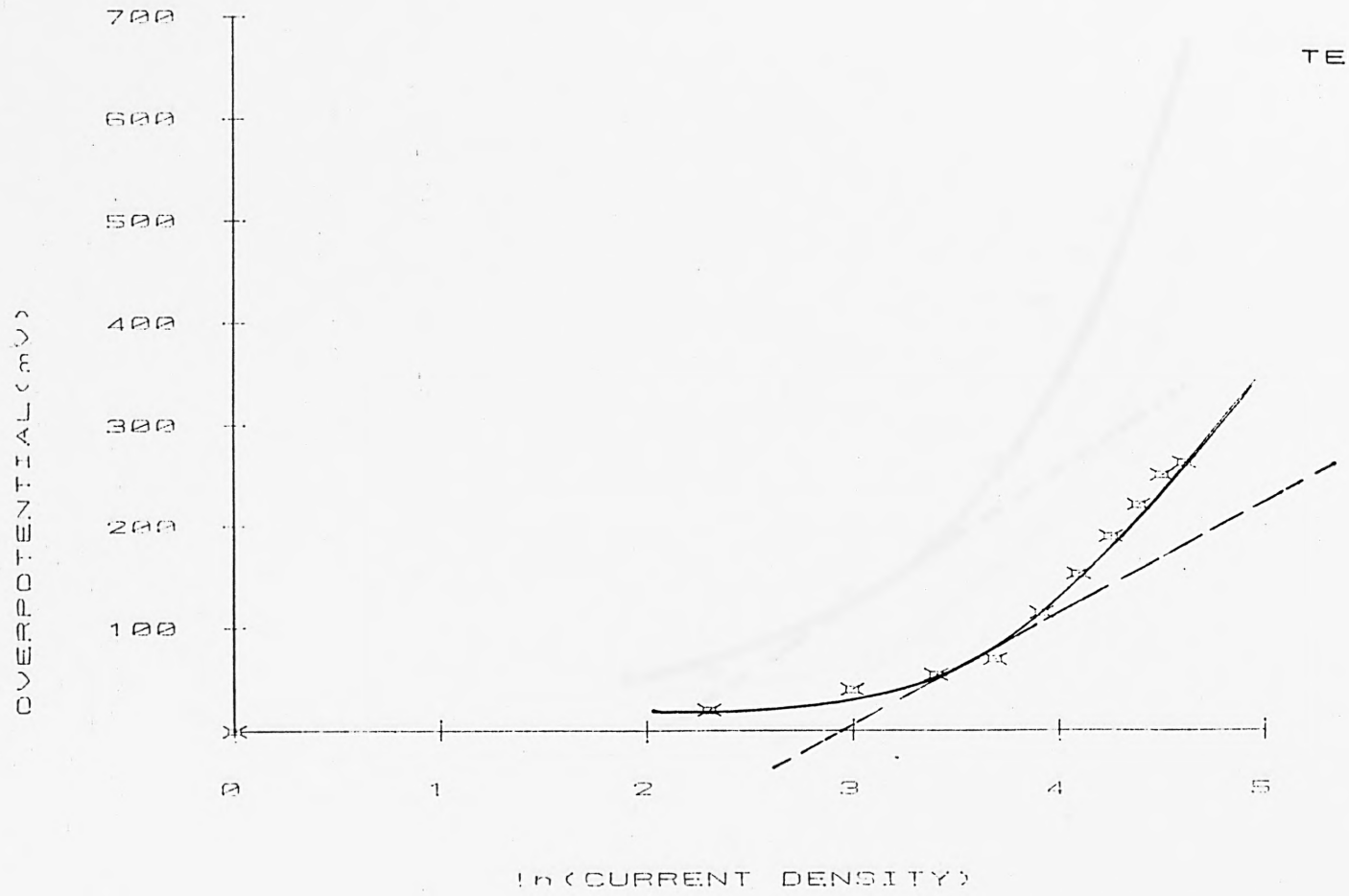

FIG. 4.25 TAFEL PLOT OF TRANSIENT STATE POLARISATION OF Q4

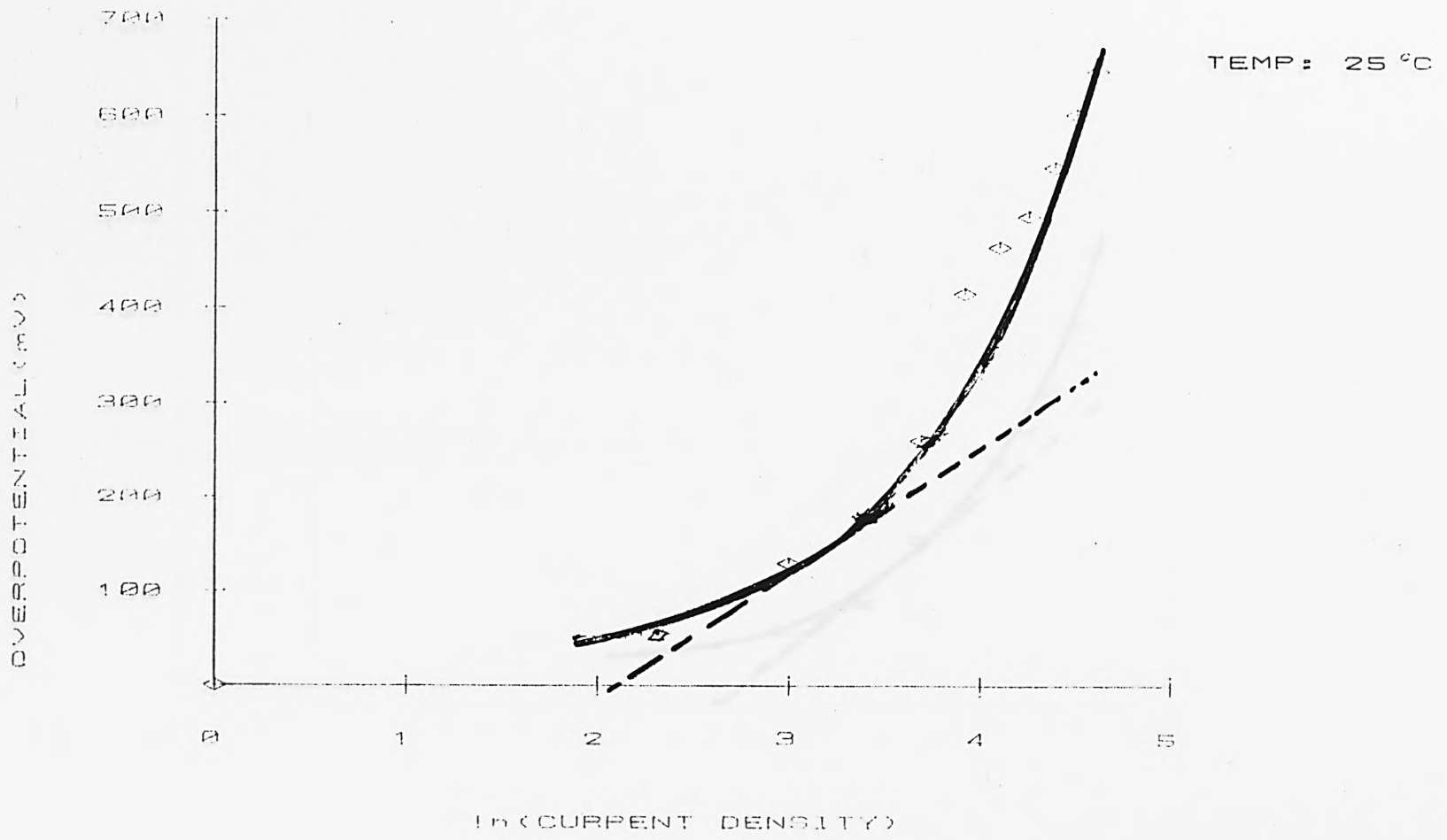

FIG. 4.26 TAFEL PLOT OF STEADY STATE POLARISATION OF Z1

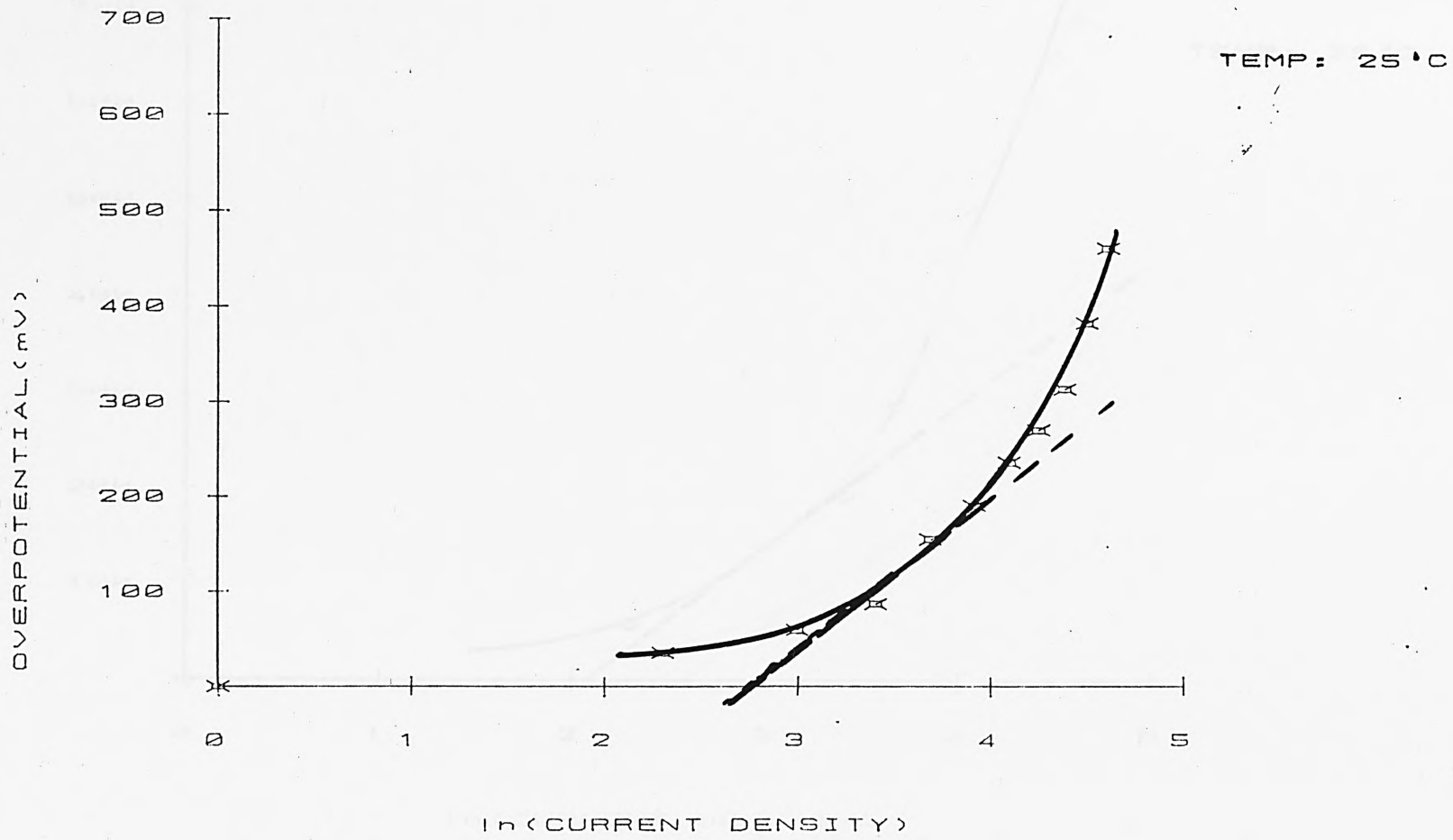

FIG. 4.27 TAFEL PLOT OF TRANSIENT STATE POLARISATION OF Z1

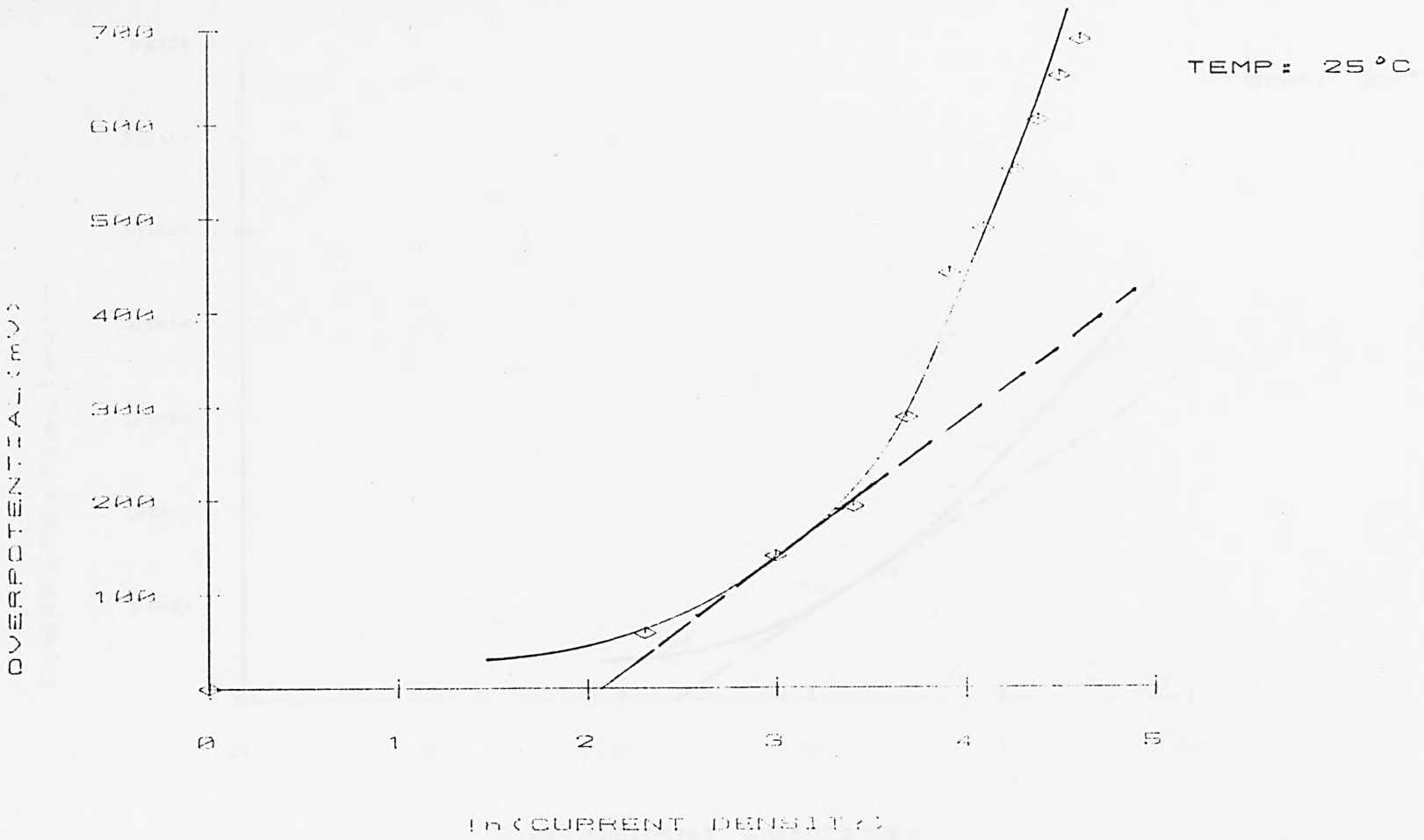

FIG. 4.28 TAFEL PLOT OF STEADY STATE POLARISATION OF Z2

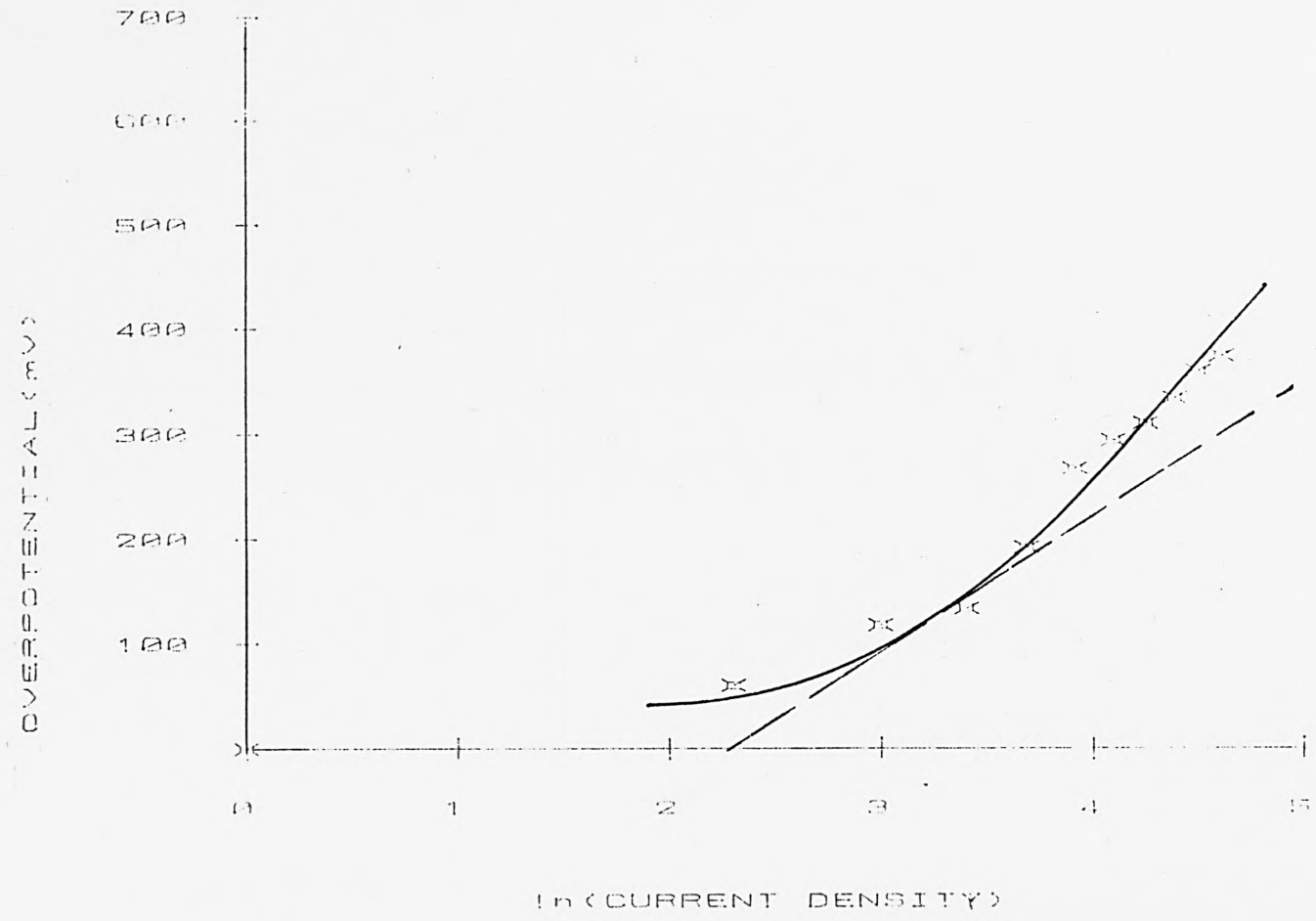

FIG. 4.29 TAFEL PLOT OF TRANSIENT STATE POLARISATION OF Z2

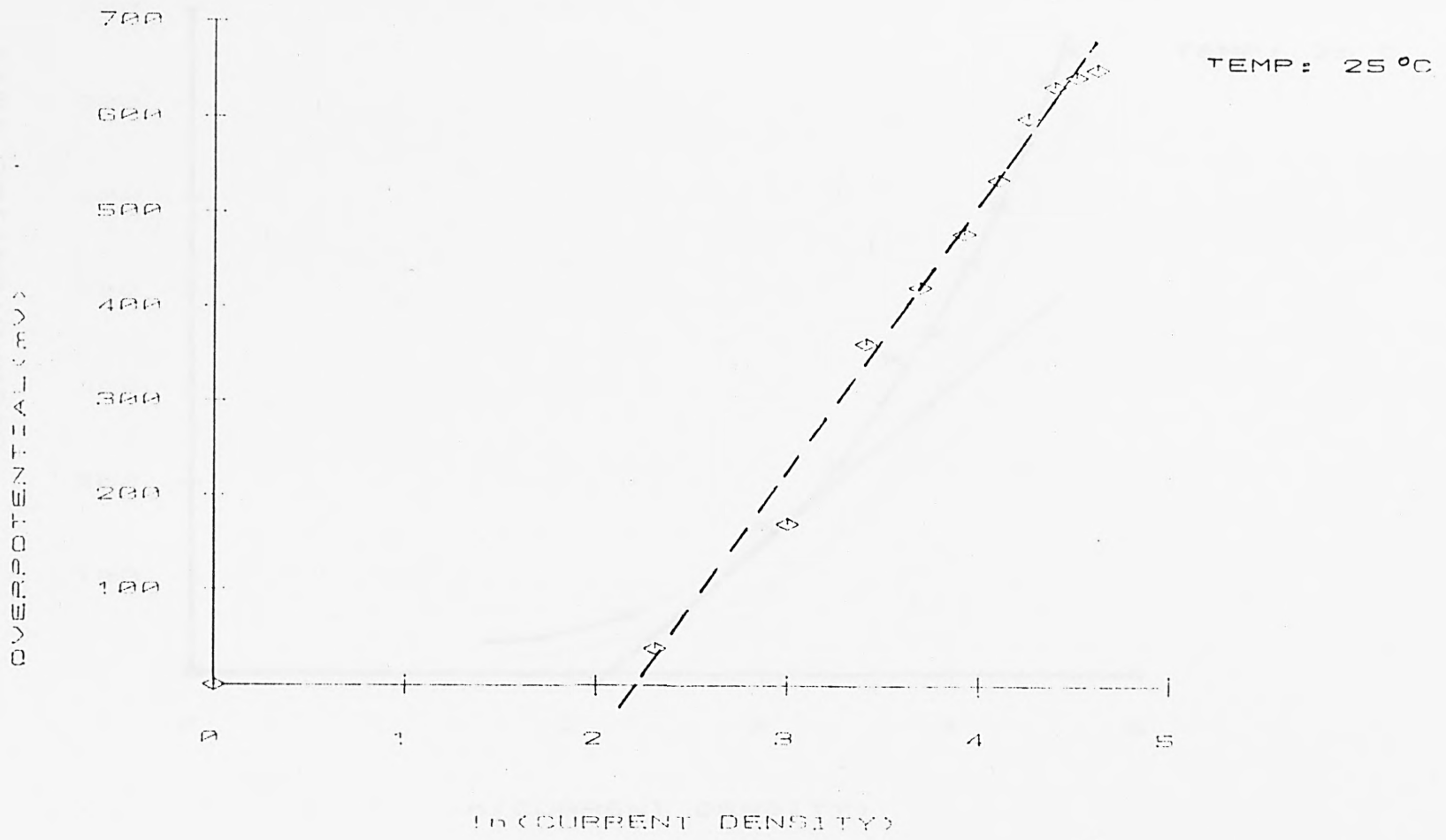

FIG. 4.30 TAFEL PLOT OF STEADY STATE POLARISATION OF Z3

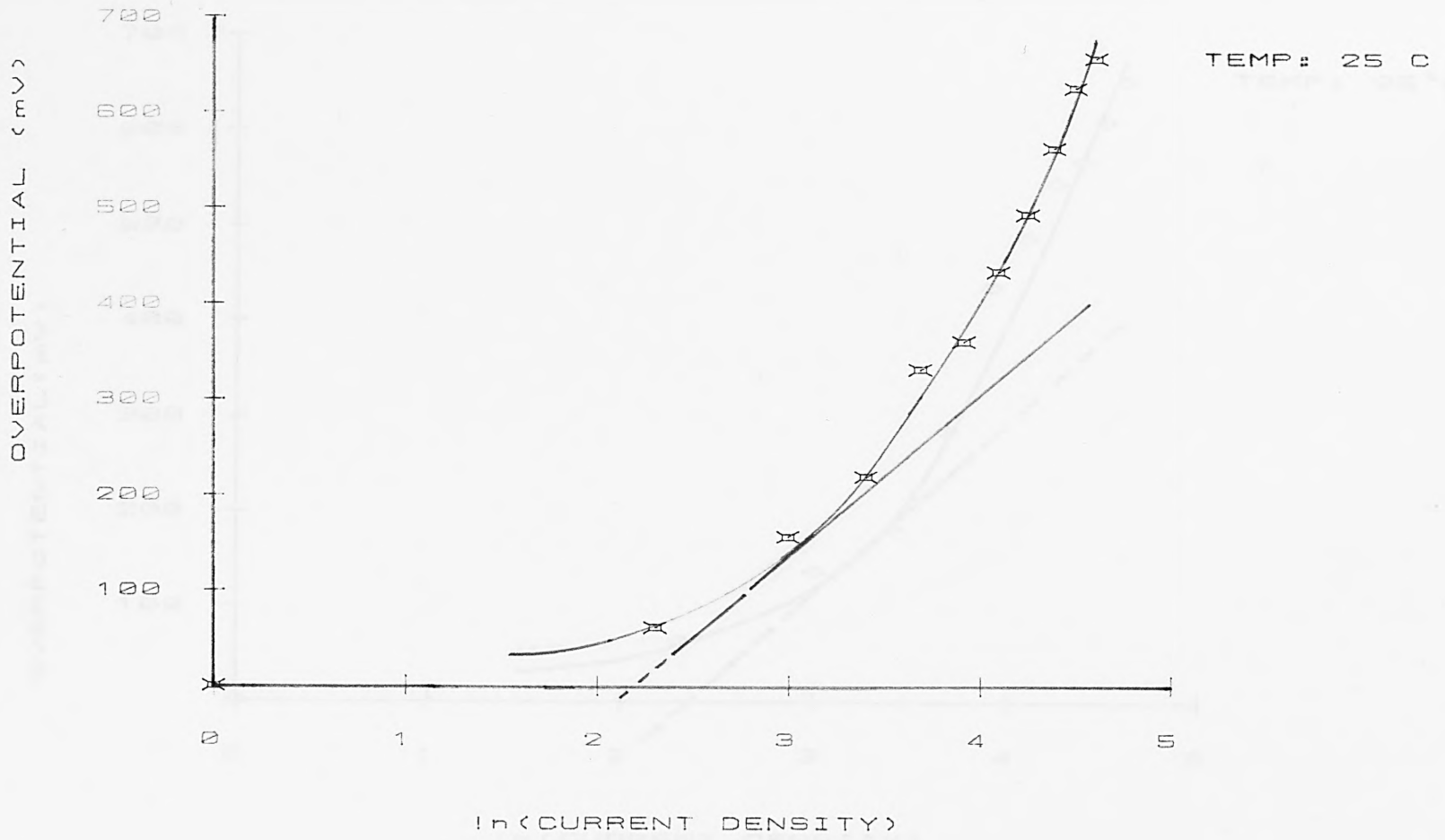

FIG. 4.31 TAFEL PLOT OF THE TRANSIENT STATE POLARISATION OF Z3

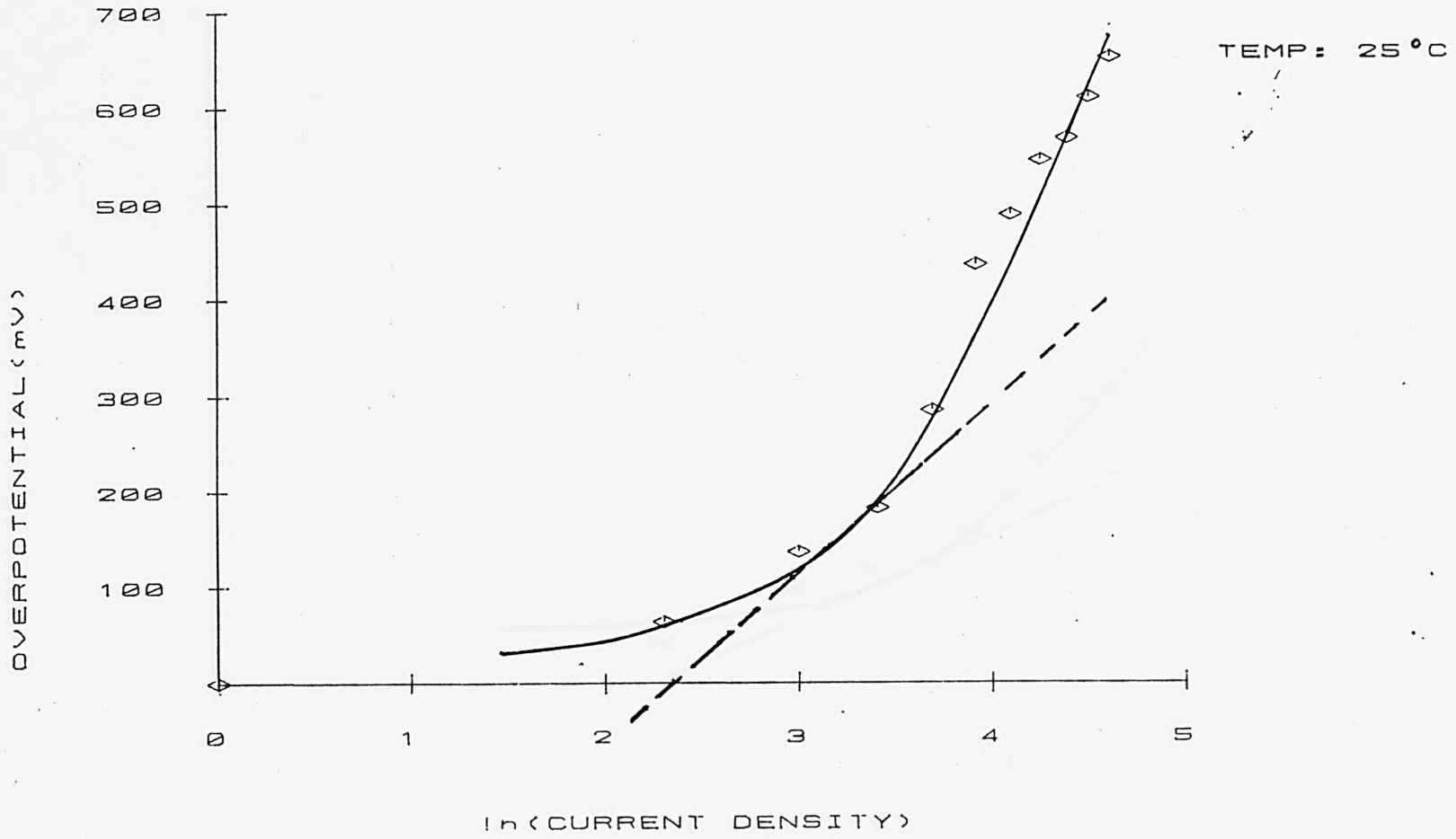

FIG. 4.32 TAFEL PLOT OF STEADY STATE POLARISATION OF ZS1

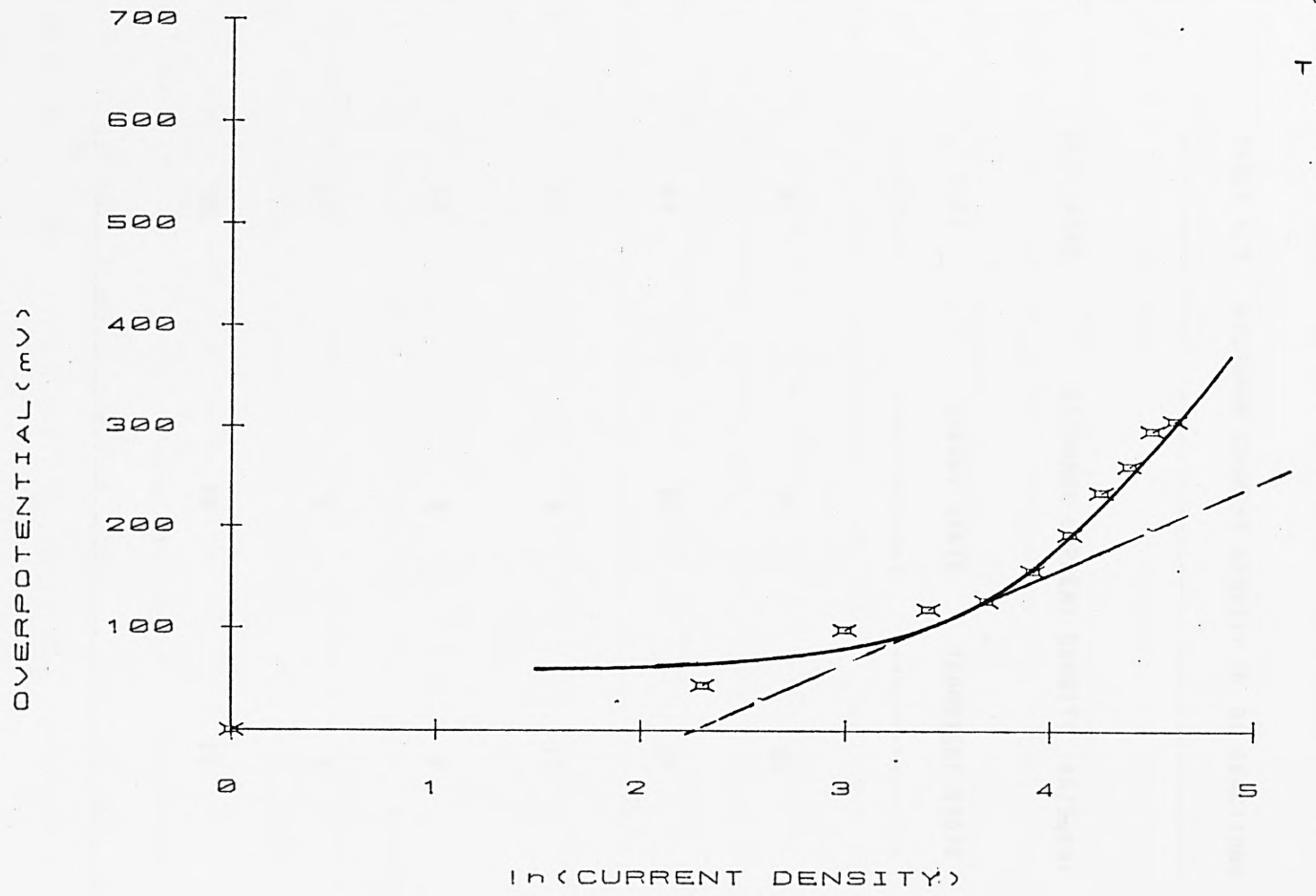

FIG. 4.33 TAFEL PLOT OF TRANSIENT STATE POLARISATION OF ZS1

TABLE 4.5 EXCHANGE CURRENT DENSITY OF Al REACTIONS

ELECTRODE TYPE	EXCHANGE CURRENT DENSITY (mA/Sqcm) STEADY STATE	TRANSIENT STATE
Al	21	22
Q4	20	20
Z1	8	15
Z2	8	8
Z3	8	9
ZS1	10	15

The transfer coefficients of the electrode reactions were ascertained from the slopes of the tangents drawn. In each case, the transfer coefficient was found to be around 0.9, much higher than the theoretical 0.5 for electrode reactions. Thus, it can only be said that the conventional Tafel plot is not useful in predicting the reaction mechanisms for aluminium reactions in concentrated solutions. This could be because there are probably different reaction mechanisms for each stage of polarisation, with respect to changing current densities.

However, the magnitude of the exchange current densities obtained, are indicative of the rapidity with which Al dissolution reactions, in strong electrolytes, occur. The differences in these values show which electrode undergoes a faster reaction and establishes the effect of concentration polarisation on the rate of reaction.

It can be seen that i_o is larger for the transient state measurements than for steady state measurements and that the extent is greater for alloys Zl and ZSl. The larger i_o for the transient state measurements infers that the rates of the electrochemical reactions are impeded by mass transfer limitations, the effect being greater for those two alloys owing to the relatively high concentration of Zn in these alloys.

4.3.2 ANODIC EFFICIENCY AND SELF-DISCHARGE CHARACTERISTICS

The data obtained from the anode utilisation tests are presented in Tables 4.6-4.11. These data were treated to find the percentage utilisation of each electrode, applying Faraday's law. The anodic efficiency, or % utilisation, of each electrode was defined as:

$$\%ut = [(IM/nF) * 60t / W] * 100$$
$$= [1.1192 * 10^{-3} t / W] * 100 \qquad (4.4)$$

where t is the time of discharge (in minutes) and W is the weight loss during discharge (in grams). The mean % utilisation of the three runs for each electrode was used to plot a histogram (Fig. 4.34). It can be seen that the utilisations of the electrodes are high and somewhat similar, the pure Al comparing favourably with the alloys.

The self-discharge characteristics of the electrodes were ascertained by measuring the amount of hydrogen evolved and the loss of active material at open-circuit. The results obtained are presented in Tables 4.12-4.17 and in Fig. 4.34. Tables 4.12-4.17 show the data for the material loss during self-discharge. The mean of the three runs for each electrode is presented as the corrosion rate of the respective electrode. The data was treated to find the amount of charge lost (in Ah) owing

TABLE 4.6 UTILISATION OF Al IN 5M KOH

	1ST RUN	2ND RUN	3RD RUN
WT CONSUMED (g)	.3466	.305	.3034
D'CHARGE TIME(MIN)	284	256	251
UTILISATION (%)	91.7	93.9	92.6

MEAN % UTILISATION 92.7

TABLE 4.7 UTILISATION OF Q4 IN 5M KOH

	1ST RUN	2ND RUN	3RD RUN
WT CONSUMED (g)	.2189	.2984	.3268
D'CHARGE TIME(MIN)	190	252	280
UTILISATION (%)	97.1	94.5	95.9

MEAN % UTILISATION 95.8

TABLE 4.8 UTILISATION OF Z1 IN 5M KOH

	1ST RUN	2ND RUN	3RD RUN
WT CONSUMED (g)	.2396	.233	.3968
D'CHARGE TIME(MIN)	202	194	287
UTILISATION (%)	94.4	93.2	81

MEAN % UTILISATION 89.5

TABLE 4.9 UTILISATION OF Z2 IN 5M KOH

	1ST RUN	2ND RUN	3RD RUN
WT CONSUMED (g)	.2118	.2368	.2846
D'CHARGE TIME(MIN)	182	206	250
UTILISATION (%)	96.2	97.4	98.3

MEAN % UTILISATION 97.3

TABLE 4.10 UTILISATION OF Z3 IN 5M KOH

	1ST RUN	2ND RUN	3RD RUN
WT CONSUMED (g)	.2832	.2288	.2452
D'CHARGE TIME(MIN)	246	197	208
UTILISATION (%)	97.2	96.4	95
MEAN % UTILISATION			96.2

TABLE 4.11 UTILISATION OF ZS1 IN 5M KOH

	1ST RUN	2ND RUN	3RD RUN
WT CONSUMED (g)	.2543	.266	.245
D'CHARGE TIME(MIN)	220	236	214
UTILISATION (%)	96.8	99.3	97.8
MEAN % UTILISATION			97.7

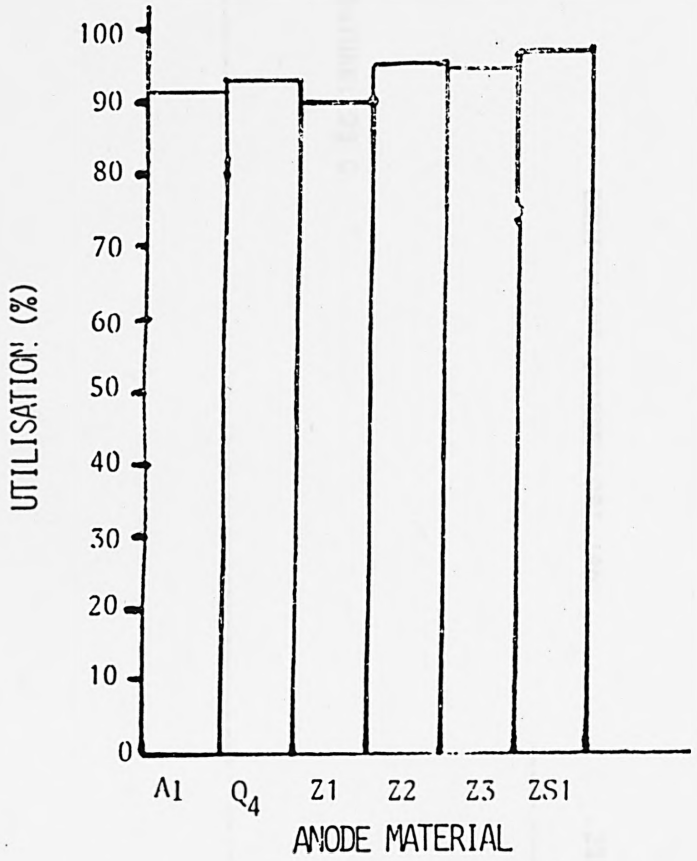

a) coulombic efficiency

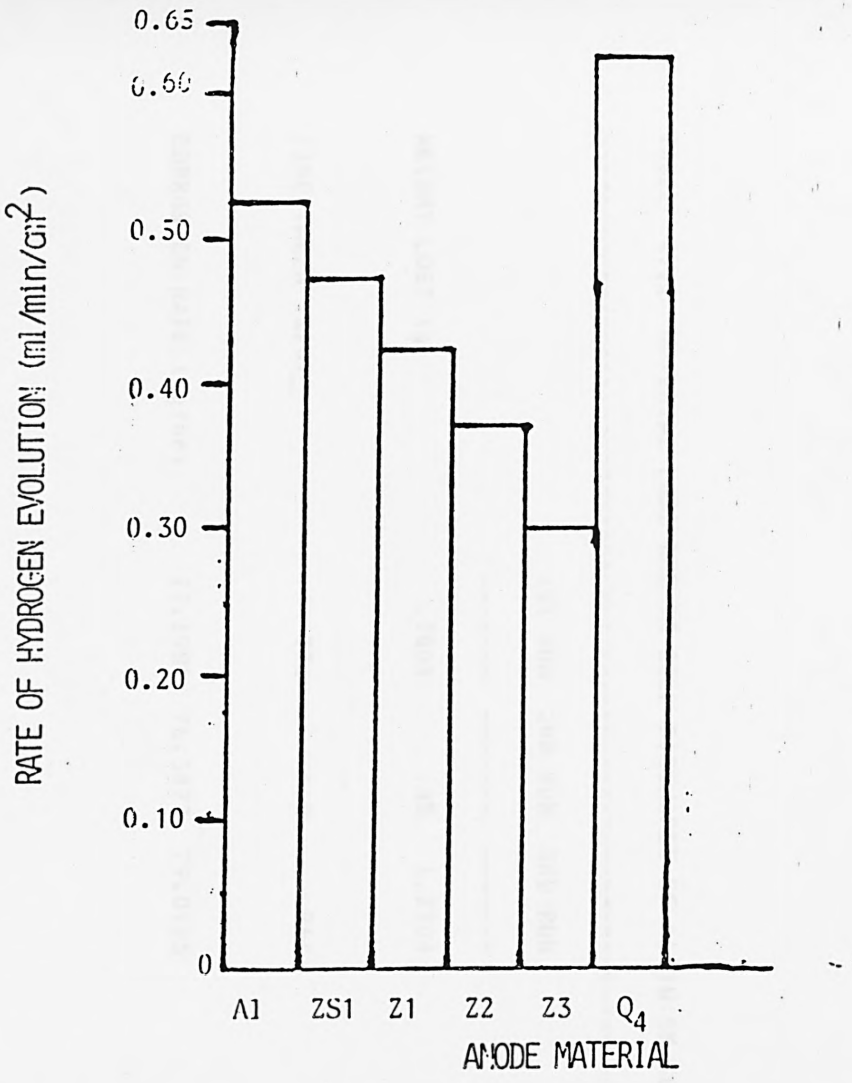

b) Hydrogen Evolution

FIG. 4.34 ANODIC EFFICIENCY AND SELF-DISCHARGE CHARACTERISTICS OF Al AND ITS ALLOYS IN 5M KOH

TABLE 4.12 MATERIAL LOSS DUE TO SELF-DISCHARGE OF Al IN 5M KOH

	1ST RUN	2ND RUN	3RD RUN
WEIGHT LOST (g)	.3804	.85	1.2704
TIME TAKEN (min)	296	668	964
CORROSION RATE (mg/hr)	77.1081	76.3473	79.0705

MEAN CORROSION RATE 77.5086 mg/hr

EQUIVALENT CHARGE LOST (Ah) .233

TEMPERATURE: 25 C

TABLE 4.13 MATERIAL LOSS DUE TO SELF-DISCHARGE OF Q4 IN 5M KOH

	1ST RUN	2ND RUN	3RD RUN
WEIGHT LOST (g)	.4651	1.1396	2.246
TIME TAKEN (min)	234	548	978
CORROSION RATE (mg/hr)	119.2564	124.7737	137.7914

MEAN CORROSION RATE 127.2738 mg/hr

EQUIVALENT CHARGE LOST (Ah) .382

TEMPERATURE: 25 C

TABLE 4.14 MATERIAL LOSS DUE TO SELF-DISCHARGE OF Z1 IN 5M KOH

	1ST RUN	2ND RUN	3RD RUN
WEIGHT LOST (g)	.2427	.5704	.894
TIME TAKEN (min)	249	648	980
CORROSION RATE (mg/hr)	58.4819	52.8148	54.7347

MEAN CORROSION RATE 55.3438 mg/hr

EQUIVALENT CHARGE LOST (Ah) .166

TEMPERATURE: 25 C

TABLE 4.15 MATERIAL LOSS DUE TO SELF-DISCHARGE OF Z2 IN 5M KOH

	1ST RUN	2ND RUN	3RD RUN
WEIGHT LOST (g)	.1812	.4312	.6728
TIME TAKEN (min)	210	664	944
CORROSION RATE (mg/hr)	51.7714	38.9639	42.7627

MEAN CORROSION RATE 44.4993 mg/hr

EQUIVALENT CHARGE LOST (Ah) .134

TEMPERATURE: 25 C

TABLE 4.16 MATERIAL LOSS DUE TO SELF-DISCHARGE OF Z3 IN 5M KOH

	1ST RUN	2ND RUN	3RD RUN
WEIGHT LOST (g)	.1668	.3832	.6056
TIME TAKEN (min)	225	656	956
CORROSION RATE (mg/hr)	44.48	35.0488	38.0084

MEAN CORROSION RATE 39.1791 mg/hr

EQUIVALENT CHARGE LOST (Ah) .118

TEMPERATURE: 25 C

TABLE 4.17 MATERIAL LOSS DUE TO SELF-DISCHARGE OF ZS1 IN 5M KOH

	1ST RUN	2ND RUN	3RD RUN
WEIGHT LOST (g)	.1296	.3508	.5236
TIME TAKEN (min)	204	652	924
CORROSION RATE (mg/hr)	38.1177	32.2822	34

MEAN CORROSION RATE 34.8 mg/hr

EQUIVALENT CHARGE LOST (Ah) .105

TEMPERATURE: 25 °C

to the self-discharge of each electrode. The amount of charge lost was obtained as follows:

$$\text{Charge lost (Ah)} = 60W / 0.333t \qquad (4.5)$$

where W is the weight (g) of material lost on self-discharge and t is the time (min) of self-discharge.

Alloy Q4 is found to lose a lot more charge than the other electrodes. This can be attributed to the instability of the adherent oxide film on the surface of the alloy compared to the stability of the ZnO film formed on alloys Z1, Z2, Z3 and ZS1. The presence of Zn in the alloys can be said to be favourable in arresting self-discharge, in terms of material loss.

Figure 4.34 shows the rate of hydrogen gas evolution on each electrode. As expected, the amount of gas evolved on Q4 was more than that evolved on pure Al and the other alloys. The large amount of hydrogen gas evolved, on each electrode, can be attributable to the presence of Fe and Cu in the alloys. These metals have very low corrosion stability in concentrated alkaline solutions. Their presence in the alloy lattice, creates an electron source for the electrochemical reduction of water and the consequent evolution of hydrogen:

$$3e + 3H_2O \text{ --- } 3OH^- + 1.5H_2$$

4.3.3 DATA REPRODUCIBILITY

All the experiments above were repeatedly conducted for each electrode as shown by the tables in Appendix B. The data obtained from the polarisation measurements, even though fluctuating, are reproducible within 10 mV. The results for the anodic efficiency and self-discharge tests virtually agree, within experimental error.

SOURCES OF ERROR

For absolute data, the errors to be accounted for will mainly be due to human and instrumental errors. Errors might have been inherrented from the type of instruments used for the polarisation measurements, with respect to their ability to reproduce each measurement and the degree of influence of ambient condtions on this ability. Similarly, for measurements invloving weights, errors might have been inherrented from the scales used. And for the gas measurements, the effect of water vapour pressure and gas solubility will be significant.

However, since the results were discussed comparatively, these errors which would have been replicated for each electrode measurements will cancel

out. Thus, the results obtained are correct for each one electrode with respect to the other.

4.4 CONCLUSION

The passivating oxide film on the surface of pure aluminium is reduced by alloying. The alloy-mix, is of a significant importance in the performance of the anode. Al-Zn alloy is found to have relatively little self-discharge, but tend to passivate at high current densities. The addition of Ga or In to the Al-Zn alloy improves its anodic performance. However, this performance is subdued if the concentration of Zn in the alloy is high (say, > 4%). Thus, even though Zn is indispensable for the improvement of the electrode properties of Al, the amount of Zn added must be closely controlled.

However, Alloy Q4 performs very well at high current densities with a high utilisation. But, the alloy has a very high self-discharge with the evolution of a relatively large amount of hydrogen. This is attributable to the comparatively high concentration of Fe present in the alloy. Thus, to reduce the rate of self-discharge, the concentration of Fe must be kept to a minimum.

Overall, Q4 is the best of all the alloys tested. The

problem of self-discharge, resulting in the loss of capacity under standby conditions can be averted by withdrawing the electrolyte from the cell, automatically, whenever power is not required and put back when needed. The hydrogen evolved can be suppressed by adding inhibitors to the electrolyte, to at least coat the surfaces of the Fe and Cu atoms in the alloys. The next chapter investigates the possibility of suppressing the hydrogen evolution in this manner.

5 SUPPRESSION OF PARASITIC HYDROGEN EVOLUTION ON ALUMINIUM

5.1 INTRODUCTION

The object of this project requires that a high current density is obtained from the anodic dissolution of aluminium. But pure aluminium is found to be somehow passive in alkaline electrolytes. To reduce the passivity, the aluminium is alloyed. However, the breakdown of the passive film on the aluminium surface and the presence of Fe and Cu, mainly as impurities, result in the anodic dissolution of the active material and a concomitant hydrogen evolution which occurs simultaneously:

$$Al + 3OH^- \text{ --- } Al(OH)_3 + 3e$$

$$3e + 3H_2O \text{ --- } 3OH^- + 1.5H_2$$

The reaction site can be considered as an electron-sink area at which de-electronation occurs, an electron-source area at which electronation occurs and an ionic conductor that functions as the medium for electrodic reactions. Such a system is like a short-circuited, self-driving cell with hydrogen

evolution and oxygen reduction as the most common cathodic (electronation) reactions. Which of these two reactions predominate in setting up a corrosion cell is decided as that which gives the largest corrosion current under the circumstances (which depends on the metal, temperature, pH, etc.).

Hydrogen deposited upon a metal surface in the course of corrosion reaction may diffuse inside it. A metal nearly always contains voids, of the order of a few tens of nanometres in length and perhaps several nanometers in the other two dimensions [154]. When H diffuses inside the metal to the walls of these voids, it adsorbs on their surface and passes into the voids. Once inside, it is molecular hydrogen, H_2. Within the void, the hydrogen builds up to a high pressure, which may exceed the limiting 'spreading pressure' of the metal constituting the walls of the void, the void then starts to spread. If such events occur in one void, they will occur in many. And if, in the course of spreading, they join up, the metal loses strength and tears. The utilisation of the anode material is then reduced. Also, when the hydrogen escapes from the metal surface it poses design, health and safety problems especially for applications in enclosed environments. There is the need therefore to suppress the hydrogen evolution.

To alleviate the problem, consider the following equation [155]:

$$I_{corr} = \left[I_{0,1} I_{0,2} \right]^{1/2} \exp\left[\frac{F(E_2 - E_1)}{4RT} \right] \qquad (5.1)$$

The equation indicates that the corrosion current can be reduced by diminishing the product ($I_{0,1}$ $I_{0,2}$); this is called corrosion inhibition [156,157]. Thus it turns out experimentally that the exchange current, $I_{0,2}$, of the electronation reaction can be reduced by adding, for example, arsenic or antimony compounds to the solution. These compunds adsorb on cathodic sites and reduce the rate of the cathodic reaction (particularly if this is hydrogen evolution) in the corrosion couple [158]. If the electronation or cathodic reaction is oxygen reduction, then a simple way to reduce the corrosion rate is to reduce the concentration of dissolved oxgyen. One way is to simply displace the air-dissolved oxygen from the solution by bubbling nitrogen through it. A similar approach can be made to reducing the reactivity of the anodic sites [159]. Here, substances which adsorb on the electron-sink areas and reduce $I_{0,1}$ can be added to solution. Another way to reduce the I_0 values is to reduce the available metal areas, by adding substances to the solution which form a film on the metal surface.

An investigation was, therefore, directed towards the search for an effective inhibitor to suppress the

hydrogen evolution reaction on the Al anode. The suitable inhibitor should suppress the hydrogen evolution without passivating the alloy.

The first part of the investigation was carried out with the object of finding the suitable inhibitors that do not passivate the alloy. Upon the success of this investigation, a further investigation to measure the amount of hydrogen evolved using the suitable inhibitors was intended. Only then will the choice of inhibitor be made. Substances with high hydrogen overvoltage and somewhat soluble in alkaline electrolytes were selected for testing.

5.2 EXPERIMENTAL

5.2.1 SELECTION OF INHIBITORS

Different concentrations of inhibitors, 0.01%, 0.1%, 1% and 2% by weight with respect to KOH, were added, in turn, to KOH pellets. The resulting mixture was dissolved in de-ionised/distilled water, sufficient enough to prepare a 5M solution. The solutions prepared were allowed to stand overnight to ensure that all undissolved particulate matter settled down before use. The inhibitors tested for, were mainly lead, phosphate,

nitrates, amines, sulphur, flouride, antimony, thallium, tin and cadmium compounds.

2 cm^2 of a 0.4 mm thick Al alloy (Q4) strip was prepared and immersed in the respective electrolyte solutions. The half-cell testing procedure was carried out. The IR drop at each selected current density was measured and used to correct for the potential reading at the selected current density.

The polarisation characteristics of the alloy in the presence of the various inhibitors were recorded and plots of potential against current density were made. All the experiments were carried out at 25°C .

5.2.2 EFFICIENCY OF SELECTED INHIBITOR(S) AS HYDROGEN EVOLUTION SUPPRESSANT(S)

The test solution was poured into a special test cell (Fig. 5.1) and immersed in a water bath maintained at the required temperatures (25 and 40°C). A test electrode was freshly prepared and immersed in the test solution. The test cell was completely sealed and a steady current density of 100 mA/cm^2 was passed through and the gas evolved was collected. After a noted time period, the amount of gas evolved was recorded.

The experiment was repeated for zero current. This

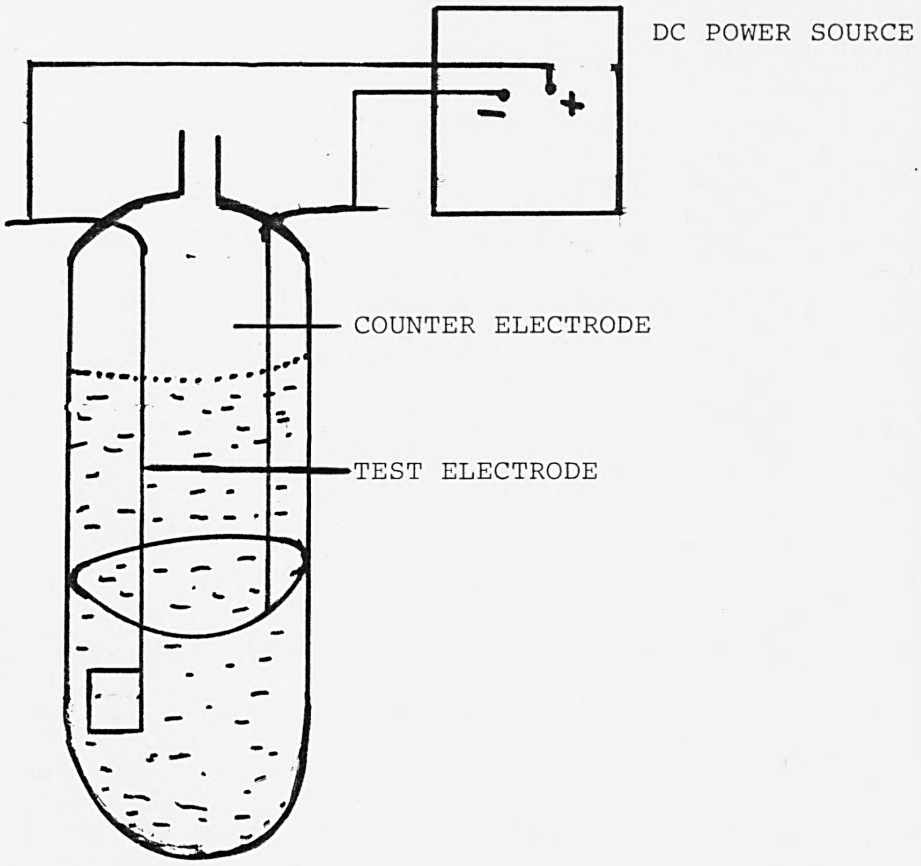

FIG. 5.1 SPECIAL TEST CELL FOR HYDROGEN EVOLUTION MEASUREMENTS

time the special test tube shown in Fig. 4.1 was used. The test electrode was freshly prepared as above, but weighed before placing into the solution. The test tube was completely sealed and the gas evolved was collected as described above. The electrode was removed from solution, washed in acetone under ultrasonic vibration, and wiped dry with a soft tissue and weighed again. The difference in weight was recorded, alongside the period of time the electrode had been in solution. The above experiments were carried out in triplicates.

5.2.3 MECHANISM OF HYDROGEN SUPPRESSION

The surfaces of the test electrodes polarised in the half-cell testings were examined using the scanning electron microscopy and X-ray flourescence techniques. Both the surface of the alloy before polarisation and after polaristion in the presence of the different inhibitors were examined. The change in the surface morphology was then analysed.

5.2.4 ANODIC EFFICIENCY AND DISCHARGE CHARACTERISTICS USING SELECTED INHIBITOR(S)

Electrode utilisation tests were carried out by preparing the test electrode as for half-cell testing. The

electrode was weighed and then immersed in the test electrolyte whilst passing through a steady current of 200 mA. The time for immersion was noted and after a considerable discharge period, the electrode was retrieved and weighed. The weight loss was noted alongside the period of discharge. The potential response with respect to time was recorded. The IR drop was measured at every ten minutes. A plot of the IR corrected potential versus discharge time was then made. The electrode was also polarised under potentiodynamic and galvanostatic transient state regimes.

5.3 RESULTS AND DISCUSSION

5.3.1 SELECTION OF INHIBITORS

The mean of the data obtained for the three polarisation runs for the performance of Q4 in the presence of the different inhibitors, at varying inhibitor-to-KOH concentration, were used to plot graphs of potential versus current density (Figs. 5.2-5.5). The plots show the polarisation characteristics of the anode in the presence of the hydrogen evolution inhibitors. It can be seen from the curves that as the concentration of inhibitors increase, they tend to passivate the alloy. Mercuric oxide can be seen as the best inhibitor, with

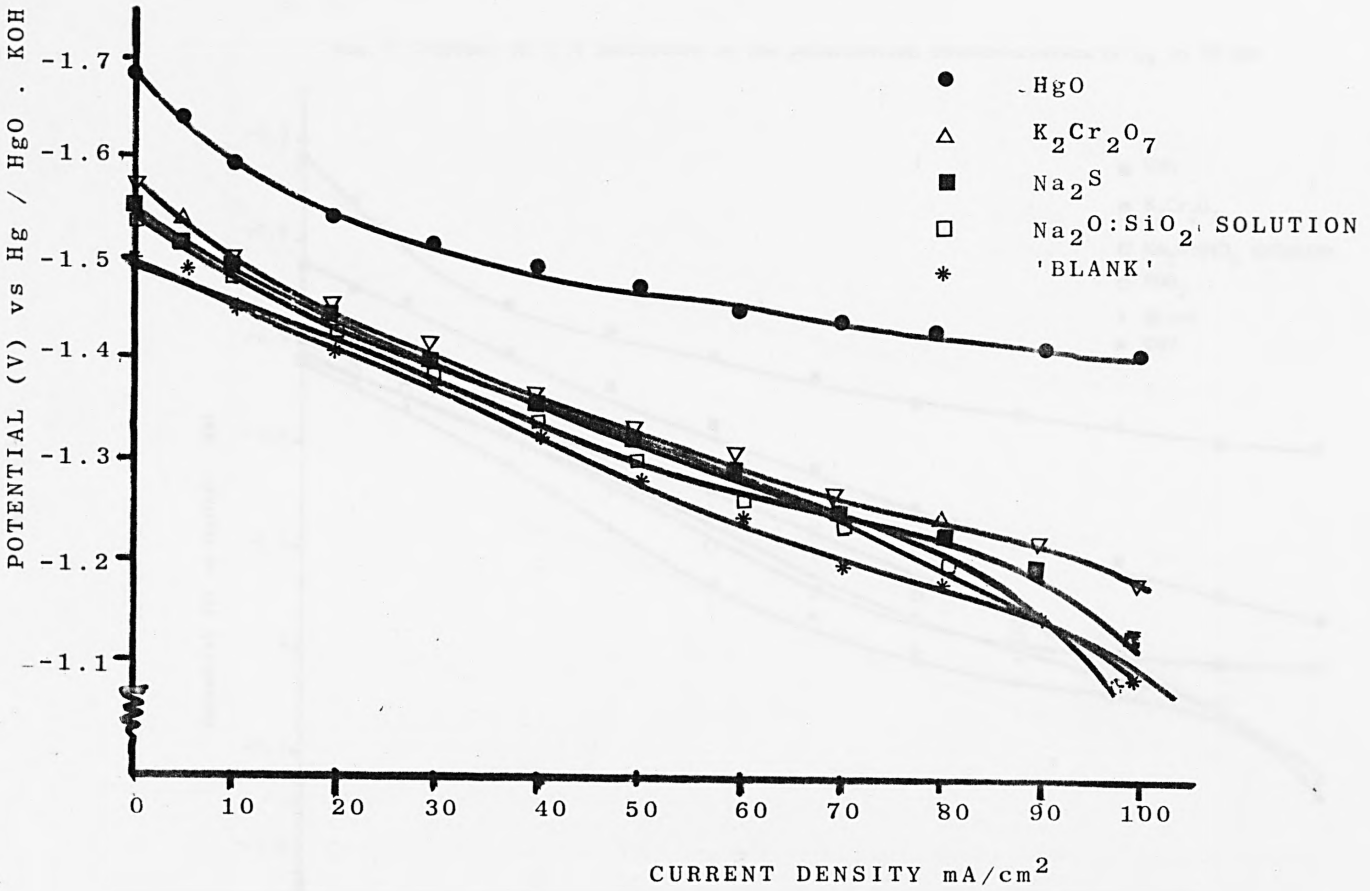

FIG. 5.2 EFFECT OF 0.01% INHIBITORS ON THE POLARISATION OF Q4

Fig. 5.3 Effect of 0.1% inhibitors on the polarisation characteristics of Q_4 in 5M KOH

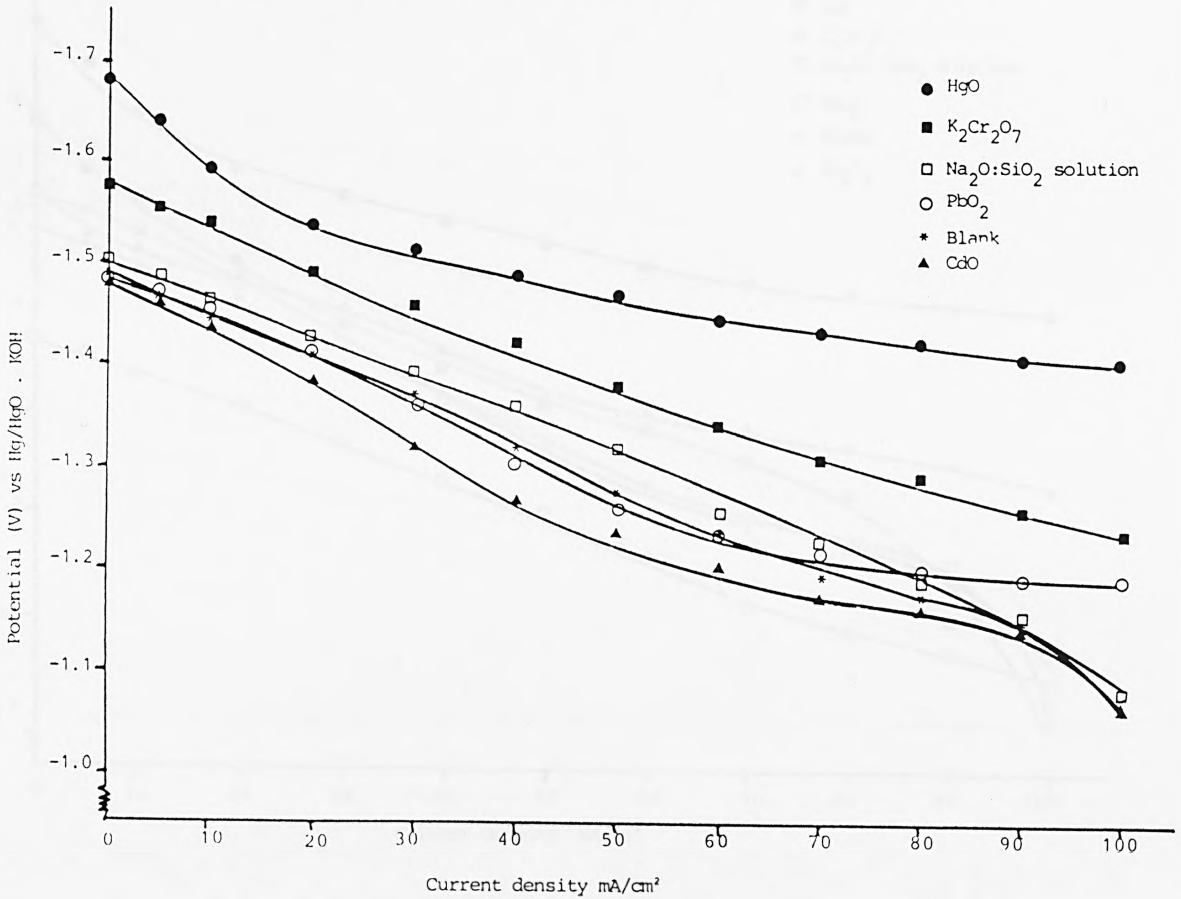

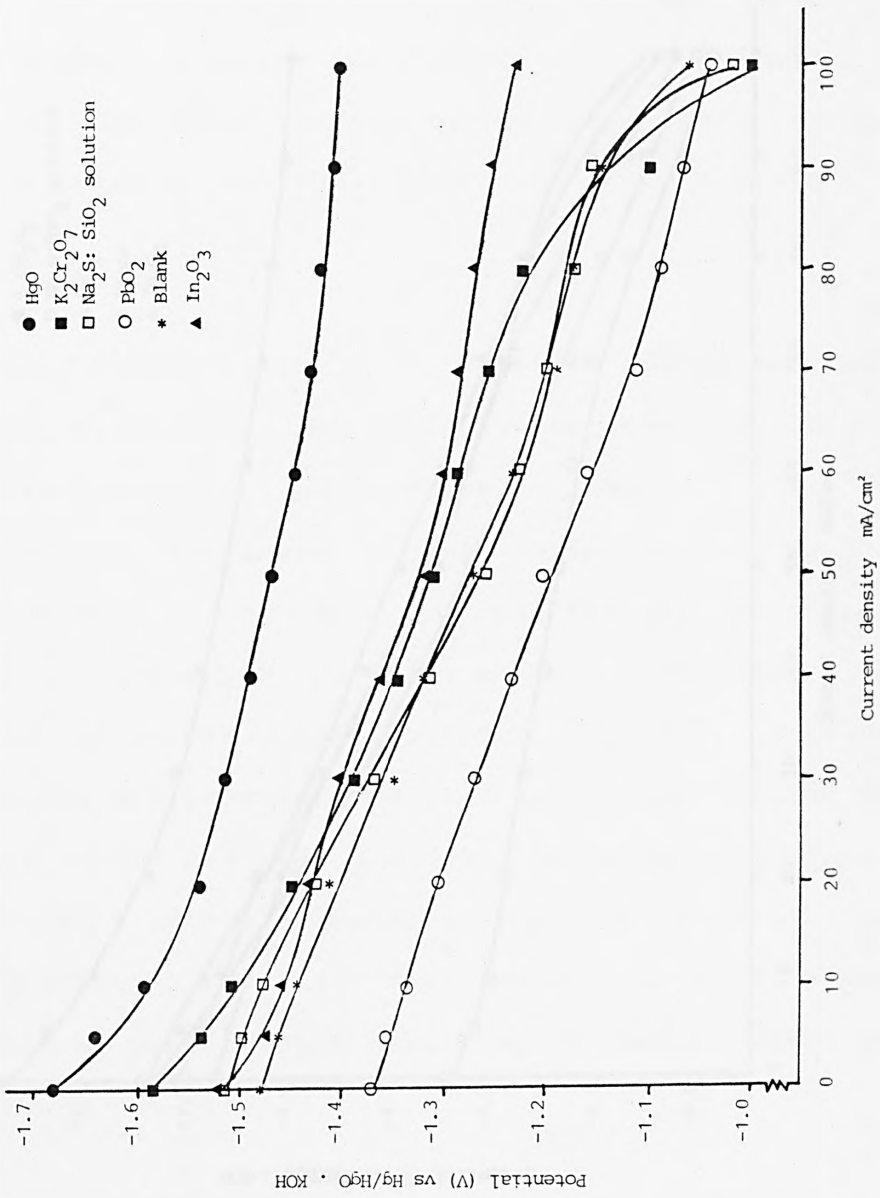

Fig. 5.4 Effect of 1% inhibitors on the polarisation characteristics of Q_4 in 5M KOH

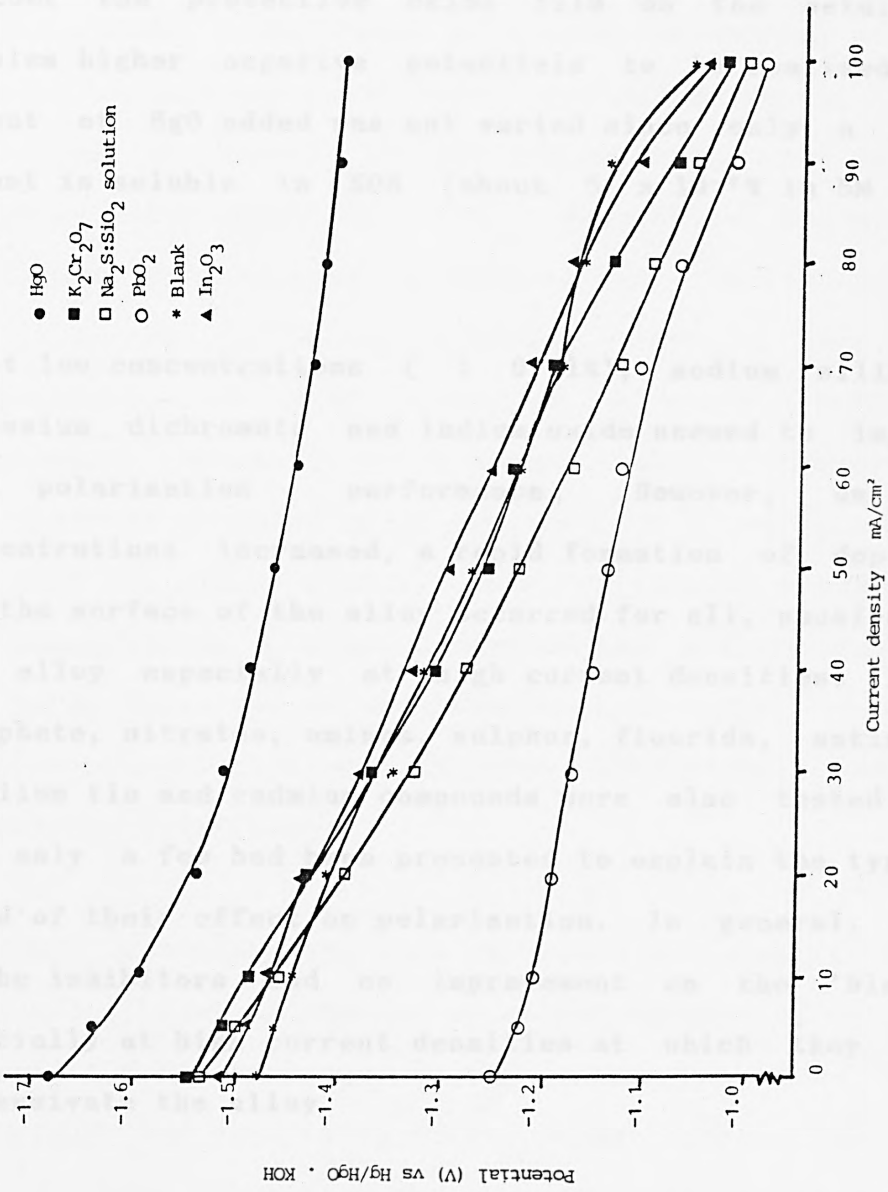

Fig. 5.5 Effect of 2% inhibitors on the polarisation characteristics of Q_4 in 5M KOH

respect to its effect on the polarisation of the alloy. The presence of Hg in the electrolyte, breaks down further the protective oxide film on the metal and enables higher negative potentials to be realised. The amount of HgO added was not varied since only a small amount is soluble in KOH (about 5 x 10^{-7}% in 5M KOH).

At low concentrations (> 0.01%), sodium silicate, potassium dichromate and indium oxide seemed to improve the polarisation performance. However, as the concentrations increased, a rapid formation of deposits on the surface of the alloy occurred for all, passivating the alloy especially at high current densities. Lead, phosphate, nitrates, amines, sulphur, flouride, antimony, thallium tin and cadmium compounds were also tested for, but only a few had been presented to explain the typical trend of their effect on polarisation. In general, most of the inhibitors had no improvement on the 'blank', especially at high current densities at which they tend to passivate the alloy.

At this point, Hg (as HgO) comes out clear as the relatively best additive in alkaline electrolytes for minimising the polarisation of the anode material, especially for the test alloy.

5.3.2 EFFICIENCY OF HgO AS A HYDROGEN EVOLUTION INHIBITOR

The ability of HgO as an effective hydrogen evolution inhibitor was established when the amount of hydrogen evolved on self-discharge and at a discharge current was collected for 'blank' KOH and KOH saturated with HgO, and compared. The amount of hydrogen evolved was measured at different temperatures for each medium. Tables 5.1 and 5.2 show the rates of hydrogen evolution. At a low temperature, the rate seems to be only marginally suppressed. However, at a higher than room temperature, the effectiveness of Hg is realised. It is worth pointing out that the almost similar rate of hydrogen evolution at low temperatures does not undermine the effectiveness of Hg as an inhibitor at such temperatures since across a working surface area, the marginal differences add up to something significant.

Table 5.3 shows the loss in active anode material, and thence the loss in charge, on self-discharge of Q4 in the presence of HgO. Compared to the results obtained for Q4 in 'blank' KOH (see Table 4.7), it can be seen that there is a vast improvement when HgO is added to the electrolyte (Fig. 5.6).

5.3.3 MECHANISM OF HYDROGEN SUPPRESSION

From Table 5.4, it can be seen that the exchange-current

TABLE 5.1 HYDROGEN EVOLUTION AT OCV

Temperature (°C)	Rate of hydrogen evolution (ml/min/cm²)	
	BLANK	HgO
40	0.420	0.162

TABLE 5.2 PARASITIC HYDROGEN EVOLUTION

Temperature (°C)	Rate of hydrogen evolution (ml/min/cm²)	
	BLANK	HgO
25	0.433	0.367
40	1.833	1.483

CURRENT DENSITY = 100 mA/cm²

TABLE 5.3 MATERIAL LOSS DUE TO SELF-DISCHARGE OF Q4 IN 5M KOH/HGO

	1ST RUN	2ND RUN	3RD RUN
WEIGHT LOST (g)	.0312	.0468	.0585
TIME TAKEN (min)	291	392	485
CORROSION RATE (mg/hr)	6.433	7.1633	7.2371

MEAN CORROSION RATE 6.9445 mg/hr

EQUIVALENT CHARGE LOST (Ah) .021

TEMPERATURE: 25 C

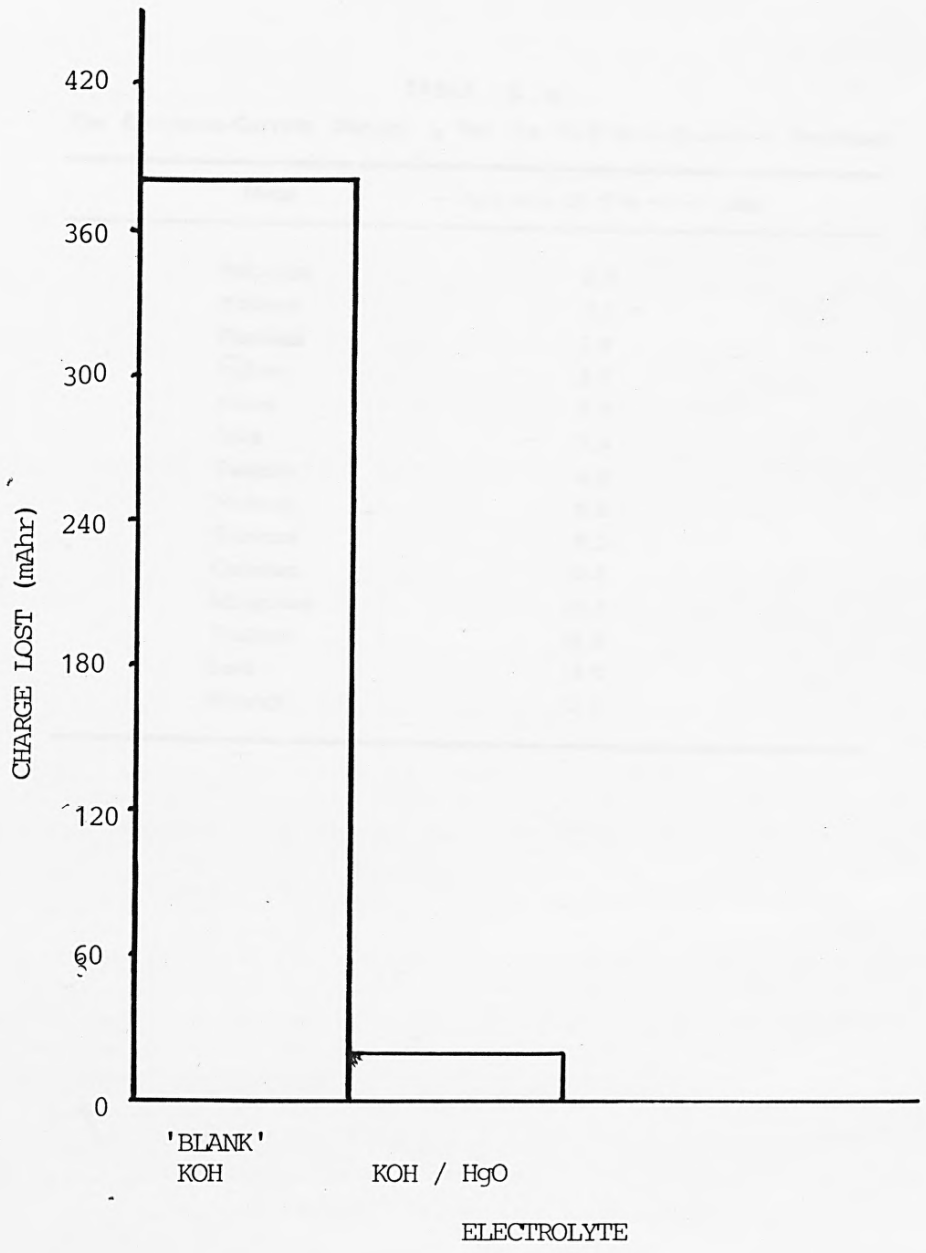

FIG. 5.6 SELF-DISCHARGE OF Q_4 IN 5M KOH SATURATED WITH HgO

Table 5.4 Exchange-current density for hydrogen-evolution reactions (p.202) has been removed for copyright reasons

density for hydrogen evolution is very small on mercury, lead, cadmium and thallium. Thus, these metals are poor catalysts for hydrogen-evolution reactions and hence, good candidates for hydrogen suppression. The presence of these metals in an aqueous electrolyte inhibits the evolution of hydrogen by suppressing the renewal of atomic hydrogen on metal surface layer [159].

The differences in the desired performance of these metals might be be due to some intrinsic property of each metal. Figs. 5.7-5.12 show scanning electron micrographs of the surface morphology of the alloy after polarisation in the prescence of the inhibitors.

From the micrographs, it can be seen that apart from Hg all the others had heavy deposits on the surface of the alloy. X-ray analyses (accompanying the micrographs) show that these deposits are largely thick oxide layers, with some detectable deposits of the inhibitor in the case of lead. These thick oxide layers are electrochemically resistive and thus inhibits the mass transfer across the reaction interface. The difference in the surface morphology for Hg as compared to the others can be used to explain the good performance of trace amount of Hg as the suitable inhibitor.

The micrograph for Hg shows only spots of oxide aggregates, quite different from the layers observed for

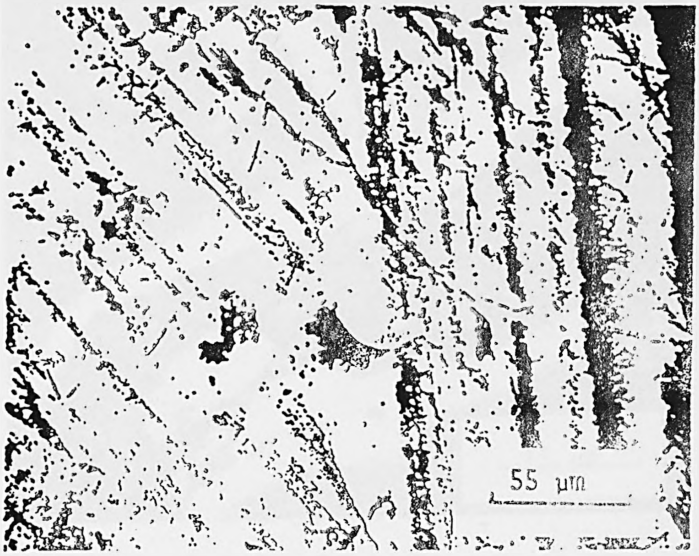

FIG. 5.7 Surface finish of Q_4 before use.

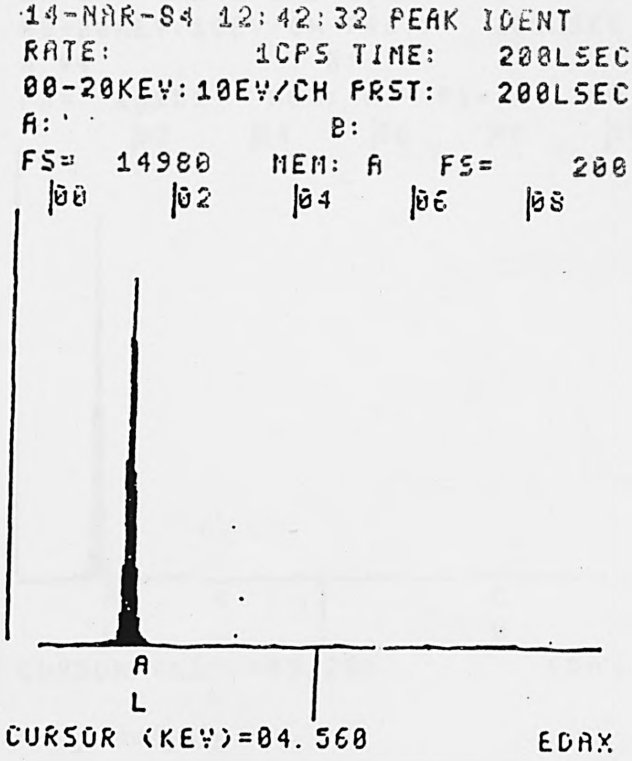

X-ray analysis

FIG. 5.8 Surface morphology of Q_4 after polarization in 5M KOH / 0.1% silicate

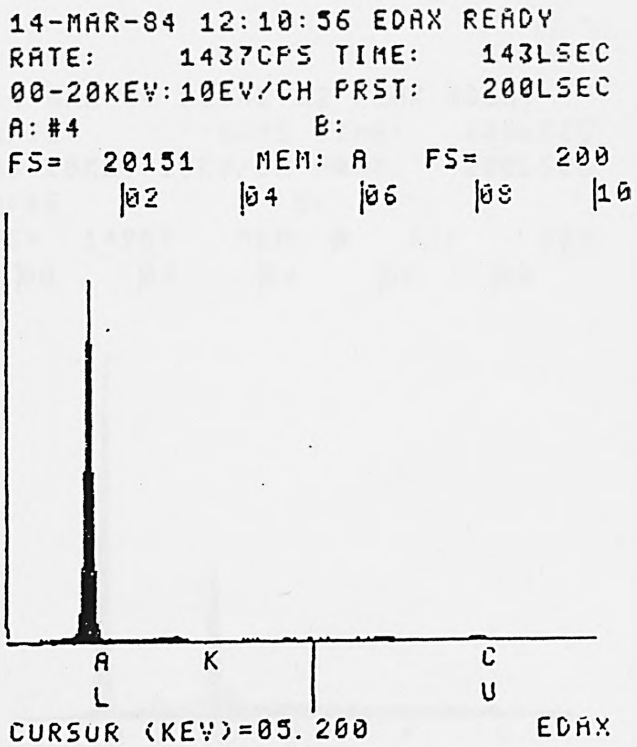

X-ray analysis

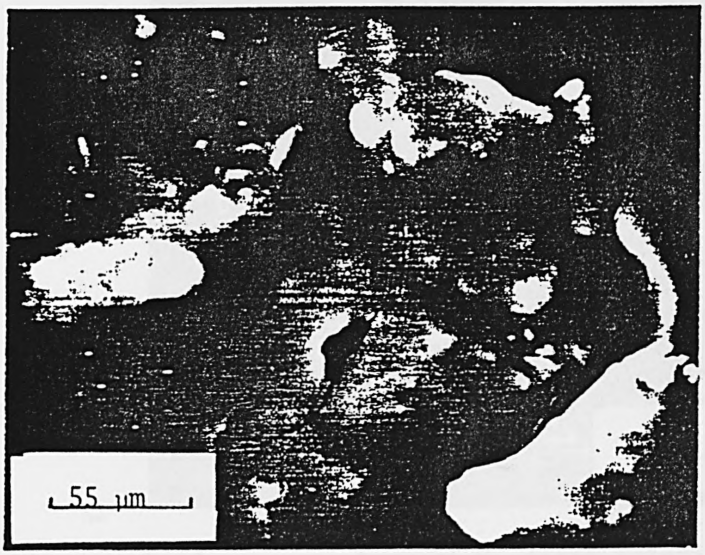

FIG. 5.9. Surface morphology of Q_4 after polarization in 5M KOH / 0.1% lead

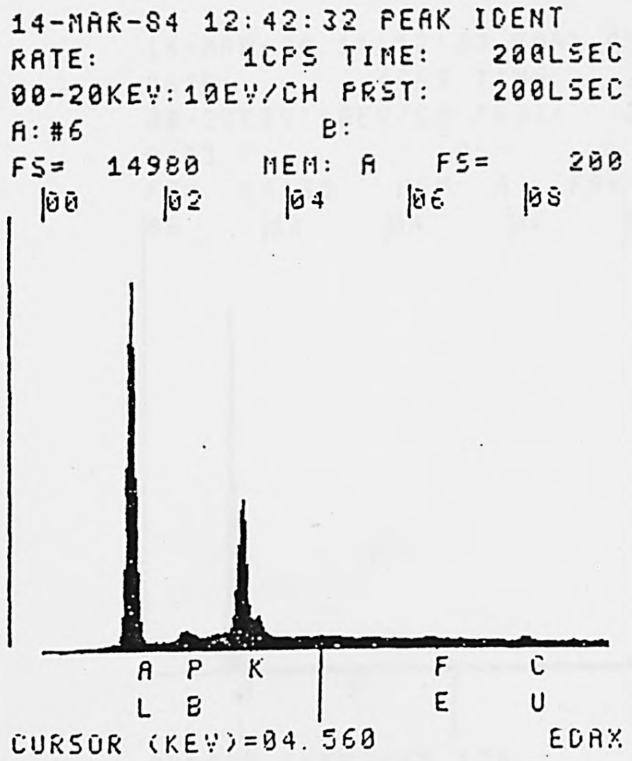

X-ray analysis

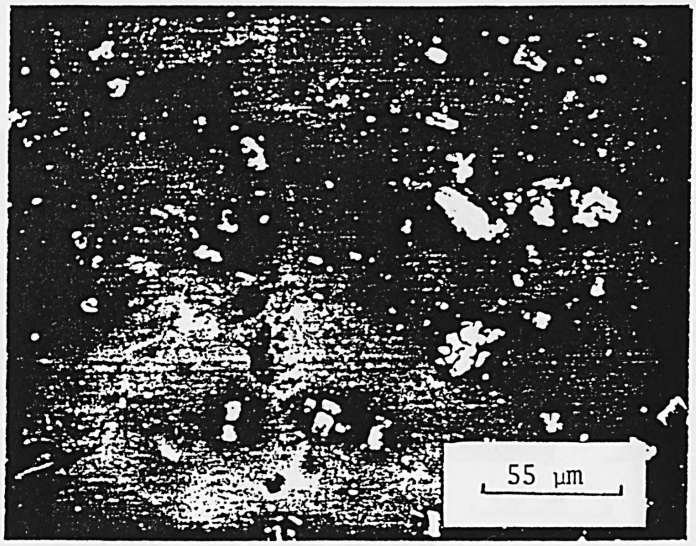

FIG. 5.10 Surface morphology of Q_4 after polarization in 5M KOH / trace amount of mercury

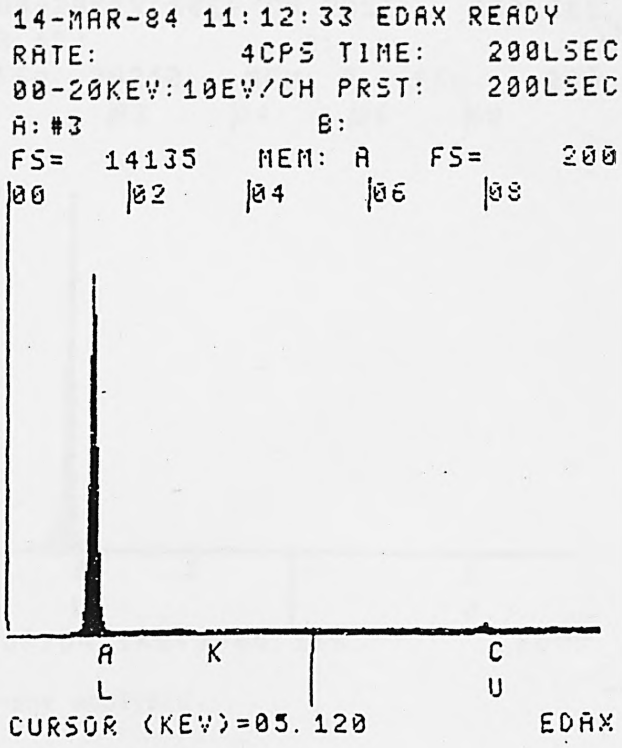

X-ray analysis

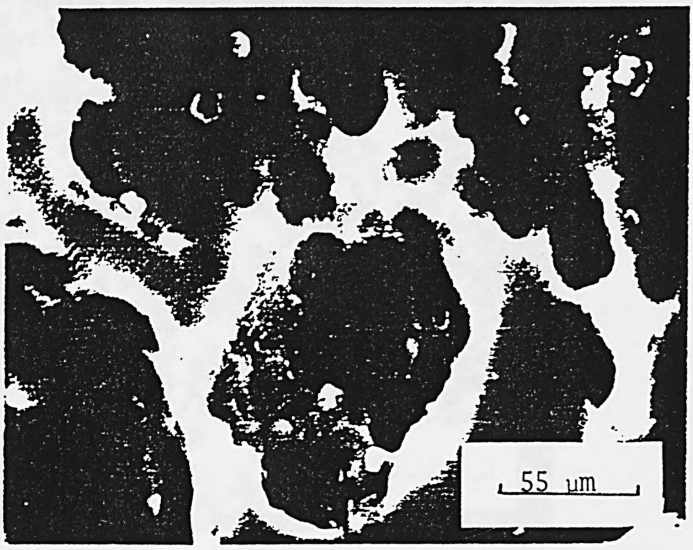

FIG. 5.11 Surface morphology of Q_4 after polarization in 5M KOH / 0.1% chromate

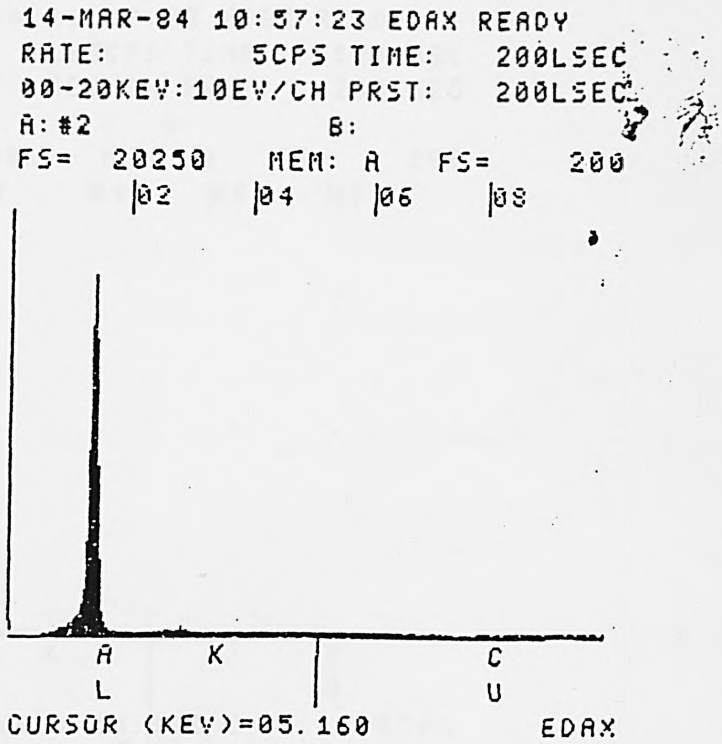

X-ray analysis.

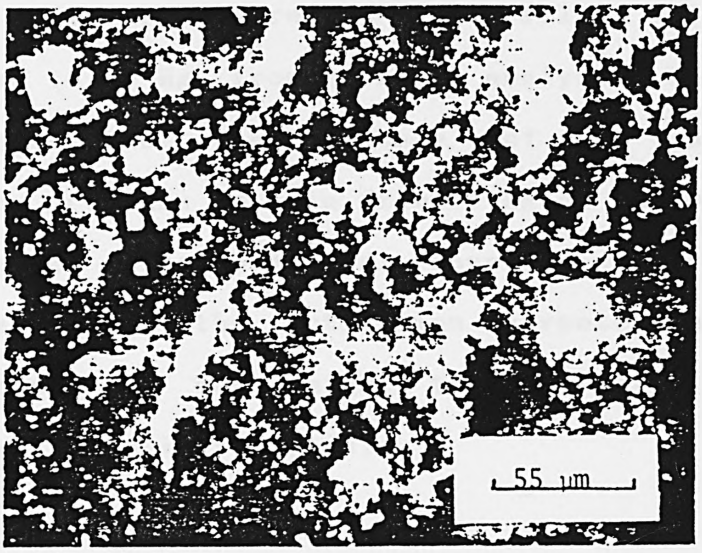

FIG. 5.12 Surface morphology of Q_4 after polarization in 5M KOH

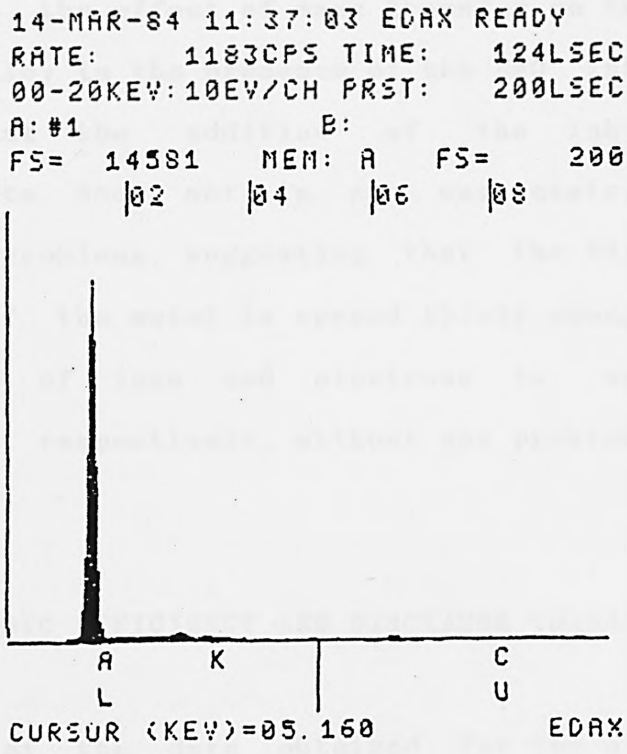

X-ray analysis

the others. Also, the surface of the metal appears to be almost uniformly covered by a thin film. This thin film is found to be Hg, from chemical analysis. Hence, it can be argued that the presence of HgO in electrolyte solution provides a thin film of Hg on the metal surface, forming an electrochemical couple in which Al is the anode and since the activation overpotential of hydrogen on mercury is very high, the cathodic evolution of hydrogen is inhibited [160].

The data obtained from the transient state polarisation of Q4 in the presence of HgO were used to plot a graph of potential versus current density. This is shown in Fig. 5.13. The curve drawn is compared to that observed for the steady state measurements in order to establish the effect of mass transfer on the polarisation of the alloy in the presence of the HgO inhibitor. It is found that the addition of the inhibitor to the electrolyte does not in any way contribute to mass transfer problems, suggesting that the film of Hg on the surface of the metal is spread thinly enough to allow the transport of ions and electrons to and from the electrode, respectively, without any problems.

5.3.4 ANODIC EFFICIENCY AND DISCHARGE CHARACTERISTICS

The mean of the data obtained for the steady state and

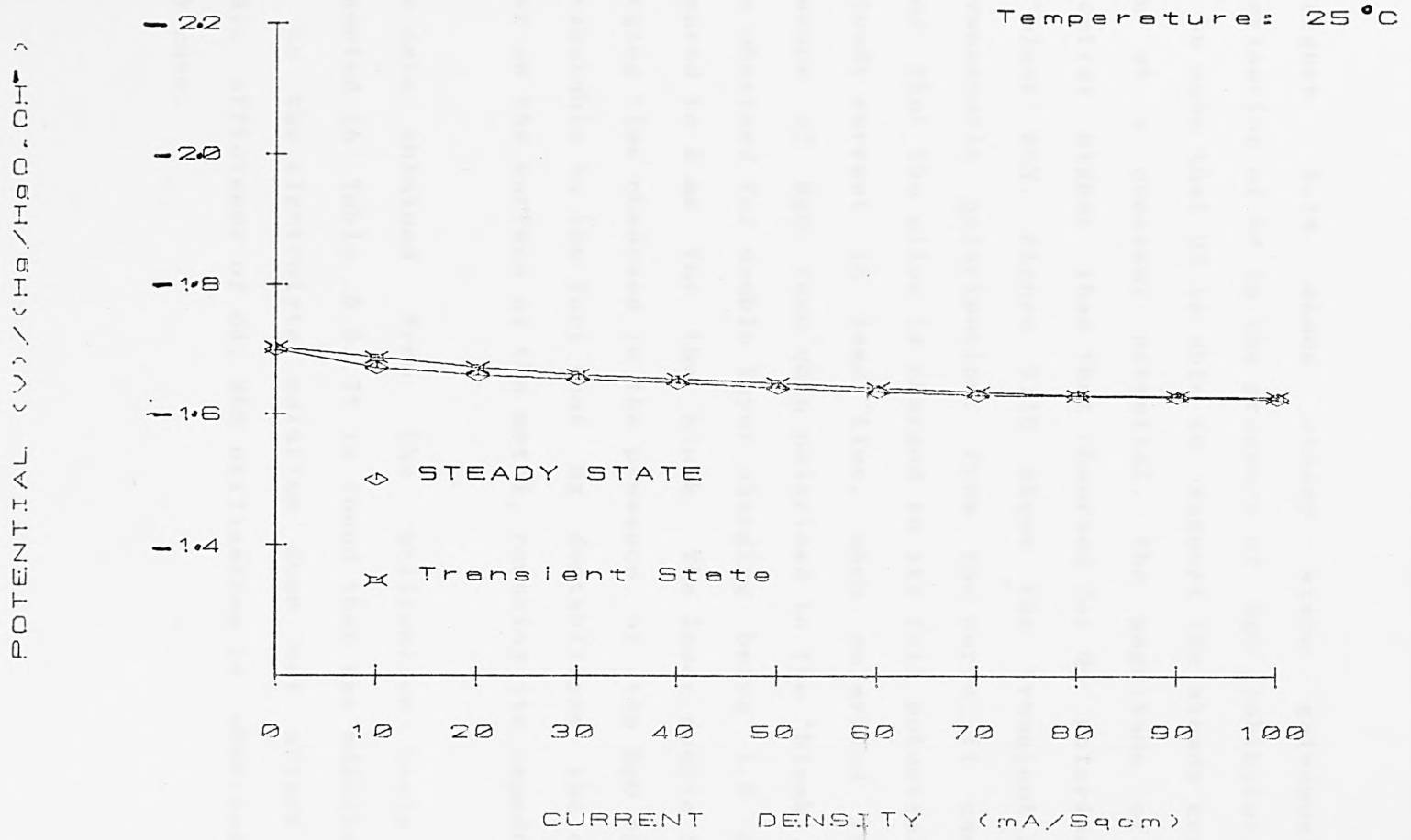

FIG. 5.13 TRANSIENT/STEADY STATE POLARISATION OF Q4 IN 5M KOH/HgO

transient state galvanostatic polarisation determinations (the mean of three runs) were used to plot graphs of potential versus time and shown as Figs. 5.14 and 5.15.

Figure 5.14 shows steady state galvanostatic polarisation of Q4 in the presence of HgO inhibitor. It can be seen that Q4 is able to support the steady current flow at a constant potential. The magnitude of the potential higher than that observed for Q4 polarisation in 'blank' KOH. Figure 5.15 shows the transient state galvanostatic polarisation. From the curve, it can be found that the alloy is charged to its full potential at a steady current in less time, when polarised in the presence of HgO, than when polarised in the 'blank'. The time observed for double layer charging being 1.8 ms as compared to 2 ms for the blank. The lower double layer charging time observed in the presence of the HgO can be attributable to the fact that Hg destabilises the oxide layer on the surface of the metal, reducing its impedance.

The data obtained from the utilisation tests are presented in Table 5.5. It is found that the addition of HgO to the electrolyte solution does not affect the anodic efficiency of Q4; 95% utilisation is observed in each case.

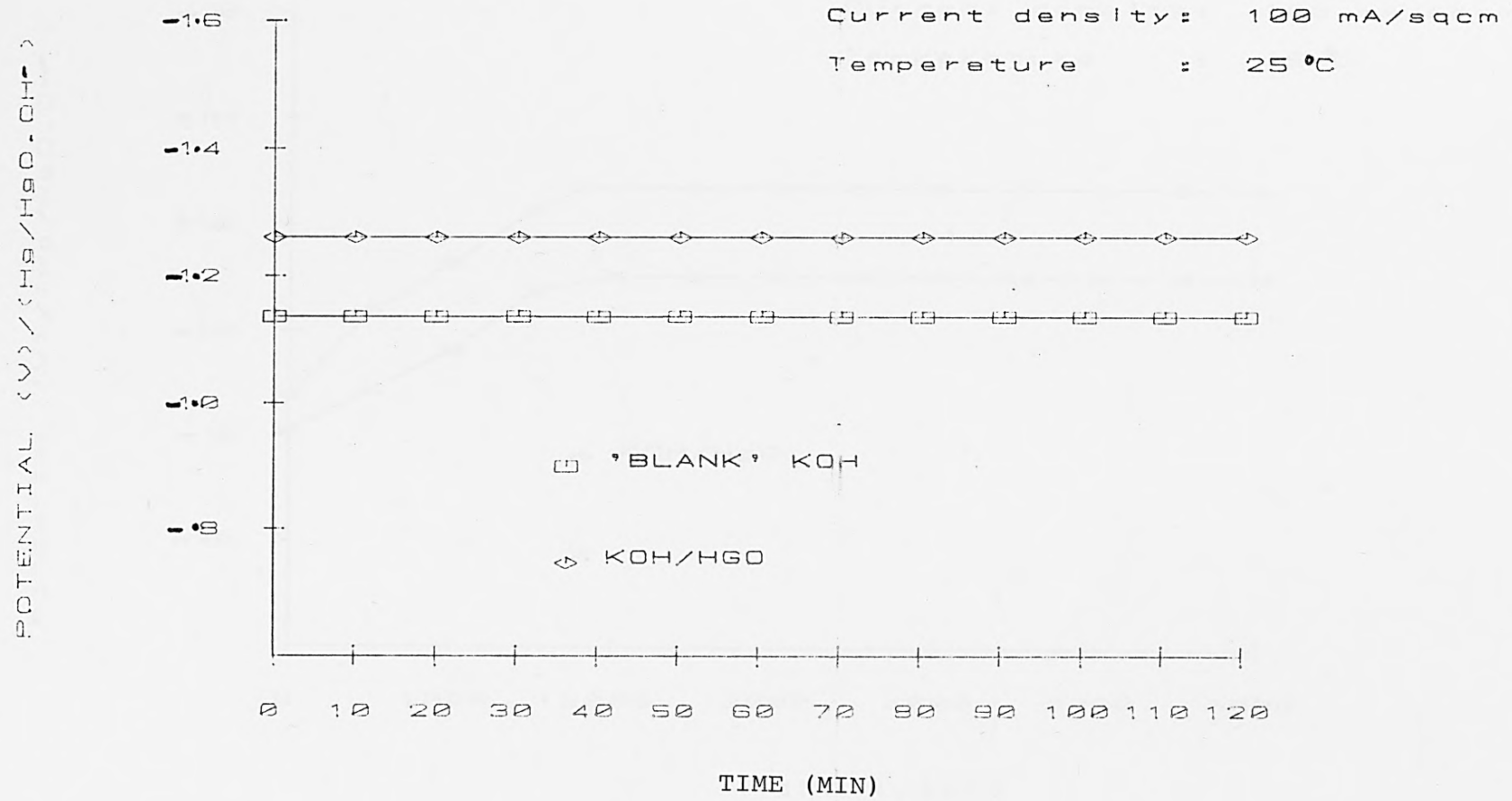

FIG.5.14 STEADY STATE GALVANOSTATIC POLARISATION OF Q4 IN 5M KOH/HgO

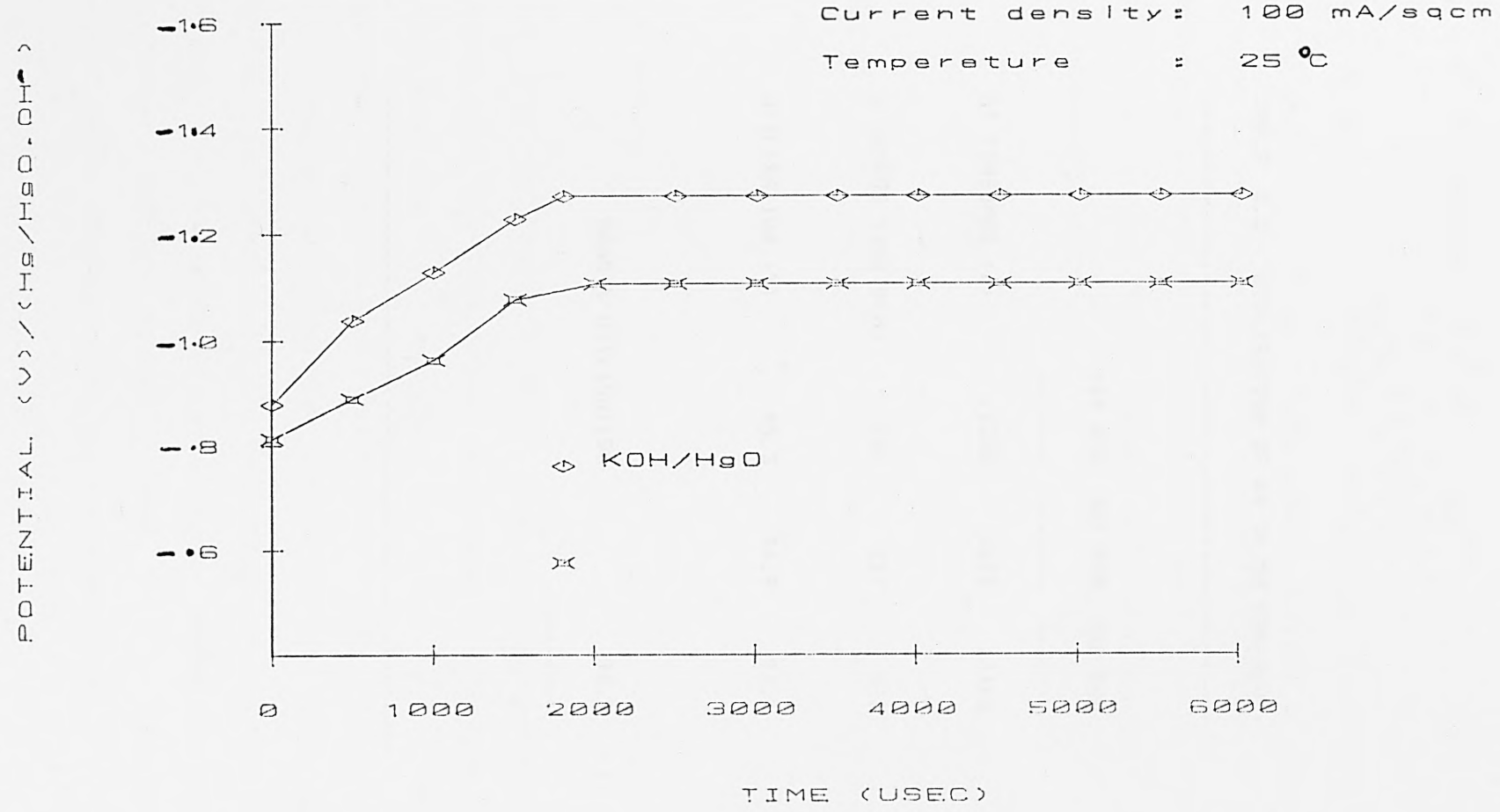

FIG. 5.15 TRANSIENT STATE GALVANOSTATIC POLARISATION OF Q4 IN 5M KOH SATURATED WITH HgO

TABLE 5.5 UTILISATION OF O4 IN 5M KOH/HgO

	1ST RUN	2ND RUN	3RD RUN
WT CONSUMED (g)	.1258	.2678	.3462
D'CHARGE TIME(MIN)	107	227	292
UTILISATION (%)	95.3	94.9	94.6

MEAN % UTILISATION 94.9

5.3.5 DATA REPRODUCIBILITY.

All the measurements involved in the experiments above were carried out in triplicates. Overall, the anodic potentials observed were reproducible within 7 mV. The hydrogen evolution measurements, anodic efficiency tests and corrosion rates were all reproducible within experimental error.

SOURCES OF ERROR

All the possible sources of errors are as discussed in chapter 4.

6.4 CONCLUSION

The problems arising from the self-discharge of the anode, with the concomitant evolution of hydrogen, can be alleviated by the addition of substances with high hydrogen overpotential and considerable solubility, to the alkaline electrolyte. For alloy Q4, trace amount of mercury is found to be the best additive. Lead, cadmium, indium, silicates and chromates were among the many other additives tested. Overall, they tend to passivate the metal, especially at high current densities.

The addition of HgO to KOH reduces the corrosion rate

of Al without causing the active anodic area to be smaller, whereas the other inhibitors greatly reduce the active anode sites by depositing resistant oxide layers onto the reaction surface of the metal. The use of mercury has a further advantage in that it reduces cell impedance by interfering with the protective oxide coating on the surface of the electrode.

6 ELECTROLYTE OPTIMISATION

6.1 INTRODUCTION

In chapter 2, the role of cell electrolyte was expounded. It was pointed out that the role it plays is very vital, since it provides the ions on which the transfer of electrons, between cell electrodes, depends.

To perform this function efficiently, the electrolyte must have a high ionic conductivity and this in turn requires a high concentration of ions; preferably of high mobility. The physico-chemical nature of these ions has already been discussed in chapter 2.

In this chapter, the contribution that an electrolyte makes towards the performance of a cell is investigated. In the optimisation of a cell performance, the electrolyte-type used is one of the parameters considered to be constraining (section 4.1). The magnitude of the rate of charge-transfer and of mass-transfer depends very much on the type of electrolyte used; the limitations being the conductivity of the respective electrolyte and the solubility of the reaction products in the electrolyte. These two variables form a major part in the following attempt to optimise the electrolyte used for

the operation of aluminium cells.

PART ONE: CONDUCTIVITY AND SOLUBILITY MEASUREMENTS

6.2 EXPERIMENTAL

6.2.1 ELECTROLYTE CONDUCTIVITY

The conductivity of an electrolyte can be said to be a measure of the current it can carry by means of its ions. The movement of these ions through the solution is induced by the imposition of an electric field - a consequence of the applied potential between electrodes.

During the operation of aluminium-air cells, the active anode material is dissolved by the electrolyte. A build-up of resistance occurs within the electrolyte owing to the presence of the reaction products. A large resistance build-up inevitably reduces the conductivity of the electrolyte and thus, results in the loss of cell potential. The magnitude of this resistance build-up is the subject of the following investigation.

A) CHANGES IN ELECTROLYTE CONDUCTIVITY DURING CELL OPERATION

In selecting an electrolyte for best cell performance, an electrolyte of a good conductivity and a less resistance build-up within the solution during cell operation will be ideal. This investigation is therefore directed towards determining the resistance build-up in various electrolytes; by looking at the changes in the conductivity of each electrolyte during cell operation.

PROCEDURE

The electrolytes used in this investigation were 5M KOH, 5M NaOH, 3M LiOH, 5M KOH saturated with HgO, equal volume mixtures of 5M KOH and 5M NaOH, 5M NaOH and 3M LiOH, 5M KOH and 3M LiOH, and 5M KOH, 5M NaOH and 3M LiOH. The electrolytes were prepared using Analar Grade chemicals and distilled/de-ionised water. They are labelled as electrolyte nos. 1 - 8 respectively. Care was taken to ensure that the solutions prepared did not absorb carbon dioxide from the atmosphere.

The electrolytes were immersed in a thermostatically controlled water bath at 25°C. Weighed amounts of alloy Q4 were dissolved in each electrolyte sample and its duplicates, until saturation. After a complete dissolution of a specific amount, the conductivity of the

electrolyte was measured by means of a digital conductivity meter. Measurements were taken on the duplicate samples as well. Where saturation was experienced before a complete dissolution, the conductivity of the saturated electrolyte was measured and recorded as such.

B) EFFECT OF TEMPERATURE ON ELECTROLYTE CONDUCTIVITY

The temperature characteristics of an electrolyte is a primary factor limiting the performance of a cell. As such, in this investigation, it is considered important to establish the effect of temperature on electrolyte conductivity.

PROCEDURE

Electrolytes nos.1-5 were used. The conductivities of each electrolyte sample, and its duplicates, were measured at different solution temperatures. The test tubes, containing the electrolytes, were immersed into the thermostatically controlled water bath. The water was then heated up to the desired temperature and maintained at that temperature for a long while, to allow the electrolyte solutions to be brought to the temperature of the bath. The temperatures of the electrolytes were confirmed by taking the temperature of each electrolyte. After ensuring complete temperature equilibration, the

conductivity of each electrolyte was determined using the digital conductivity meter. After all electrolytes had been measured, the temperature of the bath was increased (the experiment was started for the lowest temperature) to the next immediate temperature. The same procedure was followed as for the previous temperature(s).

6.2.2 SOLUBILITY MEASUREMENTS

A) SOLUBILITY OF REACTION PRODUCTS IN ELECTROLYTE TYPE

The state-of-art in the development of Al-air cells, at the moment, is culminated by the problem of cell clogging. This arises from the cell electrolyte being saturated by the reaction products formed from the dissolution of the active anode material. A highly insoluble aluminium trihydroxide is subsequently precipitated in the process.

In the dissolution reaction of aluminium, the following occurs:

Step 1: $Al + 4OH^- \longrightarrow Al(OH)_4^- + 3e$

Step 2: $Al(OH)_4^- \longrightarrow Al(OH)_3 + OH^-$

Step 2 is limiting, since it is the $Al(OH)_3$ precipitate that has deleterious effects on overall cell performance and reliability. To prevent step 2 from taking place, it is evident that step 1 must be prolonged. This can be ensured by using an electrolyte that has a high solubility for the reaction products. As such, in the selection of a suitable electrolyte, the ideal electrolyte, apart from being very conductive and remaining so throughout the operation of the cell, must have a relatively high solubility for the reaction products formed during cell operation. The following investigation is directed towards the determination of the solubility of the reaction products formed from the dissolution of active anode material in different types of alkaline electrolytes.

PROCEDURE

The saturated electrolyte solutions used in the conductivity measurements above were allowed to stand, in the water bath at 25°C, for at least 24 hours so as to ensure that all undissolved particulate matter settled down before sample preparations.

Aliquot samples of the clear saturated electrolyte

solutions were then pipetted into graduated flasks. The samples were then diluted by such factors as to enable absorbance readings to be taken, within the linearity range for aluminium, using an Atomic Absorption spectrophotometer. Each electrolyte sample was prepared in duplicate. The Atomic Absorption spectrophotometric method (section 3.4) was then used to determine the amount of aluminium dissolved in each saturated electrolyte. The average of the concentrations given by the two samples prepared for each electrolyte was then used to obtain the solubility of the aluminium part of the aluminate formed during the reaction.

B) EFFECT OF TEMPERATURE ON THE SOLUBILITY OF REACTION PRODUCTS

The reason given for the need to establish the effect of temperature on electrolyte conductivity also applies to the need to establish the effect of temperature on the solubility of the reaction products formed during cell operation.

PROCEDURE

The test tubes containing the saturated electrolyte solutions labelled 1-5, were immersed into the water bath and the desired temperatures were thermostatically

controlled in the same manner as described in section 6.2.1B. However, after confirming temperature equilibration small aliquot samples of the clear saturated solutions were pipetted into graduated flasks and diluted and analysed using the same procedure as above. Analyses were done on samples obtained for all the desired temperatures and on their duplicates.

6.3 RESULTS & DISCUSSION

6.3.1 CHANGES IN ELECTROLYTE CONDUCTIVITY

The conductivity readings taken were recorded and plots of conductivity against duration of cell operation (Fig. 6.1) were made from the data obtained. The duration of cell operation was inferred from the amount of active material dissolved, by assuming cell output of 1 Ah and a 95% Faradaic efficiency [Using Faraday's law ($w = ItM/nF$), it was calculated that 0.37g of Al was dissolved in 1 hr.].

Fig. 6.1 shows that in general, electrolyte conductivity decreases during cell operation owing to, possibly, an association between ions in solution and a consequent formation of a resistant barrier to other free moving ions. This resistance build-up increases with duration of operation as the concentration of the

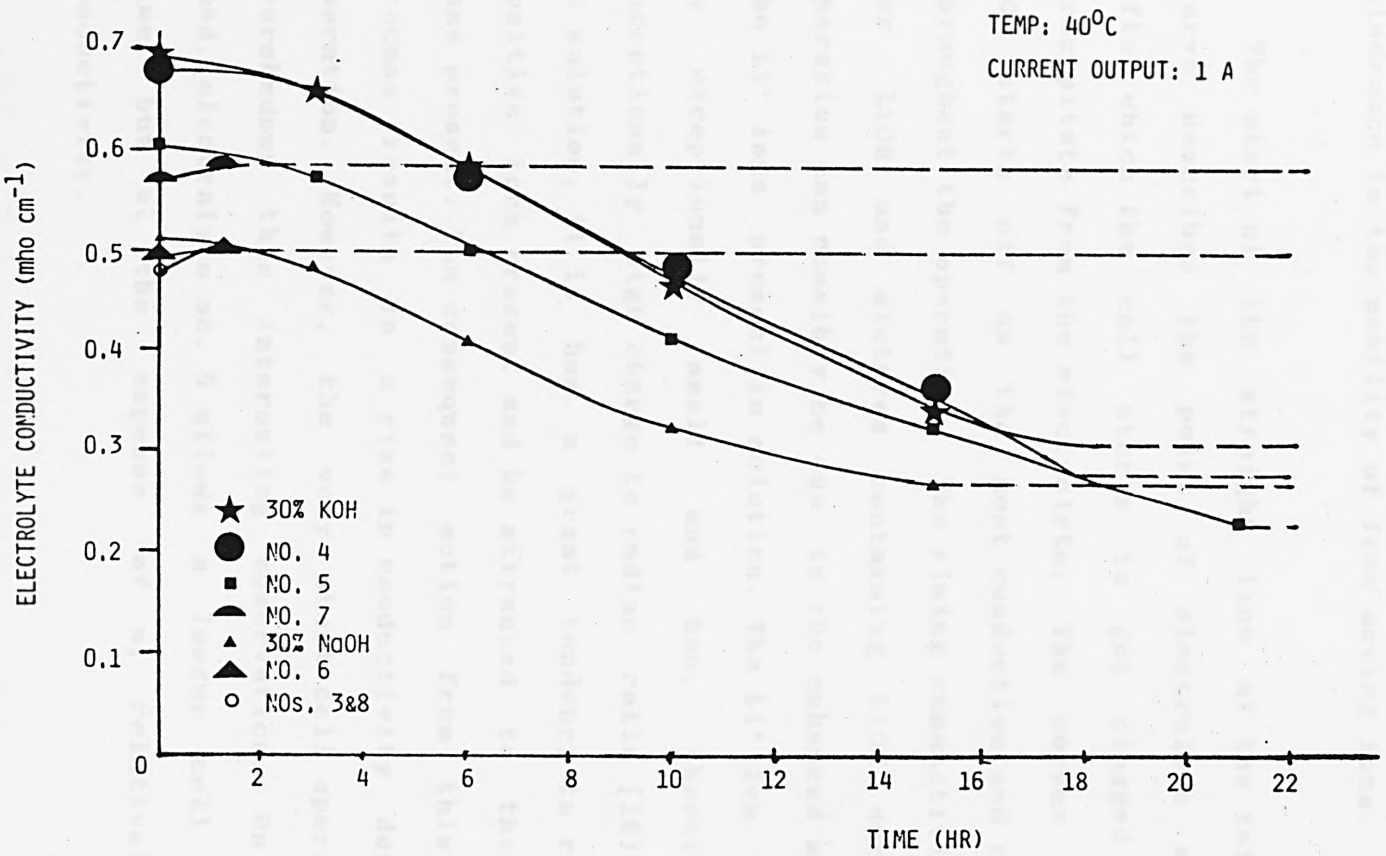

FIG. 6.1 CONDUCTIVITY CHANGES DURING CELL OPERATION

reaction product increases and thus produces a viscous hindrance to the mobility of free moving ions.

The start of the straight line at the tail of every curve describes the point of electrolyte saturation, after which the cell starts to get clogged up by the precipitate from the electrolyte. The curves show that KOH starts off as the most conductive and remains so throughout the operation. The rising conductivities shown for LiOH and mixtures containing LiOH during cell operation can possibly be due to the enhanced movement of the Li^+ ions present in solution. The Li^+ ion is exceptionally small and has, therefore, an exceptionally high charge to radius ratio [161]. Thus, in solution, it is has a great tendency to repel other positive ions present and be attracted to the negative ions present. The consequent motion from this physical process results in a rise in conductivity during cell operation. However, the very short cell operation time overshadows this interesting observation. On the other hand, electrolyte no. 5 allows a longer cell operation time, but at the expense of a, relatively, lower conductivity.

The conductivity measurements taken before dissolving Al and those taken for the saturated solutions were used to calculate the ohmic loss due to saturation, by assuming a current density (i) of 100 mA/cm^2. The

relation

$$iR = i*(1/\sigma)* \text{cell constant}$$

where cell constant = 2.0

was used to calculate the iR for the electrolyte before cell operation and after electrolyte saturation. The change in iR was then taken as the ohmic loss/gain per unit area owing to the saturation of the electrolyte (Fig. 6.2).

Fig. 6.2 shows a larger ohmic loss for NaOH and a relatively lower one for KOH. It is interesting to note that inspite of the large solubility of reaction product in electrolyte no. 5 there is only a reasonable ohmic loss; from a relative view-point. The ohmic gains shown for electrolyte nos. 3,6,7 and 8 are obviously due to the gains in conductivities during cell operation, owing to presence of Li^+ ions in solution.

6.3.2 EFFECT OF TEMPERATURE ON CONDUCTIVITY

The data obtained from the experiment to find the effect of temperature on electrolyte conductivity were used to produce plots of conductivity against temperature. These plots are shown as Figs. 6.3-6.8.

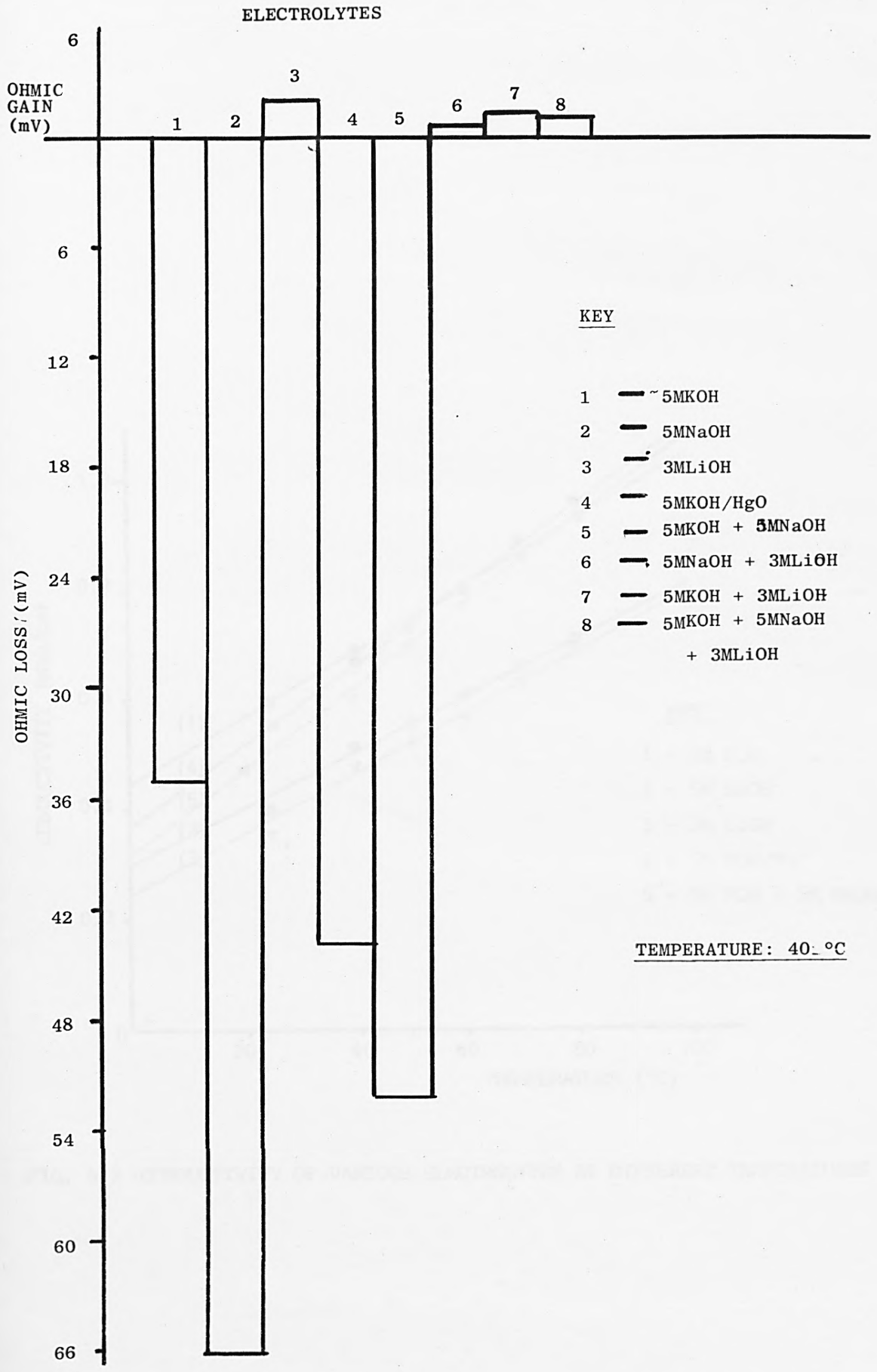

FIG. 6.2 OHMIC LOSS OWING to ELECTROLYTE SATURATION

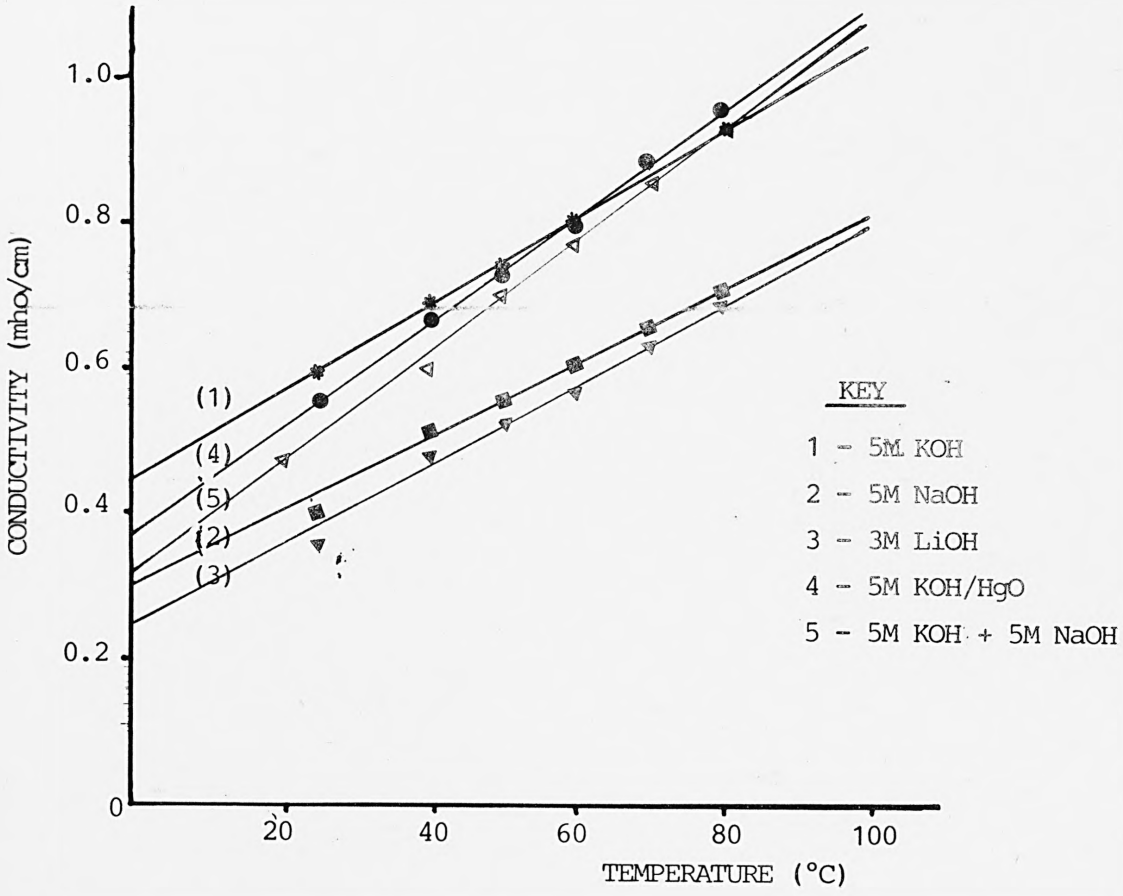

FIG. 6.3 CONDUCTIVITY OF VARIOUS ELECTROLYTES AT DIFFERENT TEMPERATURES

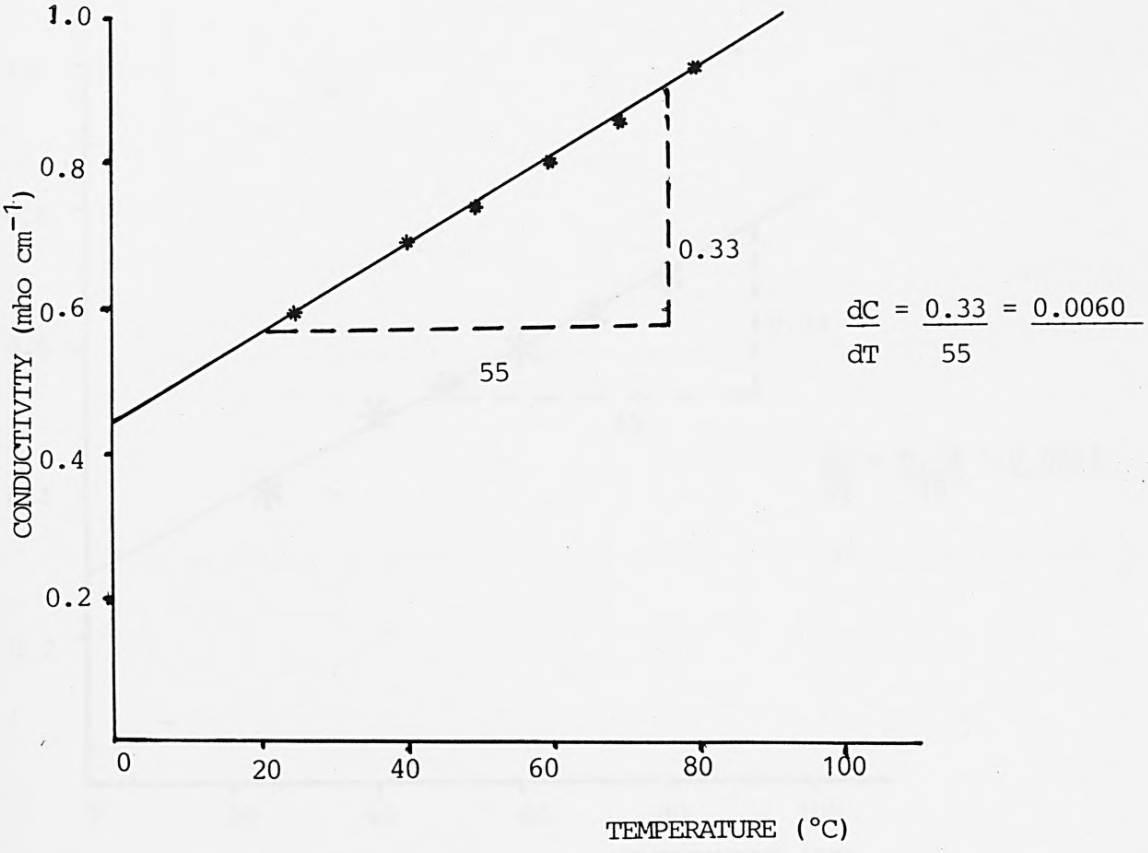

FIG. 6.4 CHANGE IN CONDUCTIVITY OF KOH W.R.T. TEMPERATURE CHANGES

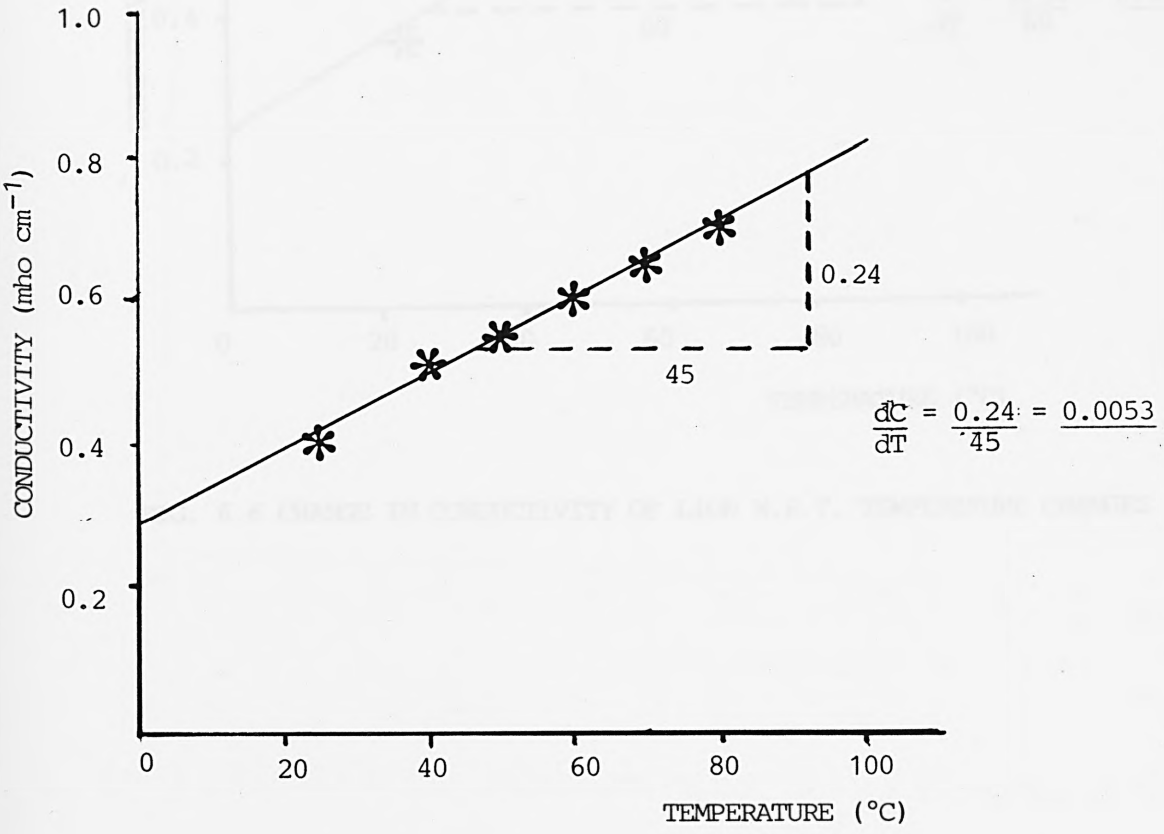

FIG. 6.5 CHANGE IN CONDUCTIVITY OF NaOH W.R.T. TEMPERATURE CHANGES

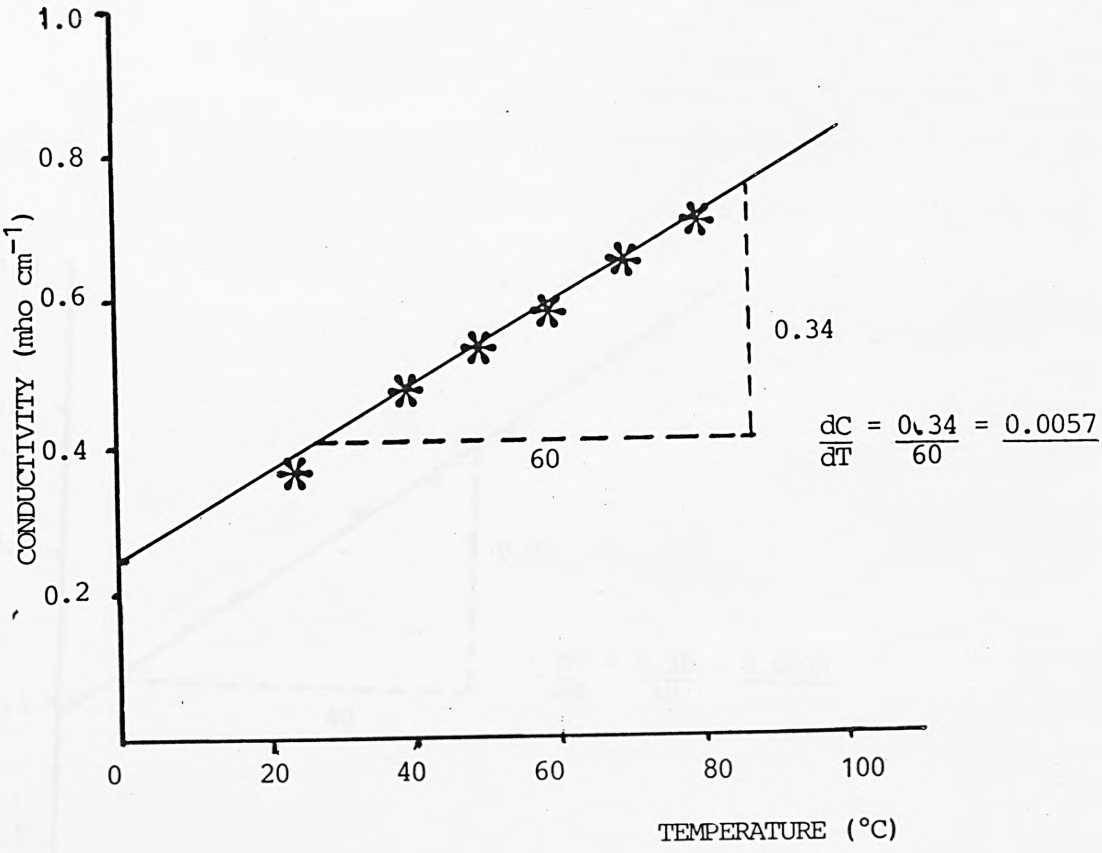

FIG. 6.6 CHANGE IN CONDUCTIVITY OF LiOH W.R.T. TEMPERATURE CHANGES

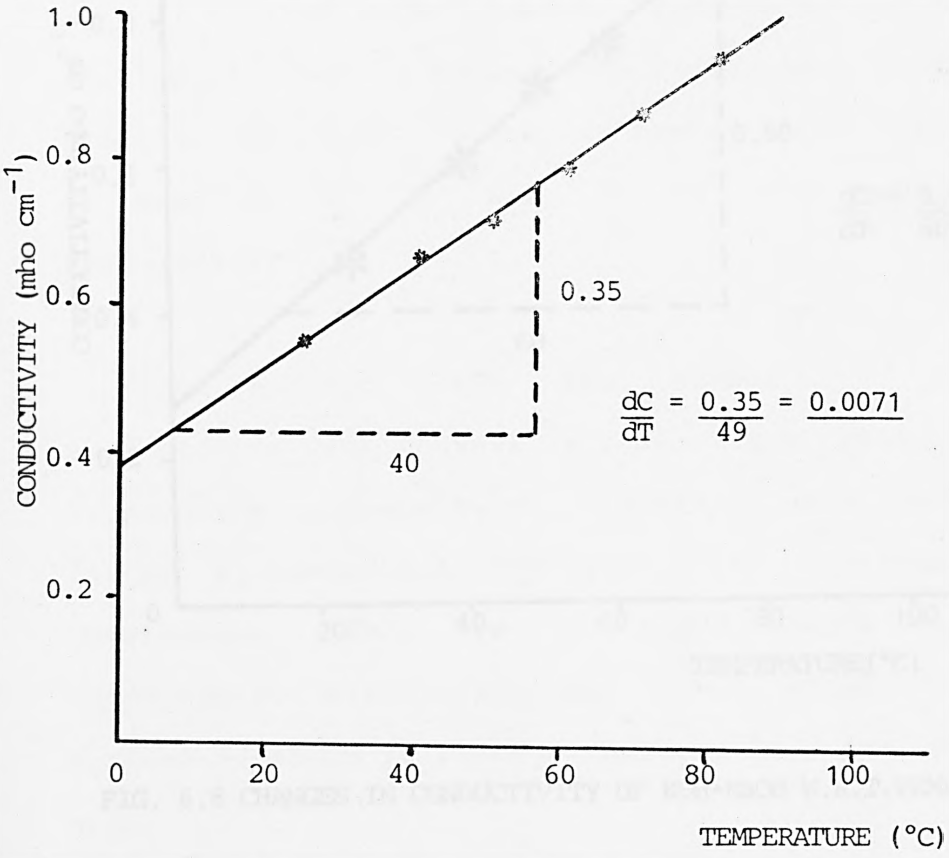

FIG. 6.7 CHANGES IN THE CONDUCTIVITY OF KOH /HgO W.R.T TEMPERATURE CHANGES

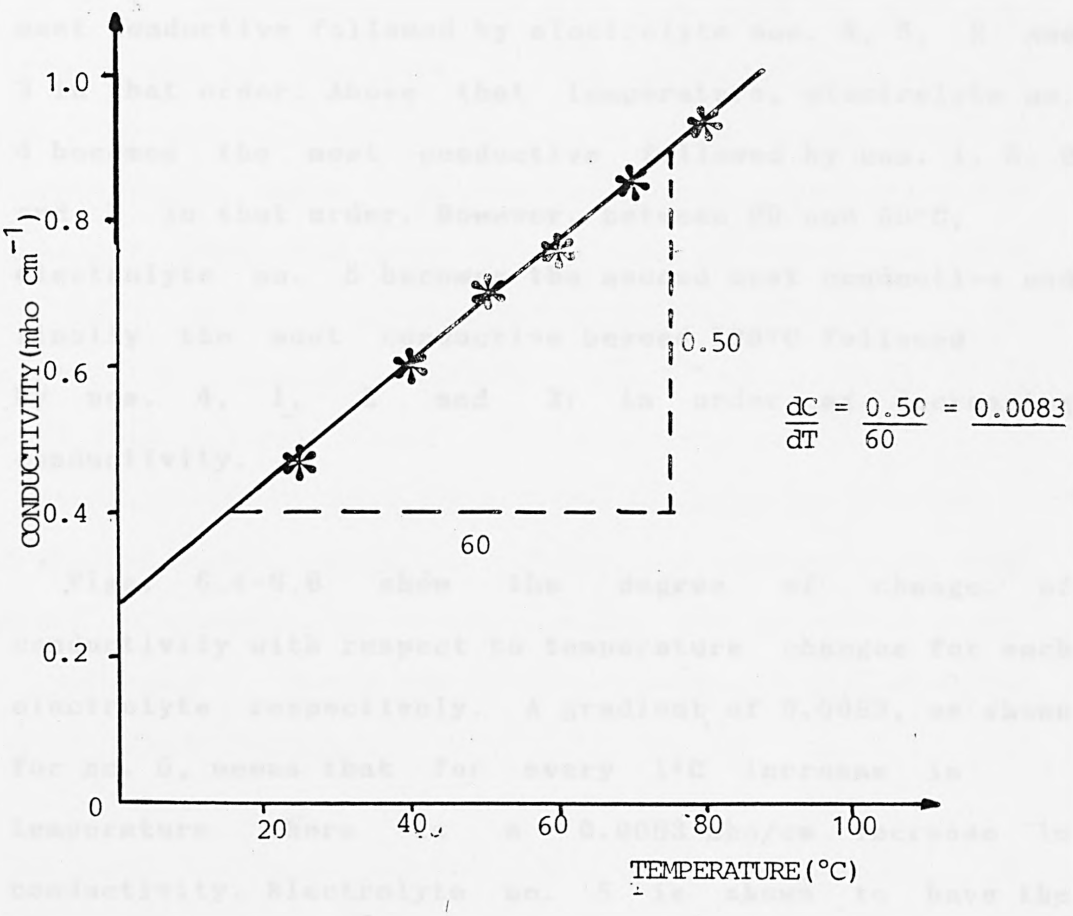

FIG. 6.8 CHANGES IN CONDUCTIVITY OF KOH+NaOH W.R.T.TEMPERATURE CHANGES

In Fig. 6.3, the plots for all electrolytes show that electrolyte conductivity increases with temperature. Below 60°C, electrolyte no. 1 is shown to be the most conductive followed by electrolyte nos. 4, 5, 2 and 3 in that order. Above that temperature, electrolyte no. 4 becomes the most conductive followed by nos. 1, 5, 2 and 3 in that order. However, between 80 and 90°C, electrolyte no. 5 becomes the second most conductive and finally the most conductive beyond 100°C followed by nos. 4, 1, 2 and 3; in order of decreasing conductivity.

Figs. 6.4-6.8 show the degree of change of conductivity with respect to temperature changes for each electrolyte respectively. A gradient of 0.0083, as shown for no. 5, means that for every 1°C increase in temperature there is a 0.0083 mho/cm increase in conductivity. Electrolyte no. 5 is shown to have the largest increase followed by nos. 4, 1, 3 and 2 in that order.

The trend of conductivity changes with temperature for all electrolytes, can be explained by considering the degree of conductivity change for each electrolyte. It depicts the effect of temperature on the rate of ion mobility, since the conductivity of an electrolyte can be said to be a function of the rate with which the constituent ions carry their charge through solution.

This rate being dependent not only upon the concentration and valency of the ions but upon their speed as well.

At high temperatures, not only does each ion activity increase; due to increase in the activation energy of each ion, but for electrolytes nos. 4 and 5, ion mobility is accelerated owing to a positive charge repulsion [162] occuring between the cations of the electrolytes. That is, there occurs a repulsion between the Na^+ ions and the K^+ ions of electrolyte no. 5 and between the K^+ ions and Hg^{2+} ions of electrolyte no. 4. The magnitude of this repulsion is greater for no. 5 and thus a larger degree of change in conductivity with respect to temperature. These changes add up over a range of temperature, hence the order of conductivity observed at high temperatures.

At lower temperatures, a different order of conductivity is observed (Fig. 6.3). At these temperatures, the contributions made by the limiting molar conductivity of each ion of an electrolyte to the total molar conductivity of the electrolyte predominates. Thus, a higher conductivity is observed for KOH; since K^+ has a higher limiting conductivity than the other cations present in the other electrolytes [163].

6.3.3 SOLUBILITY OF REACTION PRODUCTS

In the solubility measurements, the ppm readings inferred from the absorbance readings obtained for the samples were multiplied by the dilution factors and further multiplied by 10^{-6}, to convert to g/ml. The results were then computed so as to express the solubility of aluminium in each electrolyte in g/100g, by taking into account the specific gravity of each electrolyte at the working temperature.

Fig. 6.9 shows a Bar Chart constructed from the solubility data obtained; to elaborate the differences between the electrolytes. Electrolyte no. 5 is shown to have a very high solubility for aluminium, followed by nos. 1, 4, 2, and 3, 6, 7, 8 in that order. The high solubility obtained for no. 5 is probably due to the reduction in the magnitude of the common-ion effect that is pronounced in the predominately single cation electrolytes. Having said that, it is worth pointing out that the reason why the addition of HgO to KOH does not significantly affect KOH's solubility for Al might be because the Hg^{2+} ions do not partake in the formation of the reaction product. X-ray diffraction analysis (Fig. 6.10) shows no trace of Hg in the reaction product precipitate. Another reason could be because only a minute concentration of HgO is added to the KOH (about $5x10^{-7}$% of the total electrolyte

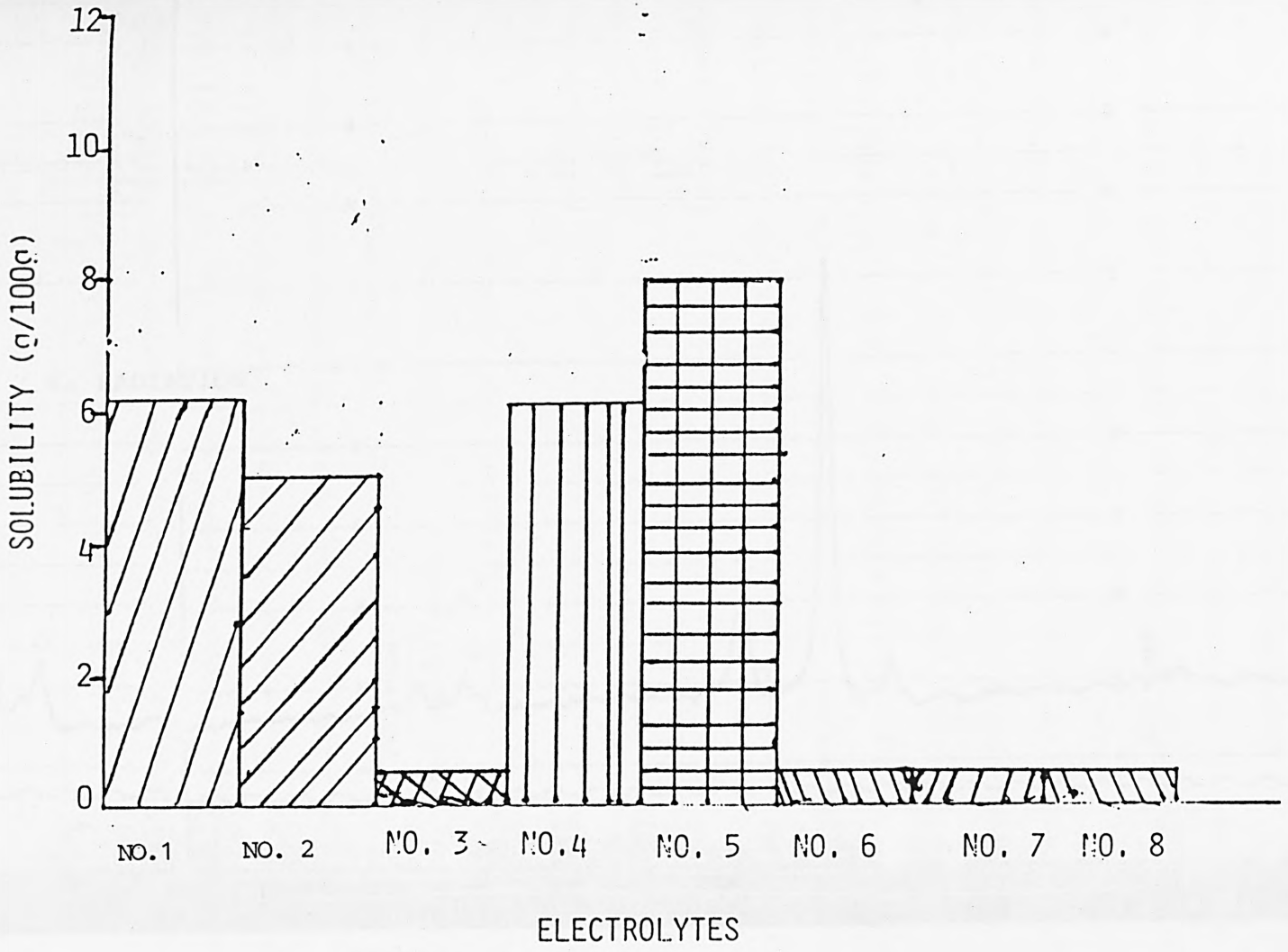

FIG. 6.9 SOLUBILITY OF REACTION PRODUCTS IN DIFFERENT ELECTROLYTES

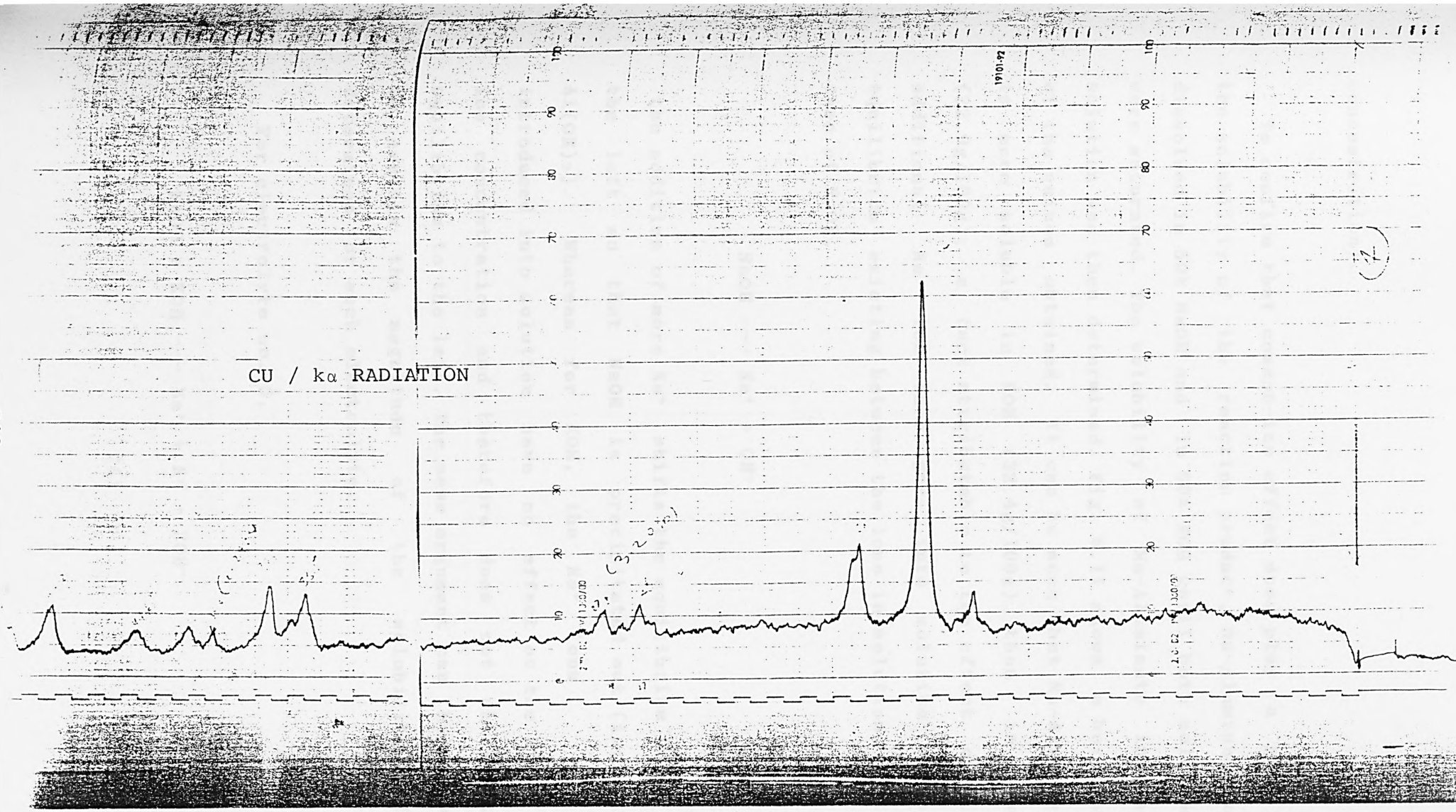

FIG. 6.10 X-RAY DIFFRACTION OF REACTION PRODUCTS FROM KOH/HgO

concentration).

To confirm that common-ion effect does play a part in the solubility of the reaction product, Na-Aluminate was dissolved in 50% NaOH and in 50% KOH until both solutions were saturated. The solubility of Na-Aluminate in each solution was then determined. Fig. 6.11 shows a bar chart of the values obtained. It can be seen that Na-Aluminate is more soluble in KOH (32.4g/100g) than in NaOH (22.9g/100g); a fact attributable to the effect of the additional Na ion that goes into solution on the equilibrium existing between the ions in solution. In the case of NaOH,

$$NaOH \text{ --- } Na^{+} + OH^{-}$$

the addition of more Na^{+} shifts the equilibrium to the left so that NaOH is precipitated out (including $Al(OH)_3$). Whereas for KOH, the Na^{+} ions introduced into solution have no effect on the K^{+} ion concentration and therefore does not shift the equilibrium to the left. The same argument can be pursued to explain the magnitude of the solubility value determined for each electrolyte.

For electrolyte no. 5,

$$NaOH + KOH \text{ --- } Na^{+} + K^{+} + 2OH^{-}$$

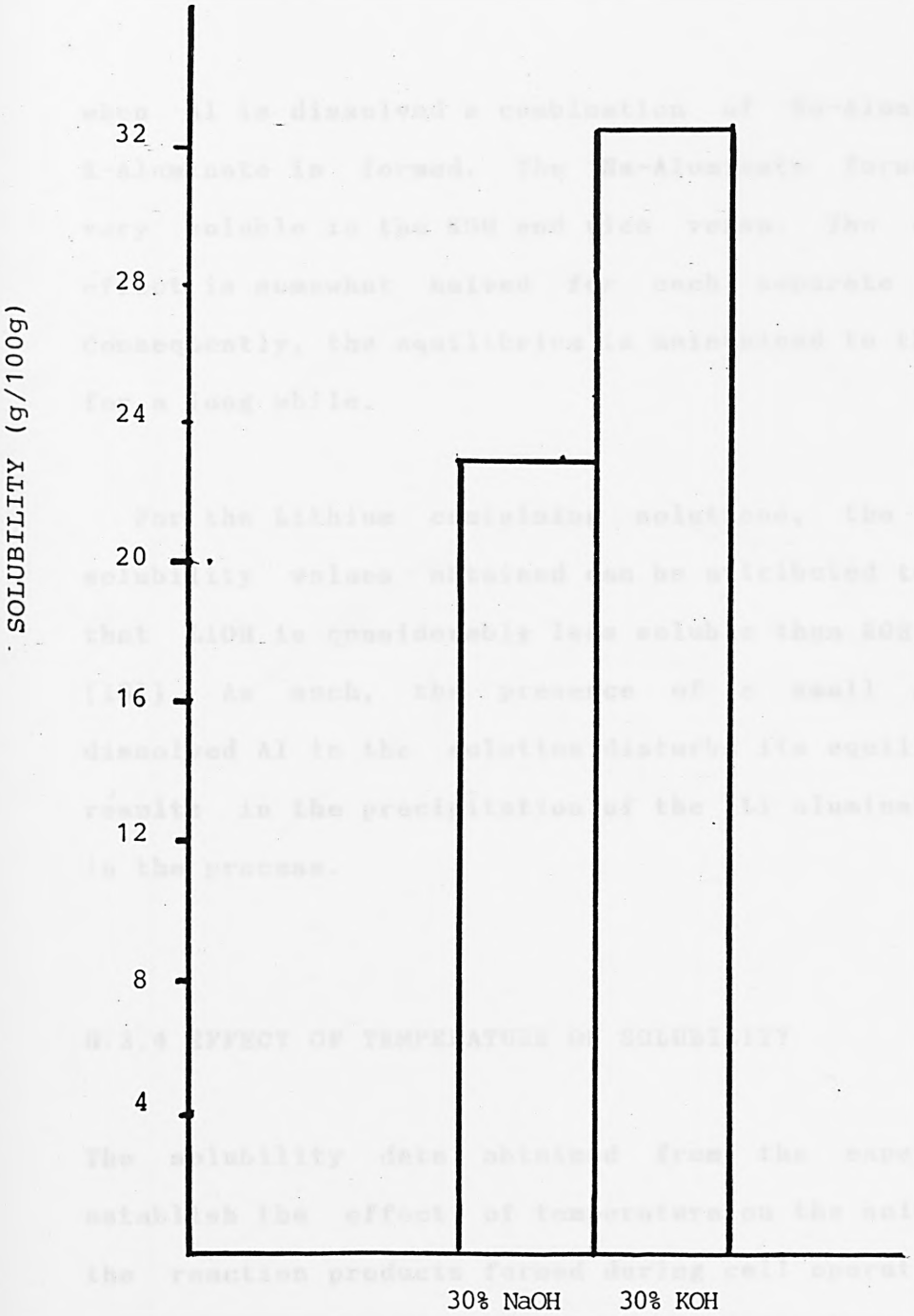

FIG. 6.11 SOLUBILITY OF SODIUM ALUMINATE IN 30% NaOH AND 30% KOH

when Al is dissolved a combination of Na-Aluminate and K-Aluminate is formed. The Na-Aluminate formed becomes very soluble in the KOH and vice versa. The common-ion effect is somewhat halved for each separate solution. Consequently, the equilibrium is maintained to the right, for a long while.

For the Lithium containing solutions, the very low solubility values obtained can be attributed to the fact that LiOH is considerably less soluble than KOH or NaOH [161]. As such, the presence of a small amount of dissolved Al in the solution disturbs its equilibrium and results in the precipitation of the Li-aluminate formed in the process.

6.3.4 EFFECT OF TEMPERATURE ON SOLUBILITY

The solubility data obtained from the experiment to establish the effect of temperature on the solubility of the reaction products formed during cell operation, were used to make plots of solubility against temperature for each electrolyte. These are shown as Fig. 6.12. Higher solubility values are shown for electrolyte no. 5 over the range of temperatures. Electrolyte nos. 1 and 4 have, significantly, same solubilities over the entire range. What is interesting here is the effect of temperature of the solubility for each electrolyte. For all

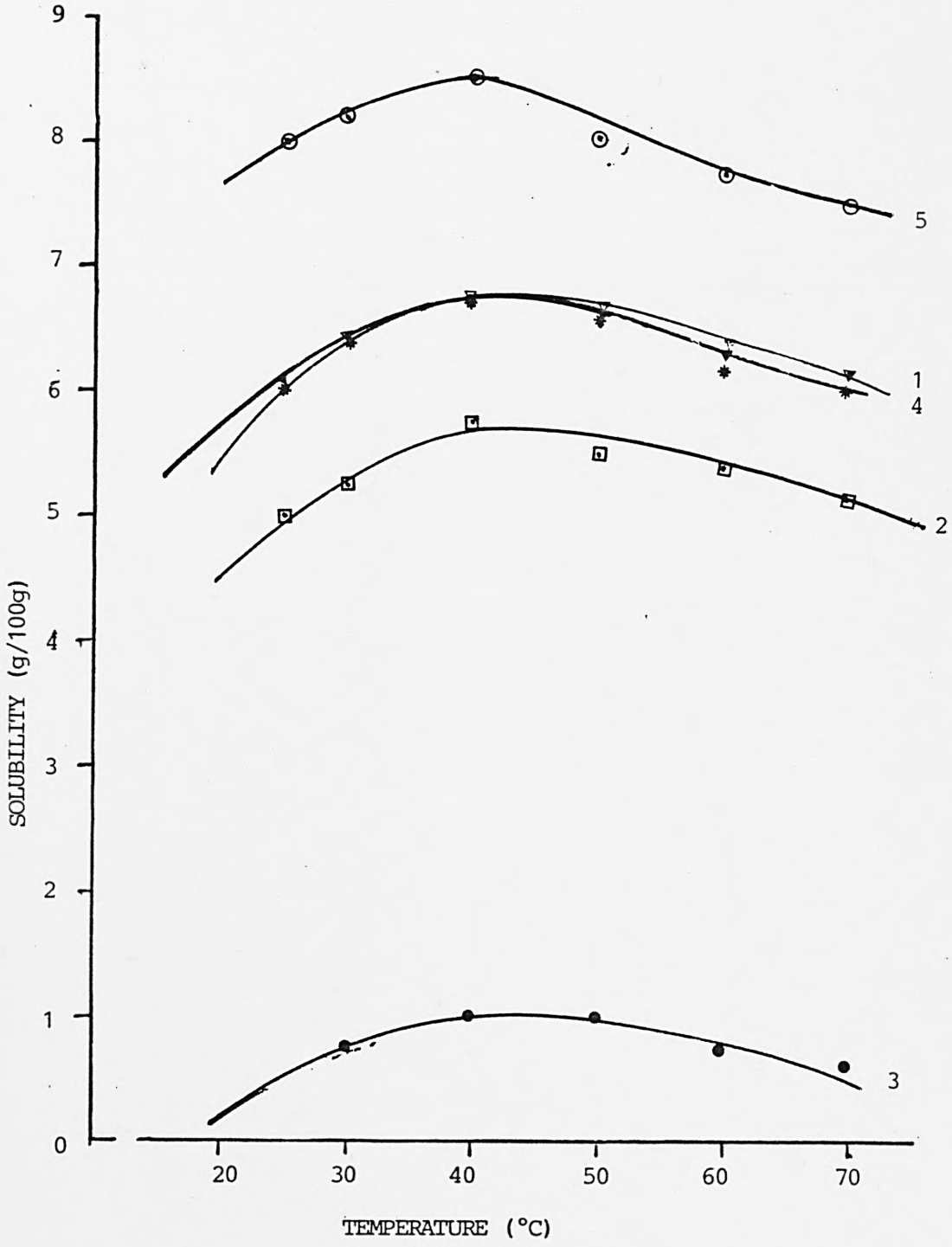

FIG. 6.12 EFFECT OF TEMPERATURE ON THE SOLUBILITY OF ALUMINATE IN DIFFERENT ELECTROLYTES

electrolytes, an increase in solubility with temperature is observed up to 40°C and then a decrease in solubility with increasing temperature, above that temperature. An explanation for that might lie in the nature of the reaction product formed at each temperature. It is put forward that, at lower temperatures a hydrated form of aluminate is formed and thus it is reasonably soluble whereas at higher temperatures, a process of dehydration takes place which significantly affects the aluminate formed, reducing its solubility.

The higher solubility values obtained for electrolyte no. 5, over the range of temperatures, prompted a further investigation into the potentials of a mixture of NaOH and KOH solution as suitable electrolyte for aluminium cells.

PART TWO: INVESTIGATING THE POTENTIALS OF A MIXTURE OF NaOH & KOH AS ELECTROLYTE FOR ALUMINIUM CELLS

A) CHOOSING SUITABLE SOLUTION CONCENTRATIONS TO MIX

For this investigation, it is requisite to obtain first the effective NaOH and KOH mixtures to be worked on since there are numerous NaOH and KOH mixtures, of different

concentrations, that can be prepared. Experiments were therefore carried out in a bid to select the mixtures that have high solubilities for the reaction products and are also highly conductive.

6.4 EXPERIMENTAL

6.4.1 EFFECT OF ELECTROLYTE CONCENTRATION ON SOLUBILITY OF REACTION PRODUCTS

It is the notion that to obtain a high solubility value for a mixture of NaOH and KOH, it will be useful to mix together the individual concentrations of NaOH and KOH that give high solubility values. Thus, the following experiment was carried out to find just those concentrations.

PROCEDURE

NaOH and KOH solutions were prepared, separately, at different concentrations. Pieces of Q4 were then dissolved in each solution until saturation. Care was taken, here also, to prevent carbon dioxide from diffusing into the solutions. The saturated solutions were left to stand, in a water bath at 25°C, for at least 24 hrs, to allow all undissolved particulate matter to settle down. Aliquot samples of the clear saturated

solutions were then pipetted into graduated flasks and diluted in the same manner as described in section 6.2.2. The same mode of analyses was followed.

6.4.2 EFFECT OF ELECTROLYTE CONCENTRATION ON CONDUCTIVITY

It is reasonable to choose the concentrations at which higher solubilities for Al were attained for the investigation. But it is very important that such solubilities are not achieved at the expense of low conductivities. In other words, a balance is required between the two variables.

PROCEDURE

The same strengths of NaOH and of KOH, as above, were prepared. The test tubes containing the solutions were immersed in the water bath at the same temperature as above. After ensuring temperature equilibration, the conductivities of the solutions were measured. Measurements were taken on duplicate samples as well.

6.5 RESULTS AND DISCUSSION

6.5.1 EFFECT OF CONCENTRATION ON SOLUBILITY

The data obtained were treated in the same manner as decribed in section 6.2.2. Plots of solubility against concentration were made for each electrolyte. These are shown as Figs. 6.13 and 6.14. For NaOH, an optimum is observed at 40% weight per volume; the solubility increases with increasing concentration up to 40% and then decreases with increasing concentration. There are only slight changes in solubility for concentrations between 30 and 50%. However, for KOH, a nonlinear increase is observed for increasing concentration.

Having noted the concentrations, of both electrolytes, which give high solubilities, their conductivities with respect to the other concentrations were also measured.

6.5.2 EFFECT OF CONCENTRATION ON CONDUCTIVITY

The conductivity data obtained were used to make plots of conductivity against concentration. These are also shown in Figs. 6.13 and 6.14. For both electrolytes, conductivity increases with concentration up to 30% electrolyte composition by weight/volume and then

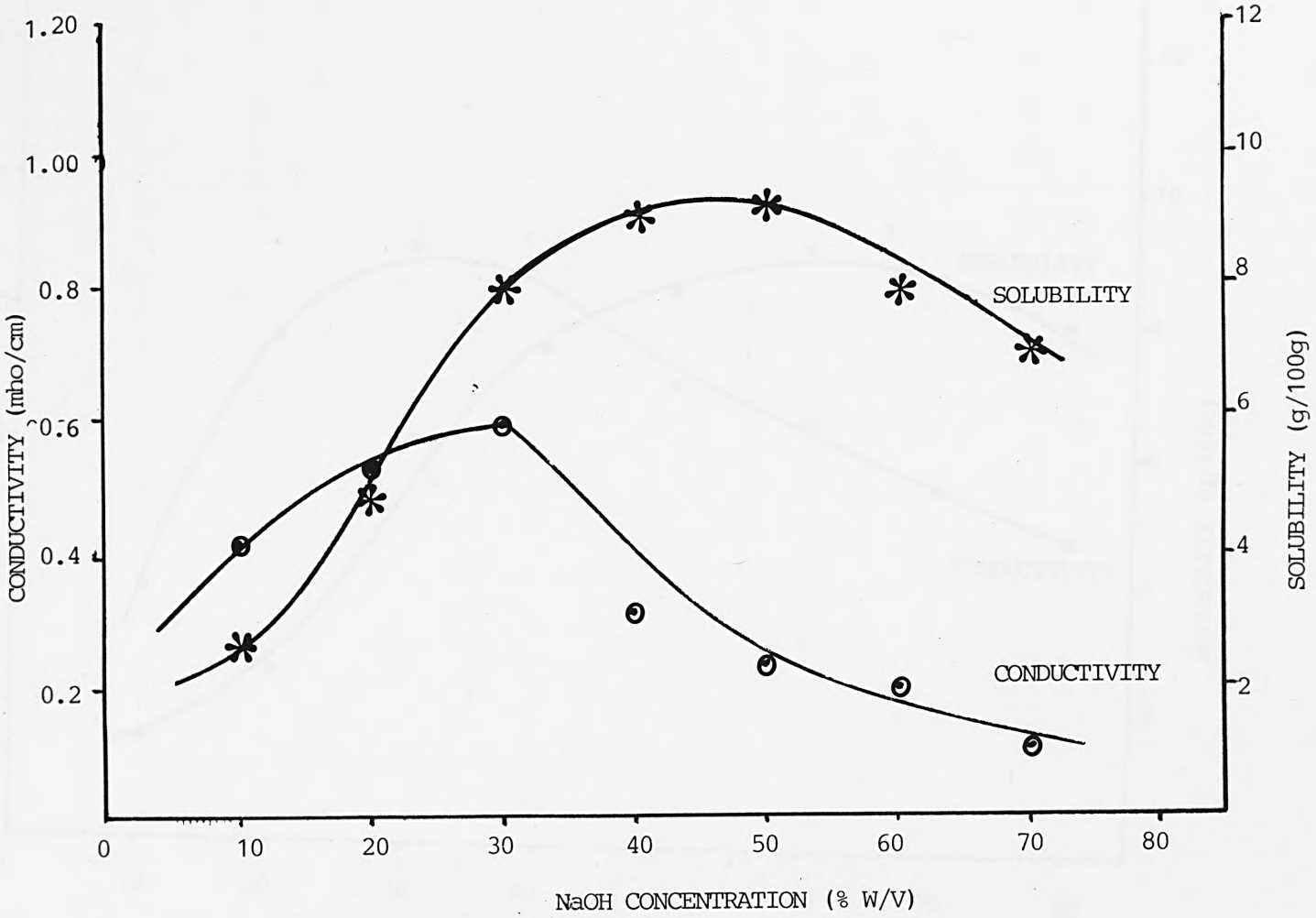

FIG. 6.13 CONDUCTIVITY EFFECT ON NaOH CONDUCTIVITY AND ON SOLUBILITY OF ALUMINATE

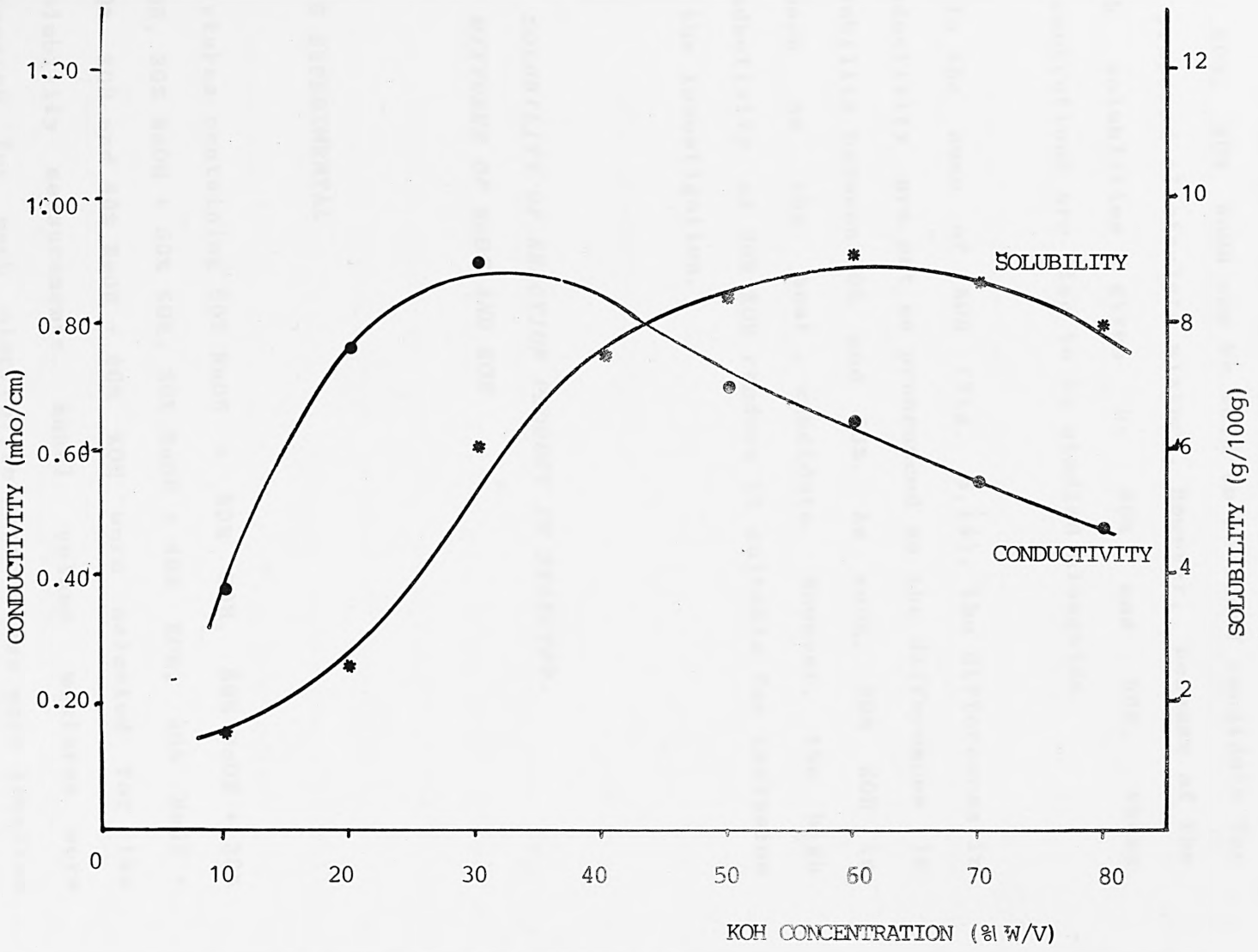

FIG. 6.14 CONCENTRATION EFFECT ON KOH CONDUCTIVITY AND ON SOLUBILITY OF ALUMINATE

decreases with further increases in concentration. The decrease in conductivity observed for concentrations beyond 30% is very pronounced for NaOH (Fig. 6.13). Since there is no significant change in solubility between 30% and 50%, 30% NaOH can be said to be ideal candidate for the proposed electrolyte mixture. However, because of the high solublities given by 40% and 50%, these concentrations are also to be studied alongside.

In the case of KOH (Fig. 6.14), the differences in conductivity are not as pronounced as the differences in solubility between 30% and 50%. As such, 50% KOH is chosen as the best candidate. However, the high conductivity of 30% KOH renders it suitable for inclusion in the investigation.

B) SOLUBILITY OF REACTION PRODUCT IN SELECTED MIXTURES OF NaOH AND KOH

6.6 EXPERIMENTAL

Mixtures containing 50% NaOH + 50% KOH, 50% NaOH + 30% KOH, 30% NaOH + 50% KOH, 30% NaOH + 40% KOH, 40% NaOH + 30% KOH and 40% NaOH + 40% KOH were selected for the solubility measurements. Equal volume mixtures were prepared for each electrolyte and these were labelled

electrolyte 9 - 14, respectively. The test tubes containing the electrolytes were immersed into a heated water bath to maintain a constant working temperature. Pieces of Q4 were then dissolved in the electrolyte until electrolyte saturation. The test tubes were cork-sealed to prevent carbon dioxide absorption. On attaining saturation, the solutions were left to stand, at the constant temperature, for at least 24 hrs to allow all undissolved particulate matter to settle down. Aliquot samples of the clear saturated solutions were pipetted into graduated flasks and diluted to the desired concentrations as explained in section 6.2.2. The same Atomic Absorption method of analyses was used here.

6.7 RESULTS AND DISCUSSION

The data obtained were used to construct bar charts. These are shown as Figs. 6.15-6.19. Fig. 6.15 shows the solubilities obtained for the electrolytes. Electrolyte no. 10 gives the highest solubility followed closely by no. 11. The solubilities obtained here are a remarkable improvement on that obtained for electrolyte no. 5 (section 6.2.2).

Figs. 6.16-6.18 compare the solubility of Al in each electrolyte mixture with the solubilities given by the individual solutions that were mixed together to form the

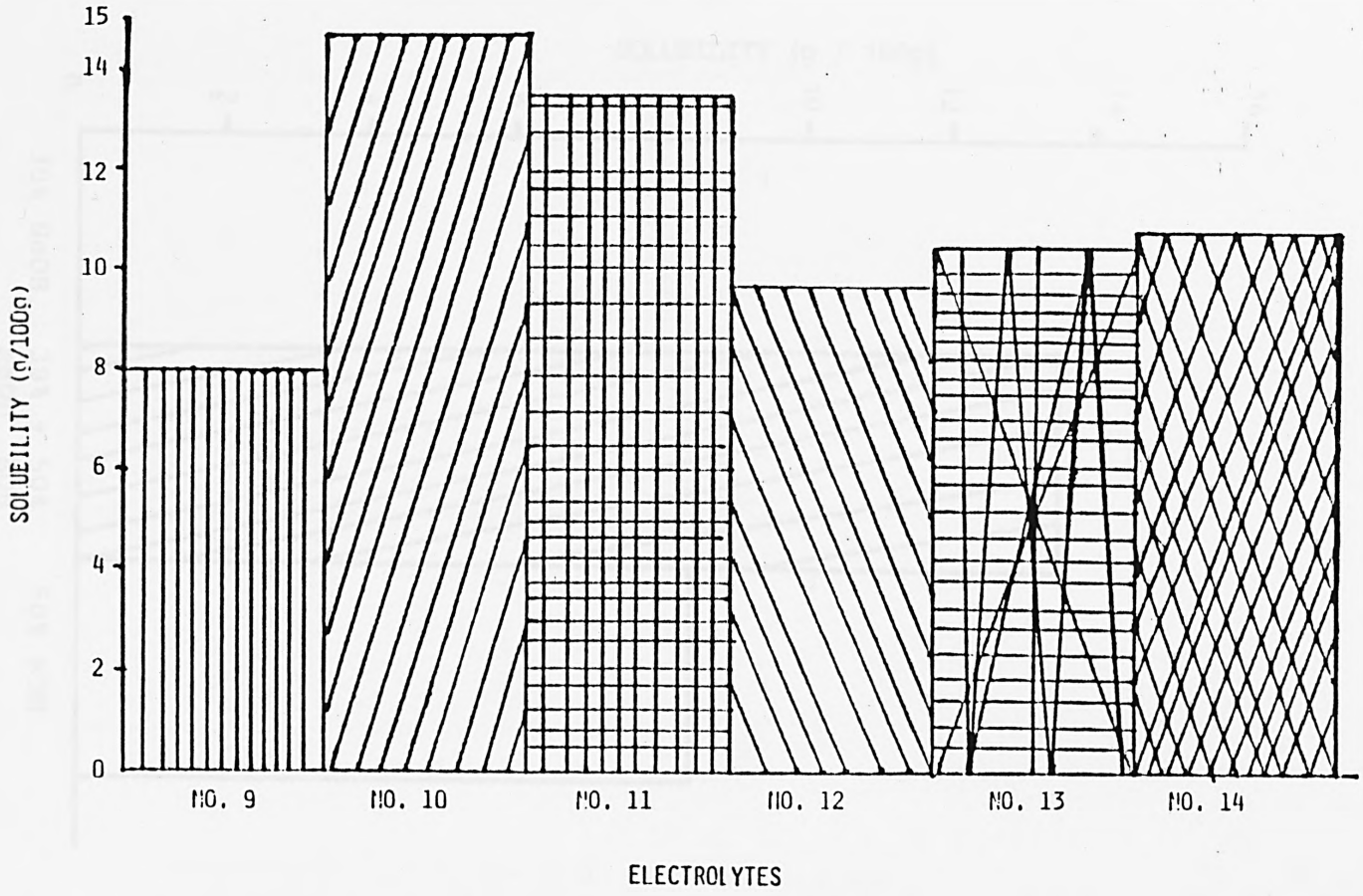

FIG. 6.15 SOLUBILITY OF REACTION PRODUCT IN ELECTROLYTE MIXTURES

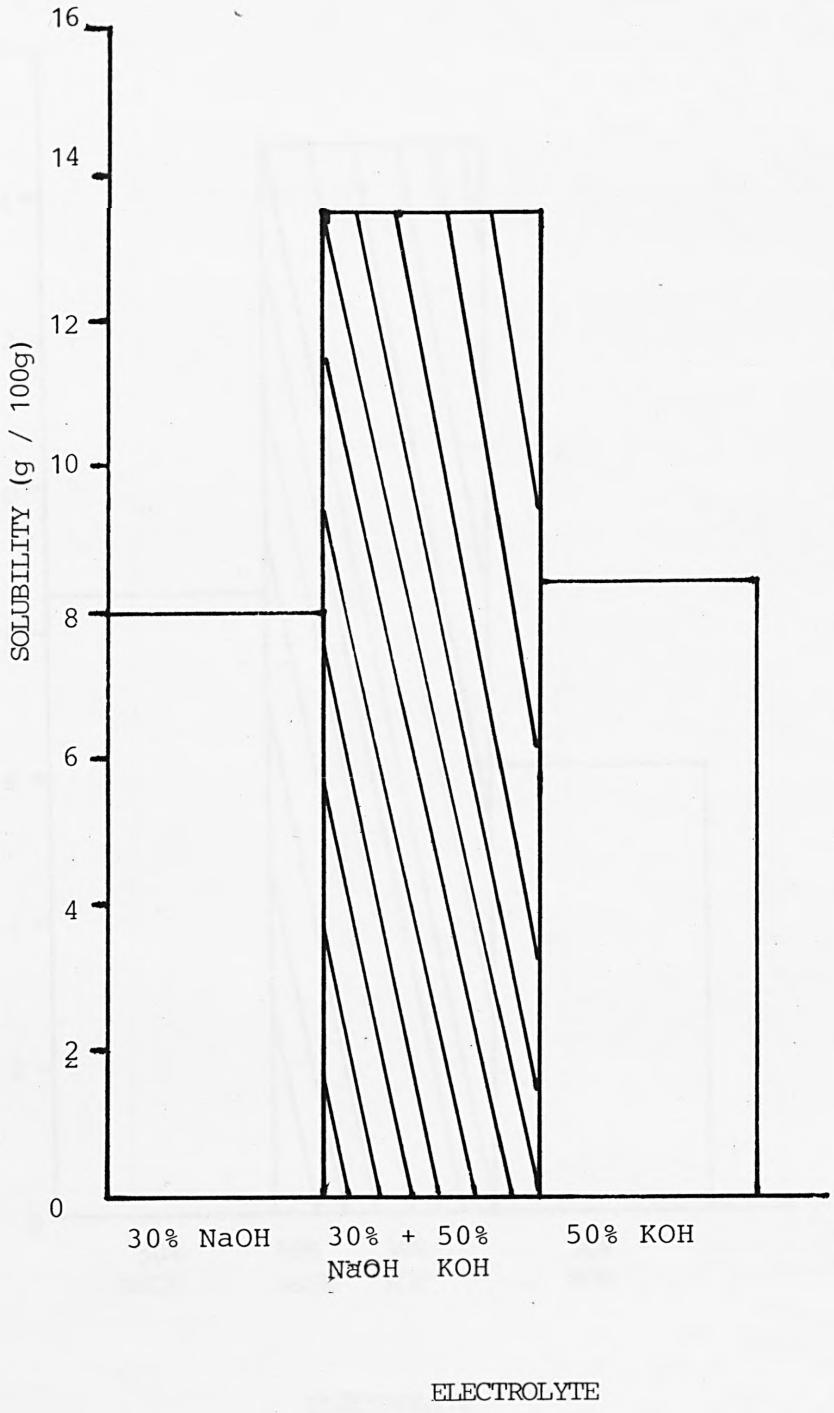

FIG. 6.16 CHANGES IN SOLUBILITY ON MIXING 30% NaOH AND 50% KOH

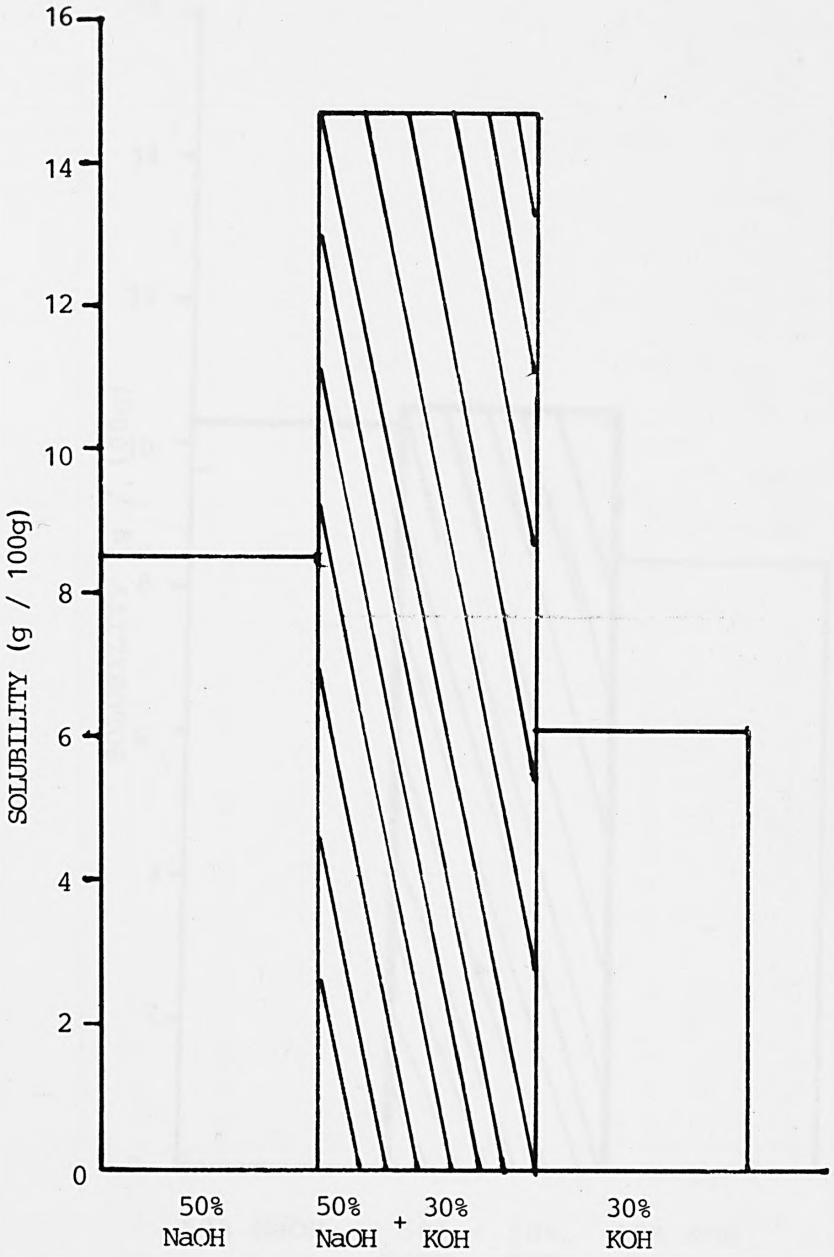

FIG. 6.17 CHANGES IN SOLUBILITY ON 50% NaOH AND 30% KOH

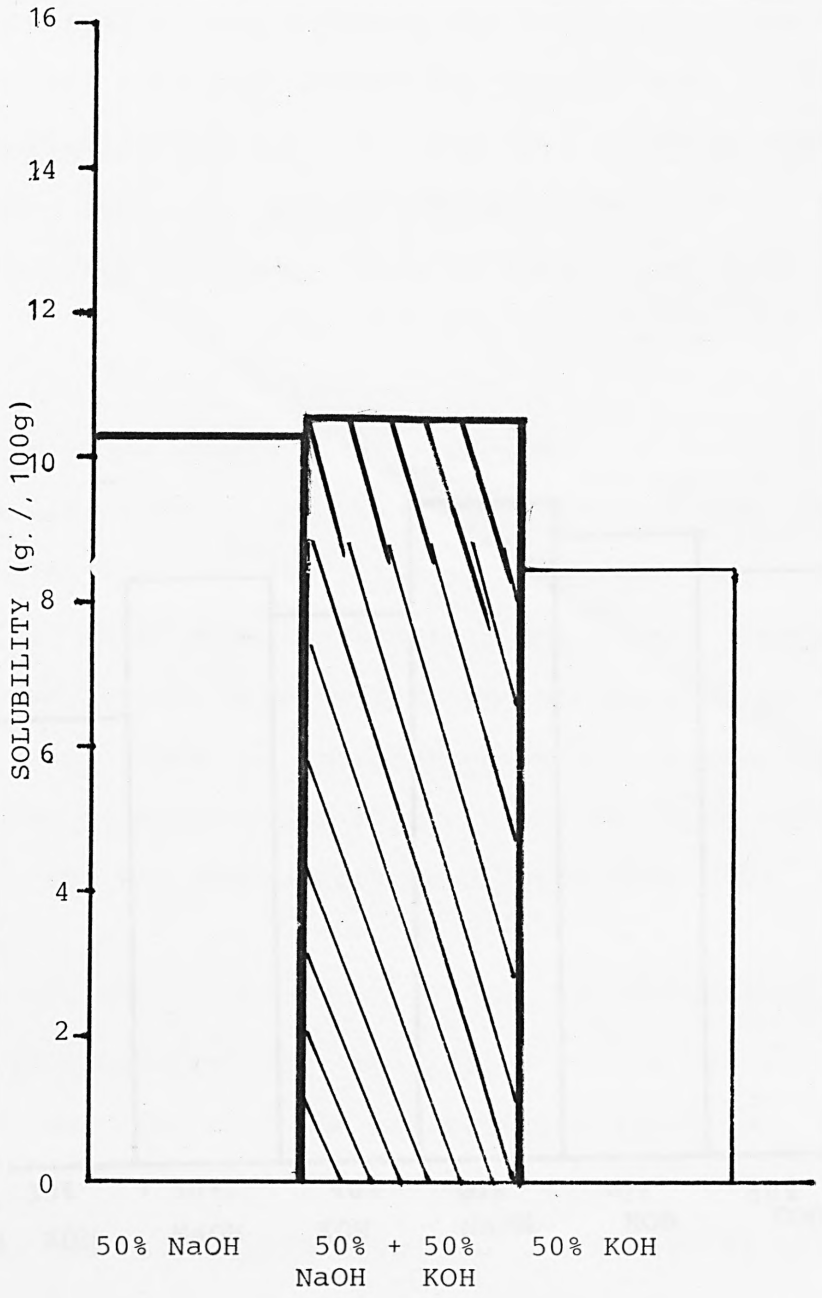

FIG. 6.18 CHANGES IN SOLUBILITY ON MIXING 50% NaOH AND 50% KOH

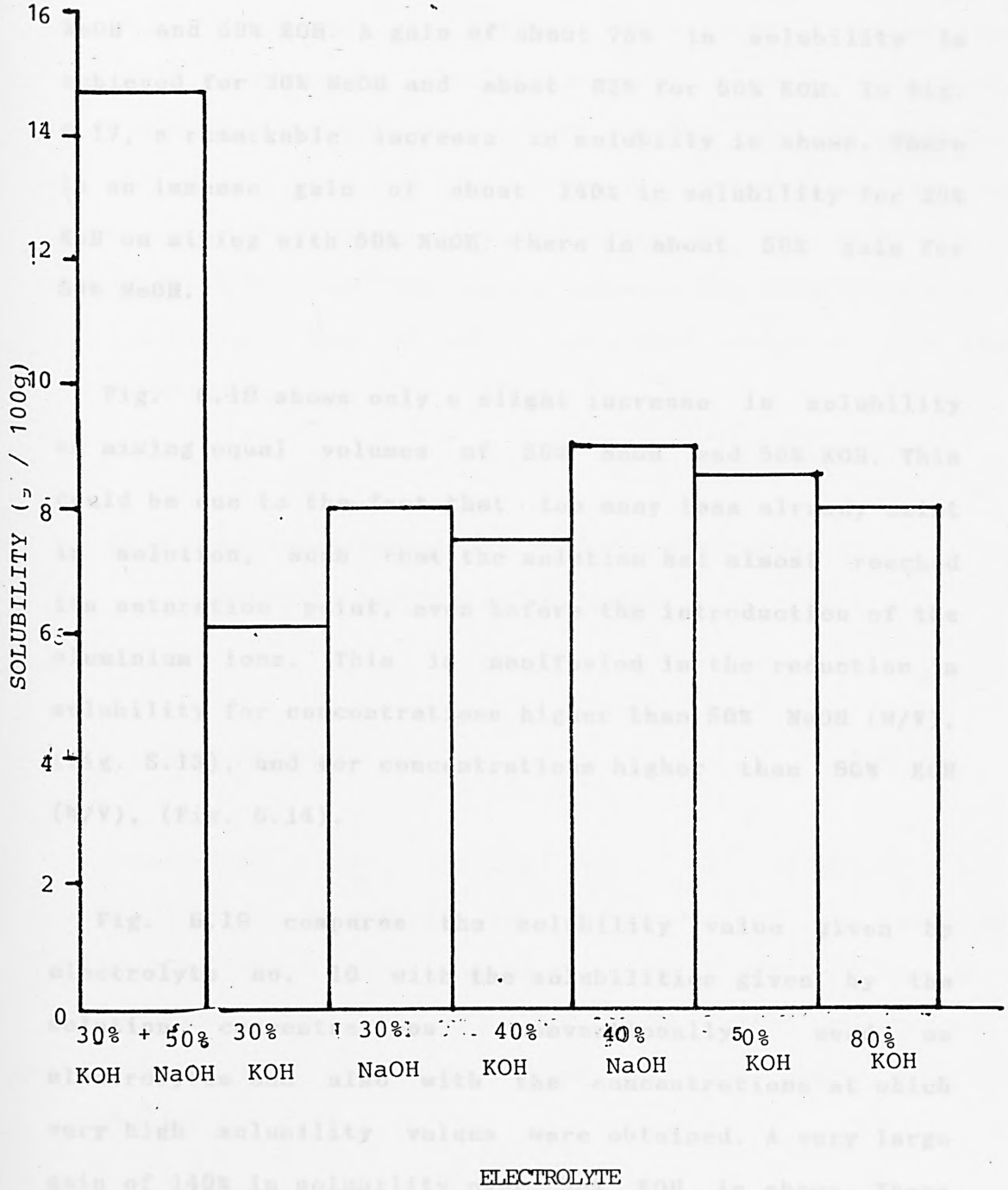

FIG.6.19 COMPARING THE SOLUBILITY OF REACTION PRODUCT IN ELECTROLYTE MIXTURE WITH THE SOLUBILITY IN CONVENTIONAL ALKALINE ELECTROLYTE

respective electrolyte mixture. Fig. 6.16 shows an increase in solubility on mixing equal volumes of 30% NaOH and 50% KOH. A gain of about 75% in solubility is achieved for 30% NaOH and about 62% for 50% KOH. In Fig. 6.17, a remarkable increase in solubilty is shown. There is an immense gain of about 140% in solubility for 30% KOH on mixing with 50% NaOH; there is about 58% gain for 50% NaOH.

Fig. 6.18 shows only a slight increase in solubility on mixing equal volumes of 50% NaOH and 50% KOH. This could be due to the fact that too many ions already exist in solution, such that the solution had almost reached its saturation point, even before the introduction of the aluminium ions. This is manifested in the reduction in solubility for concentrations higher than 50% NaOH (W/V), (Fig. 6.13), and for concentrations higher than 60% KOH (W/V), (Fig. 6.14).

Fig. 6.19 compares the solubility value given by electrolyte no. 10 with the solubilities given by the solution concentrations conventionally used as electrolytes and also with the concentrations at which very high solubility values were obtained. A very large gain of 140% in solubility over 30% KOH is shown. There is also a gain of about 84% over 30% NaOH.

The remarkable gains in solubility for the electrolyte

mixture over the conventional alkaline electrolytes means that the electrolyte mixture, when used in aluminium cells, will result in a considerable gain in discharge times. Further experiments were carried out to establish the electrochemical and physical properties of the selected electrolyte mixtures. Since in Fig. 6.15 only a slight difference is shown between the solubilities for electrolyte nos. 10 and 11, both were selected for the experiments.

PART C ELECTROCHEMICAL AND PHYSICAL PROPERTIES OF SELECTED ELECTROLYTE MIXTURES

6.8 EXPERIMENTAL

Experiments were carried out to establish the electrochemical and physical properties of the selected electrolytes; equal volume mixtures of 30% NaOH and 50% KOH and, 50% NaOH and 30% KOH. The conventional electrolytes, 30% NaOH and, 30% KOH, were studied alongside.

6.8.1 POLARISATION CHARACTERISTICS OF ALUMINIUM IN SELECTED ELECTROLYTE MIXTURES

The half-cell testing procedure was carried out. A 2

cm^2 strip of Q4 was used as the working electrode, a nickel mesh counter electrode and a $Hg/HgO.OH^-$ reference electrode were employed. Fresh aluminium strips were tested in each electrolyte. The potentials at different current densities were recorded. The IR drop at each current density was measured and plots of the IR corrected potential versus current density were made. The experiment was carried out at 25°C.

The Al electrode was further polarised under a galvanostatic regime. For this, the experimental set-up was as above, except that the Al electrode was polarised at a steady current density (100 mA/cm^2) and the corresponding potential was recorded over a period of time. The IR drop was measured at ten minute intervals and plots of the IR corrected potential versus time were made for the different electrolytes.

6.8.2 ANODIC EFFICIENCY OF Al IN SELECTED ELECTROLYTES

A 2.0 cm^2 of Q4 (0.4 mm thick strip) was fabricated, weighed and immersed into the electrolyte under test. The electrode was galvanostatically discharged at a steady current density of 100 mA/cm^2. The experiment was repeated using each different electrolyte. At an appropriate time, each experiment was terminated and the remaining alloy material dried and weighed. The loss in weight was noted

as well as the time taken. The experiments were all conducted at 25°C and repeated three times for each electrolyte.

6.8.3 SELF-DISCHARGE CHARACTERISTICS OF Al IN SELECTED ELECTROLYTES

The electrolytes were poured into the special test tubes described in section 3.2. The test tubes were allowed to stand in a heated water bath at 25°C. Fresh Al electrodes (strips of Q4), each having an exposed area of 4 cm^2, were fabricated and weighed. The weighed electrode was placed in the test electrolyte for a selected time interval. The amount of hydrogen evolved during the time period was measured, according to the procedure described in section 3.2. At the appropriate time, the remaining undissolved alloy material was weighed and the loss in weight was recorded alongside the time interval. The experiment was repeated three times for each electrolyte and the average losses in weight as well as the corresponding average times taken were used to calculate the equivalent coulombs lost; using Faraday's law.

6.8.4 CONDUCTIVITY OF SELECTED ELECTROLYTE MIXTURES

The conductivity of each electrolyte was measured at 25°C. The test tubes containing the samples were cork-sealed to prevent the diffusion of carbon dioxide into the electrolyte solutions and then immersed into a water bath. The water was then heated up to the desired temperature and maintained at that temperature for a long while, to allow the electrolyte solutions to be brought to the temperature of the bath. The temperatures of the electrolytes were confirmed by taking the temperature of each electrolyte, using a thermometer. After ensuring complete temperature equilibration, the conductivity of each electrolyte was determined using a digital conductivity meter. The readings were then noted and the average of three readings was taken as the conductivity of the particular electrolyte.

6.8.5 pH OF SELECTED ELECTROLYTES

The pH of each electrolyte was measured using a Corning pH meter. The test tubes containing the electrolyte samples and their duplicates were immersed into a water bath heated to 25°C and maintained at that temperature throughout the experiment. The meter was calibrated using 0.1 and 1M NaOH and 1M KOH. (pH readings of 13, 14 and 14 respectively [164]).

6.8.6 VISCOSITY OF SELECTED ELECTROLYTES

The viscosity measurements were carried out using an Ostwald viscometer (Fig. 6.20). The electrolytes were introduced at S, drawn by suction above P, and the time t taken for each electrolyte level to fall between the fixed marks P and Q was observed. The experiment was then repeated with the same volumes of the standard liquids; distilled water and ethyl alcohol (chosen liquids with known viscosities), and the time t' taken for each liquid to fall from P to Q was similarly observed. The experiment was repeated three times for each sample; all conducted at 25°C by immersing the viscometer in a water bath heated up to and maintained at that temperature.

6.8.7 REACTION PRODUCT ANALYSIS

The nature of the reaction products formed in the electrolytes was ascertained using the scanning electron microscopy and X-ray flourescence and diffraction techniques (see section 3.3). The samples were prepared by collecting and drying, at room temperature, the precipitates formed in each electrolyte, upon saturation. The samples were washed in acetone, under ultrasonic vibration, and then thinly dispersed onto labelled

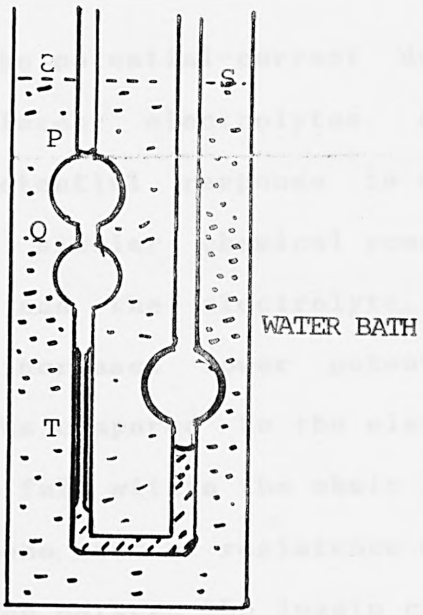

FIG. 6.20 AN OSTWALD VISCOMETER

specimen plates. Each sample was then sputerred with gold, as relayed in section 3.3. The samples were then examined, in turn.

6.9 RESULTS AND DISCUSSION

6.9.1 POLARISATION CHARACTERISTICS

Fig. 6.21 shows the potential-current density curves for Al in the different electrolytes. At low current densities the potential response is somewhat similar. This suggests a similar chemical reaction between the metal electrode and the electrolyte. However, as the current density increases lower potentials are obtained for NaOH and KOH as compared to the electrolyte mixtures. These differences fall within the ohmic region suggesting a build up of some sort of resistance within the system. Since the IR drop between the luggin capillary and the working electrode was corrected for, the other significant resistance source is that due to the electrolyte.

At lower current densities, the actual electrolyte resistances exist but do not show remarkable differences in potentials. As the current density increases, aluminium dissolution is enhanced and as such, reaction

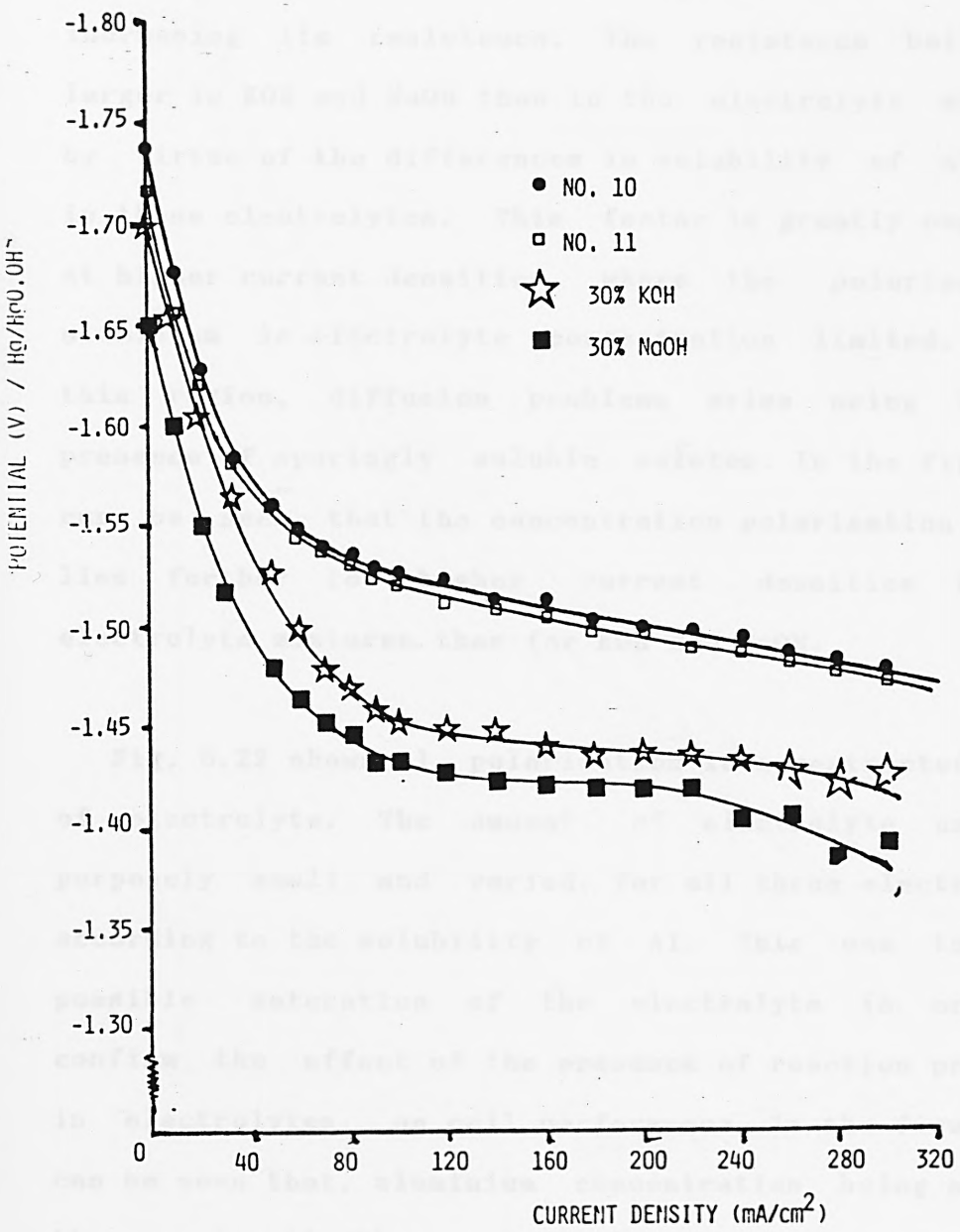

FIG. 6.21 POLARISATION OF Q4 IN SELECTED ELECTROLYTES

products are introduced into the electrolyte thereby increasing its resistance. The resistance build-up is larger in KOH and NaOH than in the electrolyte mixtures, by virtue of the differences in solubility of aluminium in these electrolytes. This factor is greatly emphasised at higher current densities, where the polarisation of aluminium is electrolyte concentration limited. Within this region, diffusion problems arise owing to the presence of sparingly soluble solutes. In the figure, it can be seen that the concentration polarisation region lies further to higher current densities for the electrolyte mixtures than for KOH and NaOH.

Fig. 6.22 shows Al polarisation in a restricted amount of electrolyte. The amount of electrolyte used was purposely small and varied, for all three electrolytes, according to the solubility of Al. This was to induce possible saturation of the electrolyte in order to confirm the effect of the presence of reaction products, in electrolytes, on cell performance. In the figure, it can be seen that, aluminium concentration being somewhat the same in all three electrolytes, the performance of the aluminium electrode is nearly the same for all the electrolytes.

Fig. 6.23 shows the galvanostatic polarisation of the aluminium electrode. A steady potential is maintained at the constant current density over a reasonable period of time. The slight potential drops were due to the reasons

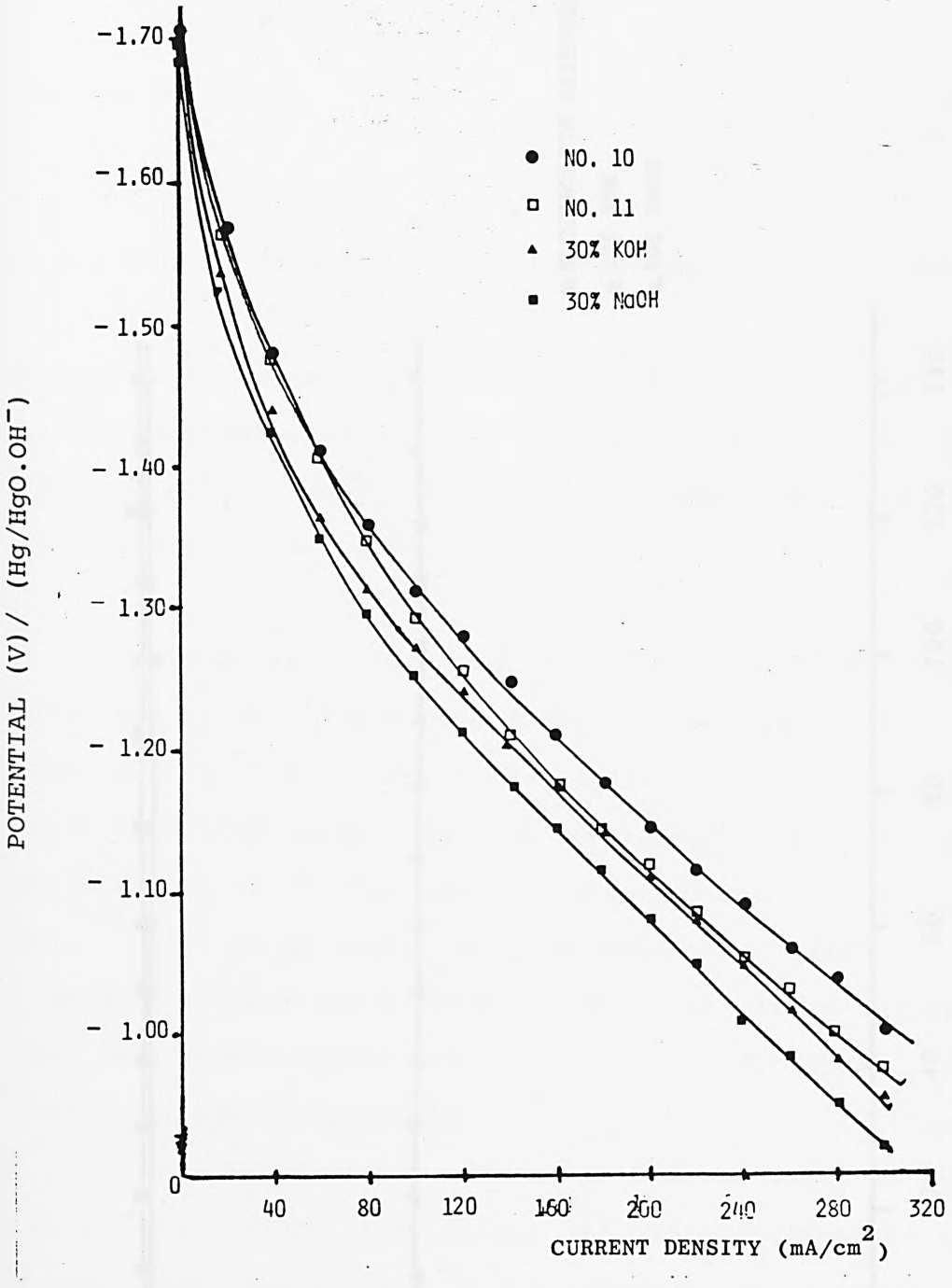

FIG. 6.22 POLARISATION OF Q4 IN RESTRICTED AMOUNT OF ELECTROLYTE

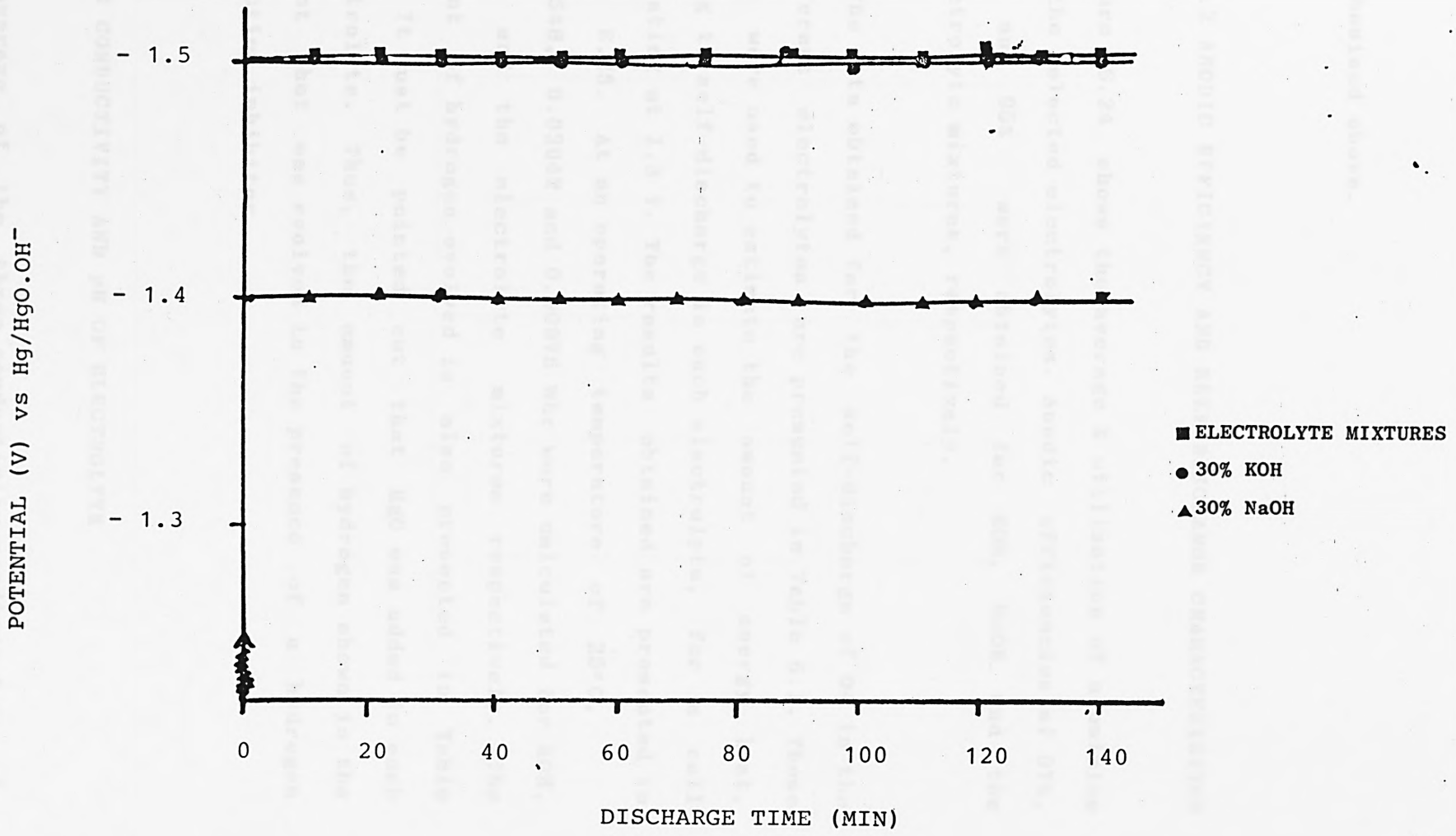

FIG. 6.23 GALVANOSTATIC DISCHARGE OF Q4 IN SELECTED ELECTROLYTES

emphasised above.

6.9.2 ANODIC EFFICIENCY AND SELF-DISCHARGE CHARACTERISTICS

Figure 6.24 shows the average % utilisation of aluminium in the selected electrolytes. Anodic efficiencies of 97%, 86% and 95% were obtained for KOH, NaOH and the electrolyte mixtures, respectively.

The data obtained for the self-discharge of Q4 in the different electrolytes are presented in Table 6.1. These data were used to estimate the amount of energy lost, owing to self-discharge in each electrolyte, for a cell operating at 1.3 V. The results obtained are presented in Fig. 6.25. At an operating temperature of 25°C, 0.02548, 0.03042 and 0.00975 Whr were calculated for KOH, NaOH and the electrolyte mixtures respectively. The amount of hydrogen evolved is also presented in Table 6.1. It must be pointed out that HgO was added to each electrolyte. Thus, the amount of hydrogen shown is the amount that was evolved in the presence of a hydrogen evolution inhibitor.

6.9.3 CONDUCTIVITY AND pH OF ELECTROLYTE

The average of the three conductivity readings for each

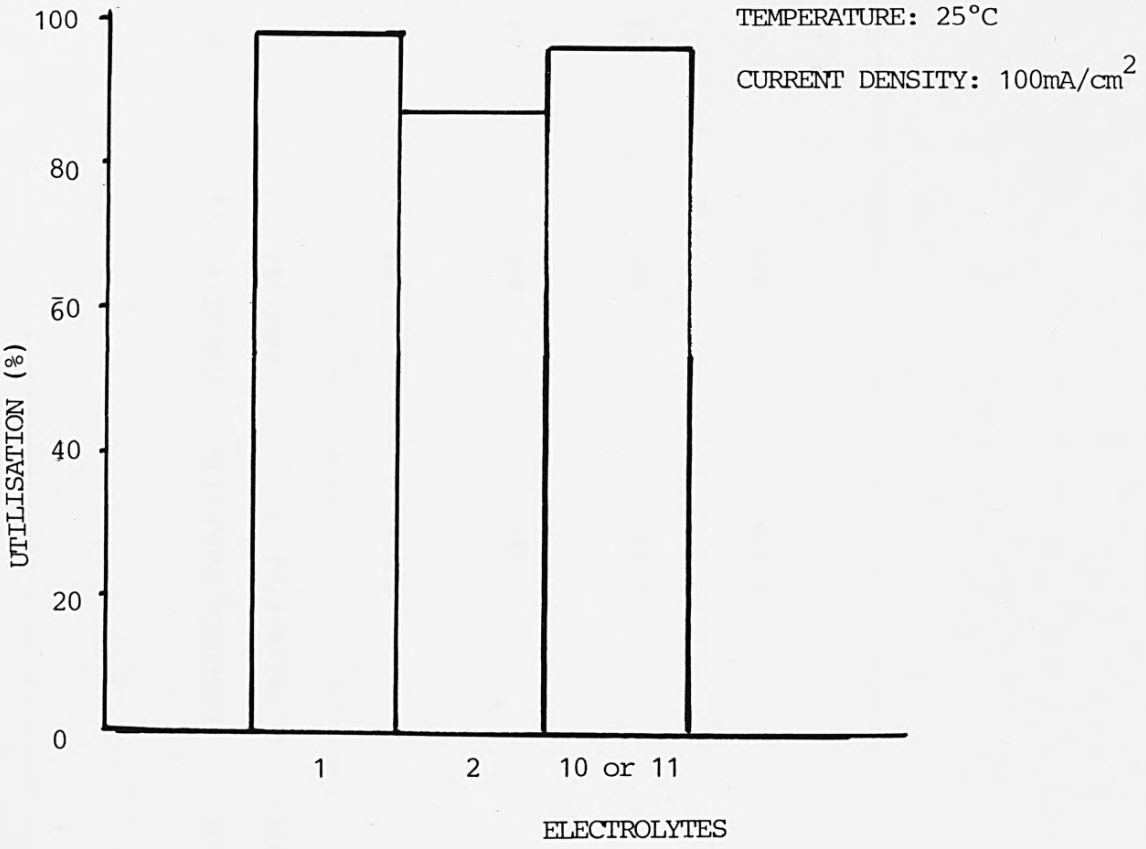

FIG. 6.24 UTILISATION OF Q_4 IN SELECTED ELECTROLYTES

TABLE 6.1 SOME ELECTROCHEMICAL PHYSICAL PROPERTIES OF SELECTED ELECTROLYTES @ 25 C

ELECTROLYTE	SELF-DISCHARGE OF Q4 (COULOMBS LOST)	HYDROGEN EVOLUTION (ml/min/cm)	CONDUCTIVITY (mho/cm)	pH	VISCOSITY ABSOLUTE(cp)	KINEMATIC
30% NaOH	84.24	2.594	.395	14	2.96	2.226
30% KOH	70.56	.383	.594	14	1.78	1.376
30%KOH+50%NaOH	27.01	1.252	.407	14	3.42	2.428
50%KOH+30%NaOH	27.01	1.238	.454	14	3.27	2.336

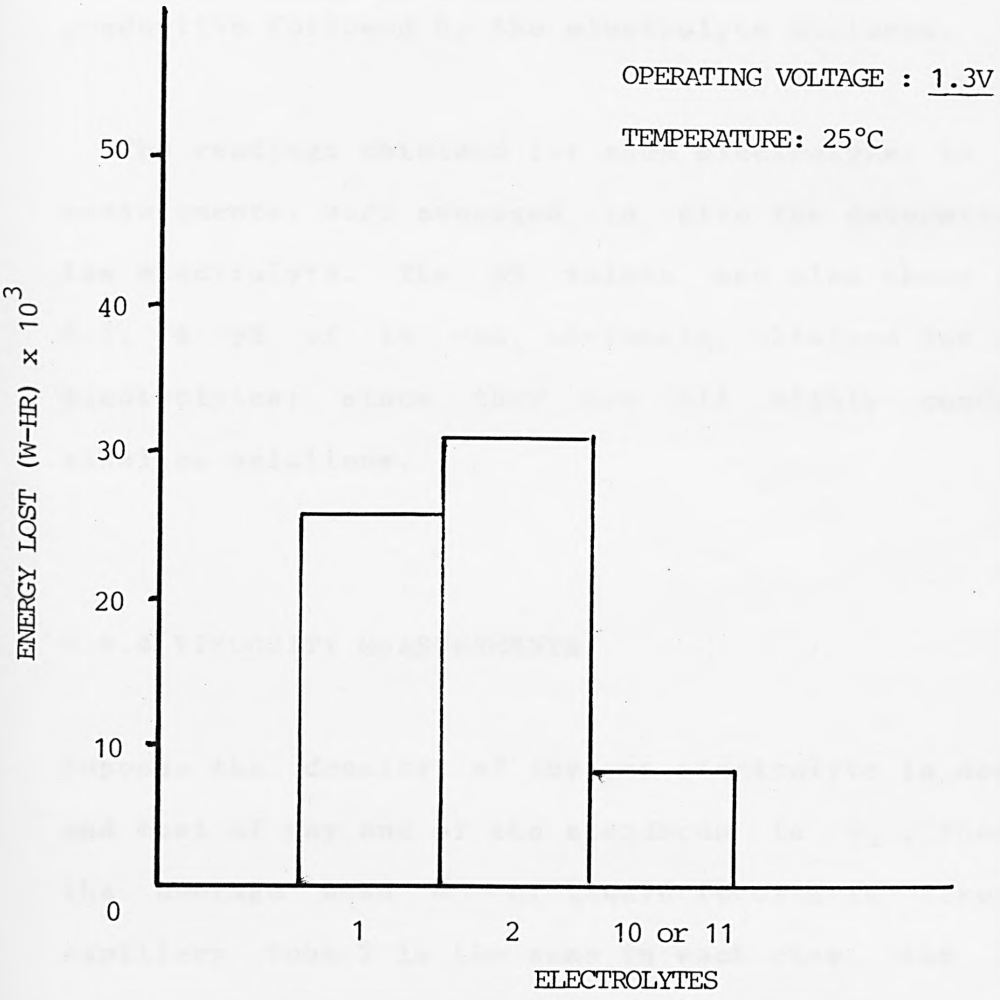

FIG. 6.25 ENERGY LOSS OWING TO SELF-DISCHARGE OF Q_4 IN DIFFERENT ELECTROLYTES

electrolyte was taken as its conductivity. The conductivity values obtained, for all the electrolytes, are also shown in Table 6.1. 30% KOH is the most conductive followed by the electrolyte mixtures.

The readings obtained for each electrolyte, in the pH measurements, were averaged to give the determined pH of the electrolyte. The pH values are also shown in Table 6.1. A pH of 14 was, obviously, obtained for all the electrolytes, since they are all highly concentrated alkaline solutions.

6.9.4 VISCOSITY MEASUREMENTS

Suppose the density of any one electrolyte is denoted by ρ_1 and that of any one of the standards is ρ_2. Then, since the average head h of liquid forcing it through the capillary tube T is the same in each case, the pressure excess between the ends of T = $h \rho_1 g$, $h \rho_2 g$ respectively. If the volume of liquid between the marks P, Q is V, then, from Poiseuille's formula, we have

$$[V/t] = [\pi h g a^4 (\rho_1)] / [8 l \eta_1] \qquad (6.1)$$

where a is the radius of T, η_1 is the coefficient of viscosity of the electrolyte and l is the length of T. Similarly, for the standard,

$$[V/t'] = [\pi hg a^4 (\rho_2)] / 8l\eta_2] \quad (6.2)$$

Dividing (6.2) by (6.1)

$$[t/t'] = \left[\eta_1 / \eta_2\right] \left[\rho_2 / \rho_1\right] \quad (6.3)$$

which implies

$$[\eta_1/\eta_2] = [t \rho_1] / [t' \rho_2] \quad (6.4)$$

Thus, determining all the other parameters, the coefficients of viscosity of the electrolytes were calculated using equation 6.4. The average time takn for each sample was used in the calculation. The coefficients of viscosity with respect to each standard were calculated and the average of the values obtained, with respect to the two standards, were taken as the coefficients of viscosity of the electrolytes. These are shown in Table 6.1. Also shown in Table 6.1 are the kinematic viscosities; the ratio of the absolute viscosity to the density of each electrolyte. The kinematic viscosity (μ) of each electrolyte gives a

measure of Diffusivity in the electrolyte [165].

6.9.5 NATURE OF REACTION PRODUCTS

The results obtained from the scanning electron microscopy examinations and the X-ray determinations are shown as Figs. 26-28. It can be seen that the precipitates agglomerate differently for each electrolyte. The nature of the agglomeration is very important in the management of the precipitates. The micrographs for NaOH and the electrolyte mixtures show large agglomerations for the precipitates formed, whereas the micrographs for the KOH shows small agglomerations. The precipitates showing large agglomerations were granular in nature unlike the fine powder obtained for the KOH precipitates. Thus, the larger the agglomeration the easier it will be to dispose off the precipitate. Therefore, an Al cell using a NaOH electrolyte or the electrolyte mixtures will have a lower maintainence problem as compared to one using a KOH electrolyte.

6.10 GENERAL CONCLUSION

The conductivity of an electrolyte is found to change during cell operation, as a result of a resistance build-up in solution. The resistance build-up is due to

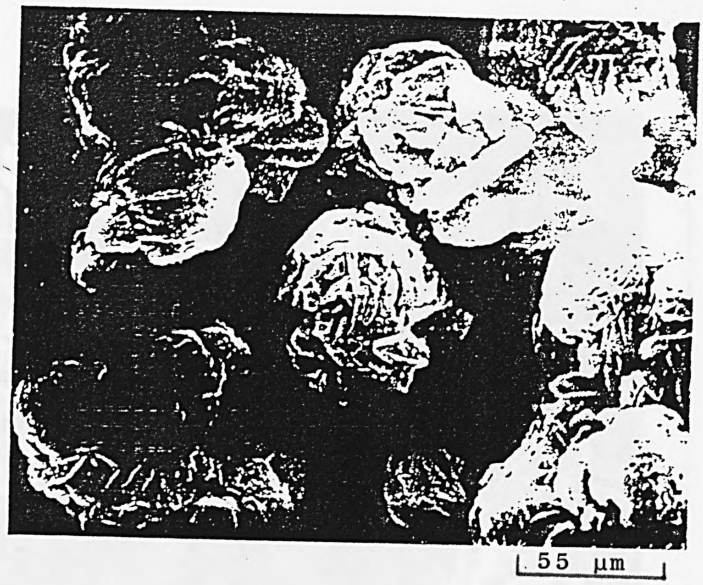

FIG. 6.26 NATURE OF REACTION PRODUCT FORMED IN ELECTROLYTE MIXTURES

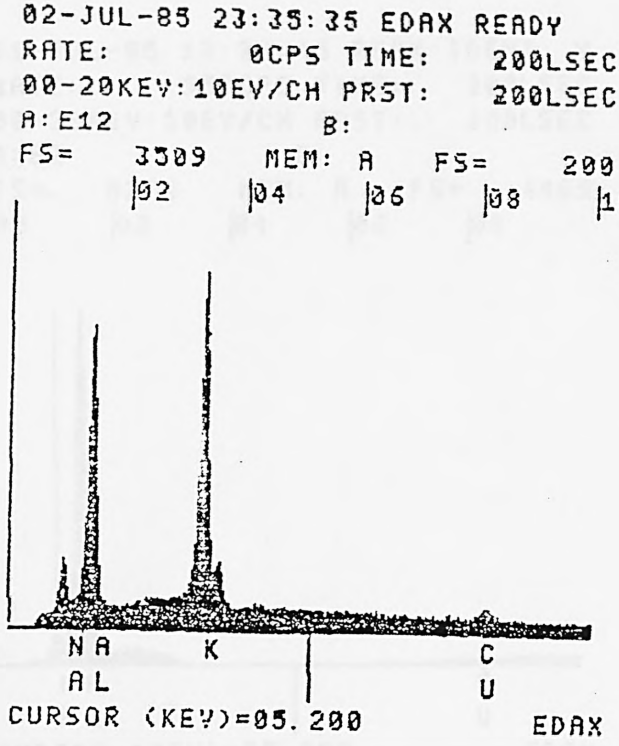

FIG. 6.27 NATURE OF REACTION PRODUCT FORMED IN 30% NaOH

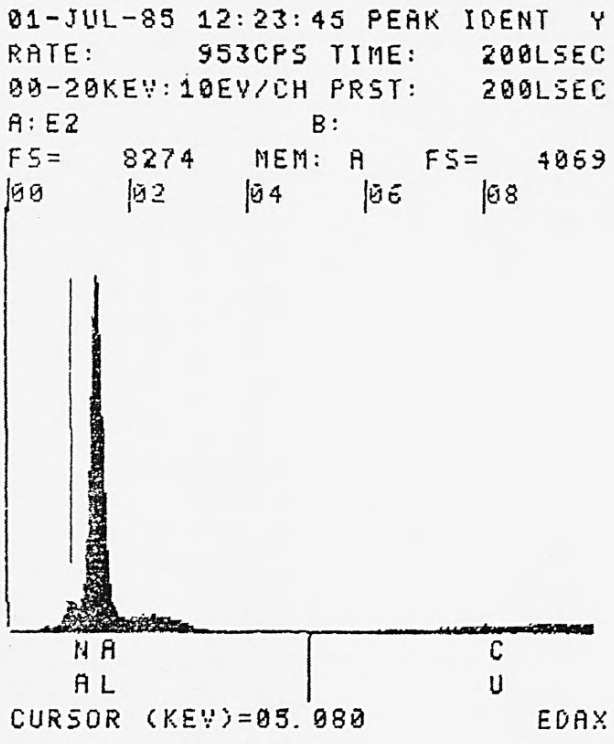

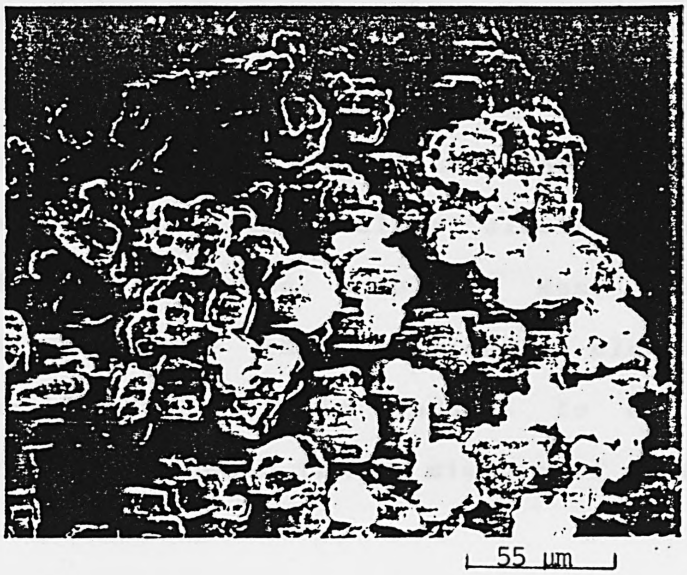

FIG. 6.28 NATURE OF REACTION PRODUCT FORMED IN 30% KOH

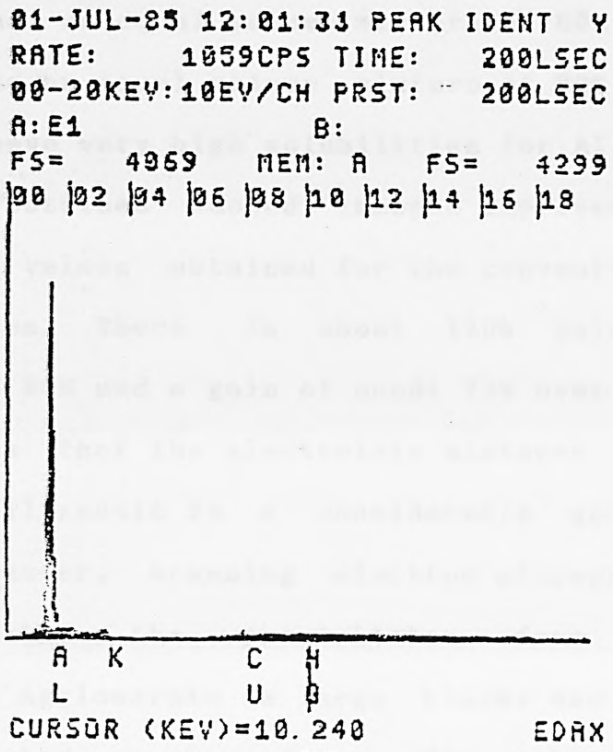

the presence of sparingly soluble reaction products, formed from the dissolution of aluminium. The performance of Al as anode material in alkaline electrolytes is, thus, limited by diffusion problems; mass transfer limitation. To ameliorate the situation, an electrolyte with high solubility for Al is thought to be ideal. Solubility measurements showed that a mixture of NaOH and KOH solutions is promising.

Investigations carried out to assess the potentials of the mixture of NaOH and KOH solutions as electrolyte for Al cells, showed that an equal volume mixture of 50% NaOH and 30% KOH (W/V) and an equal volume mixture of 30% NaOH and 50% KOH (W/V) have very high solubilities for Al. The solubility values obtained showed immense improvements over the solubility values obtained for the conventional alkaline electrolytes. There is about 140% gain in solubility over 30% KOH and a gain of about 73% over 30% NaOH. Which implies that the electrolyte mixtures when used in Al cells, will result in a considerable gain in discharge times. Moreover, scanning electron micrographs obtained showed that the precipitates from the electrolyte mixtures agglomerate in large blocks and thus can be easily flushed or cleaned away. The problem of cell clogging can therefore be alleviated if these electrolyte mixtures are used in Al cells.

The electrochemical behaviour of Al in the electrolyte

mixtures showed improvements in polarisation. Other electrochemical properties measured showed no disadvantage in using these electrolytes. For example, an anodic efficiency of 95% is obtained for the electrolyte mixtures; compared to 86% for 30% NaOH and 97% for 30% KOH. Self-discharge of Al in the electrolyte mixtures are relatively small.

Thus, overall, the best alkaline electrolyte for Al cells is either an equal volume mixture of 50% NaOH and 30% KOH or an equal volume mixture of 30% NaOH and 50% KOH. However, the former is preferred to the latter, although there is not much significant difference in their electrochemical and physical properties. The reason is, not only has the former a higher solubility for Al, but it is cheaper to make, in terms of the individual costs of NaOH and KOH solids. NaOH is cheaper than KOH and the former uses more NaOH than KOH, whereas the latter uses more KOH than NaOH, to produce the same electrolyte strength.

The effect of temperature on conductivity and solubility was also established. In general, it is found that conductivity increases with temperature; the rate of increase depending on the type of electrolyte. For the solubility measurements, it is found that the solubility of Al increases with temperature up to 40°C. At temperatures higher than that, the solubility slowly decreases. This trend in solubility suggests different

reaction schemes, for Al dissolution, at low and high temperatures.

At low temperatures, the reaction product is a combination of aluminate and aluminium trihydroxide, with the eventual precipitation of the hydroxide. Whereas at high temperatures, the reaction product is a combination of the aluminate and the least soluble aluminium oxide; due to a process of dehydration. Thus, the following reaction scheme is suggested for the dissolution of Al in alkaline electrolytes:

At low temperatures:

$$Al + 4OH^- \longrightarrow Al(OH)_4^- + 3e$$

$$Al(OH)_4^- \xrightarrow{\text{saturation}} Al(OH)_3\downarrow + OH^-$$

$$Al + 3OH^- \xrightarrow{\text{saturation}} Al(OH)_3\downarrow + 3e$$

At high temperatures:

$$Al + 4OH^- \longrightarrow Al(OH)_4^- + 3e$$

$$Al(OH)_4^- \xrightarrow{\text{saturation}} Al(OH)_3\downarrow + OH^-$$

$$Al(OH)_3 \xrightarrow{\text{dehydration}} \tfrac{1}{2}Al_2O_3\downarrow$$

$$Al + 3OH^- \xrightarrow[\text{dehydration}]{\text{saturation}} \tfrac{1}{2}Al_2O_3\downarrow + 3e$$

7 ALUMINIUM CELL RECHARGEABILITY AND THERMAL MANAGEMENT

7.1 CELL RECHARGEABILITY

7.1.1 INTRODUCTION

In chapter one, the class types under which cells are broadly classified was outlined. As explained, rechargeable cells tend to be cost effective for applications requiring continuous supply of power for a long period of time. Two ways of recharging a cell was touched upon. One way is to recharge the cell by applying external current to it, forcing the cell reaction to reverse. The other way is to refuel the cell with fresh reactants. For a cell to be recharged by the application of external current, the overall reaction involved must be reversible. Since the overall cell reaction that takes place in an aluminium-air cell is irreversible within the cell unit, it implies that, this method of recharging a cell cannot be used.

However, since in the operation of the cell the Al anode material is consumed, the spent material can be replaced by a fresh one. This can be done either manually

or automatically. For the mechanical recharging of the cell to be carried out manually and conveniently, the Al material must be safe to handle and stored at ambient conditions. These conditions will depend on the nature of the ready-to-use anode material, whether it contains any active materials that are very reactive under ambient conditions. The alloy, Q4, proposed to be used (see chapter 4) is not active at ambient conditions and is very safe to handle. Thus, manual mechanical recharging can be carried out. But, for purposes requiring continuous power usage with little supervision, mechanical recharging by manual means can be weary and dreary and expensive, in terms of labour. Here, the appropriate way is to recharge the cell automatically. This requires the Al material to be shaped in such a way that continuous automatic feeding into the cell system is possible. For this reason, Despic [33,166] developed the self-perpetuating semi-wedge anode (Fig. 7.1), which is reported to sink when it is consumed enabling a constant distance between the cell electrodes to be maintained, thereby maintaining a constant internal resistance within the cell. Along similar lines, the author's supervisor has proposed that the aluminium material used should be ball-shaped.

To establish whether the concept of using shot is acceptable, the following investigations were embarked upon.

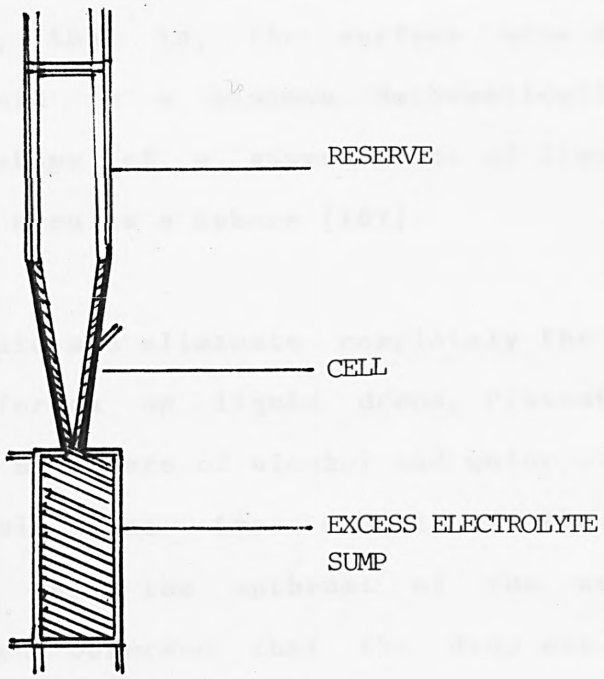

FIG. 7.1 SCHEMATIC DIAGRAM OF A MECHANICALLY RECHARGEABLE CELL WITH A SELF-PERPETUATING WEDGE ANODE

7.1.2 EXPERIMENTAL

A) FABRICATION OF ALUMINIUM SHOTS

The potential energy of any system in stable equilibrium is a minimum. Thus under surface tension forces, the area of a liquid surface will have the least number of molecules in it, that is, the surface area of a given volume of liquid is a minimum. Mathematically, it is shown that the shape of a given volume of liquid with a minimum surface area is a sphere [167].

To substantiate and eliminate completely the effect of gravitational forces on liquid drops, Plateau placed a drop of oil in a mixture of alcohol and water of the same density. In this case the weight of the drop is counterbalanced by the upthrust of the surrounding liquid. He then observed that the drop was a perfect sphere [167]. Plateau's 'spherule' experiment can be followed for the fabrication of aluminium shots by melting the aluminium in the presence of a melting salt or powder that has lower surface energy than liquid aluminium and can destroy the protective oxide film on the surface of the metal. Due to surface tension forces, the liquid metal will attain a minimum surface area by forming a sphere. If the surface is not disturbed, the liquid on cooling solidifies into a shot.

PROCEDURE

A piece of alloy Q4 was cut, rolled and dipped into a borax salt slurry (sodium tetraborate) and placed in a hole, previously drilled in a pyrolytic graphite slate. An acetylene-oxygen flame was then applied to the arrangement, to melt the aluminium. The flame was moved away as soon as a molten ball was formed. The arrangement was allowed to cool down and the resulting solid ball retrieved. The surface of the shot was then washed in a concentrated citric acid solution.

B) FEASIBILITY TESTS

The ease with which shots can be fed automatically and continuously is appreciated. However, if the performance of the anode in such a confiquration is heavily impaired, in one way or the other, it will be contrary to the aim of the project to use them. For this reason, tests were carried out to:

i) measure the electronic conductivity, through the contact-interface between two shots.

ii) determine the polarisation characteristic of the Al shot, comparing it to that of Al plate.

Also, since the active anode material is consumed in the electrochemical reaction, it is necessary to have a stable means of collecting the current that is produced in the reaction, via the negative terminal. Conventionally, the active material is plated onto a conducting material which is either inert or of a more positive potential. However, the use of shot will require a basket-like current collector into which the shot can be fed continuously. The question therefore is: can the shot so-fed provide a reasonable contact with the current collector? In other words, can the current collector collect current? A simple experiment was thus, also carried out to try to answer the question.

PROCEDURE

For the electronic conductivity measurements, two alloy strips were bent and brought together such that contact was at the bends. The area of contact was measured. The end of one of the strips was covered with paper and linked to the negative terminal of a power source; the other end was linked to the positive terminal (Fig. 7.2). Current was then passed through the contact area of the metal. The resulting voltage was read using a digital voltmeter (DVM). Two other readings were taken for different currents. The average resistance obtained was used to calculate the conductivity, across the area of contact, in air.

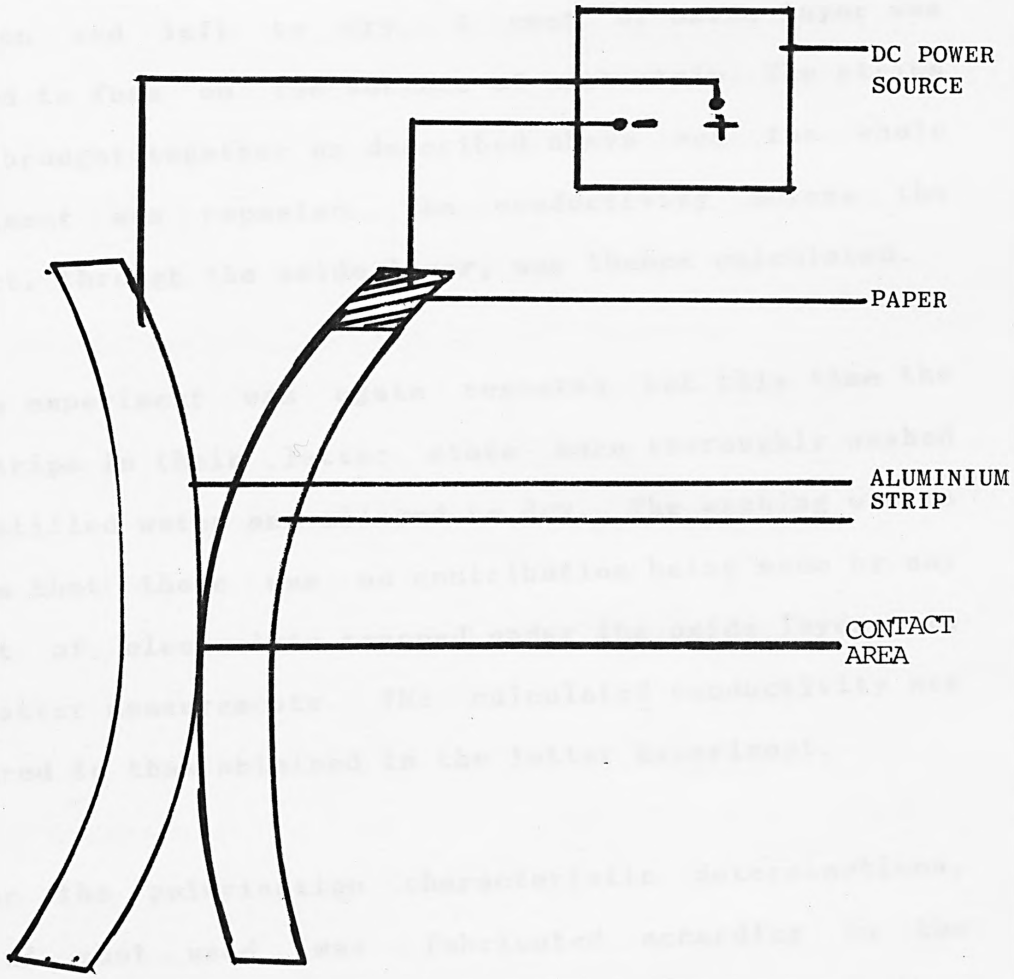

FIG. 7.2 ELECTRONIC CONDUCTIVITY MEASUREMENTS

After the above measurements, the two strips were polarised in a 5M KOH solution, saturated with HgO, at 100 mA for 10 minutes. They were then removed from solution and left to dry. A coat of oxide layer was allowed to form on the surface of each strip. The strips were brought together as described above and the whole experiment was repeated. The conductivity across the contact, through the oxide layer, was thence calculated.

The experiment was again repeated, but this time the two strips in their latter state were thoroughly washed in distilled water and allowed to dry. The washing was to ensure that there was no contribution being made by any amount of electrolyte trapped under the oxide layer, to the latter measurements. The calculated conductivity was compared to that obtained in the latter experiment.

For the polarisation characteristic determinations, the Al shot used was fabricated according to the fabrication procedure described above. Except that, immediately after the flame was moved away a thin nickel wire was gently inserted into the molten ball and then allowed to cool down as described. After washing in the citric acid solution, the nickel wire was covered with an insulating sleeve. An epoxy adhesive was used to seal the tiny gap between the metal and the brim of the sleeve.

The half-cell testing procedure (section 3.1) was

carried out using a DHE reference electrode and a nickel mesh counter electrode. Determinations were carried out, in a similar manner, for the shot and plate. To allow for the fabrication effect on the performance of the shot, some of the plate samples were subjected to the same fabrication conditions, that is, to heat and borax and, to heat only. The IR drop was measured at every current density and the potential reading corrected for. Polarisation curves were plotted for the samples.

To the answer the question surrounding the use of a basket-type current collector, a 4 cm^3 Al-air cell was constructed for the experiment. The aluminium alloy shot were packed into a basket (Fig. 7.3) made from a nickel mesh. Essentially, the current collector must have a high hydrogen overpotential in order to minimise the amount of hydrogen evolved at the anode. It must also have a more cathodic potential than the working potential of the aluminium material used. This is to ensure that the aluminium material, on dissolving, anodically protects the current collector from corroding away. Nickel mesh was used in this case, logistically, since the aim is only to test if there exists a sufficient contact between the shot and the current collector to enable current to be collected.

Pieces of copper foil were solded onto two ends of the basket and joined together to form the negative terminal (Fig. 7.3). An electrolyte was introduced into the cell

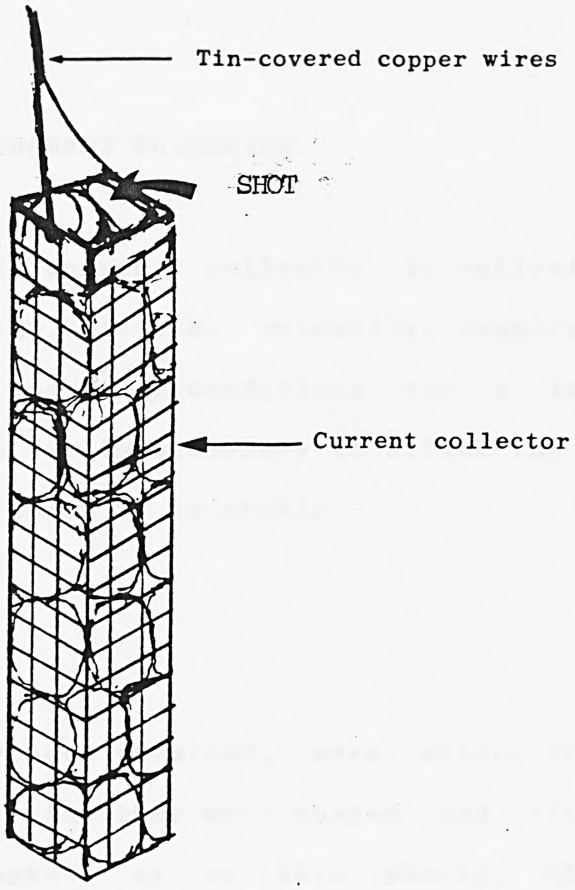

FIG. 7.3 SHOT-ASSEMBLY ELECTRODE

and the cathode and anode terminals were linked to a power sink. The cell and anode potentials were measured using a digital voltmeter. The anode potential was measured against a Zn electrode.

C) STABILITY OF CURRENT COLLECTOR

The basket-shaped current collector is entirely a novel proprietary design. It is, primarily, required to be stable under the operating conditions for a long period of time. As such, it is necessary to define the limiting conditions under which it is stable.

PROCEDURE

The current collectors examined, were either obtained as gauzes, in which case they were shaped and tin-soldered to form the basket, or as thin sheets, which were perforated before being shaped and soldered together. Once the baskets had been constructed, copper wires were tin-soldered onto two opposite ends and then joined together.

Alloy Q4 shot were fed into the basket to be tested and fitted into the test cell shown in Fig. 7.4. The shot-assembly electrode (Fig. 7.3) was held in the centre with the counter electrode and reference electrode on

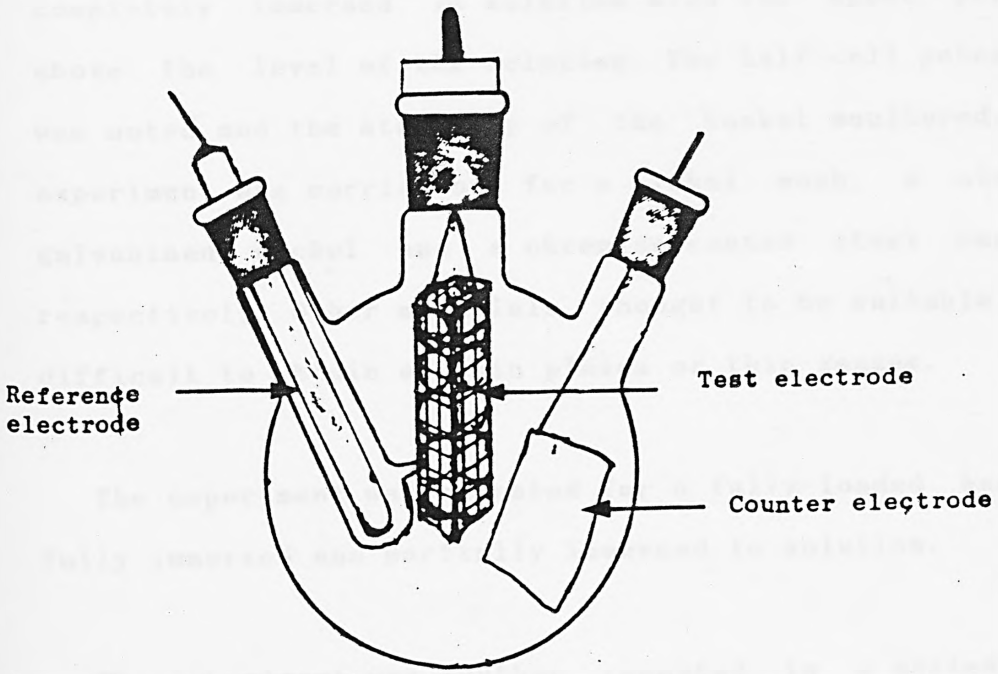

FIG. 7.4 THREE-NECK TEST CELL

either side. The flask was filled with a 5M KOH solution, saturated with HgO. The half-cell testing procedure was carried out, galvanostatically, at 100 mA/cm^2. The solution was magnetically stirred throughout the experiment. The test was conducted in the presence of excess air, with the basket half-loaded. The lower portion of the basket, containing the shots, was completely immersed in solution with the upper portion above the level of the solution. The half-cell potential was noted and the stability of the basket monitored. The experiment was carried out for a nickel mesh, a zinc, a galvanised nickel and a chromium-coated steel basket, respectively. Other materials thought to be suitable were difficult to obtain as thin plates or thin gauzes.

The experiment was repeated for a fully-loaded basket, fully immersed and partially immersed in solution.

The experiment was further repeated in a sealed cell (Fig. 7.5). The cell, so-designed, had an electrolyte reservoir from which electrolyte was circulated through the cell. A fully-loaded basket was used which was fully immersed in the electrolyte. The anodic potential was similarly measured and the stability under the operating conditions monitored. The cell was discharged at 50 mA/cm^2.

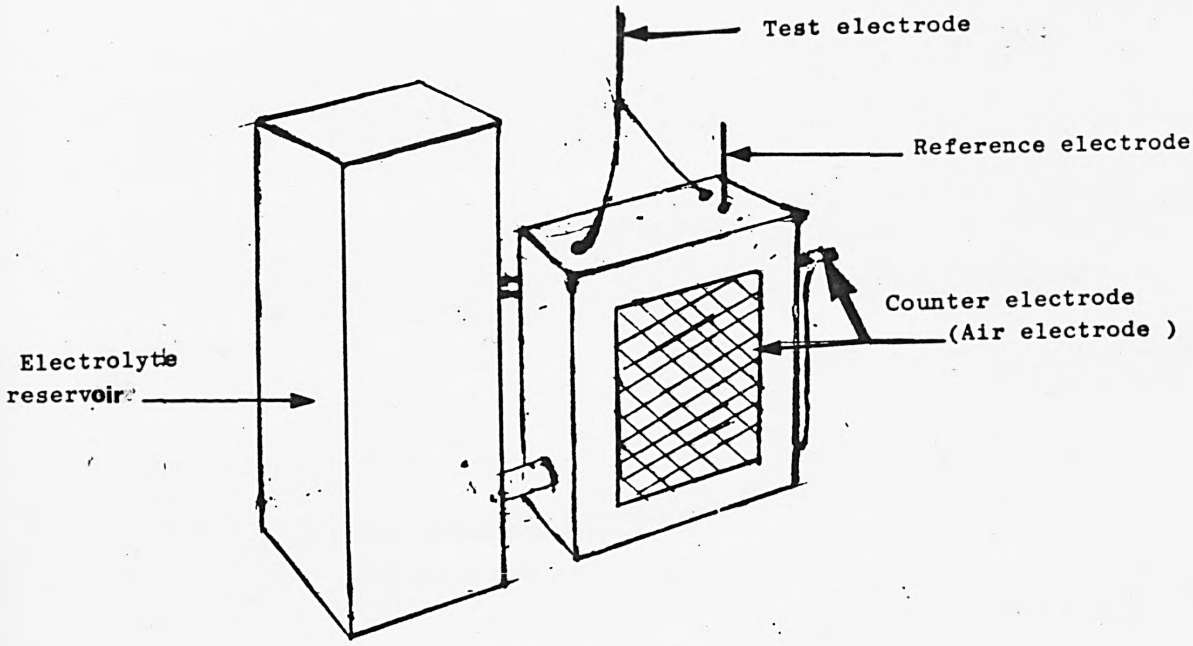

FIG. 7.5 SEALED CELL

7.1.3 RESULTS AND DISCUSSION

A) FEASIBILITY TESTS

The electronic conductivities across the contact between two shots, before and after discharging, were calculated from the measurements obtained. These are shown in Tables 7.1-7.3. Plots of voltage against current were made (Figs. 7.6 and 7.7) and the gradients given by the best fits were taken as the mean resistances.

The conductivity at each state was calculated using the equation

$$\sigma = 1/RA$$

where σ is the conductivity

R the mean resistance

l the length of contact = 2.0 cm

and A the contact area = 1.6 cm^{-2}

Thus, 87.40 mho/cm, 3.96 mho/cm and 3.40 mho/cm were calculated for conductivities before discharging and after discharging respectively. The trend of conductivity helps to establish the most important factor, as to the

TABLE 7.1 MEASUREMENTS IN AIR

current passed	voltage reading
1000 mA	14.0 mV
800 mA	11.0 mV
500 mA	6.8 mV

TABLE 7.2 MEASUREMENTS ACROSS OXIDE LAYER

(*) Before washing off electrolyte

current passed	voltage reading
1000 mA	365.0 mV
800 mA	285.0 mV
500 mA	175.8 mV

TABLE 7.3 MEASUREMENTS ACROSS OXIDE LAYER

(*) After washing off electrolyte

current passed	voltage reading
1000 mA	395.0 mV
800 mA	296.7 mV
500 mA	200.2 mV

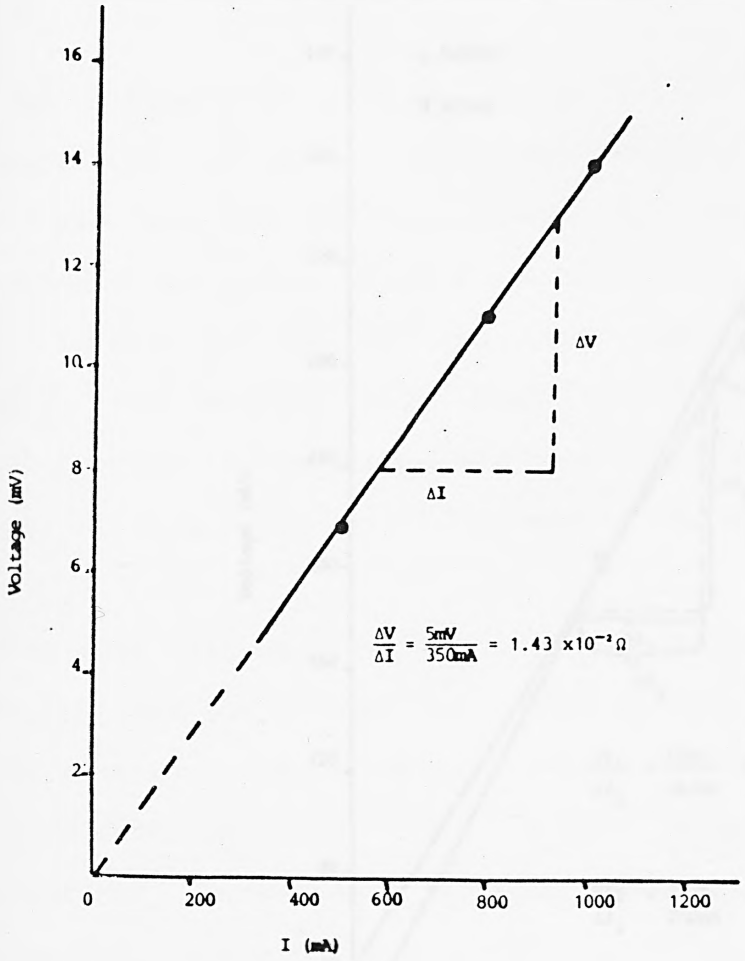

FIG. 7.6 PLOTS OF RESISTANCE MEASUREMENTS IN AIR

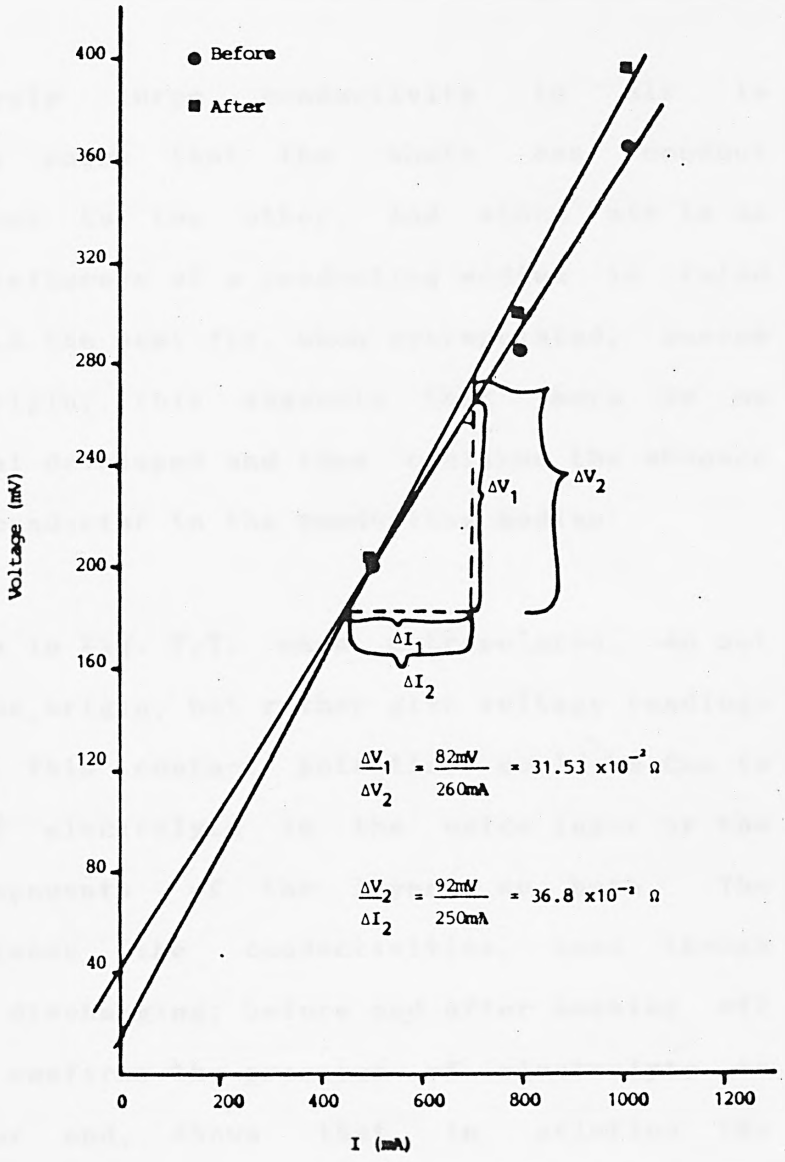

FIG. 7.7 PLOTS OF RESISTANCE MEASUREMENTS ACROSS OXIDE LAYER

electronic conductiveness between one shot and another.

The relatively large conductivity in air is encouraging. It shows that the shots can conduct electrons from one to the other. And since air is an insulator, the influence of a conducting medium is ruled out. In Fig. 7.6 the best fit, when extrapolated, passes through the origin; this suggests that there is no contact potential developed and thus confirms the absence of any foreign conductor in the conducting medium.

The best fits in Fig. 7.7. when extrapolated, do not pass through the origin, but rather give voltage readings at zero current. This contact potential could be due to the presence of electrolyte in the oxide layer or the conductive components of the layer, or both. The difference between the conductivities, even though slight, after discharging; before and after washing off 'electrolyte', confirms the presence of electrolyte in the oxide layer and, shows that in solution the conductivity is enhanced, owing to ionic conduction. The difference in contact potentials confirms the contribution made by the presence of electrolyte in the layer.

However, the relatively low conductivity or high resistance across the oxide film formed on the surfaces highlights a disadvantage in the use of shot . It is

recognised that the resistance of such films when integrated across the whole system will amount to a discouraging fact. As such, in the design of the system, steps are to be taken to ensure that there is enough electrolyte to dissolve all the reaction product. And also, that the shot are packed in a way that will ensure that they stay together during discharge.

Figs. 7.8 and 7.9 show the polarisation characteristics of shot and plates. In Fig. 7.8, it can be seen that the polarisation of a shot is somehow lower at high current densities and higher at low current densities, than that of a plates. This behaviour can be explained by considering the effect of the change in electrode area on the measured current density and, the effect of the fabrication method on the performance of the shot .

Considering the former, the change in electrode area with time can be obtained, assuming uniform dissolution across electrode surface, as follows:

In general,

$$M = V\rho$$

where M = mass, V = volume, and ρ = density.

Therefore,

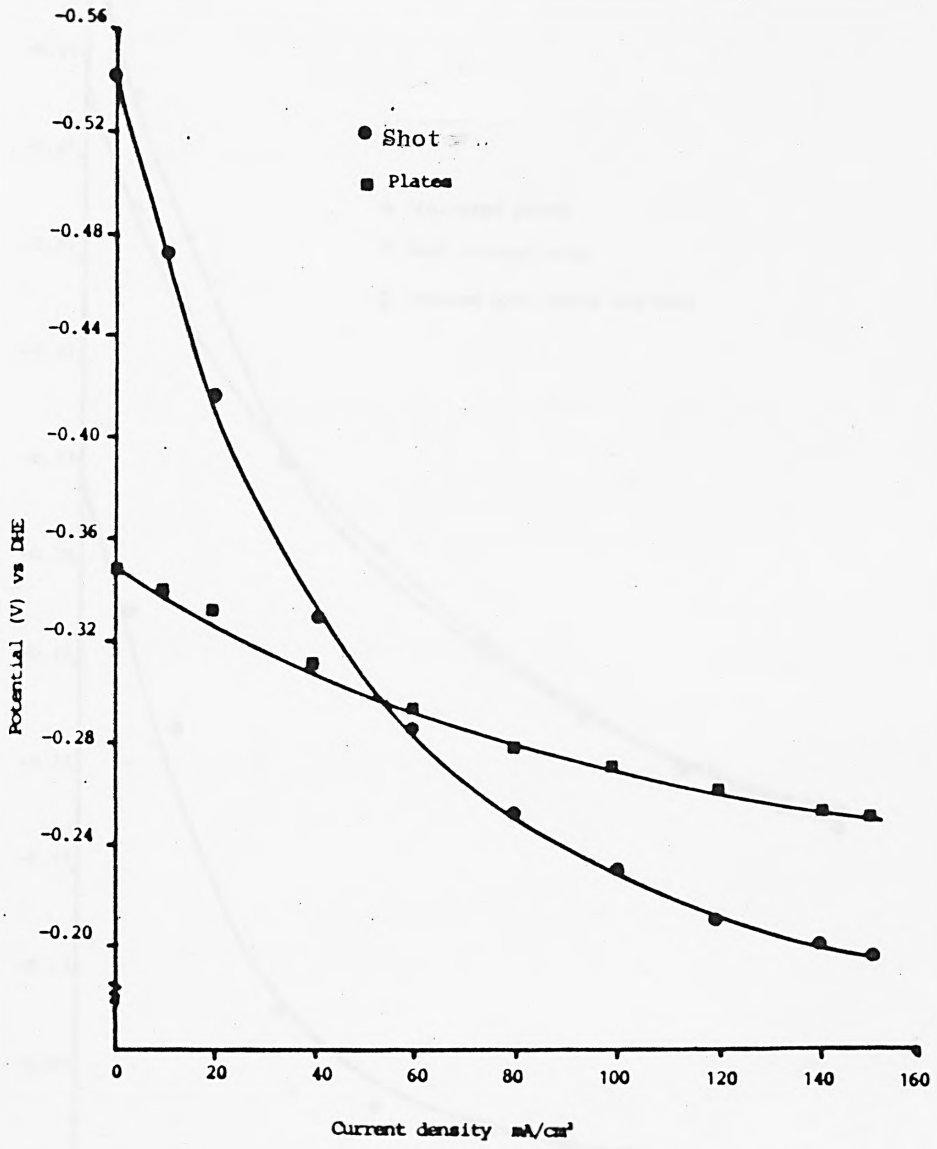

FIG. 7.8 POLARISATION CHARACTERISTICS OF SHOT AND PLATES

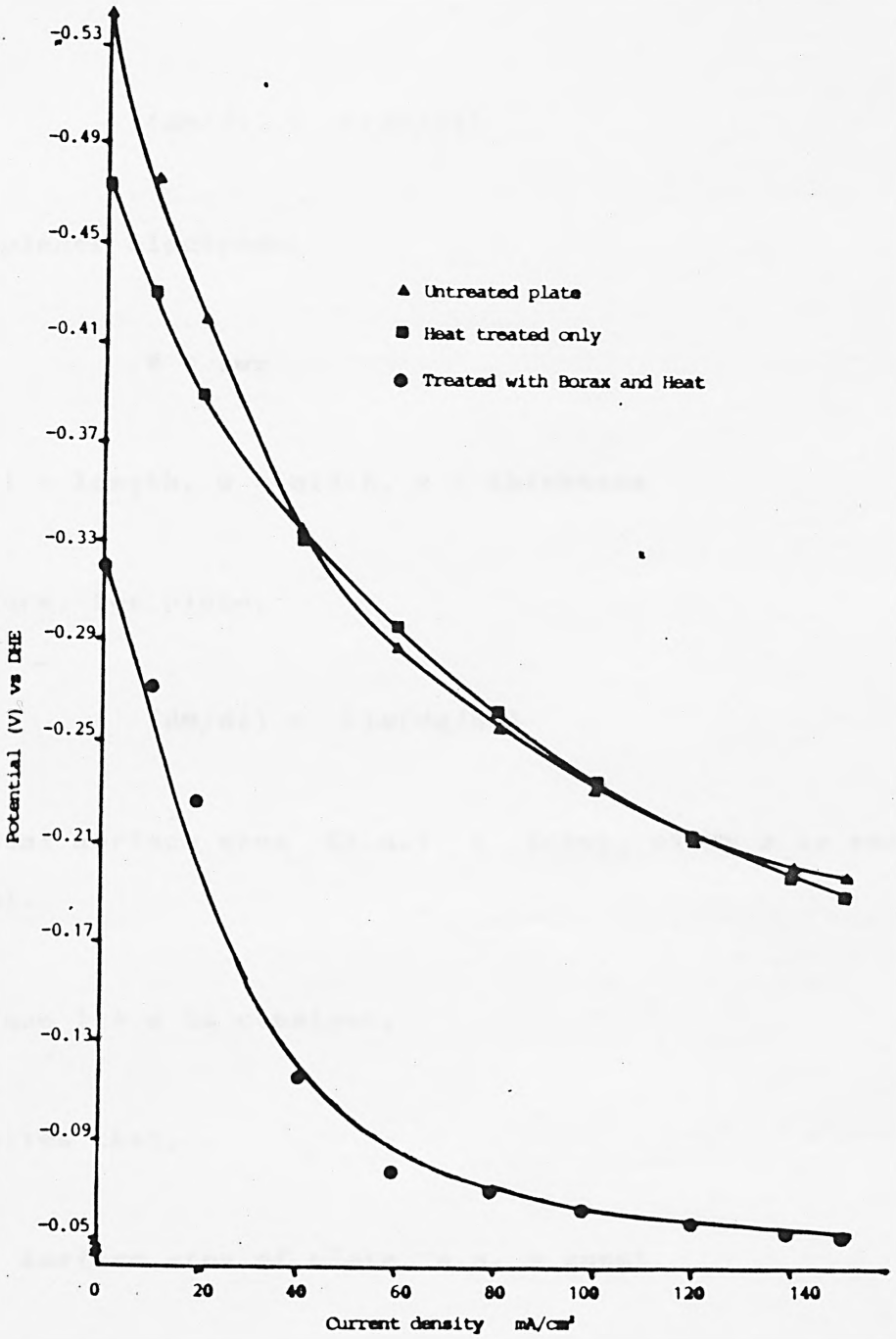

FIG. 7.9 POLARISATION CHARACTERISTICS OF PLATES SUBJECTED TO THE SHOT FABRICATING CONDITIONS

$$(dM/dt) = \rho(dV/dt)$$

For a planer electrode,

$$V = lwx$$

where l = length, w = width, x = thickness

Therefore, for plate,

$$(dM/dt) = \rho lw(dx/dt)$$

but total surface area (s.a.) = 2(lw), since x is small (0.4mm).

And since l * w is constant,

it implies that,

Surface area of plate, s.a. = const.

Therefore there is no significant change in surface area for plates at infinestmal time intervals.

For a spherical electrode,

$$V = 4/3\ \pi\ r^3$$

where r = radius of the sphere.

Therefore for shot,

$$(dM/dt) = 4/3\ \pi\rho(dr^3/dt)$$
$$= 4\ \pi r^2 \rho$$

but spherical surface area (s.a.) = $4\ \pi r^2$

Which implies,

$$s.a. = (dM/dt\ ) / \rho$$

Therefore, change in surface area of shot (Δ s.a.) is proportional to the rate of dissolution.

Since,

Current density = I / (s.a. $-\Delta$ s.a.)

where I is current passed

the actual current density (I_{actual}) tend to increase with time, in the case of shot . Thus, the lower potentials obtained for shot at high current densities could be corrected for, to obtain potentials higher than those shown. This would result in an upward shift in the polarisation curve, for shot , at high current densities.

The low potentials at these current densities can also be attributed to the conditions under which the shot were fabricated. Fig. 7.9 shows, clearly, the adverse effect of the presence of borax on polarisation. In the fabrication of the shot-electrode the use of nickel wire as the current collector may have given rise to lower potentials than actually realised, at low current densities. This is because,

$$I_{actual} = I_{passed} + I_{corrosion}$$

and since the presence of nickel in the shot could induce corrosion of the electrode the effect of the corrosion current becomes significant at low current densities. At high current densities the effect becomes negligible since the corrosion current is small and constant. Overall, the performance of a single shot is somewhat better than that of a plate.

In the experiment to find out if a basket-type current collector is capable of conducting current from the shots, at a current drain of 50 mA/cm^2, a negative potential of 0.144 V with respect to Zn, as reference electrode, was realised for the anode. Nickel by itself gave no measurable current; which meant that the current produced was solely from the shot . The high potential

realised (about -1.4 V; corrected for a Hg/HgO.KOH reference electrode) compares very well with those realised for single shot at the current density used. The current collector is, thus, capable of conducting the electrons released during the dissolution of the Al shot .

B) STABILITY OF CURRENT COLLECTORS

The data obtained from the experiments to establish the stability criteria for the anode current collector are presented in Tables 7.4-7.7. For the half-loaded, partially immersed tests (Table 7.4), a large amount of gas was evolved on the nickel mesh which enhanced the parasitic dissolution of the active material, so much so that, the faradaic efficiency, using the nickel mesh basket was only 14.5 % . A potential of -1.325 V (versus Hg/HgO.KOH) was realised. The nickel mesh was very stable in the alkaline electrolyte. However, the large gas evolution on the metal in the electrolyte makes it undesirable.

Using the zinc basket, -1.370 V was realised. But the metal lasted 80 minutes giving a faradaic efficiency of 43.1% . A longer stability was realised for the galvanised nickel and chromated steel baskets. They lasted 180 minutes and 242 minutes, giving a potential of -1.380 V and -1.249 respectively. A faradaic efficiency of 48% was calculated for the galvanised nickel and 53%

TABLE 7.4 HALF-LOADED/PARTIALLY IMMERSED CURRENT COLLECTOR

MATERIAL TYPE	POTENTIAL REALISED (V /HG/HGO.OH)	STABILITY TIME (MIN)	FARADAIC EFFICIENCY (%)
NICKEL	-1.325	STABLE	14.5
ZINC	-1.370	80	43.1
GALVANISED NICKEL	-1.380	180	48
CHROMATED STEEL	-1.249	242	53

CURRENT DENSITY: 100 mA/sqcm

TABLE 7.5 FULLY-LOADED/PARTIALLY IMMERSED CURRENT COLLECTOR

MATERIAL TYPE	POTENTIAL REALISED (V /HG/HGO.OH)	STABILITY TIME (MIN)	FARADAIC EFFICIENCY (%)
ZINC	-1.370	91	47
GALVANISED NICKEL	-1.380	183	51.3
CHROMATED STEEL	-1.249	260	53.7

CURRENT DENSITY: 100 mA/sqcm

TABLE 7.6 FULLY-LOADED/FULLY IMMERSED CURRENT COLLECTOR

MATERIAL TYPE	POTENTIAL REALISED (V /HG/HGO.OH)	STABILITY TIME (MIN)	FARADAIC EFFICIENCY (%)
ZINC	-1.350	169	71
GALVANISED NICKEL	-1.355	210	65
CHROMATED STEEL	-1.245	STABLE	69

CURRENT DENSITY: 100 mA/sqcm)

TABLE 7.7 FULLY-LOADED/FULLY IMMERSED CURRENT COLLECTOR IN A SEALED CELL

MATERIAL TYPE	POTENTIAL REALISED (V /HG/HGO.OH)	STABILITY TIME (Hrs)	FARADAIC EFFICIENCY (%)
ZINC	-1.521	3	89
GALVANISED NICKEL	-1.530	12	82.5
CHROMATED STEEL	-1.450	STABLE	85

CURRENT DENSITY: 50 mA/sqcm

for the chromated steel. Like the zinc basket, the baskets broke off at the solid-gas-liquid interface suggesting the occurrence of a local corrosion due the presence of excess air and the fact that the baskets were only half-loaded, and thence not fully protected by the Al shots. Also, the baskets were dissolving in solution. This is attributable to the large current driving the reaction. Experiments were carried out to reaffirm these causes.

The baskets were fully loaded and immersed, partially, in solution. each basket was then polarised at the current density used previously. Table 7.5 gives the data obtained. The zinc basket lasted 91 minutes with a faradaic efficiency of 47%. The galvanised nickel basket lasted 183 minutes giving a faradaic efficiency of 51.3%, whilst the chromated steel basket lasted 260 minutes with a faradaic efficiency of 53.7%. The same problems encountered with the half-loaded baskets were experienced. Since the baskets were fully-loaded, and thus protected anodically, the wearing away of the exposed part of the baskets could be attributed to hydrogen embrittlement (see section 5.1).

On fully immersing the baskets in solution, the zinc basket lasted 169 minutes with a faradaic efficiency of 71% (Table 7.6). The galvanised nickel basket was able to hold up for 210 minutes giving a faradaic efficiency of

65%. the chromated steel basket was found to be stable over a considerable period of time, giving a faradaic efficiency of 69%. The differences in stability times can be attributed to the relative stability of each basket material in the concentrated alkaline electrolyte. Also, in the case of zinc and galvanised nickel baskets, they were found to be dissolving away along with the aluminium shots, re-affirming the notion that the high driving current (1A) is also a factor responsible for the instability of the current collector.

The results obtained from the sealed cell experiments (Table 7.7) confirmed these causes. Anodic potentials of -1.521, -1.530 and -1.450 V (versus Hg/HgO.KOH) were realised for the zinc, galvinised nickel and chromated steel baskets, respectively. The zinc basket lasted for 5 hours with a faradaic efficiency of 89%. A faradaic efficiency of 82.5% was calculated for the galvanised nickel basket. The basket was stable for nearly 12 hours and only gave way when the aluminium shot had sank to the bottom of the basket, leaving the large part of the basket anodically unprotected. This poses no problem since it can be alleviated by the continuous feeding of the active anode material. The chromated steel basket was again found to be stable over an entire 44 hours of cell discharge with a faradaic efficiency of 81%.

7.2 THERMAL MANAGEMENT

7.2.1 INTRODUCTION

Thermal energy is inevitably released with electrical energy when a cell is discharged. Heat release is especially intensive in cells with negative electrodes such as aluminium, since polarisation losses for such electrodes are high.

The heat generation within a current-delivery cell gradually raises its temperature. A steady thermal situation is, however, ultimately reached, when generation is balanced out by heat transfer to the surrounding medium. The steady-state temperature difference, relative to the ambient, depends on the intensity of heat generation and on cell dimensions. It is worth pointing out that there is a non-uniformity of heat production over the cell volume and hence the temperature distribution is non-uniform within it. The latent heat and heat polarisation losses are released within the reaction zone, that is, at the electrode surface. Local overheating at the electrode surface may be observed even in steady-state conditions. On the one hand, this is a factor improving cell characteristics and on the other hand, it may intensify electrode corrosion.

Temperature is somewhat levelled off by the liquid electrolyte with its high specific heat, circulating freely in the interelectrode gap. Each cell is characterised by a certain maximum admissible temperature above which all the destructive processes (corrosion and ageing) are accelerated.

Most commercial cells are used at or near room temperature as they are contained in devices in an ambient condition where people use the devices. However, there are instances where cells are used below freezing or exposed to the direct sunlight. Therefore, cell operation at very low or very high temperatures can be important. Some systems are limited by the temperature characteristics imposed by the electrolyte, while others are limited by the polarisation of the electrode reactions.

The temperature range of the electrolyte used in a cell is a primary limiting factor. Cell operation is restricted to the range between the boiling point and freezing point of the electrolyte. In general these limits are about 100°C to -50°C, respectively, for water-based electrolytes. Variations from these limits depend on the type and concentration of the solute and the stability of the electroactive components [168].

The effects of high temperature are in contrast to low

temperature effects. At high temperature, material stability is the prime factor affecting cell operation. Stability is important for both the negative and the positive electrodes. Generally, electrolyte resistivity and diffusivity (problems experienced at low temperatures) are not problems, although at extremely high-rate of discharge the boiling point of the electrolyte may be a problem. Also, in general, increasing temperature increases chemical reaction rates and decreases electrode polarisation. It also leads to increased tendency for corrosion, and thus increasing the self-discharge rate of a cell.

Specific problems are encountered when the ambient temperature is below the minimum operating temperature of the cell. This is often the case when batteries operate in winter conditions, and also when high-temperature cells are used. In these cases the cell, prior to loading, is heated up to working temperature. If no heating means are available, self-heating is employed. The cell is shorted by a low-resistance load so that despite the low temperature the discharge current is not zero. The heat released thereby slowly increases the cell temperature, which increases current, and accelerates the process. Self-heating is not interrupted until the working temperature is reached.

7.2.2 EXPERIMENTAL

Since both the current producing and corrosion reactions of an electrode process depend very much on temperature, it is considered very important to obtain an operating temperature at which there is a minimum hydrogen evolution, a higher utilisation of the active material, a minimum polarisation (high limiting current density) as well as a high potential.

PROCEDURE

The investigation was divided into three parts:

(i) determination of alloy utilisation at different temperatures under a constant current density noting the potentials realised,

(ii) measurement of the amount of hydrogen evolved at the different temperatures, and

(iii) determination of the polarisation characteristics of the alloy at the different temperatures.

For part 'i', a 2.0 cm^2 of alloy Q4 (0.4mm thick strip) was fabricated, weighed and immersed in a 5M KOH solution, saturated with HgO. The alloy was discharged, galvanostatically, at a constant current density of 100 mA/cm^2, at different temperatures;

25, 30, 40, 50, and 60°C. The potentials realised (versus a Hg/HgO.KOH electrode) were recorded over the periods of discharge. The IR drops at selected intervals were measured. The experiment, at each temperature, was terminated after a reasonable period of discharge and the time was noted. The cell was disconnected and the remainder of the alloy was recovered, dried and weighed. Thence, the time taken for the deduced weight of the alloy to be consumed was used to calculate the utilisation at the particular temperature.

For part 'ii', the special apparatus designed to collect hydrogen (described in section 3.2) was used. The alloy was fabricated as for part 'i' and immersed in the same electrolyte solution. The alloy was similarly discharged, at the same constant current density and at the same temperatures. The amount of hydrogen evolved at the different temperatures was, thence, measured.

For part 'iii', the half-cell testing procedure was carried out for the alloy at the different temperatures. The same alloy fabrication, electrolyte and reference electrode, as for part 'i', were used. The potential at each selected current density at the different temperatures, were recorded. IR drop measurements were made at each current density and the potential readings at the selected current densities were each corrected for.

7.2.3 RESULTS AND DISCUSSION

OPERATING TEMPERATURE

In Fig. 7.10, the effect of temperature on the utilisation and potential of the anode material can be seen. In general, utilisation decreases with increasing temperature whilst potential increases with temperature. The price paid for a high potential is, therefore, a low utilisation.

Since both high potential and utilisation are the desired parameters for the optimisation of the anode performance, it is necessary to strike a balance between the two for the optimum working temperature. In striking this balance, it is necessary to consider the rate of hydrogen evolution at these temperatures, as well as the polarisation characteristics of the anode material at those temperatures.

In Fig. 7.11 the rate of hydrogen evolution is shown to increase with temperature. The shape of the curve suggests different reaction rates for temperatures below and above 40°C. Above 40°C, the rate is relatively enhanced. Since a low rate of hydrogen evolution is desired, higher temperatures are considered not suitable.

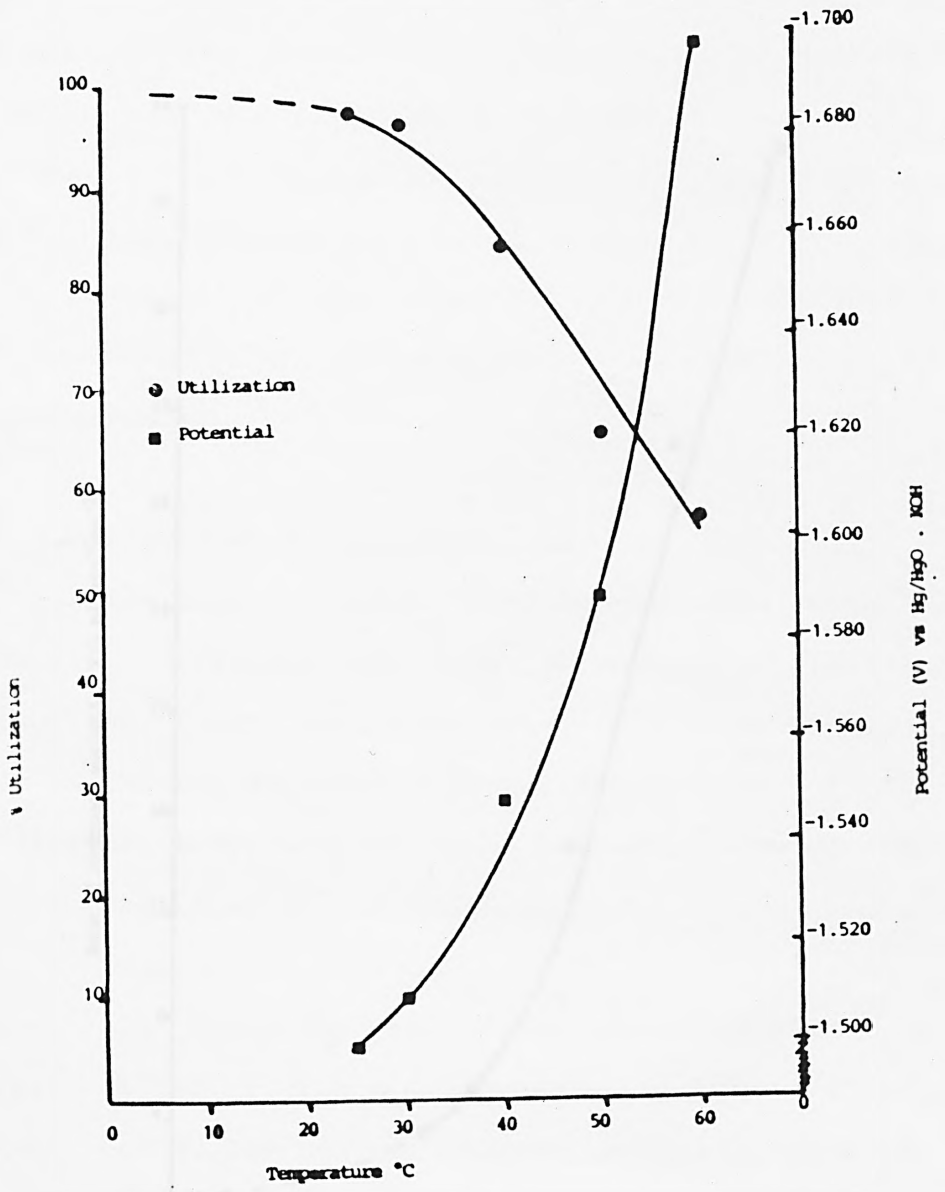

FIG. 7.10 UTILISATION AND POTENTIAL AT DIFFERENT TEMPERATURES, USING A CONSTANT CURRENT DENSITY OF 100 mA/cm^2

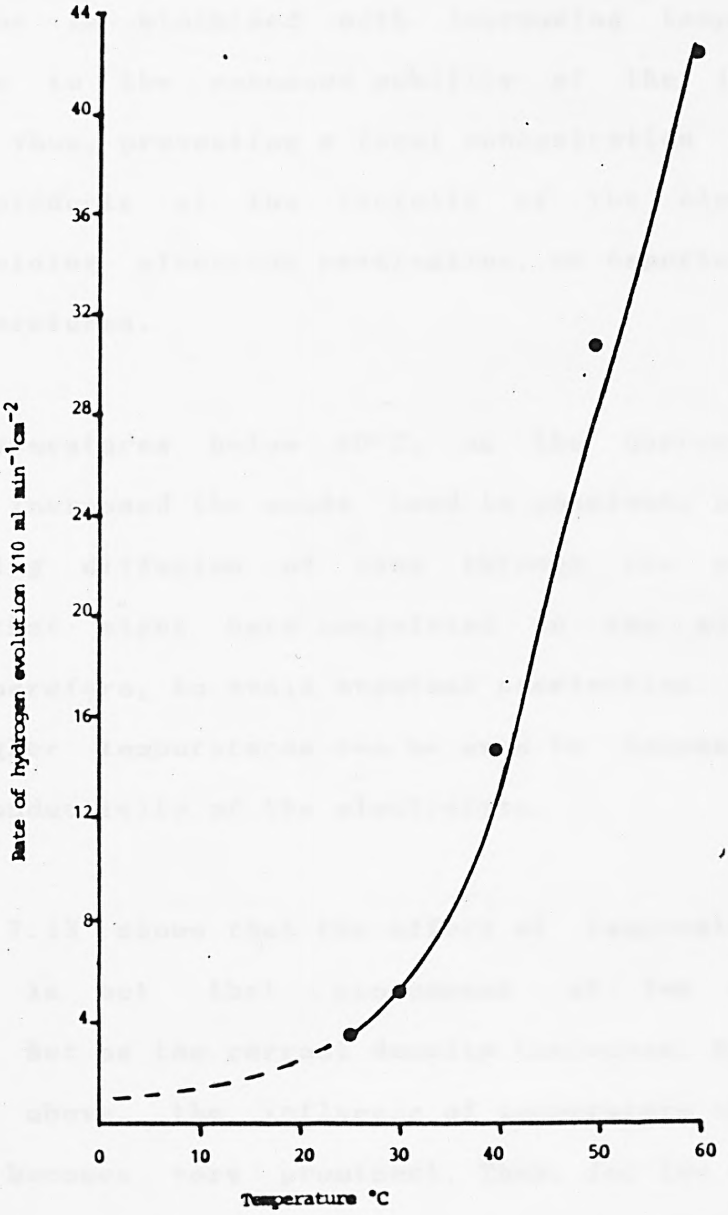

FIG. 7.11 RATE OF HYDROGEN EVOLUTION W.R.T. TEMPERATURE

Figure 7.12 shows the polarisation characteristics of the anode at the different temperatures. In general, polarisation is minimised with increasing temperature mainly due to the enhanced mobility of the ions in solution. Thus, preventing a local concentration of the reaction products at the vicinity of the electrode; thereby avoiding electrode passivation, as experienced at lower temperatures.

For temperatures below 40°C, as the current density is increased the anode tend to passivate owing to the limiting diffusion of ions through the reaction products that might have coagulated on the electrode surface. Therefore, to avoid eventual passivation of the anode, higher temperatures can be used to increase the relative conductivity of the electrolyte.

Figure 7.13 shows that the effect of temperature on potential, is not that pronounced at low current densities. But as the current density increases, from 100 mA/cm^2 and above, the influence of temperature on potential becomes very prominent. Thus, for low current density uses, low temperatures are adequate. However, for high current density uses higher potentials can be achieved, the higher the operating temperature. But it should be borne in mind that this higher potentials at higher temperature operations will be at the expense of anode utilisation and thus, at the expense of an increase

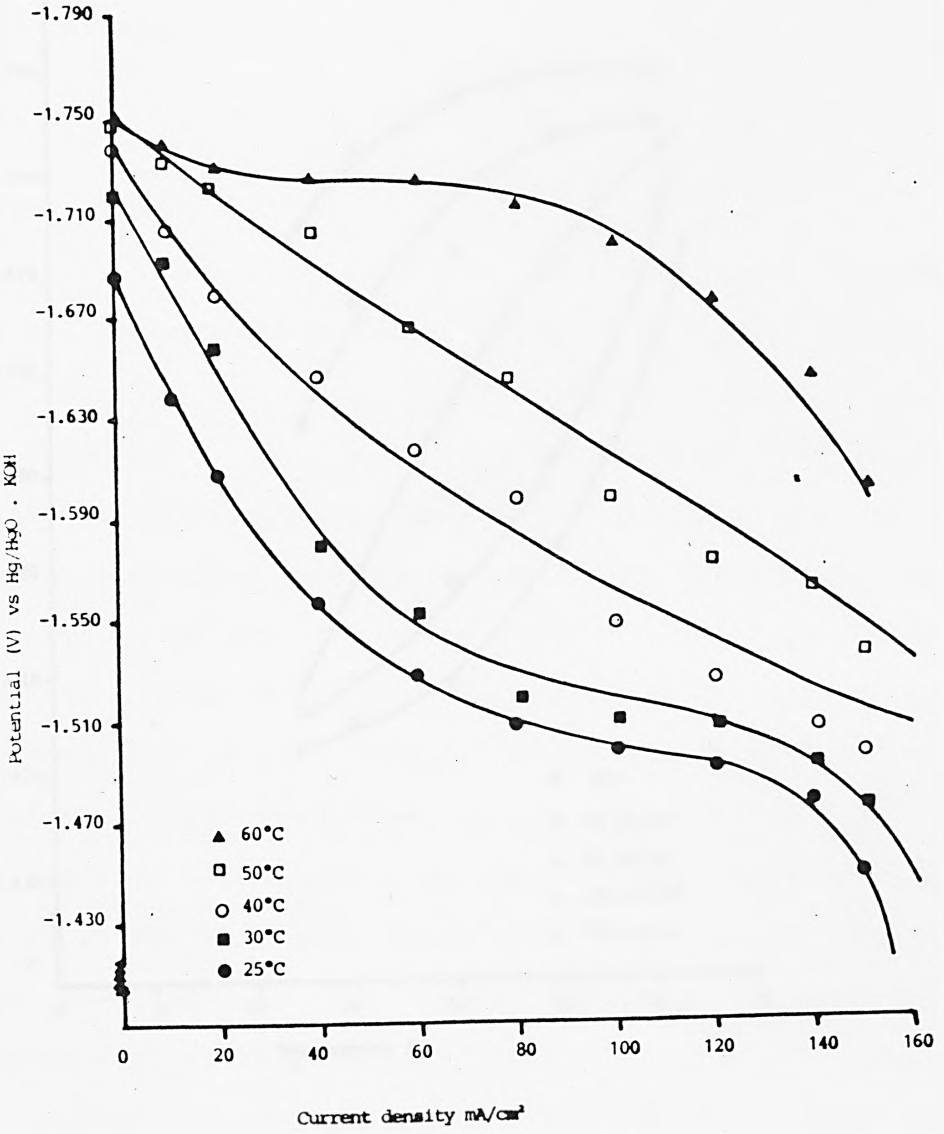

FIG. 7.12 POLARISATION CHARACTERISTICS AT DIFFERENT TEMPERATURES

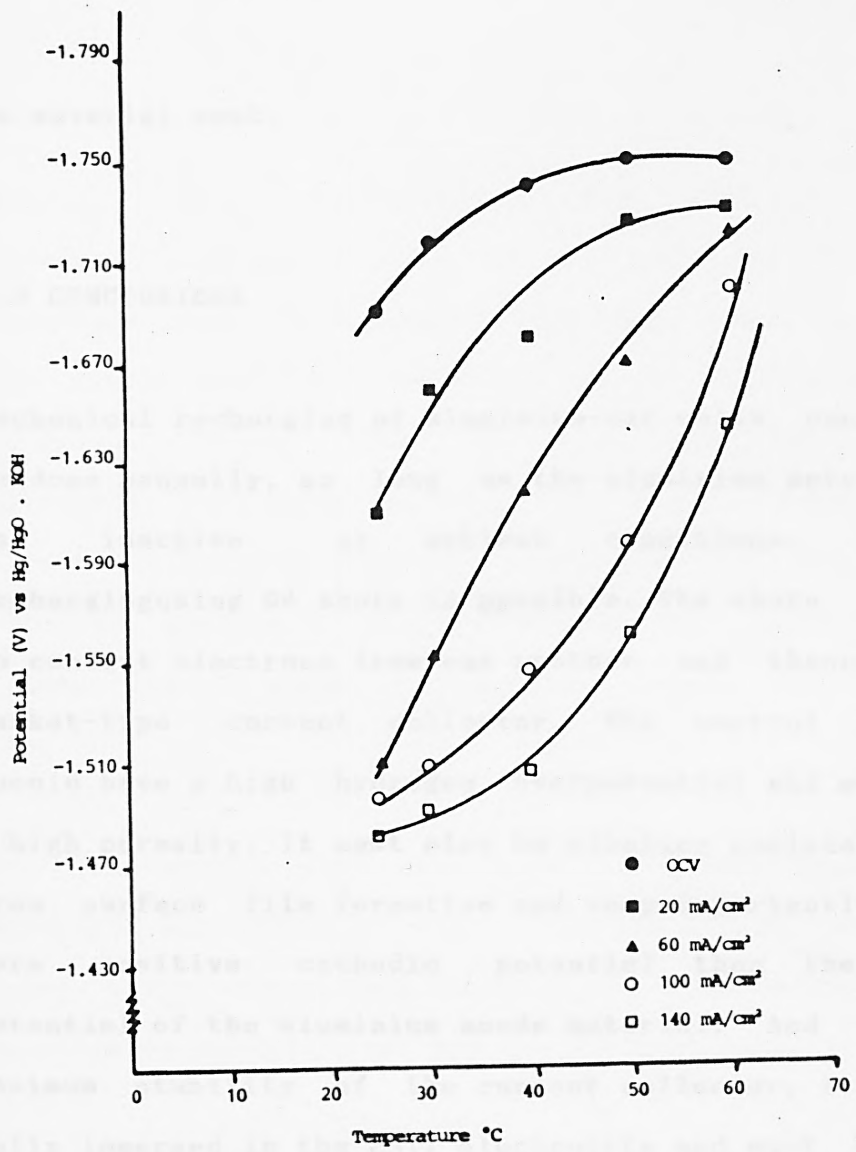

FIG. 7.13 POTENTIAL vs TEMPERATURE AT DIFFERENT CURRENT DENSITIES

in material cost.

7.3 CONCLUSIONS

Mechanical recharging of aluminium-air cells can, safely, be done manually, so long as the aluminium material used is inactive at ambient conditions. Automatic rechargingusing Q4 shots is possible. The shots are able to conduct electrons from one another and thence,to the basket-type current collector. The current collector should have a high hydrogen overpotential and must be of a 'high porosity. It must also be alkaline resistant, free from surface film formation and very importantly, of a more positive cathodic potential than the working potential of the aluminium anode material. And to ensure maximum stability of the current collector, it must be fully immersed in the cell electrolyte and must be almost fully loaded at any period of time. The cell must be sealed and operated at a reasonable current density.

For optimum operating temperature, temperatures between 40 and 45°C are desireable. At higher temperatures, utilisation of the active anode material is drastically reduced and also, hydrogen evolution is significantly increased at those temperatures. At lower temperatures, passivation of the anode occurs at high current densities.

However, high temperatures are suitable for short-time, high-power uses. This is so since for such operations, time is negligible and thus, power is P = IV (I is current and V is potential) and V increases with temperature. Where time is not negligible, high temperatures are only suitable for applications where cost is not a limiting factor; owing to the low anode utilisation. Because of the higher hydrogen evolution at high temperatures, such applications should be in open fields.

For low current density, high potential uses, low temperatures are suitable since utilisation is very high at those temperatures and there is not much influence of temperature on potential at the low current densities.

8 FULL-CELL DESIGN AND PERFORMANCE TESTING

8.1 INTRODUCTION

A full cell comprises basically of the anode, cathode and the electrolyte. In the design of the cell, all these three are brought together in contact, with the electrolyte separating the anode and the cathode.

The performance of the full cell is guided by the performances of each electrode; the electrode with the lower limiting current density, limiting its performance. As such, in the optimisation of a full cell it is a prerequisite to optimise, first, the individual electrodes.

Thus, in the optimisation of the Al-air cell, the Al anode and the air depolarising cathode were both optimised. The preceding chapters show the optimisation of Al as the anode in Al cells. The optimisation of the air electrode as the cathode, has been considered elsewhere [169,170]. However, the effect of the optimum operating conditions, suggested by the optimisation of the Al anode, on the performance of an air electrode has been investigated, here.

PART A THE AIR DEPOLARISING CATHODE

The historical background, concepts and principles of operation of the air (or oxygen) electrode, has already been detailed in chapters 1 and 2. The upsurge of the use of air cathode in fuel cells, metal-air batteries and chlor-alkali electrolyzers have meant that the typical air electrode performance should be upgraded. An attempt to realise this, involves the preparations of improved active electrocatalysts.

There are quite a number of preparations and compounds that have been suggested as electrocatalysts for oxygen reduction [171-189]. Work done at City University on Teflon bonded electrode structures using semiconducting oxide electrocatalysts [175,178,190], have resulted in the development of long-life, inexpensive and high performance air electrodes. An air electrode based on Teflon bonded Li doped cobalt oxide/graphite electrode [170] has been perfected; over 250 mA/cm^2 at 0.85 V is realised in 5M KOH at room temperature.

The Teflon bonded Li doped cobalt oxide/graphite electrode is, thus, used as the cathode in the Al-air cell studied here.

8.2 EXPERIMENTAL

8.2.1 AIR ELECTRODE FABRICATION

In the fabrication of the Teflon bonded air electrode, a mixture of high surface area graphite, the electrocatalyst powder and an aqueous dispersion of polytetrafluoroethylene (PTFE) is deposited on a metal grid (as current collector). The non-wetting properties of the PTFE, allows a gas-liquid interface to be stabilised within the pores of the electrode without the need for differential pressure [190,191]. By wet-proofing some of the pores, the contact angle is raised, and electrolyte cannot penetrate. Also, as a means of preventing the electrolyte from leaking out through the electrode pores, the oxygen side of the electrode is claded with a thin layer of a mixture of PTFE and acetylene black. The use of PTFE in the electrode structure, apart from ensuring an easy gas route, has the added advantage of increasing the mechanical strength of the electrode [192,193]. Also, the high corrosion resistance of the PTFE helps to protect the electrocatalyst from poisoning by impurities [194] and thus, allows high current densities to be realised.

The PTFE used is obtained directly from the manufacturer and so is the acetylene black. However, the

high surface area graphite and electrocatalyst are both prepared as part of the electrode fabrication procedure.

FABRICATION PROCEDURE

A) CATALYST PREPARATION

36% cobalt chloride, 20% potassium hydroxide and 6% lithium hydroxide solutions were prepared using Analar grade chemicals and de-ionised/distilled water. The KOH solution was added slowly to the $CoCl_2$ solution whilst stirring continuously, to precipitate $Co(OH)_2$. The precipitate was filtered and washed thoroughly with the distilled water until it was free from alkali. This was confirmed by taking the pH of the last wash; whose pH should be 7.

The LiOH solution was then added to the precipitate, which was still in the funnel, and left standing for some time. The water in the co-precipitate was then removed by filtering under suction. The nearly dried co-precipitate was transferred unto a flat dish and then dried in hot air, at 105°C, for 5 hours. Following that it was sintered at 300°C, in a furnace, for another 5 hours.

The resultant powder was ground in an agate mortar and stored in a tightly sealed glass jar. Samples were taken

for surface area measurements and X-ray analysis.

B) GRAPHITE PREPARATION

A fine, high surface area graphite powder was prepared by grinding a coarse graphite, under vacuum, in a vibratory ball mill. Pure nickel shots were used as grinders, in an evacuated nickel chamber.

3 kg of Ni shots and 35 g of Foliac graphite were separately weighed and loaded into the ball mill chamber in the following sequence:

i) 1 kg of Ni shots
ii) 15 g of graphite
iii) 1 kg of Ni shots
iv) 20 g of graphite

and finally, v) 1 kg of Ni shots.

The graphite was added very carefully. A dust mask was worn to protect against the graphite dust. After loading the graphite and Ni shots, the chamber lid was replaced and bolted tightly. It was then shaken from side to side to level the Ni shots and graphite, inside the chamber.

Following that, the chamber was evacuated by connecting the cylinder to a pump and, with the gas ballast closed, the pump was switched on for a minimum of

30-35 minutes. After that, the chamber was sealed using a collier clip on the rubber hose attached to the cylinder. The gas ballast was then opened, switching off the pump at the same time. The pump was disconnected from the vibrator unit. The unit was then switched on and left to operate for a long period of time.

After ball-milling for 8 hours, the graphite was retrieved from the chamber and heat-treated in nitrogen, at 900 °C. The heat-treating is necessary, since on exposure to the atmosphere, the ball-milled graphite becomes covered with strongly adsorbed oxygen which interacts with CO_2 in the atmosphere to form a carbonate complex. The complex formed, has a deleterious effect on the reactivity and stability of the graphite which is overcome by the heat-treating. After heat-treating, small samples of the graphite were taken for surface area measurements.

C) ELECTRODE FABRICATION

The complete electrode structure comprises of a current collector, a hydrophobic layer and a catalyst layer.

HYDROPHOBIC LAYER

60% of the hydrophobic layer is composed of PTFE and the remaining 40% is acetylene black. Thus, the hydrophobic layer, for a batch of electrodes, was prepared by mixing 2 g of acetylene black with 5 g of Teflon dispersion (only 60% of the dispersion is solid PTFE). After the Teflon had been mixed thoroughly into the acetylene black, small drops of water were added, as required, to the composition and kneaded into a fine dough. The dough was rolled out several times, between a glass tube and a flat base, to produce a single uniform layer. The rolled-out dough was was then wrapped in a wet paper and stored away in a dry place. (The hydrophobic layer should not be stored under water).

CATALYST LAYER

The catalyst layer comprises of 10 : 3 catalyst phase to PTFE. 10% of the catalyst phase is made up of the electrocatalyst and 90% of the high surface area (500 m^2/g) graphite. Thus, for the batch of electrodes, 0.1 g of the Li doped Co_3O_4 was added to 0.9 g of the graphite and mixed thoroughly together.

Drops of water were added to the catalyst and graphite mixture, enough to just wet it. This was to assist the dispersion of Teflon into the mixture. 0.5 g of the Teflon dispersion was added to the moist

catalyst/graphite mixture (MCP) and then worked into a fine dough. The dough was rolled out, as described for the hydrophobic layer. However, this time the rolled-out dough was stored in water, in order to prevent the dough from drying out.

CURRENT COLLECTOR

A 100 mesh nickel gauze was used as the current collector. The gauze was washed thoroughly with a laboratory detergent and then soaked in acetone, under ultrasonic vibration, to lift off grease.

ELECTRODE SET-UP

The electrode was set up as shown in Fig. 8.1. The solution side of the electrode consists of the two layers; catalyst and hydrophobic. The layers were prepared by, first, rolling a portion of the hydrophobic layer to a 0.25 mm thickness and the catalyst layer to 0.3 mm thick. The catalyst layer was placed on top of the 0.25 mm thick hydrophobic layer and the two layers were then rolled together to a 0.4 mm thickness. Care was taken to ensure that the catalyst layer was identifiable.

The air (or oxygen) side of the electrode consists of one layer, the hydrophobic layer. The layer was prepared

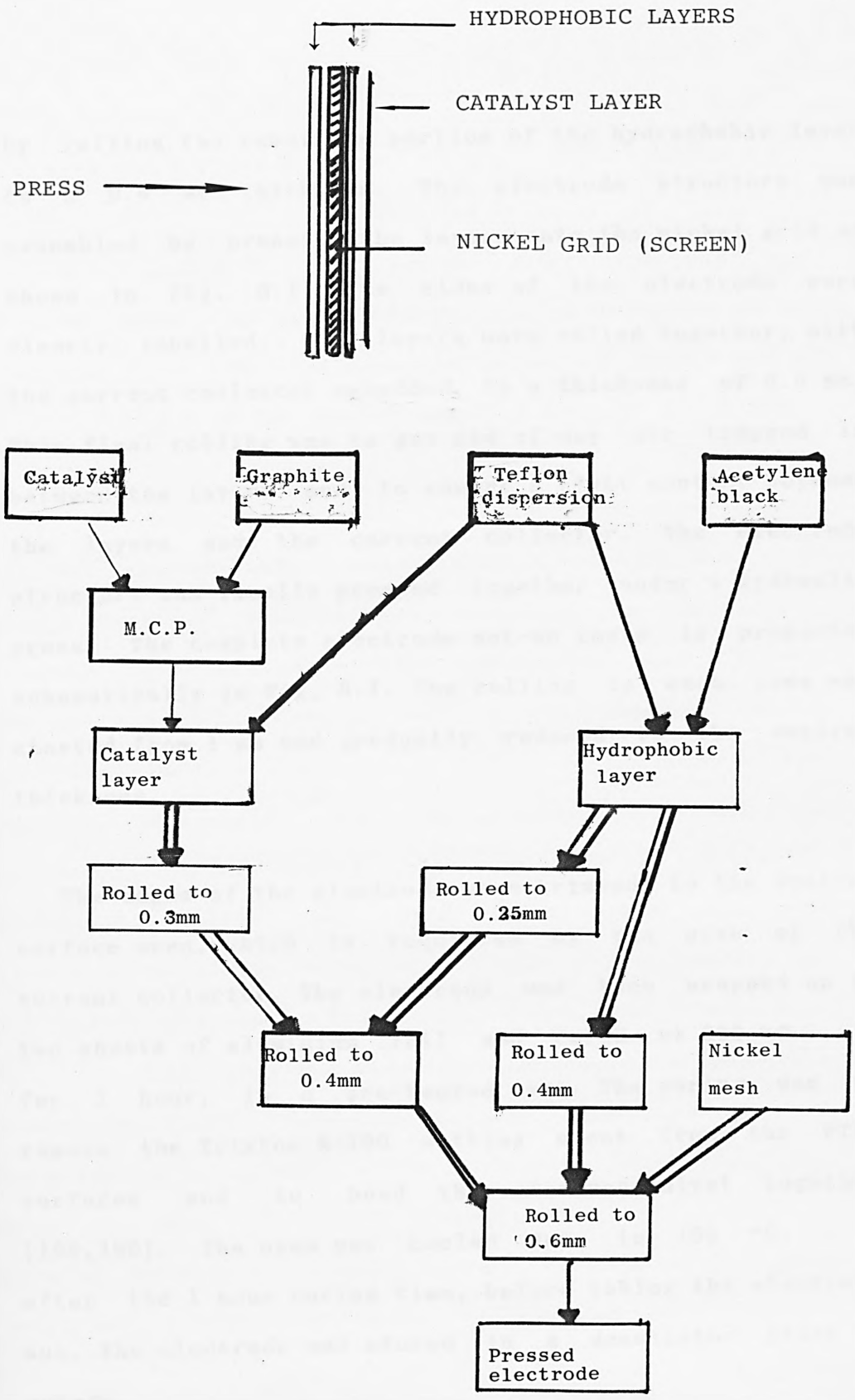

FIG. 8.1 SCHEMATIC REPRESENTATION OF AIR ELECTRODE FABRICATION

by rolling the remaining portion of the hydrophobic layer to a 0.4 mm thickness. The electrode structure was assembled by pressing the layers onto the nickel grid as shown in Fig. 8.1. The sides of the electrode were clearly labelled. The layers were rolled together, with the current collector embedded, to a thickness of 0.6 mm. This final rolling was to get rid of any air trapped in between the layers and to ensure a tight contact between the layers and the current collector. The electrode structure was finally pressed together under a hydraulic press. The complete electrode set-up route is presented schematically in Fig. 8.1. The rolling in each case was started from 1 mm and gradually reduced to the desired thickness.

The edges of the electrode were trimmed to the desired surface area, which is requlated by the size of the current collector. The electrode was then wrapped up in two sheets of aluminium foil and cured at 300 °C for 1 hour, in a pre-heated oven. The curing was to remove the Trixton X-100 wetting agent from the PTFE surfaces and to bond the electrocatalyst together [195,196]. The oven was cooled down to 100 °C, after the 1 hour curing time, before taking the electrode out. The electrode was stored in a dessicator prior to usuage.

8.2.2 HALF-CELL TESTING

The air electrode was tested under the different operating conditions suggested by the optimisation of the Al anode. This was in order to establish the effect of these conditions on the performance of the air electrode.

For the experiments, the Floating Electrode set-up [197,198] was adopted. A nickel wire was welded onto the exposed part of the current collector in the cured electrode. The electrode surface containing the catalyst layer was placed as close as possible unto the tip of the luggin capillary, as shown in Fig. 8.2. The stem of the electrode was tied to the reference electrode compartment, using Teflon tape, in order to hold the electrode in place. The test electrolyte was then introduced carefully into the cell. The amount of electrolyte was such that the electrode was just floating; with only the catalyst layer just touching the electrolyte. The test cell was immersed in a thermostatically controlled water bath. The water was heated to 40°C for all experiments, unless otherwise stated. The electrode polarisations were carried out in a cathodic mode.

A) EFFECT OF HgO ADDITIVE

The electrode was polarised in 5M KOH and then in 5M KOH

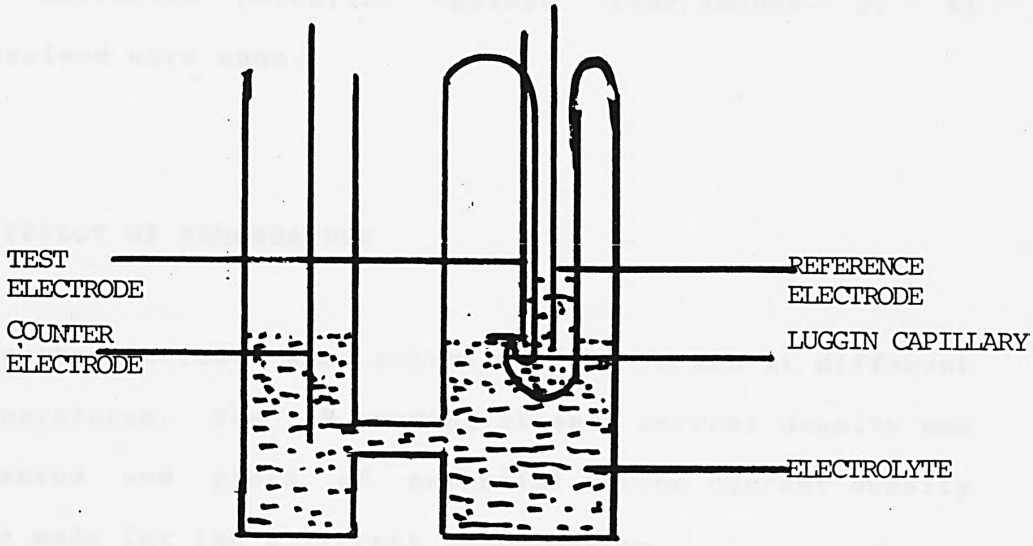

FIG. 8.2 FLOATING ELECTRODE TEST CELL

saturated with HgO. The IR drop at every current density was measured. Plots of potential versus current density were made.

B) EFFECT OF ALUMINATE CONCENTRATION

The electrode, freshly made, was polarised, galvanostatically, in 5M KOH and then in 5M KOH, in which Al was dissolved at a constant current density. Plots of IR corrected potential against time/amount of Al dissolved were made.

C) EFFECT OF TEMPERATURE

A fresh electrode was polarised in 5M KOH at different temperatures. The IR reading at each current density was measured and plots of potential versus current density were made for the different temperatures.

D) EFFECT OF OXYGEN CONCENTRATION

All the experiments above were performed in air. For this experiment, different oxygen compositions were pumped through the test cell and the polarisation of the electrode at each oxygen concentration was determined.

Apart from air, where less than 100% oxygen was fed through the cell, the other partial composition was made up of nitrogen. Thus, for a 50% oxygen feed, a 50% nitrogen and 50% oxygen gas mixture was used. Also measured was the effect of the flow rate of oxygen feed on electrode performance. For this, the electrode was polarised at different oxygen flow rates. The potential realised at each current density was recorded. The IR drops at the current densities were also measured and plots of the IR corrected potential versus current density were made.

E) PERFORMANCE IN ELECTROLYTE MIXTURES

The electrode was polarised in the selected electrolyte mixtures from chapter 6. Plots of IR corrected potential versus current were made.

8.3 RESULTS AND DISCUSSION

The plots made from the data from the above experiments are presented as Figs. 8.3-8.8. Figure 8.3 shows that the addition of HgO to the cell electrolyte has little effect on the air electrode performance. The poisoning effect of Hg is tolerable, since the electrode is Teflon bonded and the HgO concentration is very minute. Since the addition of HgO to cell electrolyte plays a positive role in the

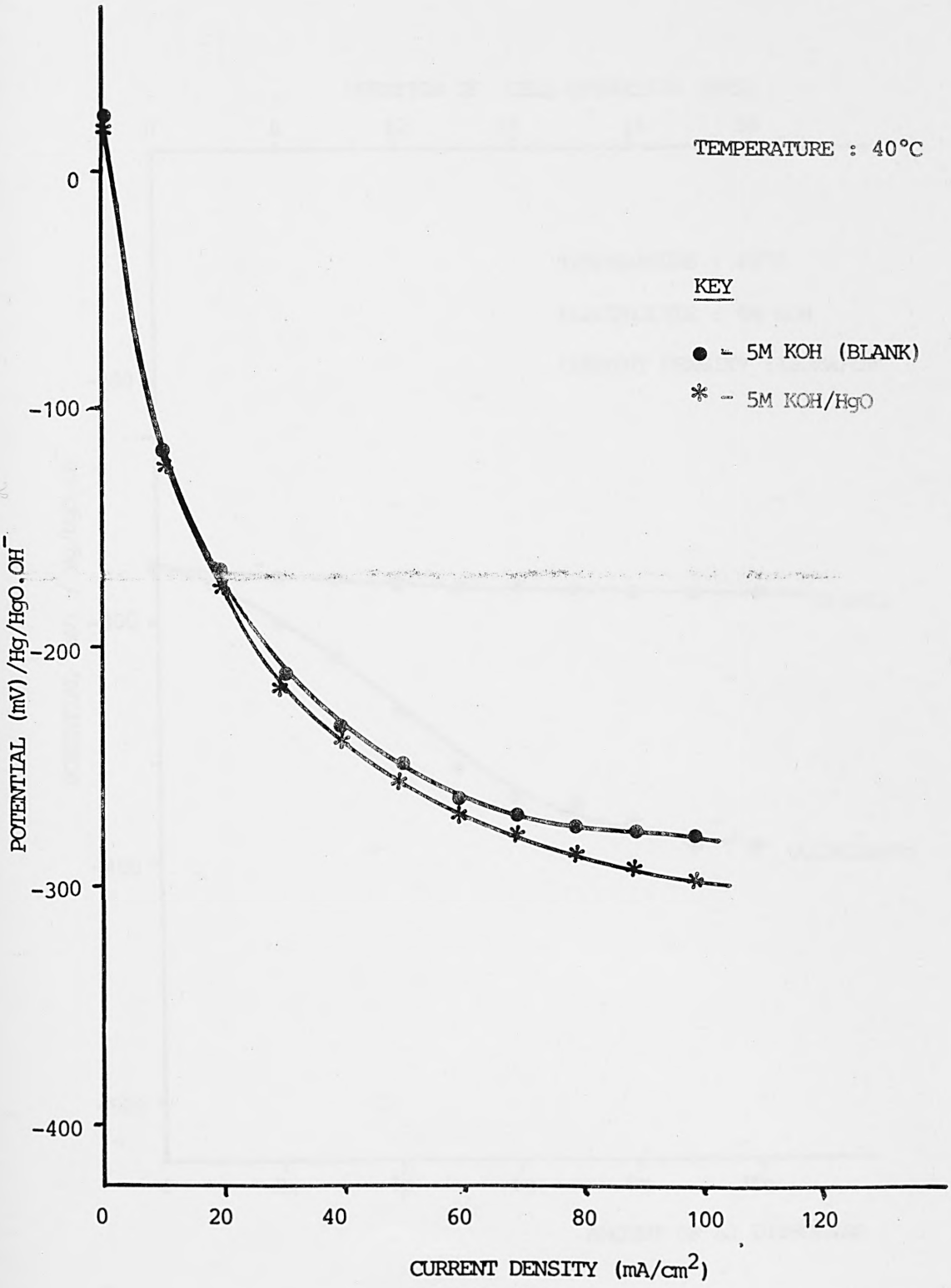

FIG. 8.3 EFFECT OF HgO ADDITIVES ON AIR ELECTRODE PERFORMANCE

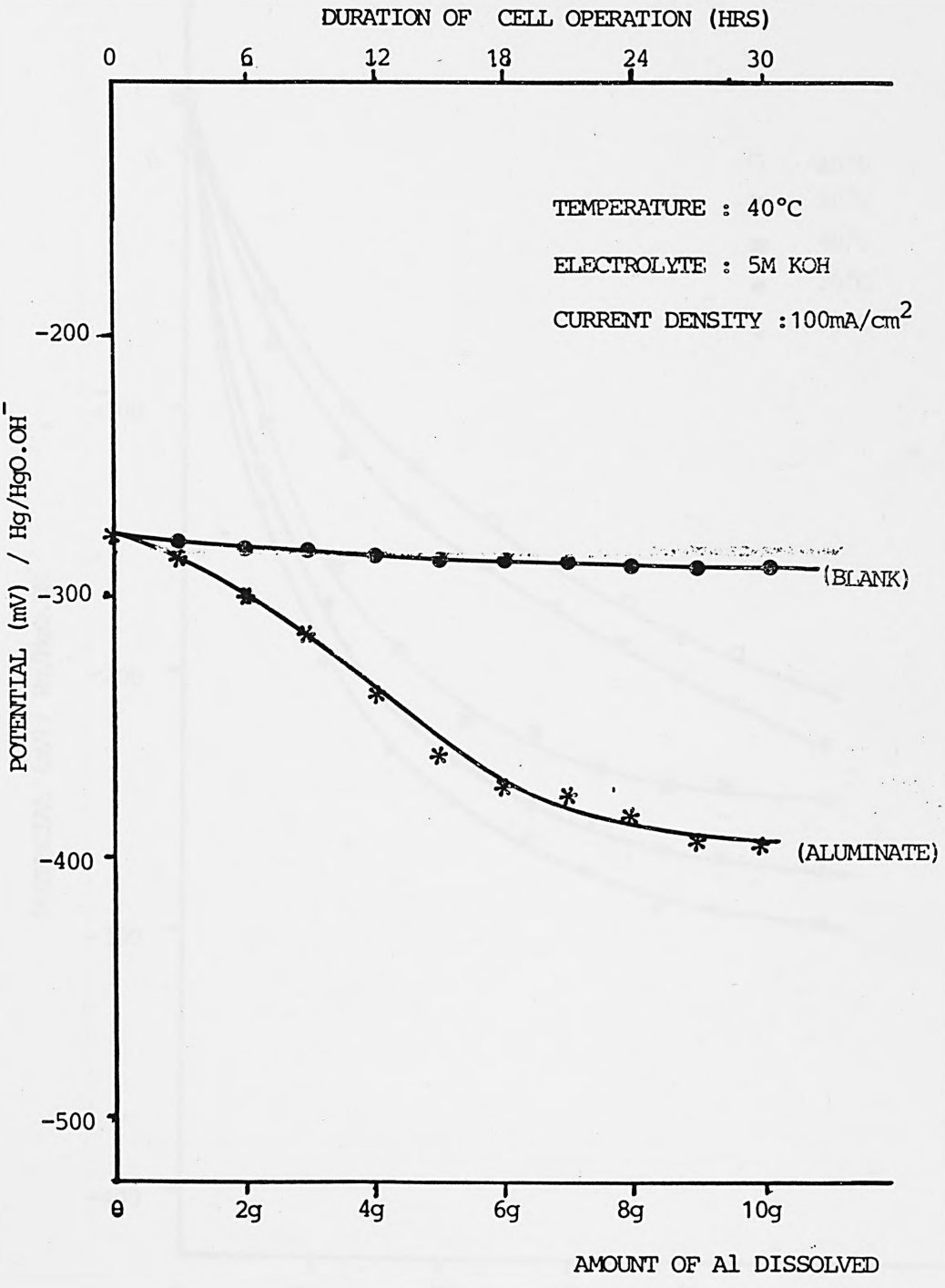

FIG. 8.4 EFFECT OF ALUMINATE CONCENTRATION ON AIR ELECTRODE PERFORMANCE

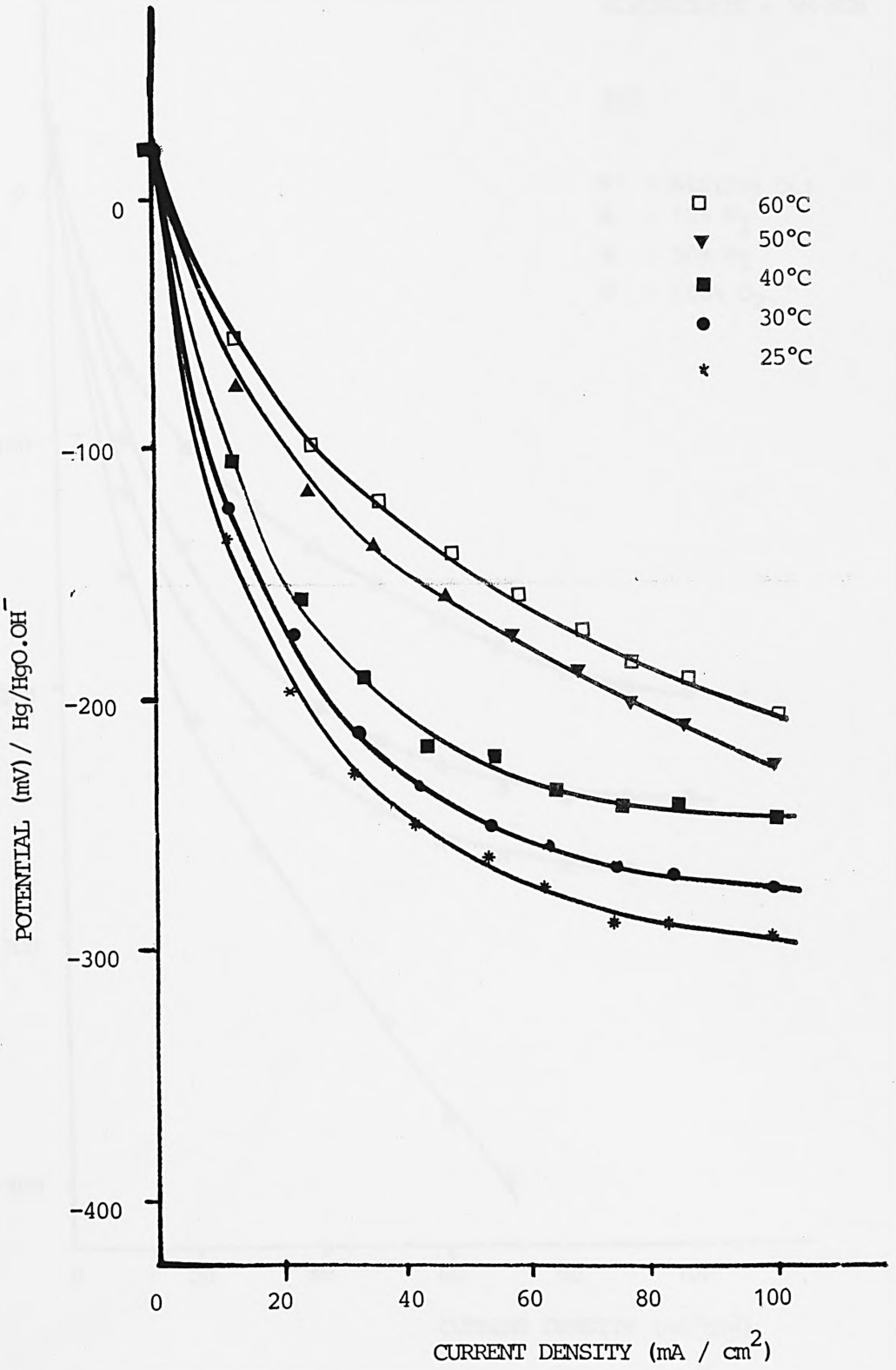

FIG. 8.5 EFFECT OF TEMPERATURE ON AIR ELECTRODE PERFORMANCE

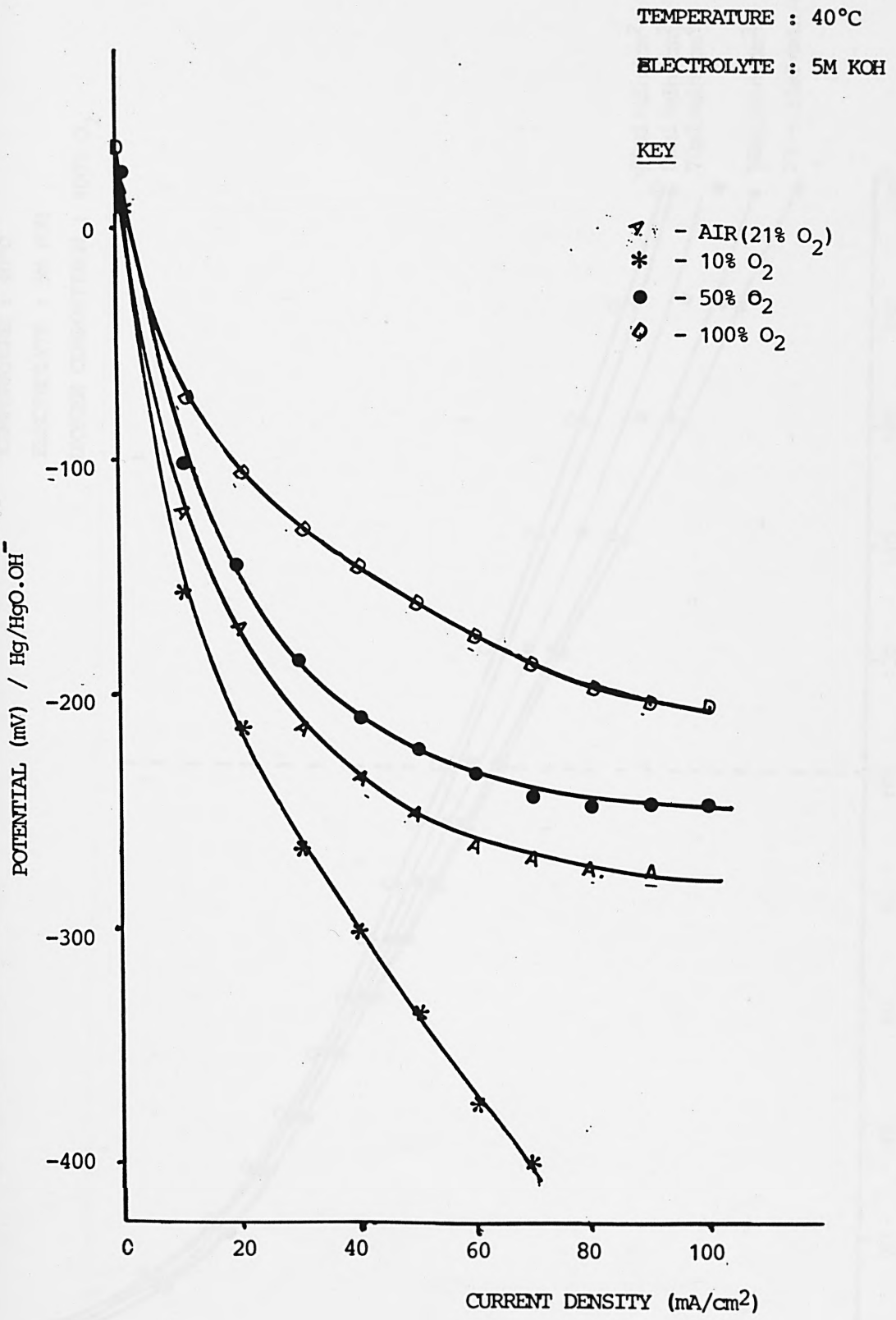

FIG. 8.6 EFFECT OF OXYGEN COMPOSITION ON AIR ELECTRODE PERFORMANCE

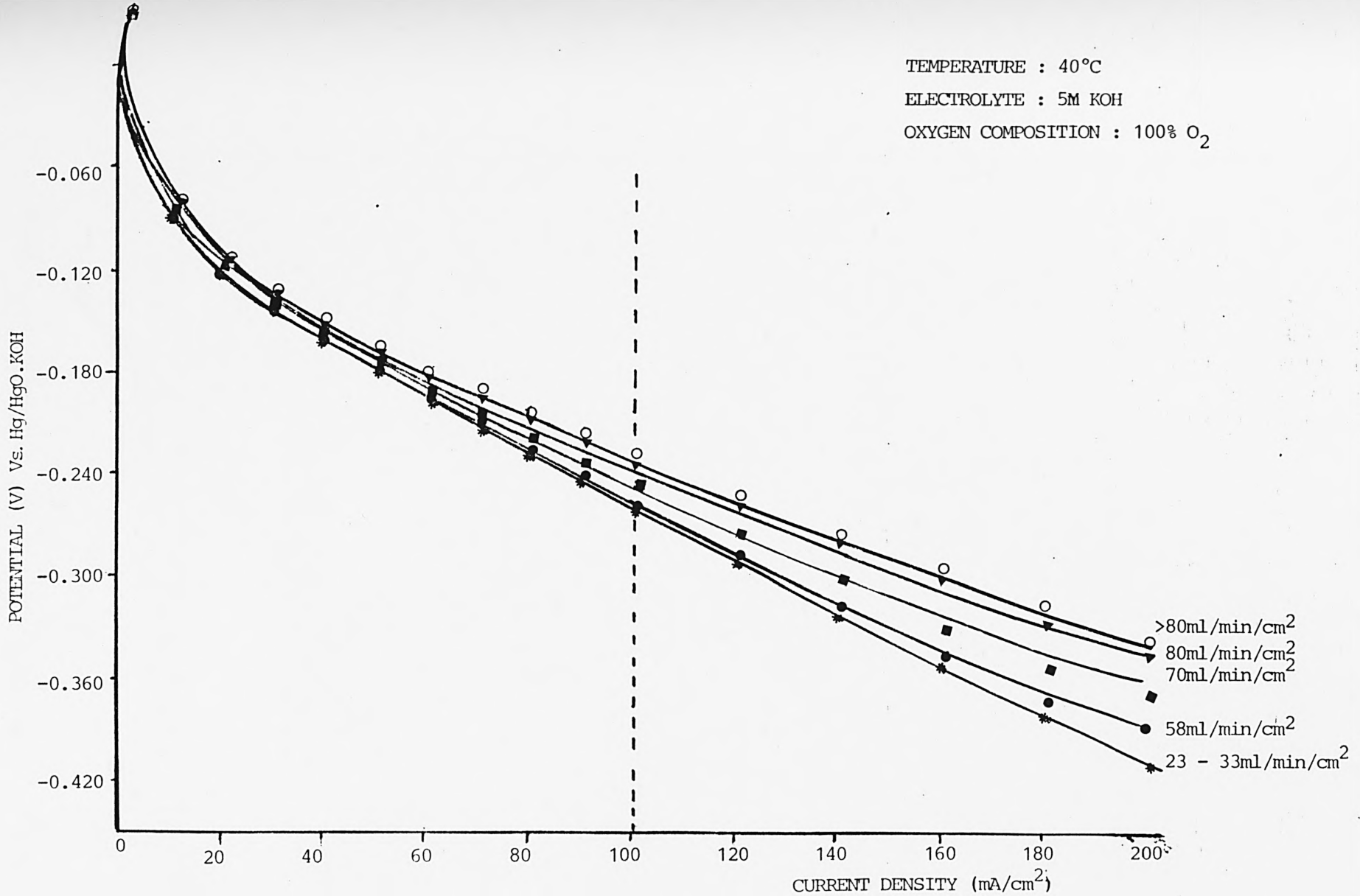

FIG. 8.7 EFFECT OF OXYGEN FEED RATE ON AIR ELECTRODE PERFORMANCE

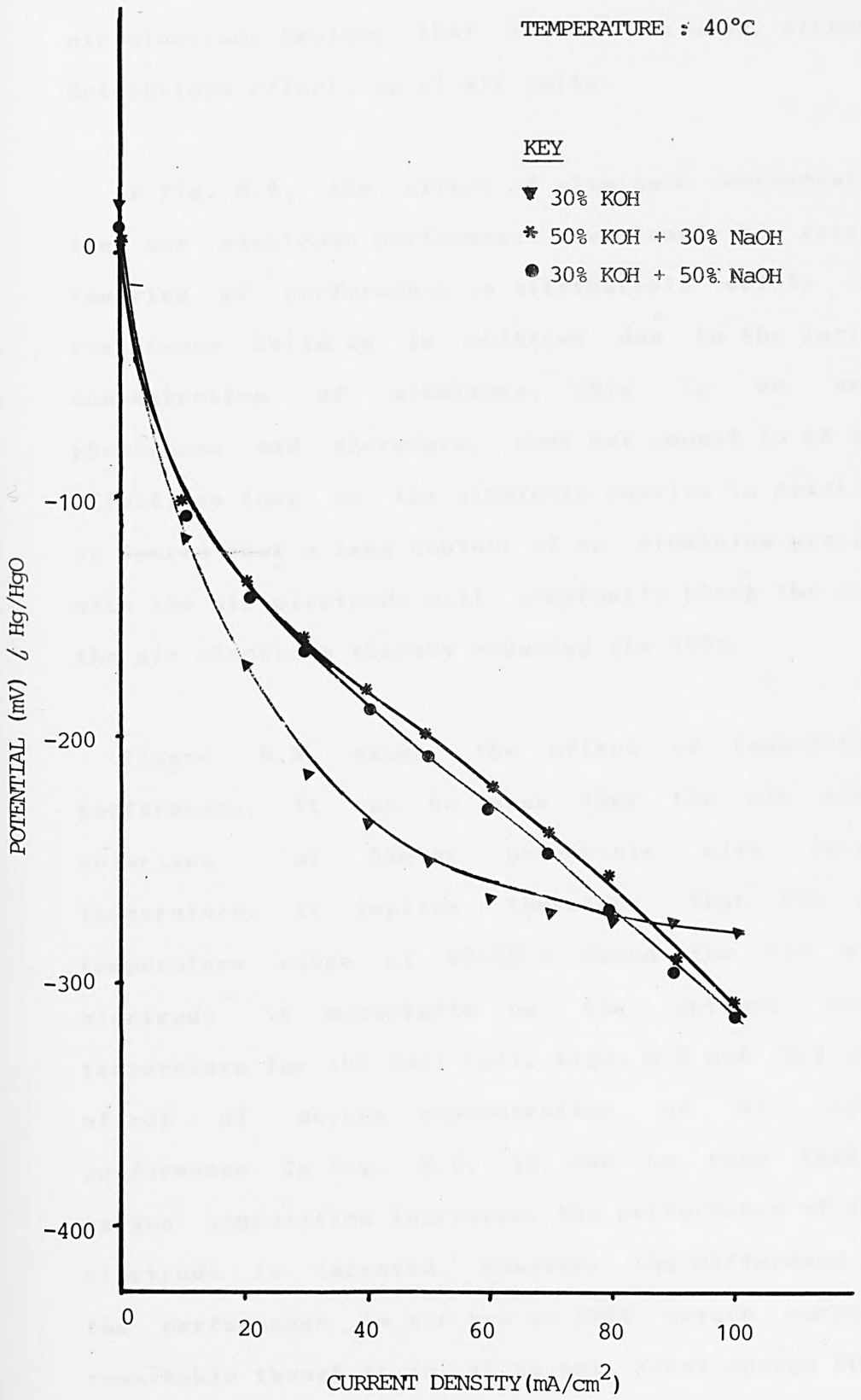

FIG.8.8 PERFORMANCE OF AIR ELECTRODE IN ELECTROLYTE MIXTURES

performance of the Al electrode, its little effect on the air electrode implies that it can be used, without any deleterious effect, in Al-air cells.

In Fig. 8.4, the effect of aluminate concentration on the air electrode performance can clearly be seen. The lowering of performance is attributable solely to the resistance build-up in solution due to the increasing concentration of aluminate. This is an expected phenomenon and therefore, does not amount to an adverse effect, so long as the aluminate remains in solution. It is feared that a long contact of an aluminium precipitate with the air electrode will eventually block the pores in the air electrode thereby reducing its life.

Figure 8.5 shows the effect of temperature on performance. It can be seen that the air electrode polarises at higher potentials with increasing temperature. It implies therefore that the optimum temperature range of 40-45°C found for the Al electrode is acceptable as the optimum operating temperature for the full cell. Figs. 8.6 and 8.7 show the effect of oxygen concentration on air electrode performance. In Fig. 8.6, it can be seen that as the oxygen composition increases, the performance of the air electrode is improved. However, the difference between the performance in air and at 100% oxygen composition, remarkable though it is, it is not great enough to offset

the energy density advantages gained by operating an Al-air cell in air. In Fig. 8.7, it can be seen that as the oxygen feed-rate is increased from 23 ml/min/cm^2 , the performance of the electrode is not affected, at current densities lower than 100 mA/cm^2 . However, at current densities higher than 100 mA/cm^2 the performance is affected. At the higher current densities, the performance of the air electrode is improved with increasing oxygen feed-rate up to 80 ml/min/cm^2 , beyond which the electrode performance is somewhat steadied. It is therefore suggested that for high power applications requiring the use of bottled oxygen, the optimum gas feed should be 80 ml/min/cm^2.

Figure 8.8 shows the performance of the air electrode in the electrolyte mixtures recommended for use in Al cells, for optimum performance. The air electrode performed comparably in all the electrolytes. The better performance of the electrode in the electrolyte mixtures, at low current densities, could be due to their higher hydroxyl ion concentration.

PART B: FULL CELL DISCHARGE CHARACTERISTICS

8.4 EXPERIMENTAL

A typical full cell used for the experiments is as shown

in Fig. 8.9. The cell casing was constructed from perspex and held together using epoxy adhesive. Two air electrodes of the same known exposed area were each fixed into a window created on each side of the rectangular cell case, with the catalyst sides facing inwards. The two air electrodes were 0.5 cm apart. The catalyst side of each electrode was covered with a thin membrane, to avoid short-circuiting and possible scratches on the air electrode when feeding in the Al metal; a thin Al alloy (Q4) plate (0.4 mm thick) was used as the anode. The cell discharges were carried out by placing a variable load across the cell circuit. The potentials realised were read off using a digital voltmeter. The following experiments show the discharges under different conditions.

8.4.1 DISCHARGE USING SELECTED ELECTROLYTES

The discharge characteristics of the full cell, constructed above, were determined for the electrolyte mixture recommended for use in Al cells (see chapter 6) and the conventional alkaline electrolytes. The cell was discharged at a steady current density of 100 mA/cm^2 (per total working area of air electrode); amounting to a total current of 1500 mA. The potentials realised during discharge were measured and plots of potential against discharge time were made.

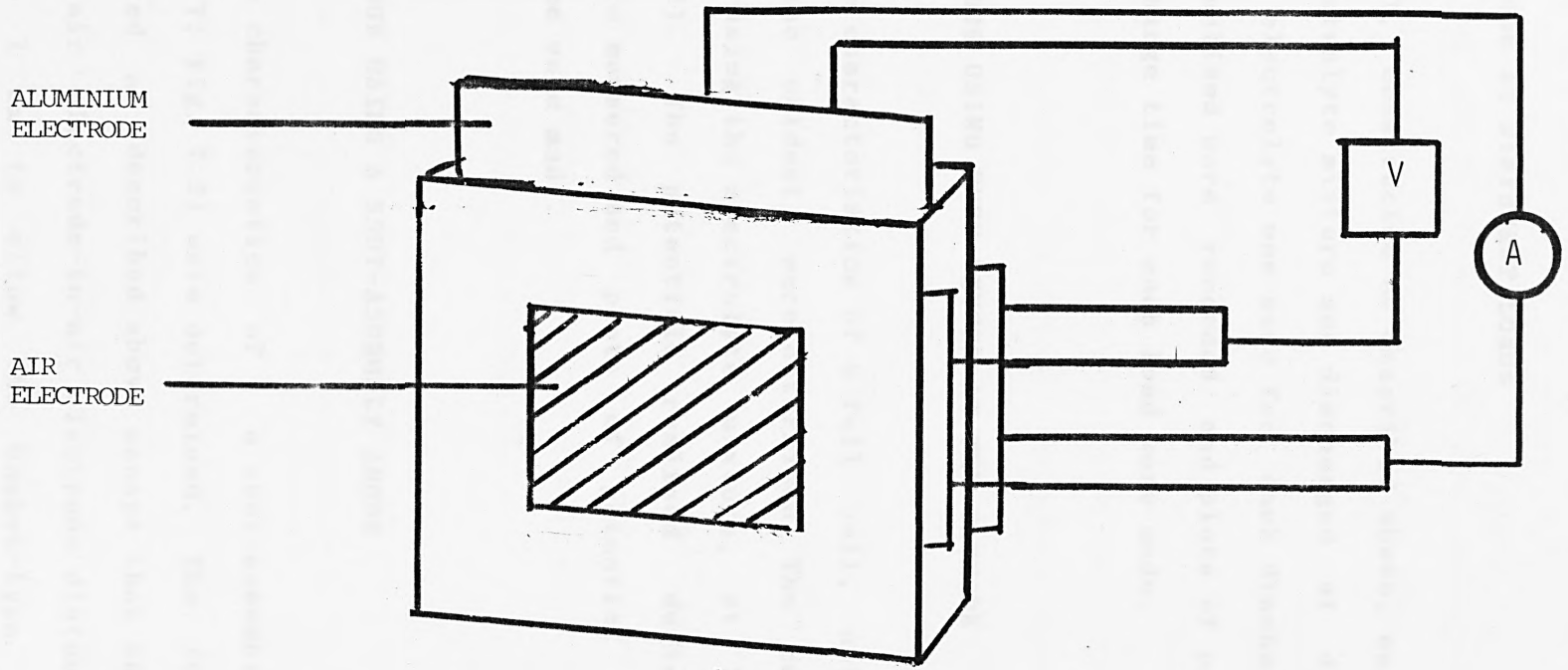

FIG. 8.9 A TYPICAL EXPERIMENTAL FULL CELL

8.4.2 DISCHARGE AT DIFFERENT LOADS

The full cell, constructed as described above, was filled with the electrolyte mixture and discharged at different loads. Fresh electrolyte was used for each discharge. The potentials realised were recorded and plots of potential against discharge time for each load were made.

8.4.3 DISCHARGE USING PURE OXYGEN AT THE CATHODE

The discharge characteristics of a full cell, using pure oxygen as the oxidant, were determined. The cell was discharged, using the electrolyte mixture, at 1500 mA (100 mA/cm^2). The potentials realised during discharge were measured and plots of potential against discharge time were made.

8.4.4 DISCHARGE USING A SHOT-ASSEMBLY ANODE

The discharge characteristics of a shot-assembly anode (see chapter 7; Fig. 7.3) were determined. The full cell was constructed as described above except that the width of the cell (air electrode-to-air electrode distance) was increased to 1 cm to allow the basket-type current collector to fit into the cell. The cell was discharged at 500 mA (50 mA/cm^2), using the electrolyte

mixture. The potentials realised were measured and plots of potential against discharge time were made.

8.5 RESULTS AND DISCUSSION

Figures 8.10-8.13 show the discharge characteristics of Al-air cell, under different operating conditions. In Fig. 8.10, it can be seen that the cell performs better when the electrolyte mixture is used as the electrolyte. The difference in performance is prominate after a long period of discharge. The electrolyte mixture allowing a longer period of discharge. This difference in performance can be attributed to the relative solubility of Al in the electrolytes. A solubility of 14.7, 6.1 and 8 g/100g were obtained for Al in the electrolyte mixture, 30% KOH and 30% NaOH respectively.

Fig. 8.11 shows the discharge of Al at different loads. The cell possesses an open circiut potential of 1.75 V. At 50 mA/cm^2, a working potential of 1.5 V is realised, giving a power density of 0.075 W/cm^2. At 100 mA/cm^2, 1.390 V is realised, giving a power density of 0.139 W/cm^2. And, at 150, 200, 250 and 300 mA/cm^2, 1.205, 1.135, 1.052 and 1.001 V were realised respectively, giving power densities of 0.181, 0.227, 0.263 and 0.3 W/cm^2 respectively. It can be seen that as the discharge load is increased, the power density of the cell is also increased. Thus, the higher

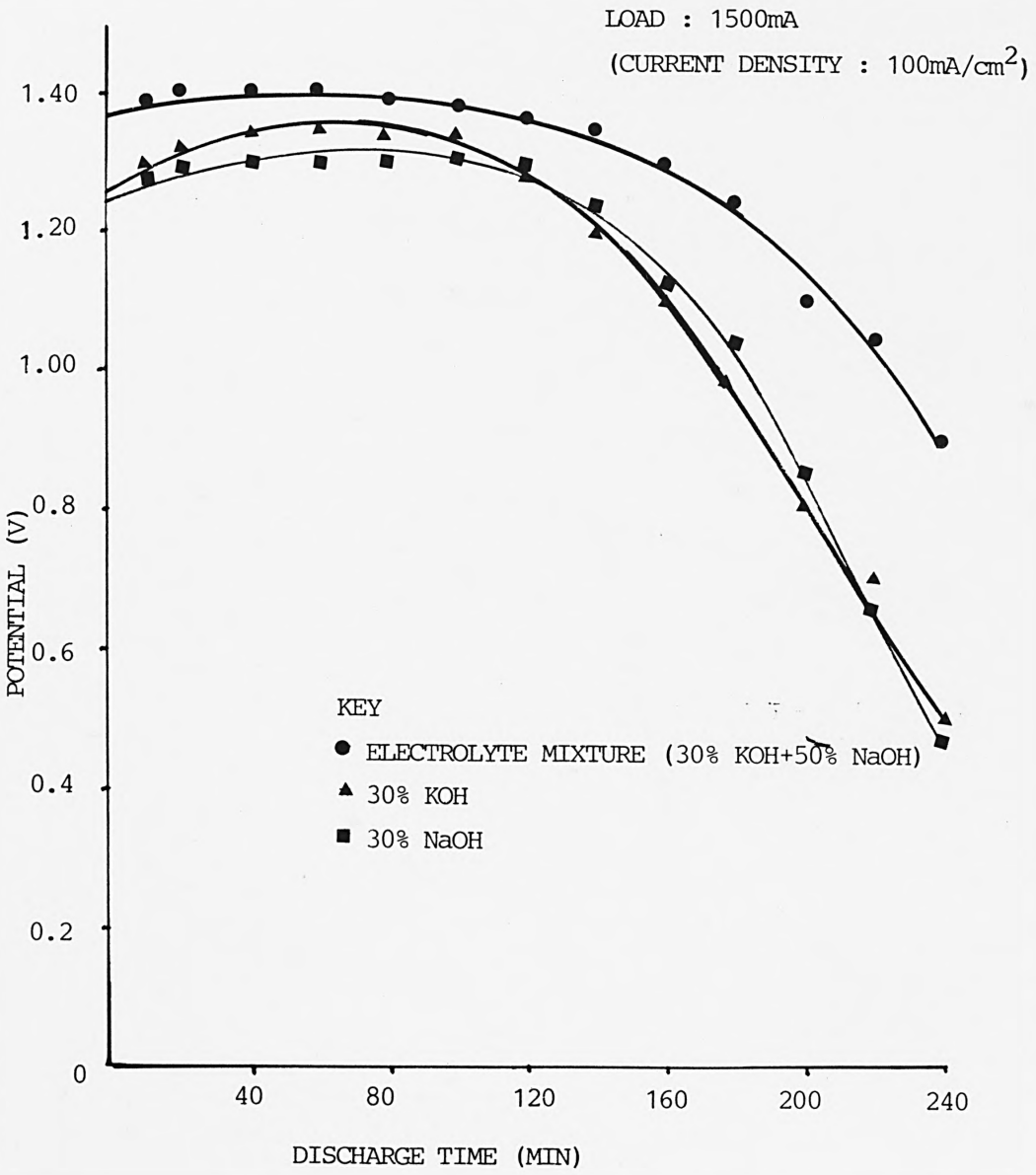

FIG. 8.10 DISCHARGE OF Al- AIR CELL USING DIFFERENT ELECTROLYTES

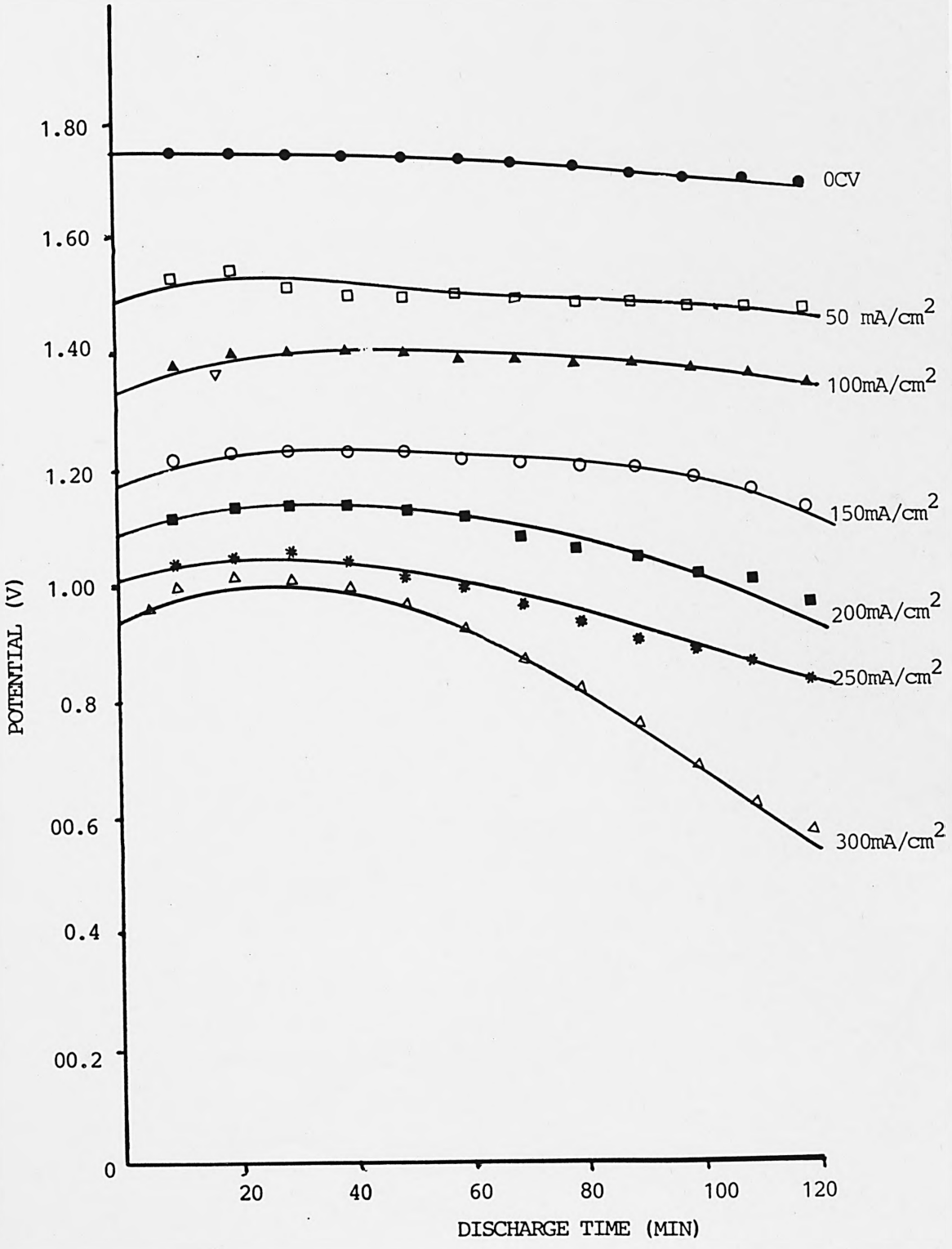

FIG. 8.11 Al - AIR DISCHARGE AT DIFFERENT LOADS

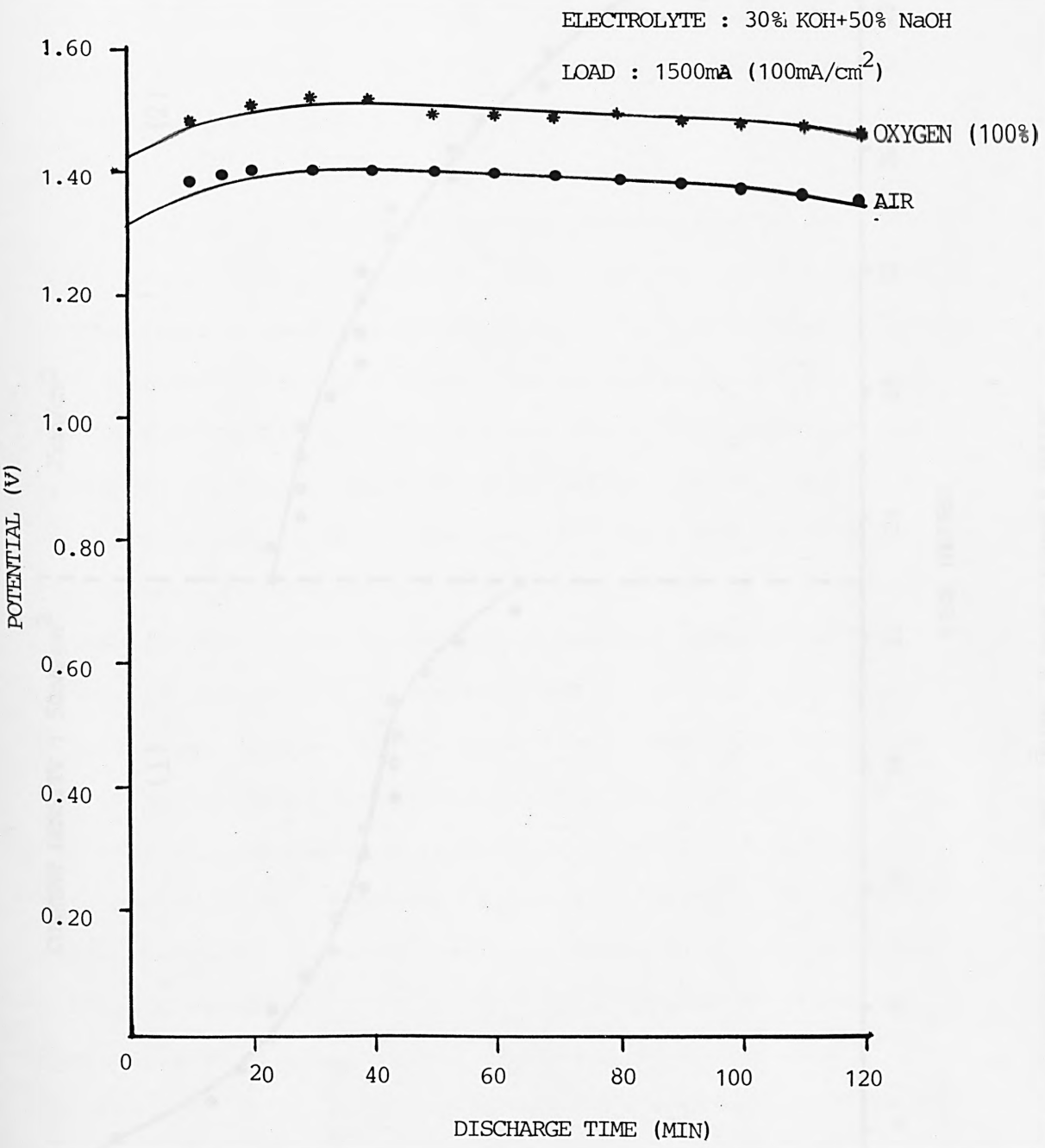

FIG. 8.12 DISCHARGE OF Al - AIR CELL USING OXYGEN AS DEPOLARISER

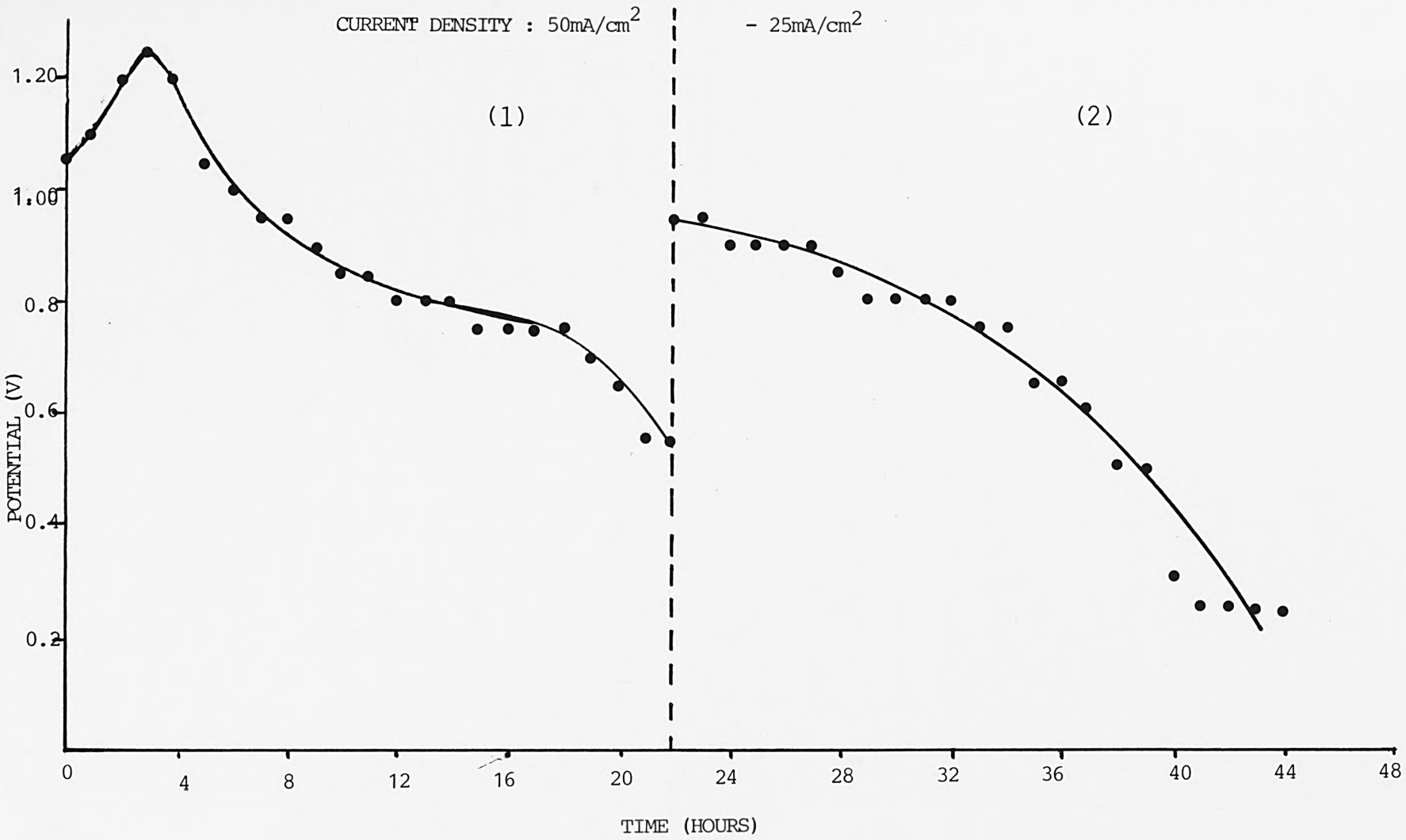

FIG. 8.13 DISCHARGE OF Al/AIR CELL USING A SHOT-ASSEMBLY ANODE

admissable steady current density of a cell the better its overall performance. The power density of a cell is further increased if the cell is operated using pure oxygen, instead of air, at the cathode. Fig. 8.12 shows the difference in performance. At 100 mA/cm^2, a working potential of 1.485 V is realised for pure oxygen, as compared to 1.390 V realised for air.

Fig. 8.13 shows the discharge characteristic of the cell, using a shot-assembly anode and twice the amount of electrolyte used above. The figure is divideded into two regions. Region 1 shows the potential response when discharged at 500 mA. The first 4 hours of operation saw a steady increase in potential after which the cell potential began to drop. However, it was not until after six hours of operation before actual drops in potential became eminent. The potential response thereafter until after 18 hours of operation falls within the Ohmic polarisation region, which signifies that the losses in potential within this period were mainly due to the build-up of resistance within the electrolyte owing to the presence of reaction products. After 18 hours, concentration polarisation predominates; suggesting diffusion problems due to the possible partial crystallisation of dissolved reaction products within the electrolyte. This is clearly shown in Region 2. Although the load was halved, accompanied by the near doubling in potential response, the trend of response exhibited the

existence of the diffusion problem. Just before the load was reduced, it appeared the amount of aluminium dissolved was enough to pose diffusion problems. However, the cell remained operationable at the reduced current output for a further 20 hours as a result of the lower demand on the cell and the concomitant reduction in the rate at which Al was being dissolved.

In general, the Al-air cell is capable of sustaining a high current density at a steady potential for a long period of time. The capacity of the cell being limited by the amount of electrolyte available. The capacity of an Al-air cell can therefore be increased if a large amount of fresh electrolyte is made available for the continuous operation of the cell. To avoid internal resistance by flooding the cell, the electrolyte can be managed in two ways:

i) the electrolyte can be fed into the cell from a reservoir to replace used one

or ii) the electrolyte can be circulated through the cell incorporating a filtering system to regenerate the used one.

To avoid the use of a pump for the circulation of the electrolyte, it is suggested that use is made of the positive gas pressure built up within the cell, for the purpose. The same positive gas pressure build-up is to be

exploited to enable automatic withdrawal of electrolyte from the cell, when it is not in use.

The following sections discuss the feasibility of these suggestions and establish the effect of electrolyte management on cell performance.

PART C: ELECTROLYTE MANAGEMENT

8.6 EXPERIMENTAL

8.6.1 CONCEPTUAL TESTS

A) ELECTROLYTE WITHDRAWAL

To alleviate the problem of self-discharge, it is suggested that the electrolyte be automatically withdrawn from the cell, when not in use, by means of the positive gas pressure that is built up at the anode. This concept of automatic withdrawal is the subject of the following test.

TESTING PROCEDURE

For the purpose, a U-shaped tube (Fig. 8.14) was used.

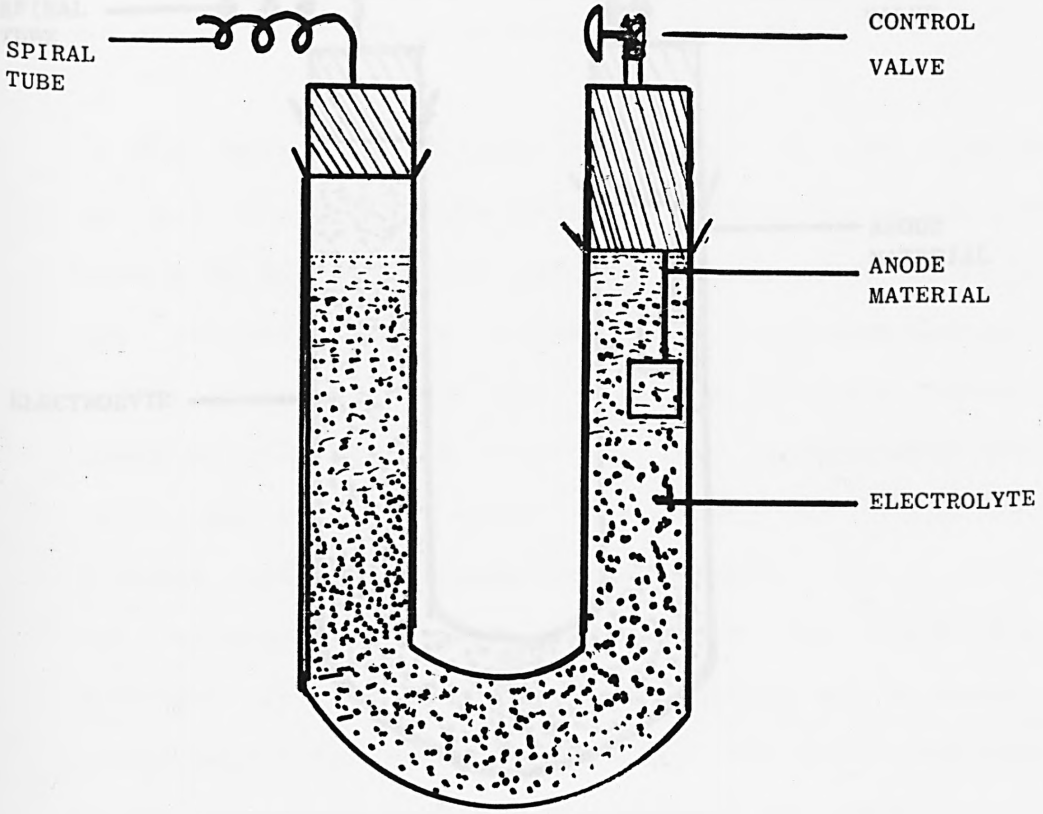

FIG. 8.14 U-SHAPED TEST CELL TO VALIDATE THE CONCEPT OF ELECTROLYTE WITHDRAWAL BY MEANS OF POSITIVE GAS PRESSURE BUILT UP WITHIN THE SYSTEM

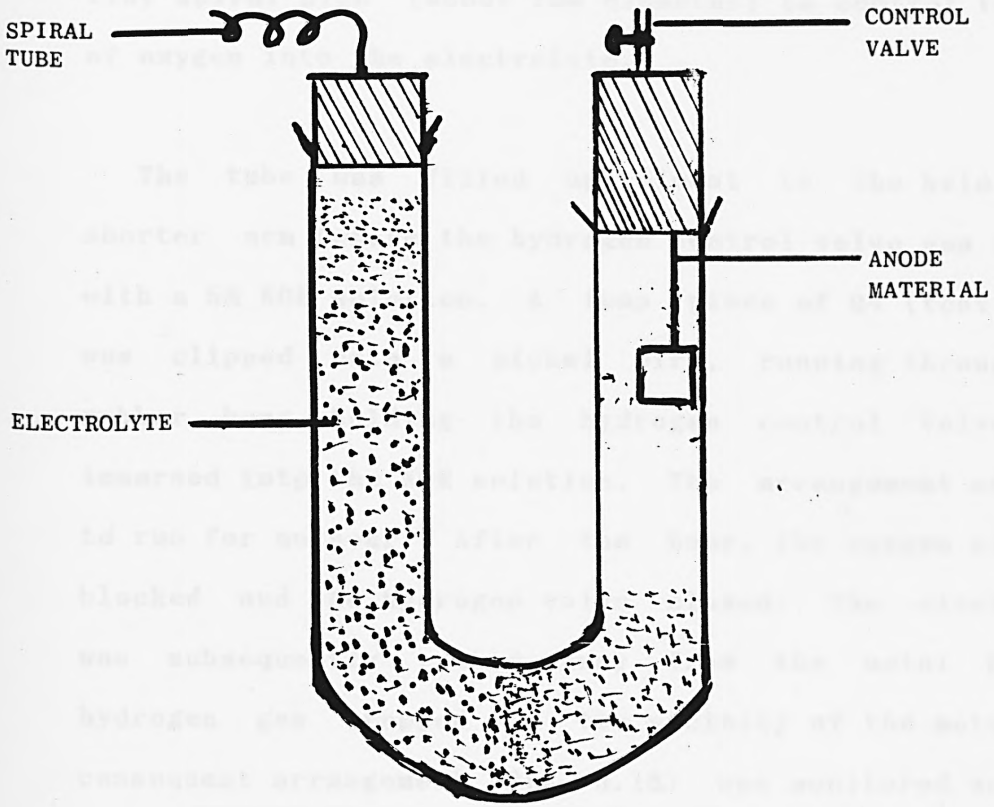

FIG. 8.15 U-SHAPED TEST CELL UPON ELECTROLYTE WITHDRAWAL

The two ends of the tube were both open. One end had a valve fitted into for the control of the flow of hydrogen out of the reaction tube. The other end was fitted with a tiny spiral pipe (about lmm diameter) to control the flow of oxygen into the electrolyte.

The tube was filled up almost to the brim of the shorter arm (where the hydrogen control valve was fitted) with a 5M KOH solution. A lump piece of Q4 (test alloy) was clipped onto a nickel wire, running through the rubber bung holding the hydrogen control valve, and immersed into the KOH solution. The arrangement was left to run for an hour. After the hour, the oxygen pipe was blocked and the hydrogen valve closed. The electrolyte was subsequently pushed away from the metal by the hydrogen gas trapped in the vicinity of the metal. The consequent arrangement (Fig. 8.15) was monitored some few hours later to find out the effect of withdrawing the electrolyte on the metal. A greyish powdery layer was formed on the surface. X-ray analysis was carried out to determine the nature of the powder.

B) ELECTROLYTE CIRCULATION

Also tested was the concept put forward for the circulation of the electrolyte. The need to circulate the electrolyte has already been mentioned in the previous

section.

TESTING PROCEDURE

A cell of the type shown in Fiq. 8.16 was used. The cell was filled with a 5M KOH solution. A lump piece of the test alloy was immersed, into the solution, at one end of the cell. Both ends of the cell were cork-sealed. The valve was opened, to allow the solution to circulate from one end to the other. To aid visual verification, a coloured piece of paper was introduced into the solution.

C) RESULTS AND DISCUSSION

Figure 8.17 shows both the X-ray analysis and scanning electron micrograph of the surface composition of the alloy on withdrawing the electrolyte. The surface was heavily coated with aluminium oxide growth, owing to the effect of the presence of dissolved oxygen, water and hydroxyl ions in the electrolyte that had remained on the surface of the metal. As such, it is suggested that the electrode should be flushed, upon electrolyte withdrawal, with an inert liquid that can displace the electrolyte on the surface; preferably a non-aqueous liquid.

The coloured paper introduced into the solution was able to move round with varying speeds; moving round the corners of the cell with ease, suggesting the build-up of

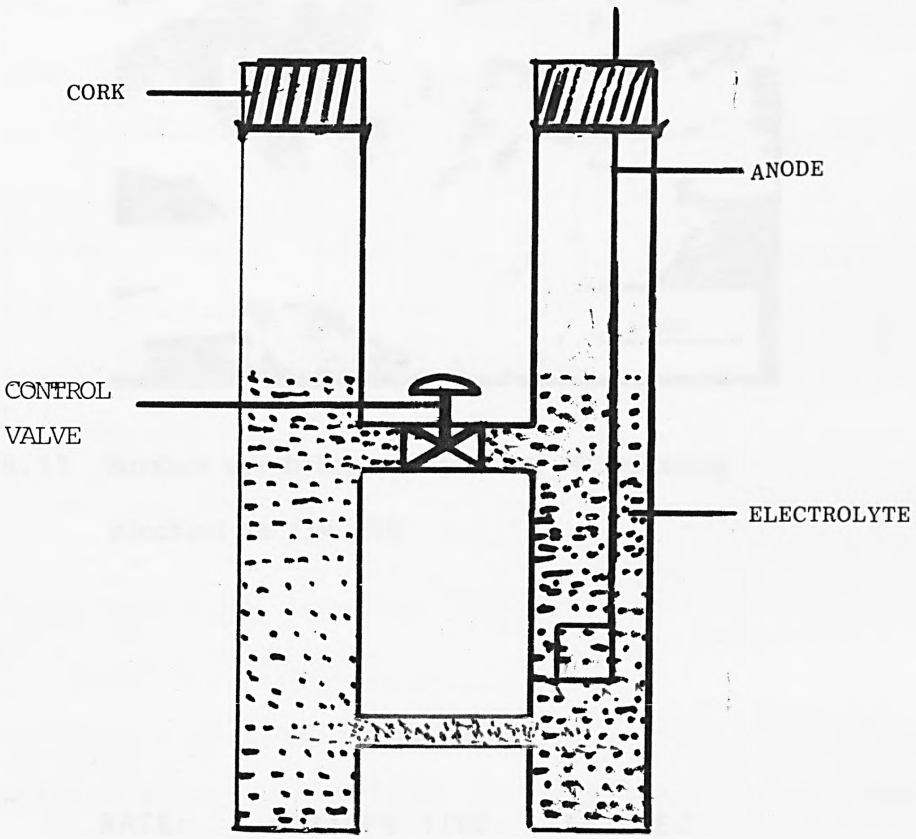

FIG. 8.16 SELF-CIRCULATION OF CELL ELECTROLYTE

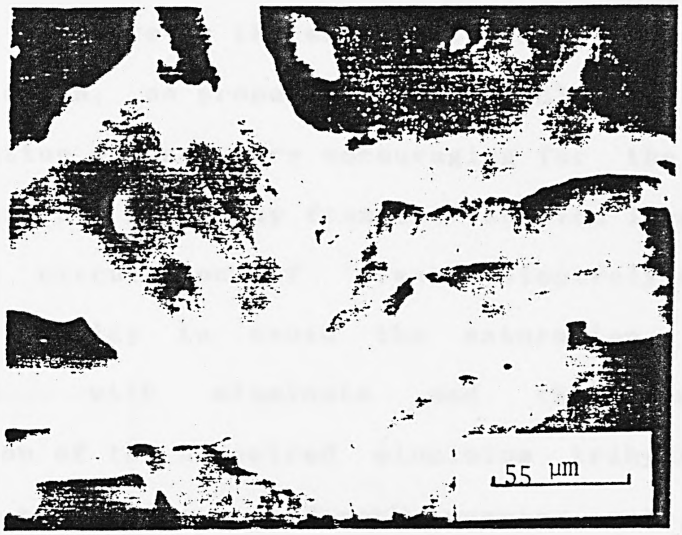

FIG. 8.17 Surface morphology of Q_4 after withdrawing electrolyte (5M KOH)

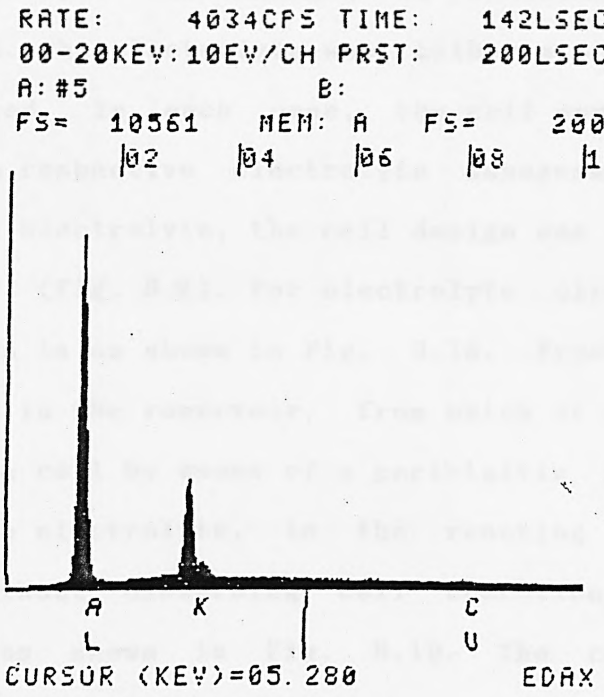

X-ray analysis

an internal pressure in the solution. This indicated that self-circulation, as proposed, was possible. But the rate of circulation was not very encouraging for the uniform distribution of heat away from the reaction locality, as well as the circulation of 'fresh' electrolyte to the reaction locality to avoid the saturation of the electrolyte with aluminate and the concomitant precipitation of the undesired aluminium trihydroxide. A peristaltic pump, of a considerable pumping rate, is thus required, to aid circulation.

8.6.2 CELL DISCHARGE CHARACTERISTICS

The discharge characteristics of a full cell, for which the electrolyte was managed in different ways, were determined. The electrolyte was either static, circulated or replaced. In each case, the cell was designed to enable the respective electrolyte management mode. For the static electrolyte, the cell design was as described previously (Fig. 8.9). For electrolyte circulation, the cell design is as shown in Fig. 8.18. Fresh electrolyte was stored in the reservoir, from which it was circulated through the cell by means of a peristaltic pump. And to enable the electrolyte, in the reacting cell, to be changed without disturbing cell operation, the cell was designed as shown in Fig. 8.19. The cell unit had a collecting vessel into which the used electrolyte was

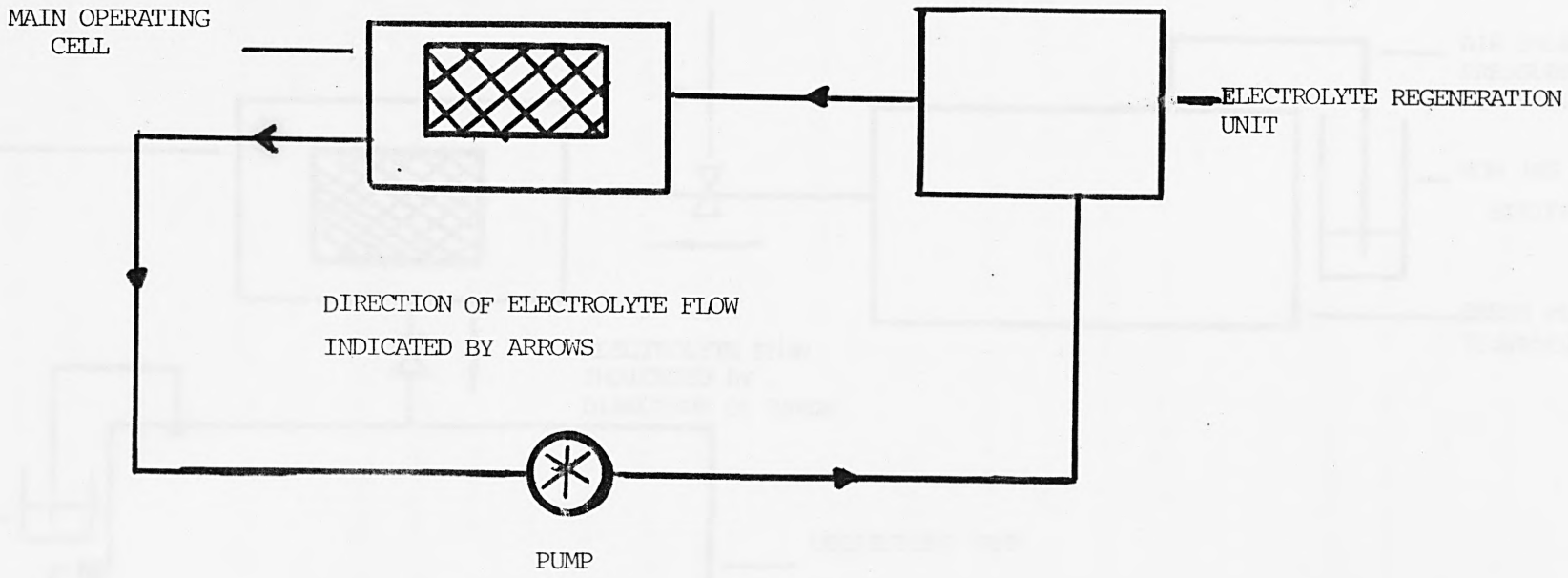

FIG. 8.18 CELL DESIGN ALLOWING ELECTROLYTE CIRCULATION BY MEANS OF A PERISTALTIC PUMP

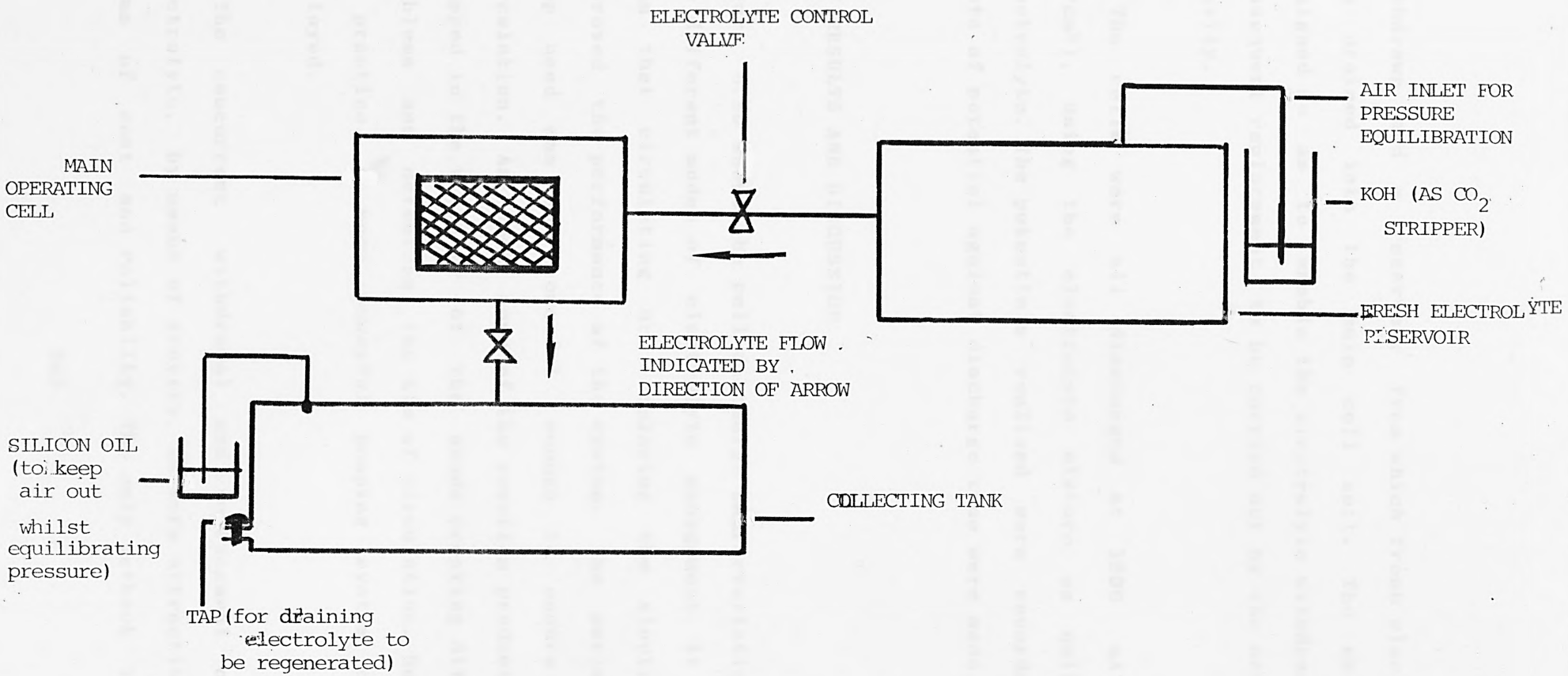

FIG. 8.19 CELL DESIGN ALLOWING CONCURRENT ELECTROLYTE WITHDRAWAL AND REPLACEMENT BY MEANS OF GRAVITATIONAL FORCES

withdrawn and a reservoir from which fresh electrolyte was drained into the main cell unit. The cell was designed so as to enable the electrolyte withdrawal and subsequent replacement to be carried out by the action of gravity.

The cells were all discharged at 1500 mA (100 mA/cm^2), using the electrolyte mixture as cell electrolyte. The potentials realised were recorded and plots of potential against discharge time were made.

8.7 RESULTS AND DISCUSSION

Figure 8.20 shows the cell discharge characteristics for the different modes of electrolyte management. It can be seen that circulating or replacing the electrolyte, improved the performance of the system. The peristaltic pump used was not powerful enough to ensure rapid circulation. As such, some of the reaction products were trapped in the vicinity of the anode creating diffusion problems and defeating the aim of circulation. However, in practice, a more powerful pumping system can be employed.

The concurrent withdrawal and replacement of the electrolyte, by means of gravity, is very attractive, in terms of cost and reliablity. The only setback is the

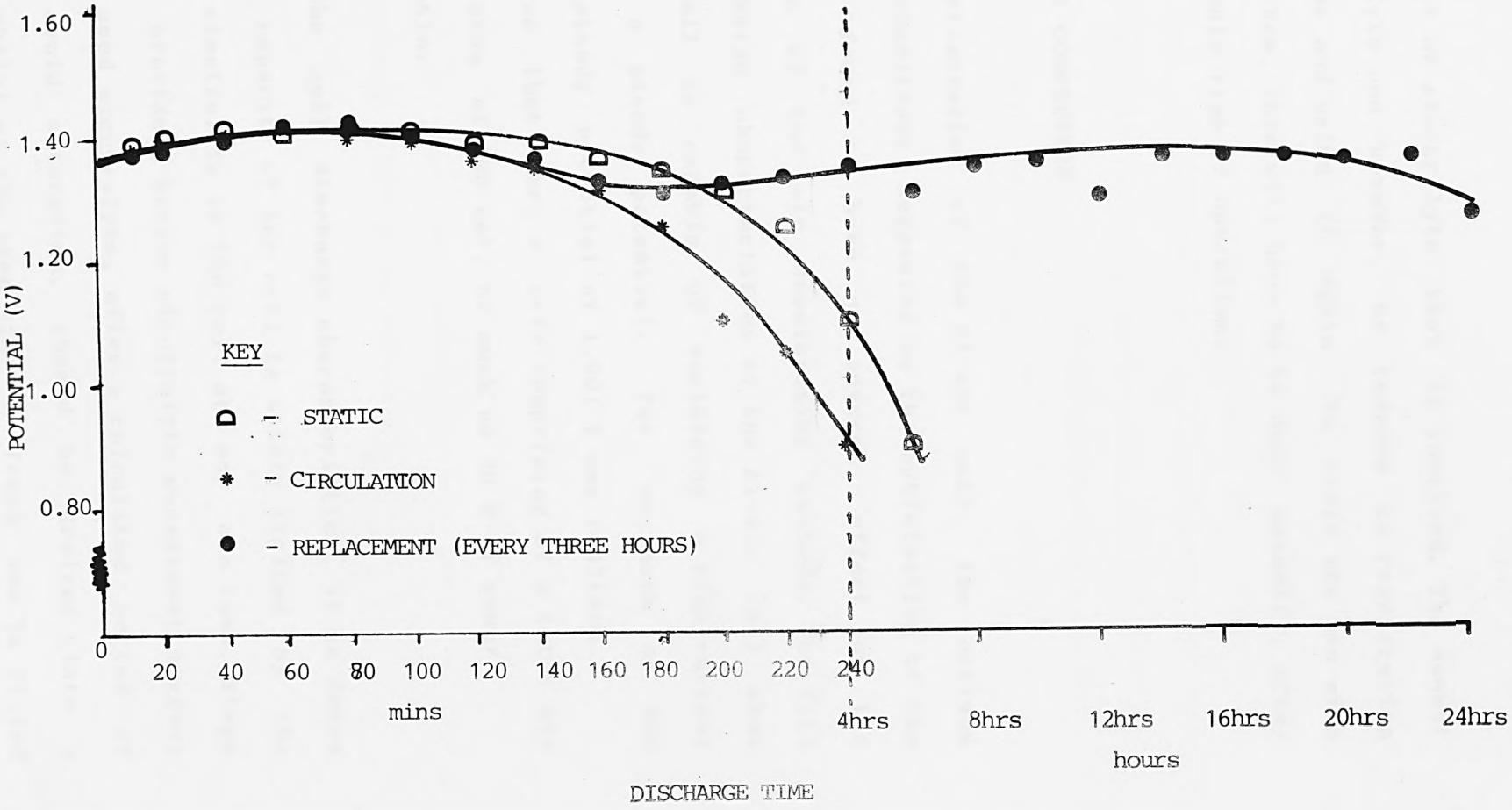

FIG. 8.20 Al – AIR CELL DISCHARGE WITH ELECTROLYTE MANAGED IN THREE WAYS

large amount of electrolyte that is involved. The amount of electrolyte can however, be reduced by regenerating the used one and using it again. To avoid the use of a pumping system, this will have to be done manually, after a considerable time of operation.

8.8 GENERAL CONCLUSION

In the optimisation of the Al-air cell, the optimum operating conditions suggested by the optimisation of the anode are found to have no adverse effect on the performance of the air depolarising cathode. The full cell discharge characteristics of the Al-air cell show that the cell is capable of sustaining a high current drain at a steady potential. For as much as 300 mA/cm^2, a steady potential of 1.001 V was realised. This implies that for a cell comprising of a total air electrode area of 100 cm^2, as much as 30 W of power is realisable.

From the cell discharge characteristics, it is found that the capacity of the cell is solely limited by the amount of electrolyte in the cell at any one time. Steps taken to provide a better electrolyte management suggest that the used electrolyte, after a calculated period of use; to avoid saturation, should be drained into a collector whilst at the same time a fresh one is filled

into the cell. The collected electrolyte is to be regenerated and and fed back into the system via the fresh electrolyte storage tank. The whole process of withdrawal and refill is to be carried out automatically by the aid of gravitational forces, in order to streamline the reliability of the system to just the reliability of the main operating cell. The reliability of the main operating cell is assured so long as there are enough reactants and electrolyte in the system.

In the management of the cell electrolyte, for applications where gravitational forces are absent, the electrolyte can be circulated through the main cell via a fresh electrolyte reservoir and a crystallizer. Here, a very powerful and highly reliable pumping system will be required.

The foregoing chapters establish the technical feasibility of an Aluminium-Air battery system capable of delivering high power outputs. In the next chapter, the economics of such a system is discussed.

9 FIELDS OF APPLICATION: A TECHNICO-ECONOMIC EVALUATION

9.1 INTRODUCTION

The use of aluminium as battery anode material, is both technologically and economically attractive. The aluminium metal is the most abundant metal in the earth's crust. The supply of the metal, governed by the primary capacity in place at any one time with adjustments for labour-caused outages or power curtailments, in the Western world is totalling up to 15.7 million tons by the end of 1985 and will increase to 16 million tons by 1987 [199]. Demand for the metal, which is lower than the supply, is estimated to total up to 13.8 million tons by the end of 1985. The demand, possibly with the exception of household foil, is derived and short-term price inelalastic; about 45% of the total consumption is made up by the two industry sectors, transport and building.

These two important markets are particularly depressed in recent times [199]. As such, the biggest challenge for the aluminium industry is the development of new applications for aluminium for further market penetration. Thus, the success of the Al-air battery is greatly supported by the aluminium industry who are even

prepared to integrate forward to ensure its cost competitiveness [200]. So with the already price competitive edge of aluminium over other metallic anodes, coupled with the availability and the compressibility of the oxidant, air or pure oxygen, the economics of the system is so far very attractive. However, the justification for any investment will require a feasible field of application. The proceeding sections take a look at such fields of application and assess their commercial viability. The type of application is discussed in two main parts; high power uses for which weight limitations apply and emergency power uses for which reserve power sources are needed. The fields of application are classified under offshore and onshore applications respectively.

PART A: OFFSHORE APPLICATIONS

The high energy-to-weight ratio of aluminium-air battery is an attractive feature in its possible use in offshore vehicles. Both in Europe and the U.S.A., vehicles for exploration and exploitation of the sea-bed are constantly being developed; owing to the expansion of interests in underwater operations. The deep diving submersible is one of the most useful vehicles developed.

9.2 APPLICATION IN SUBMERSIBLES

Basically, a submersible consists of a pressure hull that accommodates the crew. It is surrounded by an unpressurised streamlined fairing into which power supplies and other equipment that operate at ambient pressure are incorporated. Accommodation is provided for a pilot and a crew of up to five persons, depending on the size of the craft. It is fitted with port-holes, navigation and communication aids and external equipment ranging from lights and cameras to hydraulic manipulators, depending on the task at hand. Unlike conventional submarines, which depend for their buoyancy on gas or liquid ballast at ambient pressure, the submersible's pressure hull has a high strength-to-weight ratio that enables its buoyancy to support nearly all the weight of the hull's contents and external equipment. Ballast is carried for ascending and descending, for emergency use, and for altitude adjustment and surface stability.

The need for the development and deployment of low cost submersibles capable of satisfying the requirements related to: underwater surveillance, deep sea rescue, tactical deterrence, and deep ocean exploration is recognised widely by all offshore operators. The current operating submersibles have served to prove the usefulness of their potential.

An examination of current and prospective underwater operations will enable one to fully appreciate the part that can be played by Aluminium-air battery in the activities of the submersible.

9.2.1 MISSION PROFILES

The underwater world can be divided conveniently into three categories:

(i) The comparatively shallow [< 1000 ft] waters over continental shelves

(ii) The medium depth [1000-3000 ft] waters, and

(iii) The remaining deep oceans including the deepest trenches to which there have been manned descents.

The whole underwater world is therefore accessible to mankind. The same divisions can be differentiated by the human desire to exploit them and thence the effort that is willingly devoted into doing so. Oil and gas have created a near 'Gold Rush' fever of activity in shallow waters. However, though drillings have also shown these resources to be present in the medium depth, it is not economic to extract them until the shallow water reserves have been exhausted. Therefore the drive to work in

medium depths is directly related to the price of oil. Sooner or later it will become the region of greatest activity.

Although about 88% of the world's sea area is more than 3000 ft deep [201], the difficulties of working in such deep waters make it unlikely that people will want to extend their activities beyond basic scientific studies or perhaps very special military operations.

Many of the activities in shallow waters, and probably later in medium depths, require men on the spot to make detailed observations and take decisions, and power to carry out the work. These requirements can broadly be met in one of three ways:

(i) A manned submersible that is self-sufficient in power,

(ii) a manned submersible that is supplied with power via a cable, and

(iii) an unmanned vehicle with an umbilical cord.

Broadly, the first is the more flexible and easily operated within limits set by power available. The second avoids power limitation but is considerably less flexible and less easy to operate. The third seems potentially to

offer most, provided its working life justifies the expensive equipment needed to control the umbilical cord and so improve its flexibility and ease of operation to something comparable with free swimming vehicles. Umbilical cords are probably impractical for work in the deep oceans. Here, the emphasis is likely, for a long time, to be on scientific observations, their 'on the spot' interpretation and subsequent decisions. Without an umbilical cord to provide a high level communication channel to the surface, the deepsea region has to be studied using free-swimming manned submersibles.

A) MISSIONS IN SHALLOW WATER

It is appropriate to consider first underwater activities in shallow waters because they are already the scene of much commercially motivated effort, such as inspecting and examining oil rigs, finishing off wellheads, burying pipes and cable and, increasingly, clearing up after such operations. At the moment almost all such activities are executed using manned, battery powered submersibles.

These submersibles and their mother ships constitute a capital investment that is a large component of the total for the underwater service industry (over 2 million pounds for the mother ship and over 500 thousand pounds for the submersible itself) [202]. Labour cost for divers and mother ship crews are also very high, particularly

for divers in the North Sea. These two factors provide a very strong incentive to aim for as high 'diver-at-work' factors as possible, using existing vessel types.

Dives using small submersibles, whether equipped with diver lock-out facilities or not, are generally limited by crew endurance to about 10 hours duration when weather conditions permit. Free-swimming submersibles need batteries capable of meeting the maximum power demands of missions. They also have to provide enough energy at the power required for a complete mission (that is working time plus reserves for emergencies) reliably for many missions. Missions that have to be abandoned for any reason are extremely expensive. The more energy batteries can store at reasonable weights, the better use a submersible operator can make of his or her capital equipment by having more diving crews. Such a work schedule is dependent to most batteries retaining their capacity over a number of cycles.

B) MISSIONS TO THE DEEP SEA

These will be mainly for the scientific study of the deep sea itself, its physics and chemistry and the life forms it sustains. The geology and geophysics of its floor are of a second major interest. Such work requires professional scientists on the spot, working in 'laboratory coat' conditions. These scientific missions

will probably, therefore, often use manned craft in which scientists are in a sphere at near surface atmospheric pressure. The mission time is generally limited by crew endurance but the activities that can be pursued during a mission are often energy limited [203]. The type of submersible that can be used needs energy for propulsion, lighting, scientific equipment, life-support and emergencies. Each of these consumes energy at a different rate. As the use of one limits the other, the various activities in a mission have to be carefully fitted together within a craft's overall energy budget. This considerably restricts not only any scheduled programme of work but also, perhaps more importantly, curtails the scientist's freedom to change a schedule in the light of early observations and results, particularly as he or she must always consider how much energy might be needed for propulsion and life-support in unforeseen circumstances or emergency before getting back to the mother ship.

Craft mobility, a major power use, will thus always be restricted. Furthermore, the immediate environment, which the craft is there to study, is a static one with small currents, and little, if any, convective mixing [204]. Obviously then, the craft should discharge as little foreign material as possible to its surroundings and certainly nothing that seriously disturbs it, for example toxic materials. In this context, noise and possibly heat need to be considered as undesirable effluents. It is also operationally desirable not to

generate vibration and noise within the craft.

Since it is very important that the craft be recoverable under the severest conditions, the overall weight of the craft becomes limited. Therefore, deep-sea manned submersibles need power sources with the highest available energy density and preferably with minimum effluents.

C) SIMILARITIES BETWEEN THE REGIONS

Missions to all regions have several features in common. All set out to make detailed observation of their environments, often close to the sea bed or to a fixed structure. People, working with instruments, need to be in small and easily manoeuverable vessels, submersibles. These submersibles need power for navigation, propulsion, lighting, work; and for propulsion and life-support in an emergency. For the latter in particular, their power supplies have to be reliable. Because the crew knows that its survival depends ultimately on the integrity of the power supplies, the amount of work it will do on a single dive is immediately relatable to its confidence in the amount of energy available throughout the dive.

Aluminium-air battery can provide more than sufficient power needed for missions to all depths. They can give

manned submersibles sufficient energy to cover all operational dives. Because it has a high energy-to-weight ratio, it will minimise the risks that exist in recovering the submersible particularly in adverse weather conditions.

To justify the commercial viability of such a system, a brief look is taken at the market for submersibles and at the existing electrochemical power sources.

9.2.2 MARKET TRENDS

Although the modern submersible building boom was started by such famous European underwater explorers as Piccard and Cousteau, developments has since taken place largely in the USA. Of the vehicles operating in 1970, over 40 were American [205]; the rest were designed and built in the UK, Japan, the USSR, France and Canada. As with many other projects, the main impetus to the development of the manned submersible in the USA was given by the loss of Thresher [205] and, the increased awareness of the oceans that followed that disaster. In many cases, as the rush to the oceans began, submersibles were built first to demonstrate that the engineering and the technological knowledge existed to enable them to be built, and secondly to show that the company concerned was staking its claim in oceanology: and a submersible is a sufficiently exciting piece of hardware to act as

admirable proof of its builder's commitment to oceanology. In addition there was the exploratory zeal attached to building programmes: '' There are thousands of square miles of continental shelf out there that have never been seen before; let's go down to see''. This, then, was the function of the first submersible - 'to go down to see'.

A) SUBMERSIBLES FOR RESEARCH

Marine research is carried out by three main bodies: universities, government research centres and industry. Research at universities and government research centres include work on the basic oceanographical disciplines which have varying degree of relevance to industry. In this research area, lies a significant market for submersibles and, thus, aluminium-oxygen battery. The value of the submersible to date has been in its role as a passive tool and an observation device. But it is a sophisticated form of observation: no surface-controlled instrumented system of photography or measurement of the sea floor can make the choice of moving out of the line of its predetermined track to look at something a few metres to one side, but the manned submersible can.

Manned submersibles are therefore used for a wide variety of special tasks which cannot be carried out by remote-controlled instruments. A typical task is the

observation and collection of samples from inaccessible sites such as cliff faces or submarine canyons where the high manoeuvarability of the submersible and the direct observation by scientists are necessary. For these reasons, the submersible has proved of great value in scientific research. For example, biologists have been able to examine organisms in their natural environment, to collect specimens, and to make in situ measurements of salinity, temperature, illumination, and other variables. Geologists have been able to discover more about particular areas of the sea bed in two hours in a submersible than has ever been learnt before by remote methods, valuable as they are for producing generalised characteristics of a wide area. In physical oceanography the submersible has been used to measure rapid changes in salinity and temperature that occur at depths, sometimes, less than a metre apart. That, would be almost impossible to measure from a surface vessel. Also, the submersible has been used to plant oceanographic instruments on the sea bed and to return periodically to check their performance. What is even more important, is that, these programmes of observation, measurement, and sampling have not taken place on a discrete basis; by being immersed in the environment the submersible is able to integrate a series of measurements simultaneously to gain a comprehensive picture of the particular area in which it is working [204]. On a series of dives in the past for the US Naval Underwater Weapons Centre, Deepstar 4000

[205] made measurements of gravity, temperature profiles, sound velocity, sound refraction, biological sound scattering and reflecting (the effect that minute marine organisms can have on underwater sound propagation), sediment transport and layering, and enscarpment sediment shear strengths and heat flows, as well as taking water samples, planting a current meter on the bottom and releasing dye bags for water movement studies

However, because of total cost and usage considerations, research centres will usually charter submersibles for their very often intermittent research dives. Possibly, some smaller, cheaper, submersibles using under 10 KW of power will be owned by research centres for work on the continental shelves. At the end of 1973 there were only some 10 of such submersibles throughout the world. It was then predicted that by 1982, there was the likelihood that half of the non-university research centres would own one, giving a total of around 60. A realistic building-rate was predicted to be 3 per year in 1974, rising to 5 per year in 1977 and 10 per year in 1982 [206]. If this trend lived up to expectation, with the expected rise in military activities underwater and commercial offshore programmes; albeit the vigorous research before these programmes are fortefied, the future market for battery power sources for submersibles, for research, is substantial.

B) SUBMERSIBLES FOR COMMERCIAL EXPLOITATIONS

What of the submersible's role in direct exploitations of the oceans? Here, too, the vehicles have performed mainly passive work up till recent times, but they have been of great value. In the oil and gas industry, submersibles have been used for pipeline inspections and the maintenance of wellheads. Currently, the principal outlets for submersibles in the oil and gas industry are for:

(i) wellhead servicing and

(ii) pipeline and structure inspection.

Unless the water is very deep (say over 300 m) or there are strong currents, a submersible operating from a mother ship does not have much advantage over a lowered capsule. Rough weather hinders both the docking of the capsule on the cellar, and the launch and retrieval of the submersible. The use of a larger submarine as the mother ship for either capsule or submersible is a possibility, but it would be very expensive in both capital and operating cost.

The alternative is, therefore, a relatively high-speed submersible which would operate from a shore base. This will eliminate the support ship cost. The power required for such a high-speed submersible can be adequately met

by the aluminium-air battery.

The world building rate for submersibles for the above purposes is, however, very uncertain. Taking upper limit fiqures for offshore oil production, and assumming that sea bed production systems requiring submersible access were predominant, it was predicted in 1973 that by 1982 the total number of submersibles in service would be 40 [206]. Assuming a world building rate of 5 per year, it can be estimated that by 1986 the total number will be 60, for the above purposes.

C) SUBMERSIBLES FOR RECREATION

The popularity of the underwater tourist sightseeing bus [206] will depend largely on the development of reliable, low cost, high energy density, batteries for the propulsion and other power requirements of free-swimming, tourist submersibles. For such submersibles to be economically viable, they will have to provide accommodation for about 25 persons, each time. Thus, the successful development of the proposed low cost, very high energy density system will make tourist submersibles very common means of recreation, since a large number of people can be carried as well as the amount of energy needed.

D) OTHER MARKET AREAS

Submersibles have been used in the past in other industries. In the fishing industry, 'Aluminaut' had surveyed scallop beds off Florida [205], confirming in one dive the results of preliminary surveys by trawlers, and determining the distribution, density, and size of the resource. As a result, a new fishery has been set up.

In search and salvage operations, there was the now famous search by 'Alvin' and 'Aluminaut' for the H-bomb lost off Spain in 1966, and in 1968 the rescue of 'Alvin' by 'Aluminaut' when she fell from her support ship and sank in 4900 ft of water [205]. The U.S. Navy is working on a project for a fast-reaction underwater rescue system capable of reaching a stricken submarine within hours, and at the heart of the project is the unique Deep Submergence Rescue Vehicle (DRSV) - a free-swimming manned submersible [207].

The sucessful use of submersibles in these industries defines yet other market areas for aluminium-oxygen battery. Another significant area is in the use of submersibles for underwater tactical deterrence by the military.

9.2.3 EXISTING ELECTROCHEMICAL POWER SOURCES

According to Busby [208], ''all submersibles constructed in the seventies and now under construction specify lead-acid batteries''. Almost the same applies to all free-swimming submersibles today; only a few use other batteries instead.

Table 9.1 shows some of the high energy density batteries now commercially available. Compared to Pb/acid [1], the Ni/Fe [2] has a higher energy density but it is more rugged and gasses severely on charge. Which apart from the need frequently to top-up the electrolyte, can create an explosion hazard.

Similarly, the only clear advantage in using Ni/Cd [3], and much more Ag/Zn [4], is their higher energy densities. Both are however, much more expensive; Ni/Cd x 2 and Ag/Zn x 10, the cost of Pb/acid. Silver-zinc (Ag/Zn) has the further disadvantage of having only about 10% the cycle life of the other two [4]; its reliability must be similarly reduced. Also, Ni/Cd, though used in a few submersibles, suffers from the major drawback that there is no reliable method of estimating its state of charge [3].

Also commercially available is the Hydrogen/oxygen fuel cell [5]. However, it is very expensive and suffers from the disadvantage of cryogenic storage: requiring a

TABLE 9.1 SOME HIGH ENERGY DENSITY BATTERIES USED IN SUBMERSIBLES

	Ni/Zn	Ni/H_2	Li/Cl_2	$Li(Si)/FeS_2$	Na/S	$Zn/Cl_2.6H_2O$	$Li/SOCl_2$	$Al/CrCl_3$
Temperature (^oC)	Am	Am	450-550	400-450	350	Am	Am	Am
Open Circuit Voltage (v)	1.7	1.3	3.6	2.1	2.08	2.1	3.5	2.3
Achieved Energy Density $Whkg^{-1}$	55-77	55-60	350	187	75	66-88	500	150-200
Energy Density $kWhm^{-3}$	50-100	200	440	210	250	200	750	-
Cycle life	300-1500	2,000-10,000	300	1000	800/65%	>100	1^o	1^o
Pressure	Am	1-35 Atm	-	-	-	1 Atm	Am	Am
Problems	shape change, dendrite formation on Zn electrode	some self-discharge on stand	fire, corrosion, thermal insulation			refrigeration Zn morphology	fire risk on short circuit, passivation on stand	Self-discharge once activated

pressure shell, and boil-off during long missions.

Clearly, the overhelming predominance of lead-acid batteries in this field of application can be seen. However, its inherently low energy density poses power or weight limitations and thus, curtails the productiveness of the submersible during a particular dive. Table 9.2 shows a comparison of the energy to weight ratio for Pb/acid and the proposed system. It can be realised that for about 7 times less weight, allowing for the weight of oxygen bottles and other auxillaries, the aluminium-oxygen battery can provide the same amount of energy as lead-acid battery. The very high energy obtainable, for a very small overall weight, from the proposed system will allow more diving crew and equipment to be carried on board the submersible; allowing high 'diver-at-work' factors to be realised. Moreover, since it is very expensive to abandon missions, mission failures due power failures can be averted using the proposed system. The fuel (aluminium), oxidant (oxygen) and electrolyte needed for the provision of power are carried and fed from outside the main battery operating unit. Therefore, to provide for such emergencies, only the already lightweight oxygen electrodes need be carried in excess, as standby units. In the event of any fault with the operating unit, the same fuel, oxidant and electrolyte provided can be fed into the standby unit to obtain the power needed to continue the mission; instead

TABLE 9.2 ENERGY DENSITY OF ALUMINIUM-OXYGEN BATTERY

EXPERIMENTAL DATA

CURRENT OUTPUT (A)	8
CELL OPERATING VOLTAGE (V)	1.485
VOLUME OF ELECTROLYTE/CELL (ml)	45
DENSITY OF ELECTROLYTE SOLUTION (g/ml)	1.2821
SOLUBILITY OF ALUMINIUM IN ELECTROLYTE (g/100g)	14.7
COULOMBIC EFFICIENCY OF ALUMINIUM (%)	95
WT OF AIR ELECTRODES AND CELL STACK (g)	76.5
OXYGEN REQUIREMENTS (g/hr)	2.3875
WT OF OXYGEN + BOTTLE (g)	5800
AMOUNT OF OXYGEN/BOTTLE (g)	576

SCALING UP FOR A 1 KW UNIT FOR A 10 Hr MISSION

SCALE-UP FACTOR	84
MISSION TIME (hr)	10
WT OF ALUMINIUM REQUIRED (g)	2379.949
WT OF ELECTROLYTE SOLUTION REQUIRED (g)	16190.13
WT OF AIR ELECTRODES AND CELL STACKS (g)	6439.394

TOTAL WEIGHT OF OXYGEN + BOTTLES (g)	23200
WT OF AUXILIARY EQUIPMENT; PUMPS, CONTROL GEAR, ETC. @ 25% THE WT OF AIR ELECTRODE & CELL STACKS (g)	1609.848
TOTAL WT OF COMPLETE BATTERY SYSTEM (Kg)	49.819
ENERGY DENSITY (Whr/Kg)	200.73
ENERGY DENSITY OF Pb-ACID BATTERY (Wh/kg)	30

of abandoning it. This cannot be said for Pb/acid since, being a secondary battery, almost twice the amount of energy actually needed will have to be carried, under the already existing weight limitations, in order to achieve that.

Also, the overall weight of aluminium-air system can be further decreased, for long mission times, by carrying the hydroxides used in preparing the electrolyte in the solid form. The aqueous electrolyte needed can then be prepared in situ using water from the sea. This will not only reduce the weight due to the amount of water that will be carried otherwise, but will also reduce remarkably the vast storage space that might be needed. An experimental investigation was carried out to determine the effect of using seawater, instead of distilled water, to prepare the cell electrolyte.

The performance of an 8 x 8 cm air electrode full-cell was tested for the the control electrolyte, Electrolyte no. 10, which was prepared by dissolving the 30% KOH and 50% NaOH in distilled water. The electrolyte under investigation was prepared by using artificial seawater, containing 2.5% NaCl concentration by weight and some Mg and Ca impurities, to dissolve the solid hydroxides. This is labelled as Electrolyte no. 19. Sufficient seawater was added to ensure the same hydroxide concentration, by weight, as that of the control electrolyte. The

artificial seawater was used, by itself, as one of the test electrolytes. It is labelled Electrolyte no.20. Trace amount of Hg was added to each electrolyte. The cell was discharged at 8 amperes in each case and the start-up times as well as the potential changes with time noted. The cell was thoroughly washed after each test before being used again.

The results obtained for the full cell testings are shown as Figs. 9.1 and 9.2. Fig. 9.1 shows the start-up times for the cell using the different electrolytes. The delay period is divided into three regions, assuming a full load of 9.6 Watts is required. The beginning of the first region, labelled 'WL', is the time at which a significant loading level starts to be achieved. It is called the working loading level because from that time power for at least a one shot application is realised. The beginning of the second region is labelled 'EL', the effective loading level. It is the time from which power can be provided for effective use, for a reasonable time period. The third region starts from the time at which the required full load is achieved. From this time, reliable power that ensures continuity of operation is provided.

A working loading level is achieved after 65 secs for electrolyte no. 10 and after 95 secs for electrolyte no. 19. After 124 and 185 secs, an effective loading level is achieved for nos. 10 and 19 respectively. Also, full load

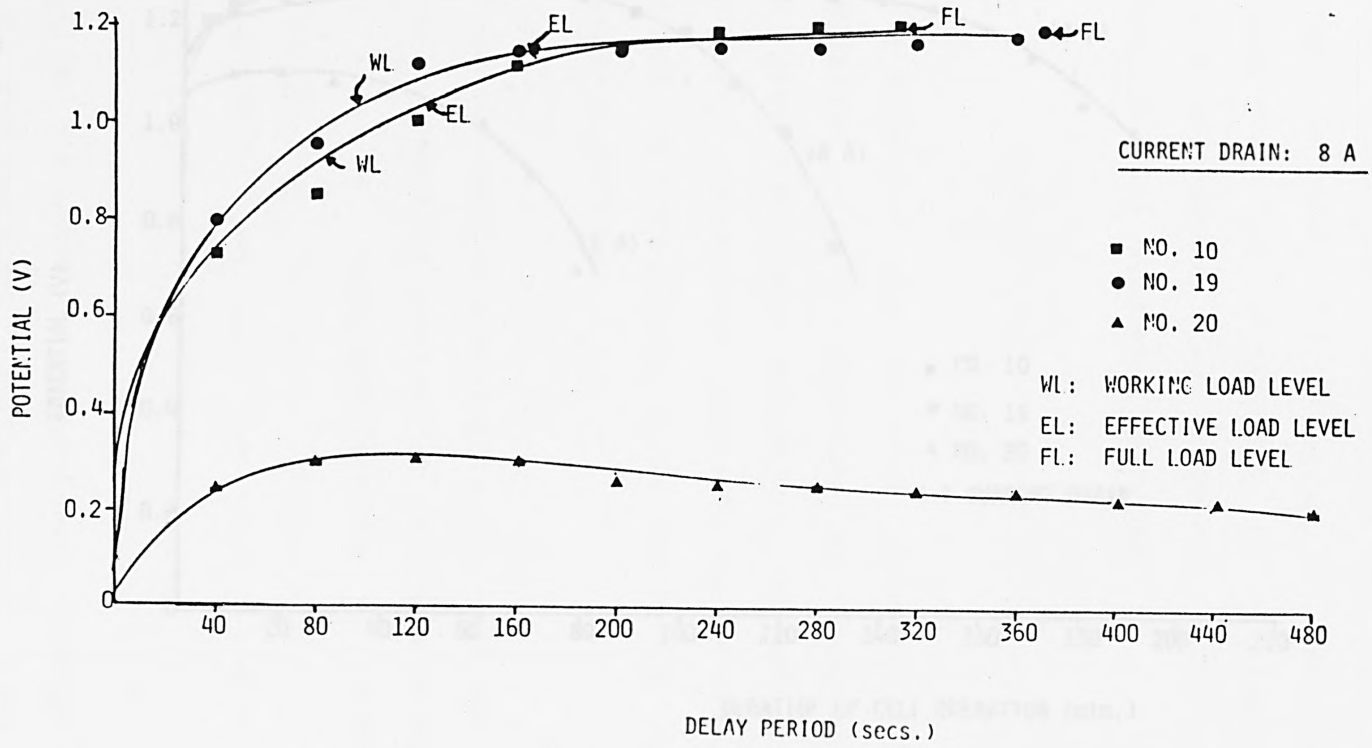

FIG. 9.1 START-UP CHARACTERISTICS OF Al-AIR CELL FOR OFFSHORE APPLICATIONS

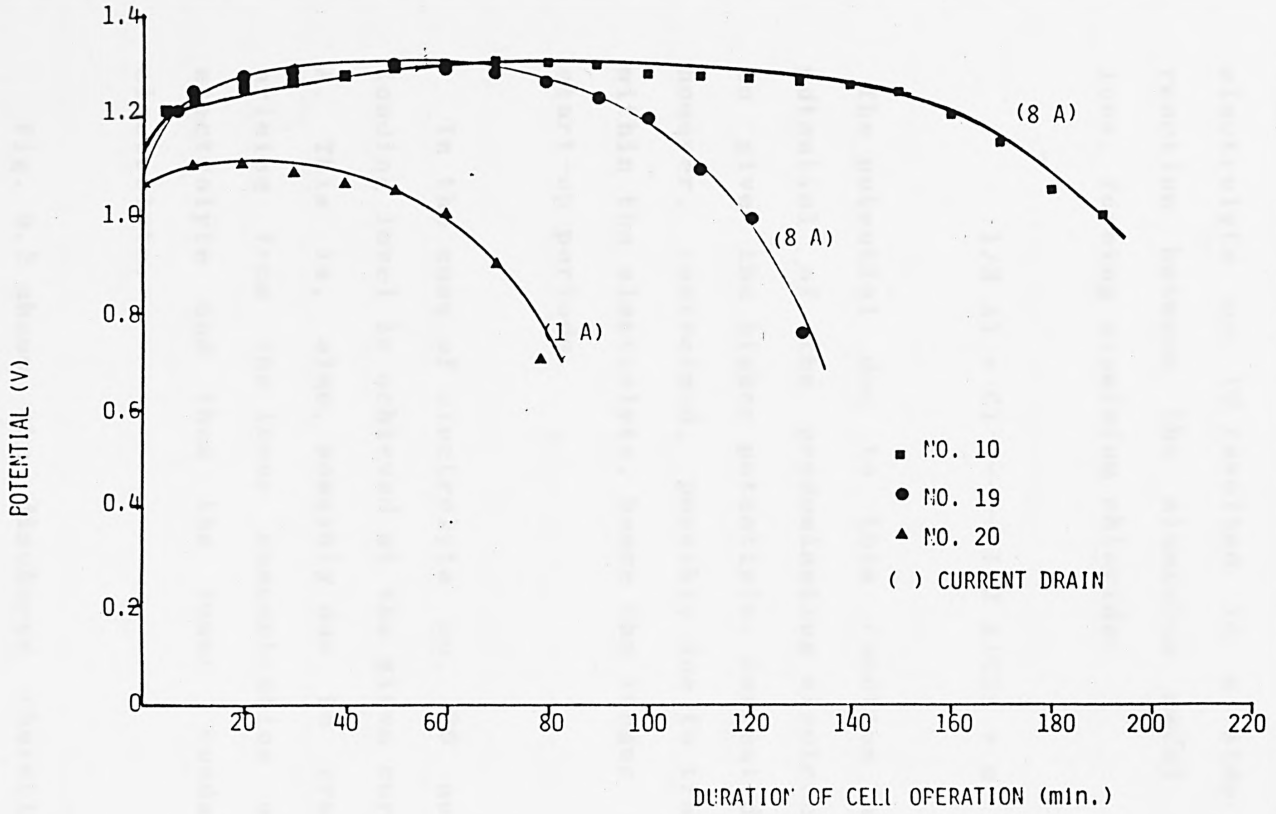

FIG. 9.2 DISCHARGE CHARACTERISTICS OF Al-AIR CELL FOR OFFSHORE APPLICATIONS

is achieved after 314 secs and 375 secs for nos. 10 and 19 respectively. It can be noted that the working and effective loading levels for electrolyte no. 19 are achieved at higher potentials than those for no. 10. This might be that the presence of chloride ions in the electrolyte no. 19 resulted in a side electrochemical reaction between the aluminium metal and the chloride ions, forming aluminium chloride:

$$1/3\ Al + Cl^- \text{ ---- } 1/3\ AlCl_3 + e$$

The potential due to this reaction adds up to the potential of the predominating electrochemical reaction to give the higher potentials. Current distribution is, however, restrained, possibly due to transport problems within the electrolyte, hence the longer delays for the start-up periods.

In the case of electrolyte no. 20 not even a working loading level is achieved at the given current drain of 8 A. This is, also, possibly due to transport problems arising from the lower concentration of ions in the electrolyte and thus the lower conductivity of the electrolyte.

Fig. 9.2 shows the discharge characteristics of the cell for the different electrolytes. Owing to the mass transfer problems realised for electrolyte no. 20 at 8 A,

the cell using this electrolyte, was discharged at 1 A instead. The other two electrolytes were tested at 8 A. In Fig. 9.2, it can be seen that even though the cell was discharged at 1/8 the current of the other electrolytes, the performance of electrolyte no. 20 is very low. The cell could only be operated for a very short time. It starts to get clogged up after the short time of operation. Solubility data obtained show a solubility of only 1.4 g/100g for aluminium, in the electrolyte.

At the 8 A current drain, electrolyte no. 10 is found to operate for a longer time than electrolyte no. 19. This can be explained again by the difference in the solubility of aluminium in these electrolytes. Fig. 9.3 shows the solubility of aluminium. It is more soluble in electrolyte no. 10 than in electrolyte nos. 19 and 20. The shorter operating time for no. 19 is also due to the lower coulombic efficiency of the anode material in the electrolyte. Coulombic efficiency of 80% is obtained for the electrolyte, compared to 95% for no. 10. This implies that a lot more aluminium is consumed within a given time for no. 19 than for no. 10. And with the lower solubility of aluminium in the test electrolyte, saturation occurs after a shorter operation time. The precipate formed in this case is a foamy white gel consisting of a mixture of complex aluminium hydroxide and aluminium chloride compounds. The gel formed cloggs up the cell if not removed.

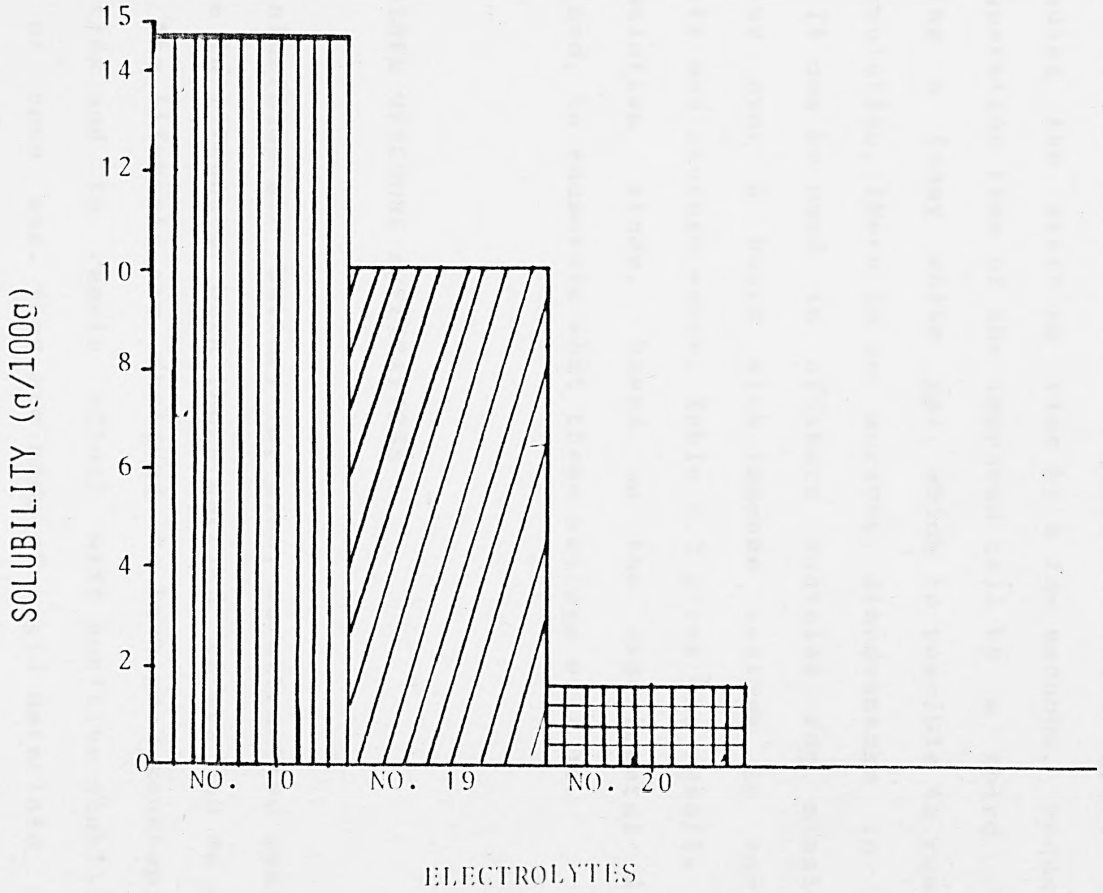

FIG. 9.3 SOLUBILITY OF ALUMINIUM IN ELECTROLYTES RECOMMENDED FOR OFFSHORE APPLICATIONS

Seawater, by itself, is not a very suitable electrolyte to use in aluminum-air cells, to meet high power demands. However, its use, instead of distilled water, to make up the alkaline electrolyte for aluminium-air cells is highly feasible. Apart from extending the start-up time by a few seconds, reducing the operation time of the improved cell by a third and forming a foamy white gel, which is possible to remove from solution, there is no serious disadvantage in its use. It can be used in offshore vehicles for missions lasting over 3 hours with immense savings in energy density and storage space. Table 9.3 gives the results of a simulation study, based on the experimental data obtained, to enumerate what these savings will be.

9.3 OTHER OFFSHORE APPLICATIONS

The aluminium-air battery is, also, an attractive system to use in lifeboats; both those carried at sea and on oil rigs. The lifeboats are designed to have good seakeeping qualities and to remain afloat with positive stability when at open sea. They are made of rigid materials and are of sufficient strength to enable them to be lowered in the fully laden condition to the water. The number and speed of lifeboats, at sea, depend on the size and service of the ship on which they are carried. In general, however, at least one motor lifeboat is carried

TABLE 9.3 USING SEAWATER TO PREPARE CELL ELECTROLYTE, INSTEAD OF DISTILLED WATER

EXPERIMENTAL DATA	ELECTROLYTES MADE WITH	
	DISTILLED WATER	SEAWATER
CURRENT OUTPUT (A)	8	8
CELL OPERATING VOLTAGE (V)	1.2	1.2
VOLUME OF ELECTROLYTE/CELL (ml)	45	45
DENSITY OF ELECTROLYTE SOLUTION (g/ml)	1.2821	1.2821
BULK DENSITY OF SOLID HYDROXIDES (g/ml)	-	1.2
ELECTROLYTE STRENGTH (% WT OF HYDROXIDES/VOL)	40	40
SOLUBILITY OF ALUMINIUM (g/100g)	14.7	10
COULOMBIC EFFICIENCY OF ALUMINIUM (%)	95	80
WT OF AIR ELECTRODES AND CELL STACK (g)	76.5	76.5
CALCULATIONS		
WT OF ELECTROLYTE SOLUTION/CELL (g)	57.694	57.694
WT OF SOLID HYDROXIDES/CELL (g)	-	18
MAXIMUM AMOUNT OF Al DISSOLVED IN THE OPERATING QUANTITY OF ELECTROLYTE WITHOUT PRECIPITATE (g)	8.481	5.769
RATE OF AL CONSUMPTION (g/hr)	2.779	3.3
CELL OPERATION TIME BEFORE ELECTROLYTE CHANGE (hr)	3.05	1.74

A) ASSUMING A 3 hr MISSION TIME

MISSION TIME (hr)	3	3
NUMBER OF ELECTROLYTE CHANGES	0	1
WT OF ELECTROLYTE SOLUTION REQUIRED (g)	57.694	57.694
WT OF SOLID HYDROXIDES REQUIRED (g)	-	18
WT OF Al REQUIRED (g)	8.337	9.9
WT OF AIR ELECTRODES AND CELL STACK (g)	76.5	76.5
TOTAL WT OF COMPLETE CELL SYSTEM (g)	142.531	162.094
ENERGY DENSITY (Whr/Kg)	202.061	177.674
INCREASE IN ENERGY DENSITY (%)		-12.07
VOLUME OCCUPIED BY ELECTROLYTE SOLUTION (ml)	45	45
VOLUME OCCUPIED BY SOLID HYDROXIDES (ml)	-	15
TOTAL VOLUME OCCUPIED BY ELECTROLYTE (ml)	45	60
SAVINGS IN ELECTROLYTE STORAGE SPACE (%)		-33.33

In practice, there must be sufficient electrolyte already prepared, with distilled water, for the first few hours of operation. The comparison for the 3hr mission is therefore, irrelevant. For longer missions allowance must be made for the initial 3hr use of distilled water, in the calculations for seawater.

Thus,

B) ASSUMING A 6 hr MISSION TIME

	ELECTROLYTES MADE WITH	
	DISTILLED WATER	SEAWATER
MISSION TIME (hr)	6	6
NUMBER OF ELECTROLYTE CHANGES	1	2
WT OF ELECTROLYTE SOLUTION REQUIRED (g)	115.389	57.694
WT OF SOLID HYDROXIDES REQUIRED (g)	-	36
WT OF Al REQUIRED (g)	16.6737	18.2368
WT OF AIR ELECTRODES AND CELL STACK (g)	76.5	76.5
TOTAL WT OF COMPLETE CELL SYSTEM (g)	208.5627	188.4308
ENERGY DENSITY (Whr/Kg)	276.176	305.683
INCREASE IN ENERGY DENSITY (%)		10.7

VOLUME OCCUPIED BY ELECTROLYTE SOLUTION (ml)	90	45
VOLUME OCCUPIED BY SOLID HYDROXIDES (ml)	-	30
TOTAL VOLUME OCCUPIED BY ELECTROLYTE (ml)	90	75

SAVINGS IN ELECTROLYTE STORAGE SPACE (%)	16.7

C) ASSUMING A 12hr MISSION TIME

	ELECTROLYTES MADE WITH	
	DISTILLED WATER	SEAWATER
MISSION TIME (hr)	12	12
NUMBER OF ELECTROLYTE CHANGES	3	5
WT OF ELECTROLYTE SOLUTION REQUIRED (g)	230.778	57.6945
WT OF SOLID HYDROXIDES REQUIRED (g)	-	90
WT OF Al REQUIRED (g)	33.3478	38.0368
WT OF AIR ELECTRODES AND CELL STACK (g)	76.5	76.5
TOTAL WT OF COMPLETE CELL SYSTEM (g)	340.6258	262.2313
ENERGY DENSITY (Whr/Kg)	338.201	439.307

INCREASE IN ENERGY DENSITY (%)	29.9

VOLUME OCCUPIED BY ELECTROLYTE SOLUTION (ml)	180	45
VOLUME OCCUPIED BY SOLID HYDROXIDES (ml)	-	75
TOTAL VOLUME OCCUPIED BY ELECTROLYTE (ml)	180	120

SAVINGS IN ELECTROLYTE STORAGE SPACE (%)	33.3

D) ASSUMING A 24hr MISSION TIME

	ELECTROLYTES MADE WITH	
	DISTILLED WATER	SEAWATER
MISSION TIME (hr)	24	24
NUMBER OF ELECTROLYTE CHANGES	7	11
WT OF ELECTROLYTE SOLUTION REQUIRED (g)	461.556	57.6945
WT OF SOLID HYDROXIDES REQUIRED (g)	-	198
WT OF Al REQUIRED (g)	66.6947	77.6368
WT OF AIR ELECTRODES AND CELL STACK (g)	76.5	76.5
TOTAL WT OF COMPLETE CELL SYSTEM (g)	604.7507	409.8313
ENERGY DENSITY (Whr/Kg)	380.9834	562.1825

INCREASE IN ENERGY DENSITY (%)	47.6

VOLUME OCCUPIED BY ELECTROLYTE SOLUTION (ml)	360	45
VOLUME OCCUPIED BY SOLID HYDROXIDES (ml)	-	165
TOTAL VOLUME OCCUPIED BY ELECTROLYTE (ml)	360	210

SAVINGS IN ELECTROLYTE STORAGE SPACE (%) 41.7

SCALING UP FOR A 30 KW UNIT

	ELECTROLYTES MADE WITH	
	DISTILLED WATER	SEAWATER
SCALE-UP FACTOR	3125	3125
MISSION TIME (hr)	24	24
NUMBER OF ELECTROLYTE CHANGES	7	11
WT OF ELECTROLYTE SOLUTION REQUIRED (Kg)	1442.363	180.2953
WT OF SOLID HYDROXIDES REQUIRED (Kg)	-	618.75
WT OF Al REQUIRED (Kg)	208.4211	242.6151
WT OF AIR ELECTRODES AND CELL STACKS (Kg)	239.0625	239.0625
WT OF AUXILLARY EQUIPMENT; PUMPS, CTRL GEAR, ETC. @ 50% THE WT OF AIR ELECTRODE & CS (Kg)	119.5313	119.5313
TOTAL WT OF COMPLETE BATTERY SYSTEM (Kg)	2009.377	1400.254
ENERGY DENSITY (Whr/Kg)	358.32	514.192

INCREASE IN ENERGY DENSITY (%)		43.5
VOLUME OCCUPIED BY ELECTROLYTE SOLUTION (1)	1125	140.625
VOLUME OCCUPIED BY SOLID HYDROXIDES (1)	-	515.625
VOLUME OCCUPIED BY Al ANODE MATERIAL (1)	77.193	89.857
VOLUME OCCUPIED BY MAIN BATTERY FRAME (1)	106.25	106.25
VOLUME OCCUPIED BY AUXILLARY EQUIPMENT @ 50% MAIN BATTERY FRAME (1)	53.125	53.125
TOTAL VOLUME OCCUPIED BY COMPLETE SYSTEM (1)	1361.568	905.482
SAVINGS IN SPACE (1) (%)		33.5

COST OF SYSTEM (30KW) AND CONSUMABLES FOR 24hr MISSION

UNIT COST OF Al ALLOY (£/Kg)	10	10
UNIT COST OF ELECTROLYTE (£/Kg)	2	2
COST OF Al ALLOY (£)	2084.21	2426.15
COST OF ELECTROLYTE (£)	900	1350
COST OF BATTERY	4500	4500
COST OF AUXILLARY EQUIPMENT @ 15% COST OF BATTERY	675	675
TOTAL COST OF COMPLETE SYSTEM (£)	8159.21	8951.15
COST/KWhr (£)	11.33	12.43
RUNNING COST/KWhr (£)	4.14	5.24

in cargo ships and two in passenger ships and tankers [209]

Special requirements are made on lifeboats for tankers and oil rigs to take into account the greater possibility of fire at sea. Ideally, personnel should be able to board the boats safely, launch them through fire, cast off and get away safely, and the boat should be suitable as a normal lifeboat. A totally enclosed self-righting lifeboat meeting such requirements is made of glass reinforced plastic with fire-resistant additives; canopy of orange colour. Water sprinklers are fitted to spray sea water over the outside of the boat, all external surfaces being shaped to ensure maximum coverage. Embarkation is through two inward-opening doors in the canopy amidships. The coxswain's position is forward [near lowering cable), provided with viewing port, steering wheel, controls for engine and release gear. Occupants are strapped-in to minimise injury in event of capsize. Excess pressure in boat prevents fumes entering. The totally enclosed boat without the sprinkler system, providing maximum protection from exposure and fumes, is available for ships other than tankers.

On a life-boat engine, the starting mechanism would have to be infallible even after periods of non-use, while the engine itself would need to be mounted in a water-tight but not air-tight compartment, with all

controls on the outside. And, once battened down, it had to be capable of continuing to run for long periods without attention. Lubricating, fuel and electrical systems would all have to function unfailingly on a wildly gyrating engine. Furthermore, with the self-righting type of boat, the engine would have to stop automatically in the event of a capsize, but must be ready for instant re-start once the crew had regained control of their boat. For hour after hour such an engine would have to withstand the screw-racing, bolt and shaft shearing shocks as boat, engine bearers and engine crashed into a trough, followed by labouring of deeply biting propellers as the boat climbed the crest of a new onslaught.

Propulsion, at the moment, is by a diesel engine with a closed fresh water cooling system which allows the engine to be run up and warmed through whilst the boat is still at the davits. A large capacity compressed-air cylinder in the bottom of the boat supplies air to the occupants and the engine, and drives a pump for delivering water to the sprinkler system. Such a power source is lacking in the rapid start-up times required and is very inefficient in terms of the energy it provides per the weight that is carried, let alone the enviromental hazards created by exhausts from the combustion process. The use of Al-air battery in its place will ensure greater efficiency in terms of the engine requirements stated in the previous paragragh. The

Al-air battery will allow lifeboats to grow in size and power. More electricity could be generated on board, leading to the introduction of such welcome benefits as sophiticated searchlights, deck floodlighting, adequate cabin navigation lighting, loud-hailers, signalling lamps, power to operate the various instruments: echo sounder, radio transmission with its attendant direction-finding equipment, culminating in this present-day boom in computer-aided navigation-radar.

PART B: APPLICATIONS ONSHORE

Because of the available cheap power, provided by high voltage generators, for continuous usage onshore, the use of Al-air battery, onshore, will be restricted to emergency and tactical uses.

9.4 APPLICATION AS EMERGENCY POWER SOURCE

The effects of power loss is very well known. Apart from obvious inconveniences, essential services, such as hospitals, telephone exchanges, etc., are badly affected. Also, public buildings turn into safety hazard areas. People get injuried in trying to find their way out, let alone the psychological effect that getting stuck in a dark lift has. Industry also stands to lose out on oportunity sales, customer credibility and machine

shutdown and restart costs. In effect everybody suffers during a blackout. The need therefore, for emergency power cannot be stressed enough.

According to a market survey conducted for emergency power sources, at this research centre, there is an uptrend need for emergency power as more and more automation is sought after and society, in its sophistication, becomes health, safety and security conscious. In the survey [210], it is noted that the main areas where batteries are employed as emergency power sources, include (i) emergency lighting, (ii) alarms, (iii) specialist applications, e.g. computer memory circuits and (iv) compensates for the delay in generator start-up.

Health and safety requirements demand that, among other requirements, all public buildings must have escape routes that are adequately lit and all fire alarms must be in good working condition (BS 5266). Emergency lighting systems are therefore fitted in these buildings, conforming with the legislation, to provide lighting in the case of power failure. Burglar alarms and fire alarms are mostly powered by battery units that possess similar features as in emergency lighting systems. At the moment, the available emergency lighting system consists of a rechargeable Nickel-Cadmium or Lead/acid battery, a charger, an invertor, a change-over device and an 8 W flourescent tube. In the event of a mains failure, the

change-over device switches over to the battery which then provides power for a minimum of three hours. Each system as a whole costs at least £62.00 to purchase. There is also a running and maintenance cost totalling up to 40p a year; assuming power failure occurs on two occasions in a year. In replacing this system with an aluminium-air system several pounds will be saved in the long run. Cost projections (Table 9.4) show that it will cost at most £27.12 to buy a complete aluminium-air system. Running cost will be small, as the only cost is to replinish the aluminium and electrolyte (10p) after power failure for a total of about three hours.

The other area where aluminium-air can be used to provide emergency power is in the specialised industries where computers are heavily depended upon. Computer memory circuits normally have small rechargeable batteries mounted in their circuit boards to ensure data storage is not lost while the computer performs its different functions. The current involved here is in the region of microamperes, and thus, it is of no use in the event of power failure since what is needed is the ability to save data onto a hard system, such as a floppy disk, in order to prevent the loss of a day's or even a week's transaction. For this reason, most commercial firms such as banks, have standby generators to continue running until power is restored. However, some generators, e.g. gas turbines, require a starting-up period of up to 30 minutes before achieving full loading

TABLE 9.4 COST ANALYSIS OF Al-AIR CELL AS AN EMERGENCY POWER SOURCE

EXPERIMENTAL DATA

CURRENT OUTPUT (A)	8
CELL OPERATING VOLTAGE (V)	1.2
VOLUME OF ELECTROLYTE/CELL (ml)	45
DENSITY OF ELECTROLYTE SOLUTION (g/ml)	1.2821
ELECTROLYTE STRENGTH (% WT OF HYDROXIDES/VOL)@ 25'C)	40
SOLUBILITY OF ALUMINIUM (g/100g)	14.7
COULOMBIC EFFICIENCY OF ALUMINIUM (%)	95
WT OF AIR ELECTRODES AND CELL STACK (g)	76.5

CALCULATIONS

WT OF SOLID HYDROXIDES/CELL (g)	18
MAXIMUM AMOUNT OF Al DISSOLVED IN THE OPERATING	
QUANTITY OF ELECTROLYTE WITHOUT PRECIPITATE FORMATION (g)	8.481
RATE OF AL CONSUMPTION (g/hr)	2.779
CELL OPERATION TIME BEFORE ELECTROLYTE CHANGE (hr)	3.05

FOR A 3 HOUR EMERGENCY LIGHTING

OPERATING TIME (hr)	3
NUMBER OF ELECTROLYTE CHANGES	0
WT OF SOLID HYDROXIDES REQUIRED (g)	18
WT OF Al REQUIRED (g)	8.337
WT OF AIR ELECTRODES AND CELL STACK (g)	76.5

COST OF SYSTEM

UNIT COST OF Al ALLOY (£/Kg)	10
UNIT COST OF ELECTROLYTE (£/Kg)	3
COST OF Al ALLOY (£)	.08
COST OF ELECTROLYTE (£)	.04
COST OF BATTERY @ £150/KW (£)	1.44
COST OF AUXILIARIES; INVERTOR, HOLDER, LED INDICATOR, 8W TUBE, COVER AND SOLENOID VALVE (£)	12
TOTAL COST OF COMPLETE SYSTEM (£)	13.56
ALLOWING FOR 100% MARK UP; COST OF SYSTEM (£)	27.12
COST/Whr (p)	94
RUNNING COST/POWER CUT-OFF (p)	10

capacity. This necessitates a back-up system, usually a battery, before the standby power becomes fully operational. Another potential customer for the aluminium-air system, for emergency use, could be a large department store with several branches where the possible losses through shoplifting, during a blackout, could be considerable.

9.5 OTHER APPLICATIONS

The greatest advantage of aluminium-air battery lies in the great savings in reactant weight. High capacity batteries can be made with low overall weights. Thus, aluminium-air cells are attractive propositions for applications which require portable power in relatively large amounts. In general, all portable electrical devices which use electric motors are potential users.

Nowadays, increasing number of toys are being produced with electric motor drive. Aluminium-air cells can be used to power these toys. It can also be used to replace the noisy, low efficency, high pollutant electric generators used by the military. The noise and IR-dectability of such generators has prompted the military to look for other means of power generation for field use [211]. It can be used to provide power for activities, such as 'RECCE' patrols (reconnoitring), for

which the noiseless operation of the system will be welcomed.

In the area of commuter vehical propulsion, since the cost of energy is a predominant factor in the day to day running of such vehicles, the continuous use of aluminum as fuel will be too costly.

9.6 CONCLUSION

Not only will the use of aluminium as battery anode material be heavily patronised by aluminium producers; who will be prepared to intergrate forward to ensure its cost competitiveness, but when coupled with oxygen it is capble of providing the energy requirements of most offshore vehicles at less weight than existing power sources do. The less weight carried for the power source will imply that, in the case of submersibles, a larger amount of work can be done at anyone dive in terms of the number of men at work and the range of equipment carried. And, in the case of lifeboats, it will mean that more lives can saved by a single boat, at any one time. There is a large market, even though somewhat conservative, for these offshore applications. Here, the market relies very much on the operational abilities of the system rather that its cost. Thus, an investment in this area can easily be magnified, upon the technical success of the system.

The system can also be used to provide emergency power for lighting, computer memory banks and for engine start-ups. There exists also, a large market for such applications. Here, the cost of the system plays an important role and from cost projections, the system is found to compete with existing systems.

10 CONCLUDING REMARKS

10.1 GENERAL CONCLUSION

10.1.1 REDUCING THE PASSIVITY OF PURE ALUMINIUM

The passivating oxide film on the surface of pure aluminium, which is greatly responsible for its poor performance as galvanic anode, can be broken down by dissolving in a highly concentrated electrolyte and also, by alloying the metal with other suitable elements.

The alloy-mix is of a significant importance in the anodic performance of the metal. The self-discharge and high current density performance depends very much on that. Alloying elements with high hydrogen overpotentials are, thus, preferred. Zn, Ga, In, Pb, Bi and Sn are found to be highly indispensible. Nevertheless, the concentrations of these elements in the metal are to be closely controlled and kept as low as possible. Fe and Cu have deleterious effect on the self-discharge of the anode and thus, they are to be significantly removed. The Fe and Cu elements in Al and its alloys exist as impurities and are very difficult and expensive to remove totally. From the alloys tested, alloy Q4 was found to

perform very well at high current densities with a high utilisation. The composition of the alloy is given in chapter 4.

10.1.2 SUPPRESSION OF HYDROGEN EVOLUTION

The breakdown of the passive film on the aluminium surface on alloying results in an enhanced electrochemical reduction of water molecules at the surface of the metal, owing to the corrosion action of the exposed active surface atoms. The hydrogen evolved in the process, poses design, health and safety problems especially for applications in enclosed environments. It is, therefore, suppressed by the addition of inhibitors to the electrolyte.

Substances with high hydrogen overpotential and somewhat soluble in alkaline electrolytes were tested. The addition of trace amounts of Mercuric oxide (HgO) was found to be the best inhibitor. It did not only reduce the rate of hydrogen evolution on the Al surface, but it coupled with the atoms on the metal surface to produce a negative shift in potential. As much as 200 mV was gained by the action of HgO. The amount of mercury dissolved in the electrolyte is very small (1.5 ppb) to be of a health hazard. Also, It is found that the mercury is not precipitated with reaction products but remains in solution and at the surface of the anode. The optimum

operating temperature range of the anode is too low for possible vaporisation of the Hg. Electrochemically, tests run on a Teflon bonded Li-doped cobalt oxide/graphite electrode showed that the use of HgO in the electrolyte has very little effect on its performance, suggesting the absence of a possible electrocatalyst poisoning.

The relatively small amount of hydrogen still evolved at the anode can be got rid off by including a Hydrogen-Oxygen recombination catalyst [212] in the design of the real life battery.

10.1.3 SOLVING THE PROBLEM OF CELL CLOGGING

In Chapter 1, it was recounted that the state-of-art in the development of Al-air cells, at the moment, is characterised by the problem of cell clogging. The problem is widly appreciated and efforts had been made by many researchers in the field to control the reaction products formed from the dissolution of aluminium [213]. It is recognised that in the engineering of the system, a balance should be made between electrolyte and alloy composition. It is also known that the electrolyte composition greatly influences the type of product that is precipitated. As such, some workers have tried to reduce the volume of the reaction products formed by the addition of anionic, cationic and nonionic surfactants to the electrolyte, without any success [213].

In the dissolution reaction of aluminium, the following occurs:

Step 1 $Al + 4OH^- \longrightarrow Al(OH)_4^- + 3e$

Step 2 $Al(OH)_4^- \xrightarrow{\text{saturation}} Al(OH)_3\downarrow + OH^-$

$$Al + 3OH^- \xrightarrow{\text{saturation}} Al(OH)_3\downarrow + 3e$$

Step 2 is regarded as a limiting factor, since it is the $Al(OH)_3$ precipitate that cloggs up the cell and thus has deleterious effects on overall cell performance and reliability. To prevent cell clogging, it is evident that step 1 must be prolonged. To ensure this, it is thought that an electrolyte that has a high solubility for the reaction products must be used.

Investigations directed toward the determination of the solubility of the reaction products formed in different types of electrolytes, as well as the conductivity and the conductivity changes that occur during cell operation resulted in unearthing that a mixture of NaOH and KOH solutions possesses very high solubility for Al with relatively little detrimental effect on conductivity. The high solubility was proved to

be due to a reduction in the magnitude of the common-ion effect that is pronounced in the predominantly single cation electrolytes.

For the electrolyte mixtures, the following solution equilibrium is observed:

$$NaOH + KOH \text{ --- } Na^{+} + K^{+} + 2OH^{-}$$

When Al is dissolved a combination of Na-Aluminate and K-Aluminate is formed. The Na-Aluminate formed becomes very soluble in the KOH and vice versa. The common-ion effect is thus, somewhat halved for each separate solution. Consequently, the equilibrium is maintained to the right, for a longer time than experienced when using each individual solution. Because the equilibrium is maintained to the right, more Al is dissolved until a balance in equilibrium and then finally a shift to the left, with the precipitation of the Na and K as an aluminium hydroxide. As much as 14.7 g/100g solubility was obtained for the electrolyte mixture (an equal volume mixture of 30% KOH + 50% NaOH), as compared to 6.1 and 8 g/100g for 30% KOH and 30% NaOH (conventionally used as aqueous alkaline electrolytes), respectively.

The higher solubility obtained for the electrolyte mixture means that its use in aluminium cells, results in a reduction in the amount of reaction product

precipitated and thus reduces the tendency of cell clogging. There is also a considerable gain in discharge times, as well as some gains in discharge potentials. Moreover, the precipitate formed in the electrolyte is granular, unlike the powdery nature of that formed in the 30% KOH conventional electrolyte, and can therefore be easily pumped or cleaned away.

10.1.4 THERMAL MANAGEMENT

The temperature effect on a cell performance is one of the primary limiting factors. The optimum working temperature range for the Al-air cell was found to be between 40 and 45°C. In using the electrolyte mixture, the heat evolved at room temperature measures between 55 and 60°C. This implies that the cell can be used from as low as -20°C and it can be expected to self-heat itself to a working temperature. For room temperature uses, steps are to be taken in the designs of the cell, which varies depending on the type of application, to ensure cell operation within the optimum temperature range.

10.1.5 CELL RECHARGEABILITY

One of the problems encountered in the use of existing

Al-air systems is the the storage capability of the Al anodes. Many workers use Al alloys that are active in the atmosphere [213]. These alloys are activated, ready for use, since a ready-to-use anode material is requisite in the mechanical recharging of the cell. They are therefore stored in airtight packs and normally lasts up to a month. Longer storage times cause problems. Moreover, these replacement anodes are expected to be handled with caution, which in turn limits the field of applications for the system.

The problem of electrode handling and storage is dealt with, in this work, by finding an alloy that is electrochemically active in the operating medium but behaves like the bare metal, aluminium, under atmospheric conditions. The alloy Q4, possesses these qualities. The alloy has a thin oxide film cover, about 0.4 - 0.6 x 10^{-2} microns, which provides it with an appreciable amount of resistance under atmospheric conditions. Once in the cell electrolyte, the film is broken down instantaneously and it becomes very active. Since the alloy is stable in the atmosphere, it can be stored openly and infinitely. And since it behaves just like aluminium, it can be handled anyhow without any damaging effect. The system, using this anode, can therefore be recharged conveniently and safely; thereby widening the field of application.

For applications that demand long time use with minimal supervision, an automatic means of recharging has been validated. The anode material is fabricated into shots, which are fed into a basket-type current collector, to enable a continuous automatic feeding of the active material into the cell. Experiments carried out validate the concept. The problem now, is the need for a conductor with a high hydrogen overpotential, highly alkaline resistant and of a low electronic resistivity. The system, as designed at the moment, is suffering from a low limiting current density due to electronic resistivity experienced between the shots and the current collector.

10.1.6 PROPERTIES OF THE IMPROVED CELL

The aluminium anode material used in the cell has a high limiting current density; it remains active at high current densties. It thus, allows high currents to be drawn from the cell, depending on the limiting current density of the air electrode. With a very good air electrode, the high current density potential of the cell (over 400 mA/cm^2) could be realised.

Since the anode material used is stable under atmospheric conditions and can be stored till infinity under those conditions, the cell can safely be said to

possess an infinite shelf-life. And moreover, since the anode material does not need any pretreatment, whatsoever, before use, the cell can be easily and safely recharged, manually. However, if necessary, the cell can be recharged automatically.

Since aluminium is comparatively more soluble in the electrolyte used, the cell can operate at a longer discharge time, than normal, without getting clogged up. A typical cell (Fig. 10.1) containing about 57 g of electrolyte, can be discharged at 8A, 1.2-1.3 V for three continuous hours, without a problem. The cell can be recharged, by putting in more aluminium and fresh electrolyte, to operate over any length of time. At a lower current drain, 3A (25 mA/cm^2) the same cell was able to operate continuously (without being recharged) for over 48 hours without any serious problems; e.g the problem of cell clogging. The precipitate formed, from the dissolution of the active anode material, is granular in nature and can therefore be easily cleaned away if the need arises.

The energy density of the cell, calculated for a 24 hour operation time, was nearly 400 Wh/Kg; 3,714 Wh/Kg for the Al anode. The cell can be operated from as low as $-20^{o}C$ without the use of an external heater to warm it up.

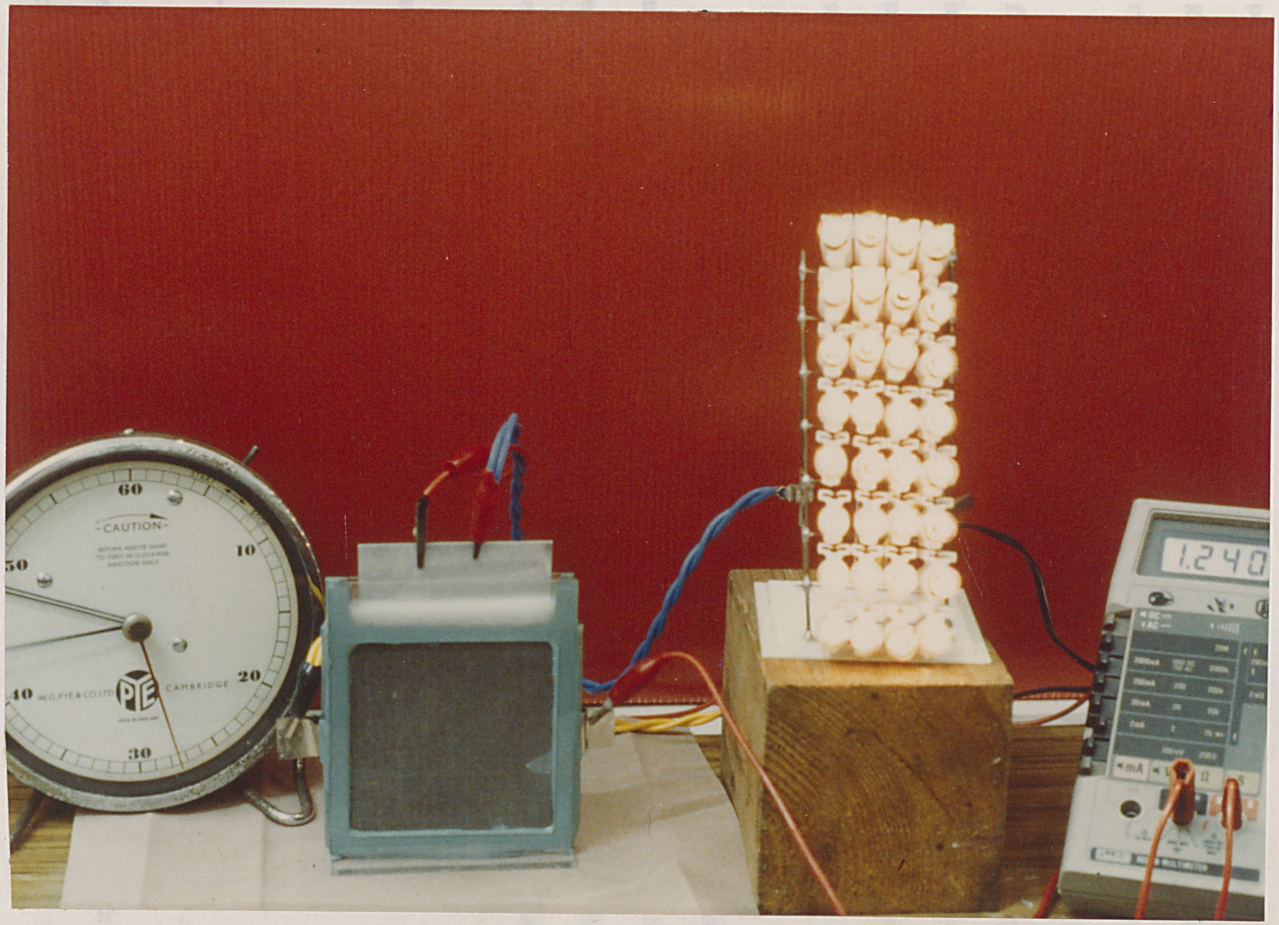

FIG. 10.1 PHOTOGRAPH OF A TYPICAL Al-AIR CELL (LABORATORY VERSION)

10.1.7 COMMERCIAL VIABILITY

The Al-air battery can be used to provide power for applications both onshore and offshore. Because of the high energy-to-weight ratio of the system, it is particularly attractive for applications offshore. It can be used as the main power source in submersibles, life-boats, military field equipment and reconnaissance vehicles. For these applications, even though cost is not constraining, the Al-air batterry can be said to project a very good value for money.

The battery system can also be used as emergency power source for lighting, for which it is projected to be cheaper than the existing Ni-Cd cells. It can also be used for burglar and fire alarms, computer memory banks, as start-up for car engines and as back-ups for generators.

10.2 SUGGESTIONS FOR FURTHER WORK

The alloy Q4 can be further improved by reducing the Fe and Cu concentrations considerably. The reason for this has already been summarised above. Apart from the alloy composition, the only other area for improvement is the type of material that could be used as the current collector for the shot-assembly anode. As pointed out

previously, the material should be a conductor of a low electronic resistivity, having a high hydrogen overpotential and must be stable in aqueous alkaline and must also be capable of being perforated or woven. A lead-tin alloy is suggested to be tested for its suitability. Also, provided a 40 mesh titanium can be obtained, it is worth experimenting on that.

Apart from the individual suggestions made above, it can be said that the fundamental drawbacks on the commerciability of the Al-air cell have been overcome. However, it is recognised that problems do occur on engineering scale-ups and thus, it is recommended that the next immediate work on the system should be done on a prototype model. It is only then that the practicability of the system can be evaluated. If the scale-up should bear the same properties as the laboratory version, then the only problems left to be solved are the engineering design problems, as to the versatility, non-spillage and mechanical strength of the system; to name but a few.

It is also suggested that the aluminium anode should be coupled with known metallic oxides, such as manganese dioxide, to produce dry cells for basic domestic uses and to test the full potentials of the electrolyte mixture. It is recommended that a small concentration of aluminium chloride (about 3%) and about 3% sodium gluconate be added to the slurry that might be prepared from the electrolyte mixture composition. The sodium gluconate is

to soften the precipitate that might result owing to the lack of water, in order to avoid any clogging. The aluminium chloride is to provide chloride ions for an increase in anodic potential, to compensate for the low conductivity that might be experienced.

REFERENCES

[1] Taylor, A.H., Goebel, F. and Giner, J., 'Factors influencing the Design of a High Power Density Lead-acid Battery for Electric Propulsion', Power Sources 4 (ed. Collins, 1973), p 541

[2] Lexow, K.W.; Kramer G. and Oliapuam, V.A., 'Ni-Fe (Fenox) Module Battery', Power Sources 8 (ed. J. Thompson, 1981), p 389

[3] Milner, P. and Thomas, U., 'The Ni/Cd Cell', Advances in Electrochem. and Electrochem. Eng., Vol.5 (ed. Delahay and Tobias, 1967) p 1

[4] The Electrochem. Soc. Series, 'Zinc-Silver oxide Batteries, (ed. Fleischer and Lander), J. Wiley and Sons (1970).

[5] Gillibrand, M., Gray, J. and Twentyman, F., 'Fuel Battery for Underwater operations', Power Sources 3 (ed. Collins, 1971), p 405

[6] Mennons, M.A.F., Brit. Pat. 296 (1858)

[7] Eager, H. T. and Milburn, R.P., Brit. Pat. 6924 (1891)

[8] ibid., Brit.Pat. 899 (1891)

[9] Brown, C.H., US Pat. 503,567 (1893)

[10] Anderson, E.L., US Pat. 706,631 (1902)

[11] Noble, J. and Anderson, E.L., US Pat. 759,740 (1904)

[12] Vince, C.H., Brit. Pat. 399,561 (1933)

[13] Pennock, A.G.L. and Lee, S., Brit. Pat. 437,536 (1935)

[14] Heise, G.W.; Schumacher, E.A. and Cahoon, N.C., J. Electrochem. Soc., 94 (1948) p99

[15] Sargent, D.E., US Pat. 2,554,447 (1951)

[16] Ruben, S., US Pat. 2,638,489 (1953)

[17] Lozier, et al, Us Pat. 2,874,079 (1959)

[18] Zaromb, S., US Pat. 3,513,031 (1970)

[19] ibid., US Pat. 3,554,810 (1971)

[20] Katsoulis, E.G., US Pat. 3,533,845 (1970)

[21] Martin, D.J., Brit. Pat. 1,213,647 (1970)

[22] Takeshi, S. and Kazuo, T., Jap. Pat. 2003 (1959)

[23] Hulot, M., Compt. rend., Vol. 40 (1855) p 148

[24] Cazin, A., Piles Electriques, Gauthier-Villars, Paris (1881) p 131

[25] Tommasi, D., Trait des Piles Electriques, Georges Carre, Paris (1889) p 131

[26] Stokes, J.J., Jr., US Pat. 2,796,456 (1957)

[27] ibid., US Pat. 2,838,591 (1958)

[28] ibid., US Pat. 3,307,976 (1967)

[29] Gregory, D.P., Metal-Air Batteries, Mills & Boon (1972) p 10

[30] ibid., p 14.

[31] Zaromb, S., J. Electrochem. Soc., 109 (1962) p 1125

[32] Tseung, A.C.C., Wan, B.Y.C. and King, W.J., Ger. Offen 2,051,235 (1971)

[33] Despic, A.R., Yugoslav Patent Application P-1224/83

[34] Despic, A.R.; Drazic, D.M.; Purenovic, M.M. and Cikovic, N., J. Appl. Electrochem. 6, (1976) p 527

[35] Cooper, J.F., 13th IECEC, (1978) p 738

[36] Proc. 1st Int. Workshop Reactive Metal-air Batteries, Lockheed, Palo Alto, Res. Lab. (1979).

[37] Despic, A.R. and Drazic, D.M., Electrochim. Acta, Vol.25 (1980)

[38] Despic, A.R.; Drazic, D.M.; Gajic, Lj. and Zecevic, S., Electrochim. Acta 26, (1981) p 1625

[39] Valand, T.; Mollestad, O. and Nilsson, G., in Power Sources 8 (ed. J. Thompson, 1981) p 523

[40] Polcich, G., US Pat. 1,771,190 (1926)

[41] Keir, D.S.; Pryor, M.J. and Sperry, P.R., J. Electrochem. Soc., Vol.116, No.3 (1969) p 319

[42] Sarangapani, K.B., J. Applied Electrochem. Vol.14 (1984) p 475

[43] Mance, A.; Cerovic, D. and Mihajlovic, A., ibid., p 459

[44] Tye, F.L., in 'Electrochem. Power Sources', (ed. M. Barak), IEE, London, (1980) p107

[45] As Ref 29, p 43

[46] Sully, J., U.S. Pat. 585,855 (1897)

[47] Littaeur , E.L. and Cooper, J.F., in 'Handbook of Batteries and Fuel Cells' (ed. D. Linden), McGraw-Hill, N.Y., (1984) p 30.

[48] Yeager, E.B. and Schwartz, E.P., in ''The Primary Battery'', Vol. 1 (ed. Heise and Cahoon), John Wiley & sons, N.Y., (1971) p 60

[49] Thirsk, H.R, in (as REF. 44) p 27

[50] Lewis, G., Randall, M., Pitzer, K. and Brewer, L., ''Thermodynamics, McGraw-Hill, N.Y. (1961)

[51] Gladstone, S., Introduction to Electrochemistry, D. Van Nostrand Co., N.Y., (1942)

[52] Kirkwood, J. and Oppenheim, I., Chemical Thermodynamics, McGraw-Hill, N.Y., (1961) Ch 11-13

[53] Beck, W.H. and Wynne-Jones, W.F.K., Trans. Faraday Soc., Vol 50 (1954) p 136

[54] Bagotzky, V.S. and Skundin, A.M., Chemical Power Sources, Academic Press, London (1980) p14

[55] Mackowiak, J., 'Physical Chemistry for Metallurgists', George Allen & Unwin, London, (1965).

[56] Latimer, W., The oxidation states of the elements and their potentials in aqueous solutions, Prentice-Hall, (1952)

[57] Davies, C.W., Electrochemistry, George Newness Ltd., London (1967) p 128

[58] Heald, C. and Smith A.C.K., Applied Physical Chemistry, MacMillan Press, N.Y. (1974) p 307

[59] Atkins, P.W., Physical Chemistry, Oxford University Press, London (1978) p 155

[60] Antropov, L., 'Theoretical Electrochemistry', Mir, Moscow, (1977).

[61] As REF. 48 p 81

[62] Moeller, T. and O'Connor, R., Ions in Aqueous Systems, McGraw-Hill, N.Y. (1972) Ch 7

[63] Kortum, G. and Bockris, J.O'M., Textbook of Electrochemistry Vol. 1, Elsevier Pub. Co., N.Y., (1951) p 99

[64] Samoilov, O. Ya., Structure of Aqueous Electrolyte Solutions, Consultants Bureau, N.Y. (1965)

[65] Robinson, R.A. and Stokes, R.H., 'Electrolyte Solutions', Butterworths, London, (1968), p 242.

[66] Brown, G.I., Intro. to Physical Chemistry, Longman, London (1978) p 88

[67] As REF. 63 (Vol 2) p 400

[68] As REF. 57 p 37

[69] Delahay, P., ''Double layer and Electrode Kinetics'', Interscience, N.Y. (1965) Ch 2-6

[70] As REF. 67 p 353

[71] Bockris, J. O'M., Bonciocat, N. and Gutmann, F., ''An introduction to Electrochemical Science'', Wykeham Publications, London (1974) p 41

[72] Friend, J.A. and Gutmann, F., ''Electrochemistry'', Pergamon Press, Oxford (1965) p 199

[73] Stillinger, F.H., J. Chem. Phys., 35 (1961) p 1584

[74] Frank, H.S. and Thompson, P.T., J. Chem. Phys. 31 (1959) p 1086

[75] Vetter, K.J., ''Electrochemical Kinetics'', Academic Press, London (1967)

[76] Mulvey, T. and Webster, R.K., ''Modern Physical Techniques in Materials Technology'', Oxford Press, London (1974)

[77] As REF. 71 p 53-56

[78] Caldin, E.F., ''Fast reactions in solution'', Blackwell, London (1964)

[79] As REF. 59 p 966.

[80] Tafel, J., Z. Phys. Chem., 50 (1905) p 641.

[81] As REF. 59 p 834.

[82] As REF. 60 p 162.

[83] As REF. 71 p 74.

[84] Bard, A.L., and Faulkner, L.R., 'Electrochemical Methods, John Wiley & Son, N.Y., (1980) p 89.

[85] Hickling, A., Trans. Faraday Soc., 38 (1942) p 27.

[86] Schwartz, W.M., and Shain, I., Anal. Chem., 35 (1963) p 1770.

[87] Lowe, K., J. Chem. Educ., 47 (1970) p 846.

[88] Lingane, J.J., Ind. Eng. Chem., Anal. Ed., 17 (1945) p 332.

[89] ibid., Anal. Chem., 21 (1949) p 497.

[90] Lingane, J.J. and Jones, S.L., Anal. Chem., 22 (1950) p 1169.

[91] Allen, M.J., Anal. Chem., 22 (1950) p 804.

[92] Coche, A., J. Chim. Phys., 48 (1951) p 146.

[93] Greenough, M.L., Williams, W.E. and Taylor, J.K.,

Rev. Sci. Instr., 22 (1951) p 484.

[94] Damaskin, B.B., 'The Priniples of Current Methods for the Study of Electrochemical Reactions', McGraw-Hill, N.Y., (1967) p 31

[95] ibid., p 1.

[96] Berzins, T. and Delahay, P., J.Chem. Phys. 23 (1955) p 972.

[97] Birke, R.L. and Roe, D.K., Anal. Chem., 37 (1965) p 455.

[98] Delahay, P., 'New Instrumental Methods in Electrochem.', Interscience, N.Y., (1966) p 47,196.

[99] ibid., p72

[100] ibid., 'Advances in Electrochem. and Electrochemical Engineering', Vol. 1, Interscience, N.Y. (1961) p 247.

[101] ibid., p 254.

[102] Gerischer, H. and Krause, M., Z. Physik. Chem., N.F., 14 (1958) p 184.

[103] ibid., 'New Instrumental Methods in Electrochemistry', Interscience, N.Y., (1966) p 59,146.

[104] ibid., 'Advances in Electrochem. and Electrochemical Engineering', Vol. 1, Interscience, N.Y. (1961) p 265.

[105] Ives, D.J.G. and Janz, G.J., 'Reference Electrodes', Academic Press, N.Y. (1961)

[106 Epson corporation, 'HI-80 Plotter; Operation Manual', Japan, (1984).

[107] Booker, G.R., 'Modern Diffraction and Imaging Techniques in Materials Science', North-Holland, Amsterdam, (1970) p 553.

[108] Clarke, D.R., J. Mater. Sci., 5 (1970) p 689.

[109] Oatley, C.W., Nixon, W.C. and Pease, F., Adv. Electron. Elecron Phys., 21 (1965) p 181.

[110] Oatley, C.W., 'The Scanning Electron Microscope', Cambridge University Press, (1972).

[111] Thornton, P.R.,'Scanning Electron Microscopy', Chapman and Hall, London, (1968).

[112] Birks, L.S., 'X-ray Spectrochemical Analysis', Interscience, London, (1969).

[113] Ashley, D.G. and Andrews, K.W., Analyst, 97 (1972) p 841.

[114] Pantony, D.A. and Hurley, P.W., ibid. p 497.

[115] Seligson, D., 'Standard Methods of Clinical Chemistry', Vol.2, Academic Press, N.Y. (1958) p 165

[116] Christian, G.D., 'Analytical Chemistry', John Wiley, N.Y., (1980) p 421.

[117] ibid., p 349.

[118] As REF. 98 p 369.

[119] Salvin, W., 'Atomic Absorption Spectroscopy', Interscience, N.Y., (1968).

[120] Walsh, A., Spectrochim. Acta, 7 (1955) p 108.

[121] L'vov, B.V., ibid, B24 (1969) p 53.

[122] As REF. 85, ch 12.

[123] Garside, J.E. and Claret, P.A., 'Semi-Micro Inorganic Qualitative and Volumetric Analysis', Pitman, London (1954).

[124] Vogel, A.I., 'Quantitative Inorganic Analysis', Longman, (1972).

[125] Carlsen, K.M., J. Electrochem. Soc., 104, (1957) p147

[126] Kaesche, H., in Localized Corrosion, Williamsburg conference, 1971. NACE, Houston (1974) p 516.

[127] Beck, T.R., Electrochemica Acta, 29 (1984) p485

[128] Foley, R.T. and Nguyen, T.H., J. Electrochem. Soc., 129 (1982) p27 & p464

[129] ibid, 126 (1979) p1855

[130] Alkire, R.C. and Siitari, D., ibid., 129 (1982) p481

[131] Van Lancker, M., 'Metallurgy of Aluminium Alloys', Chapman & Hall, London (1967) ch 14.

[132] Binger, W., Corrosion, 9 (1953) p 440.

[133] Glicksman, R., J. Electrochem. Soc., 106 (1959) p457

[134] Ruben, S., U.S. Pat. 1,920,151 (1933).

[135] Lozier, G.S.; Glicksman, R. and Morehouse, C.K., US Pat. 2,976,342 (1961)

[136] Petrocelli, J. Electrochem. Soc., 97 (1950) p10

[137] Vince, C.H. (Jnr), Brit. Pat. No. 397,475 (1933)

[138] As REF. 43 p 415

[139] As REF. 131, ch 1.

[140] Varley, P.C., 'The Technology of Aluminium and its Alloys', Newnes-Butterworths, London (1970).

[141] Smallman, P.E., 'Modern Physical Metallurgy', Butterworths, London (1970).

[142] As REF. 131 p 98.

[143] Van Lanck, L.H., 'Materials Science for Engineers', Addison-Wesley, Massachussetts, (1970) p 149.

[144] ibid. 'Elements of Materials Science', Addison-Wesley, Massachussetts, (1964) Ch 4.

[145] Massalki, T.B., 'Physical Metallurgy', North-Holland, Amsterdam, (1965) p 149

[146] As REF. 143 p 63.

[147] Reding, J.T. and Newport, J.J., US Pats. 3,337,332-3

(1967).

[148] Hori, Y., Takao, J. and Shomon, H., Electrochim. Acta., 30 (1985) p 1121

[149] Rohrman, F.A., US Pat. 2,758,082 (1956).

[150] Rutemiller, H.C., US Pat. 3,227,644 (1966).

[151] ibid., US Pat. 3,418,230 (1968).

[152] Raclot, B., US pat. 3,318,692 (1967).

[153] As REF. 143 p 479.

[154] Heise, G.W. and Cahoon, N.C., J. Electrochem. Soc., 99 (1952) p 179C.

[155] As REF. 71 p 93.

[156] Morehouse, C.K., Hammer, W.J. and Vinal, J. Research Natl. Bur. Standards, 40 (1948) p 151.

[157] Mears, R.B. and Brown, R.H., J. Electrochem. Soc., 97 (1950) p 75.

[158] Bockstie, L., Trevethan, D. and Zaromb, S., J. Electrochem. Soc., 110 (1963) p 267.

[159] Vijh, A.K., J. Phys. Chem., 72 (1968) p 1148.

[160] Schumacher, E.A. and Heise, G.W., J. Electrochem., Soc., 99 (1952) p 191C.

[161] Cotton, A.F. and Wilkinson, G., 'Advanced Inorganic Chemistry,', Interscience, N.Y., (1972) p 191.

[162] The Chemical Society, 'Electrochemistry', Vol. 1, (1970) p12.

[163] As REF. 161 p 198.

[164] Weast, R.C., (ed.), 'Handbook of Chemistry and Physics', CRC press, Florida (1982).

[165] As REF. 60 p 344.

[166] Despic, A.R., J. Applied Electrochem., 15 (1985) p191.

[167] Nelkon, M. and Parker, P., Advanced Level Physics, 4th ed., Heinemann (1977) p 156

[168] Heise, G.W. and Cahoon, C.N., 'The Primary Battery', John Wiley & Sons, N.Y., (1971)

[169] Tseung, A.C.C. and Elbeik, S., Unpublished Work, Catalytic Electrodes Ltd., London.

[170] Tseung, A.C.C., Rasiyah, P. and Hibbert, D.B., British Patent Application, 804483 (1980).

[171] Littauer, E.L. and Tsai, K.C., J. Electrochem. Soc., 126 (1979) p 1924.

[172] Sepa, D.B., Vojanovic, M.V. and Damjanovic, A., Electrochim. Acta 25 (1980) p 1491.

[173] Bevan, H.L. and Tseung, ibid. 9 (1974) p 201.

[174] Tseung, A.C.C. and Bevan, H.L., Electroanal. Chem., 45 (1973) p 429.

[175] Yeung, K.L.K. and Tseung, A.C.C., J. Electrochem. Soc., 125 (1978) p 878.

[176] Tseung, A.C.C., ibid., 125 (1978) p 1660.

[177] Hibbert, D.B. and Tseung, A.C.C., ibid., 125 (1978) p 74.

[178] King, W.J. and Tseung, A.C.C., Electrochim. Acta, 19 (1974) p 201.

[179] Tseung, A.C.C. and Jasem, S.M., ibid. 22 (1977) p 31.

[180] Tseung, A.C.C. and Yeung, K.L.K., J. Electrochem. Soc., 125 (1978) p 1003.

[181] Jasem, S.M. and Tseung, A.C.C., ibid. 126 (1979) p 1353.

[182] Kozowa, A., Zillionis, V.E. and Brood, R.J., ibid., 118 (1971) p 1705.

[183] ibid. 117 (1970) p 1470.

[184] Savy, M., Bernard, C. and Magner, G., Electrochim. Acta, 20 (1975) p 383.

[185] Appleby, A.J. and Savy, M., ibid., 22 (1977) p 1315.

[186] Magner, G., Savy, M. and Scarbeck, G., J. Electrochem. Soc., 127 (1980) p 1076.

[187] Zagal, J., Bindra, P. and Yeager, E., ibid. 27 (1980) p 1506

[188] Collman, J.P., Marroco, M. and Denisevich, P., J. Electroanal. Chem., 101 (1979) p 117.

[189] Yeager, E., Electrochim. Acta, 29 (1984) p 1527

[190] Tseung, A.C.C., Hobbs, B.S. and Tantram, A.D.S., ibid. 15 (1970) p 473

[191] Tantram, A.D.S. and Tseung, A.C.C., Nature, 221 (1969) p 167

[192] Vassie, P.R. and Tseung, A.C.C., Electrochim. Acta, 20 (1975) p 759.

[193] ibid., p763.

[194] Tseung, A.C.C., J. Applied Electrochem., 15 (1985) p 575.

[195] Aldhart, O.J., Proceedings 19th Power Source Conference, PSC Publications Committee, N.Y. (1966).

[196] Shropshire, J.A., Albert, R.H. and Horowitz, H.H., in 'Hydrocarbon Fuel Cell Technology', (ed. B.S. Baker), Academic Press, N.Y. (1965) p 539.

[197] Giner, J., Parry, J.M., Swette, L. and Cattabriga, R., NASA Contract CR-97624, Final Report, (1968).

[198] Giner, J., Parry, J.M., Smith, S. and Turchan. M., J. Electrochem. Soc., 116 (1969) p 1692.

[199] Metal Bulletin, 2nd Int. Aluminium Congress, 1982.

[200] Scamans, G., Paper delivered at the SCI Meeting on Advances in Battery Technology, London, (october, 1985).

[201] Fleming, R.H., The Oceans, Prentice Hall, New York (1946) p 21.

[202] Sea Technology, February, 1977.

[203] Grassie, J.F. and Heirtzler, J.R., 'Deep-sea Research by Manned Submersibles', Science, vol 194 (1976) p 294

[204] Myers, J.; Holm, C. and McAllister, R., Handbook of Ocean and Underwater Engineering, McGraw-Hill (1969)

[205] Barton, R., Oceanology Today, Aldus, London (1970)

[206] Economic Planning Department, Report UR5 (1973).

[207] King, T.E. and Moroz, W.J., 'Survey of Continuous Sources of Electrical Power for Under-ice Propulsion of Small Submersibles, part 2, US NTIS A REP.1977, AD-A037721

[208] Busby, R.F., Manned Submersibles, Office of the Oceanographer (1976), p 310.

[209] Simon, H.S., 'Survival At Sea', Plenum, London (1974).

[210] Tseung, A.C.C. and Tang, T.S.K., 'Emergency Power Sources; Market Survey', Chemical Energy Research Centre, TCU (1983).

[211] O'Connor, T.W., Army Research and Development News Magazine, 12 (1977) p 19.

[212] Tseung, A.C.C., Ho, T.M. and Worthington, C., Patent Application 1982, assigned to Chloride-Alcad.

[213] Valand, T.; Mollestad, O. and Nilsson, G., in Power Sources 8 (ed. J. Thompson, 1981) p 523

APPENDICES

(A2) COMPUTER PROGRAM FOR AA DATA HANDLING

(A1) PROGRAM FOR PLOTTING ON THE HI-80 USING V1SICALC

have been removed for copyright reasons

TABLE B1 STEADY STATE POLARISATION OF PURE Al IN 5M KOH

CURRENT DENSITY (mA/Sqcm)	POTENTIAL (V)/(Hg/HgO.OH⁻) 1ST RUN	2ND RUN	3RD RUN	MEAN
OCV	-1.351	-1.369	-1.361	-1.360
10	-1.337	-1.358	-1.355	-1.350
20	-1.325	-1.341	-1.343	-1.336
30	-1.311	-1.324	-1.324	-1.320
40	-1.285	-1.302	-1.299	-1.300
50	-1.261	-1.269	-1.267	-1.266
60	-1.221	-1.231	-1.228	-1.227
70	-1.191	-1.188	-1.182	-1.187
80	-1.155	-1.144	-1.142	-1.147
90	-1.121	-1.112	-1.119	-1.117
100	-1.088	-1.083	-1.088	-1.087

TEMPERATURE: 25°C

TABLE B2 STEADY STATE POLARISATION OF Ø4 IN 5M KOH

CURRENT DENSITY (mA/Sqcm)	POTENTIAL (V)/(Hg/HgO.OH⁻) 1ST RUN	2ND RUN	3RD RUN	MEAN
OCV	-1.544	-1.546	-1.545	-1.545
10	-1.521	-1.521	-1.521	-1.521
20	-1.495	-1.489	-1.489	-1.491
30	-1.454	-1.449	-1.451	-1.451
40	-1.404	-1.402	-1.404	-1.403
50	-1.362	-1.356	-1.354	-1.357
60	-1.321	-1.313	-1.311	-1.315
70	-1.277	-1.271	-1.269	-1.272
80	-1.256	-1.252	-1.248	-1.252
90	-1.231	-1.226	-1.224	-1.227
100	-1.193	-1.193	-1.193	-1.195

TEMPERATURE: 25 °C

TABLE B3 STEADY STATE POLARISATION OF ZI IN 5M KOH

CURRENT DENSITY (mA/Sqcm)	POTENTIAL (V)/(Hg/HgO.OH⁻) 1ST RUN	2ND RUN	3RD RUN	MEAN
OCV	-1.661	-1.661	-1.656	-1.659
10	-1.609	-1.607	-1.605	-1.607
20	-1.531	-1.528	-1.527	-1.529
30	-1.489	-1.482	-1.472	-1.481
40	-1.407	-1.401	-1.389	-1.399
50	-1.253	-1.246	-1.236	-1.245
60	-1.204	-1.197	-1.187	-1.196
70	-1.172	-1.165	-1.155	-1.164
80	-1.121	-1.114	-1.104	-1.113
90	-1.067	-1.059	-1.051	-1.059
100	-1.022	-1.015	-1.005	-1.014

TEMPERATURE: 25°C

TABLE B4 STEADY STATE POLARISATION OF Z2 IN 5M KOH KOH

CURRENT DENSITY (mA/Sqcm)	POTENTIAL (V)//(Hg/HgO.OH⁻) 1ST RUN	2ND RUN	3RD RUN	MEAN
OCV	-1.672	-1.661	-1.653	-1.662
10	-1.621	-1.611	-1.607	-1.613
20	-1.542	-1.529	-1.525	-1.532
30	-1.487	-1.479	-1.471	-1.479
40	-1.394	-1.381	-1.377	-1.384
50	-1.241	-1.228	-1.224	-1.231
60	-1.191	-1.181	-1.181	-1.184
70	-1.127	-1.118	-1.118	-1.121
80	-1.075	-1.067	-1.065	-1.069
90	-1.028	-1.021	-1.019	-1.023
100	-.992	-.981	-.979	-.984

TEMPERATURE: 25°C

TABLE B 5 STEADY STATE POLARISATION OF Z3 IN 5M KOH

CURRENT DENSITY (mA/Sqcm)	POTENTIAL (V)/(Hg/HgO.OH⁻) 1ST RUN	2ND RUN	3RD RUN	MEAN
OCV	-1.661	-1.661	-1.651	-1.658
10	-1.603	-1.629	-1.627	-1.620
20	-1.463	-1.507	-1.491	-1.487
30	-1.284	-1.312	-1.295	-1.297
40	-1.226	-1.245	-1.241	-1.237
50	-1.172	-1.185	-1.183	-1.180
60	-1.117	-1.131	-1.121	-1.123
70	-1.055	-1.065	-1.057	-1.059
80	-1.022	-1.031	-1.025	-1.026
90	-1.013	-1.021	-1.014	-1.016
100	-1.008	-1.012	-1.005	-1.008

TEMPERATURE: 25°C

TABLE B 6 STEADY STATE POLARISATION OF ZS1 IN 5M KOH

CURRENT DENSITY (mA/Sqcm)	POTENTIAL (V)/(Hg/HgO.OH⁻) 1ST RUN	2ND RUN	3RD RUN	MEAN
OCV	-1.673	-1.681	-1.681	-1.678
10	-1.609	-1.617	-1.616	-1.614
20	-1.536	-1.544	-1.543	-1.541
30	-1.491	-1.498	-1.497	-1.495
40	-1.387	-1.395	-1.394	-1.392
50	-1.236	-1.245	-1.242	-1.241
60	-1.184	-1.193	-1.191	-1.189
70	-1.125	-1.136	-1.135	-1.132
80	-1.102	-1.113	-1.112	-1.109
90	-1.061	-1.071	-1.069	-1.067
100	-1.018	-1.029	-1.028	-1.025

TEMPERATURE: 25°C

TABLE B 7 . TRANSIENT STATE POLARISATION OF Al IN 5M KOH

CURRENT DENSITY (mA/Sqcm)	POTENTIAL (V)/(Hg/HgO.OH⁻) 1ST RUN	2ND RUN	3RD RUN	MEAN
OCV	-1.381	-1.389	-1.394	-1.388
10	-1.371	-1.378	-1.385	-1.378
20	-1.356	-1.364	-1.369	-1.363
30	-1.329	-1.336	-1.343	-1.336
40	-1.295	-1.302	-1.306	-1.301
50	-1.262	-1.267	-1.267	-1.265
60	-1.201	-1.201	-1.202	-1.201
70	-1.156	-1.158	-1.157	-1.157
80	-1.102	-1.089	-1.105	-1.099
90	-1.021	-1.006	-1.019	-1.015
100	-.958	-.954	-.955	-.956

TEMPERATURE: 25°C

TABLE B 8 TRANSIENT STATE POLARISATION OF Q4 IN 5M KOH

CURRENT DENSITY (mA/Sqcm)	POTENTIAL (V)/(Hg/HgO.OH⁻) 1ST RUN	2ND RUN	3RD RUN	MEAN
OCV	-1.544	-1.545	-1.545	-1.545
10	-1.524	-1.526	-1.525	-1.525
20	-1.504	-1.506	-1.504	-1.505
30	-1.491	-1.492	-1.491	-1.491
40	-1.475	-1.478	-1.476	-1.476
50	-1.429	-1.432	-1.431	-1.431
60	-1.388	-1.399	-1.396	-1.394
70	-1.351	-1.362	-1.359	-1.357
80	-1.319	-1.329	-1.327	-1.325
90	-1.292	-1.299	-1.297	-1.296
100	-1.281	-1.286	-1.284	-1.284

TEMPERATURE: 25°C

TABLE B 9 TRANSIENT STATE POLARISATION OF Z1 IN 5M KOH

CURRENT DENSITY (mA/Sqcm)	POTENTIAL (V)/(Hg/HgO.OH⁻) 1ST RUN	2ND RUN	3RD RUN	MEAN
OCV	-1.575	-1.588	-1.579	-1.581
10	-1.531	-1.552	-1.543	-1.545
20	-1.515	-1.528	-1.519	-1.521
30	-1.488	-1.501	-1.492	-1.494
40	-1.421	-1.433	-1.424	-1.426
50	-1.385	-1.398	-1.389	-1.391
60	-1.339	-1.353	-1.343	-1.345
70	-1.305	-1.318	-1.309	-1.311
80	-1.262	-1.275	-1.266	-1.268
90	-1.193	-1.206	-1.197	-1.199
100	-1.116	-1.128	-1.119	-1.121

TEMPERATURE: 25 °C

TABLE B 10 TRANSIENT STATE POLARISATION OF Z2 IN 5M KOH

CURRENT DENSITY (mA/Sqcm)	POTENTIAL (V)/(Hg/HgO.OH⁻) 1ST RUN	2ND RUN	3RD RUN	MEAN
OCV	-1.669	-1.681	-1.666	-1.672
10	-1.659	-1.671	-1.656	-1.662
20	-1.612	-1.624	-1.609	-1.615
30	-1.596	-1.608	-1.593	-1.599
40	-1.538	-1.551	-1.535	-1.541
50	-1.463	-1.475	-1.461	-1.466
60	-1.436	-1.448	-1.433	-1.439
70	-1.421	-1.432	-1.417	-1.423
80	-1.396	-1.408	-1.393	-1.399
90	-1.371	-1.383	-1.368	-1.374
100	-1.356	-1.368	-1.353	-1.359

TEMPERATURE: 25°C

TABLE B 11. TRANSIENT STATE POLARISATION OF Z3 IN 5M KOH

CURRENT DENSITY (mA/Sqcm)	POTENTIAL (V)/(Hg/HgO.OH⁻) 1ST RUN	2ND RUN	3RD RUN	MEAN
OCV	-1.718	-1.741	-1.713	-1.724
10	-1.677	-1.699	-1.672	-1.683
20	-1.582	-1.605	-1.577	-1.588
30	-1.519	-1.542	-1.514	-1.525
40	-1.407	-1.431	-1.402	-1.413
50	-1.378	-1.401	-1.373	-1.384
60	-1.305	-1.328	-1.301	-1.311
70	-1.245	-1.268	-1.241	-1.251
80	-1.161	-1.184	-1.156	-1.167
90	-1.066	-1.089	-1.061	-1.072
100	-.961	-.983	-.955	-.966

TEMPERATURE: 25 °C

TABLE B 12 TRANSIENT STATE POLARISATION OF ZS1 IN 5M KOH

CURRENT DENSITY (mA/Sqcm)	POTENTIAL (V)/(Hg/HgO.OH-) 1ST RUN	2ND RUN	3RD RUN	MEAN
OCV	-1.692	-1.676	-1.678	-1.682
10	-1.648	-1.632	-1.634	-1.638
20	-1.593	-1.577	-1.579	-1.583
30	-1.573	-1.557	-1.559	-1.563
40	-1.565	-1.549	-1.551	-1.555
50	-1.535	-1.519	-1.521	-1.525
60	-1.497	-1.486	-1.485	-1.489
70	-1.455	-1.444	-1.443	-1.447
80	-1.429	-1.418	-1.417	-1.421
90	-1.393	-1.382	-1.381	-1.385
100	-1.383	-1.372	-1.371	-1.375

TEMPERATURE: 25°C

TABLE B 13 STEADY STATE GALVANOSTATIC POLARISATION OF AL IN 5M KOH

TIME (mIN.)	POTENTIAL (V)/(Hg/HgO.OH⁻) 1ST RUN	2ND RUN	3RD RUN	MEAN
0	-1.111	-1.119	-1.111	-1.114
10	-1.111	-1.119	-1.111	-1.114
20	-1.111	-1.119	-1.111	-1.114
30	-1.111	-1.119	-1.111	-1.114
40	-1.111	-1.119	-1.111	-1.114
50	-1.111	-1.119	-1.111	-1.114
60	-1.111	-1.119	-1.111	-1.114
70	-1.111	-1.119	-1.111	-1.114
80	-1.111	-1.119	-1.111	-1.114
90	-1.111	-1.119	-1.111	-1.114
100	-1.111	-1.119	-1.111	-1.114
110	-1.111	-1.119	-1.111	-1.114
120	-1.111	-1.119	-1.111	-1.114

CURRENT DENSITY: 100 mA/SQCM

TEMPERATURE : 25°C

TABLE B 14 STEADY STATE GALVANOSTATIC POLARISATION OF Q4 IN 5M KOH

TIME (mIN.)	POTENTIAL (V)/(Hg/HgO.OH⁻) 1ST RUN	2ND RUN	3RD RUN	MEAN
0	-1.209	-1.165	-1.165	-1.180
10	-1.209	-1.165	-1.165	-1.180
20	-1.209	-1.165	-1.165	-1.180
30	-1.209	-1.165	-1.165	-1.180
40	-1.209	-1.165	-1.165	-1.180
50	-1.209	-1.165	-1.165	-1.180
60	-1.209	-1.165	-1.165	-1.180
70	-1.209	-1.165	-1.165	-1.180
80	-1.209	-1.165	-1.165	-1.180
90	-1.209	-1.165	-1.165	-1.180
100	-1.209	-1.165	-1.165	-1.180
110	-1.209	-1.165	-1.165	-1.180
120	-1.209	-1.165	-1.165	-1.180

CURRENT DENSITY: 100 mA/SQCM

TEMPERATURE : 25°C

TABLE B 15 STEADY STATE GALVANOSTATIC POLARISATION OF Zi IN 5M KOH

TIME (mIN.)	POTENTIAL (V)/(Hg/HgO.OH⁻) 1ST RUN	2ND RUN	3RD RUN	MEAN
0	-1.011	-1.059	-1.011	-1.027
10	-1.011	-1.059	-1.011	-1.027
20	-1.011	-1.059	-1.011	-1.027
30	-1.011	-1.059	-1.011	-1.027
40	-1.011	-1.059	-1.011	-1.027
50	-1.011	-1.059	-1.011	-1.027
60	-1.011	-1.059	-1.011	-1.027
70	-1.011	-1.059	-1.011	-1.027
80	-1.011	-1.011	-1.001	-1.008
90	-1.011	-1.011	-1.001	-1.008
100	-1.011	-1.011	-1.001	-1.008
110	-1.011	-1.011	-1.001	-1.008
120	-1.011	-1.011	-1.001	-1.008

CURRENT DENSITY: 100 MA/SQCM

TEMPERATURE : 25°C

TABLE B 16 STEADY STATE GALVANOSTATIC POLARISATION OF Z2 IN 5M KOH

TIME (mIN.)	POTENTIAL (V)/(Hg/HgO.OH⁻) 1ST RUN	2ND RUN	3RD RUN	MEAN
0	-1.109	-1.109	-1.109	-1.109
10	-1.109	-1.109	-1.109	-1.109
20	-1.075	-1.109	-1.109	-1.098
30	-1.061	-1.085	-1.085	-1.077
40	-1.045	-1.059	-1.075	-1.060
50	-1.035	-1.039	-1.059	-1.044
60	-1.011	-1.025	-1.059	-1.032
70	-1.001	-1.011	-1.059	-1.024
80	-.985	-1.001	-1.049	-1.012
90	-.961	-.961	-1.035	-.986
100	-.961	-.961	-1.011	-.978
110	-.961	-.961	-1.011	-.978
120	-.961	-.961	-1.011	-.978

CURRENT DENSITY: 100 MA/SQCM

TEMPERATURE : 25 °C

TABLE B 17 STEADY STATE GALVANOSTATIC POLARISATION OF Z3 IN 5M KOH

TIME (mIN.)	POTENTIAL (V)/(Hg/HgO.OH⁻) 1ST RUN	2ND RUN	3RD RUN	MEAN
0	-1.011	-1.011	-1.059	-1.027
10	-1.011	-1.011	-1.059	-1.027
20	-1.011	-1.011	-1.059	-1.027
30	-1.011	-1.011	-1.059	-1.027
40	-1.011	-1.011	-1.059	-1.027
50	-1.011	-1.011	-1.059	-1.027
60	-1.011	-1.011	-1.059	-1.027
70	-1.011	-1.011	-1.059	-1.027
80	-.985	-1.011	-1.011	-1.002
90	-.961	-1.011	-1.011	-.994
100	-.961	-1.011	-1.011	-.994
110	-.961	-1.011	-1.011	-.994
120	-.961	-1.011	-1.011	-.994

CURRENT DENSITY: 100 MA/SQCM

TEMPERATURE : 25°C

TABLE B.18 STEADY STATE GALVANOSTATIC POLARISATION OF ZS1 IN 5M KOH

TIME (mIN.)	POTENTIAL (V)/(Hg/HgO.OH⁻) 1ST RUN	2ND RUN	3RD RUN	MEAN
0	-1.011	-1.011	-1.011	-1.011
10	-1.011	-1.011	-1.011	-1.011
20	-1.011	-1.011	-1.011	-1.011
30	-1.011	-1.011	-1.011	-1.011
40	-1.011	-1.011	-1.011	-1.011
50	-1.011	-1.011	-1.011	-1.011
60	-1.011	-1.011	-1.011	-1.011
70	-1.011	-1.011	-1.011	-1.011
80	-1.011	-1.011	-1.011	-1.011
90	-1.001	-1.011	-1.011	-1.008
100	-1.001	-1.011	-1.011	-1.008
110	-1.001	-1.011	-1.011	-1.008
120	-1.001	-1.011	-1.011	-1.008

CURRENT DENSITY: 100 mA/SQCM

TEMPERATURE : 25 °C

TABLE B 19 TRANSIENT STATE GALVANOSTATIC POLARISATION OF AL IN 5M KOH

TIME (USEC)	POTENTIAL (V)/(Hg/HgO.OH⁻) 1ST RUN	2ND RUN	3RD RUN	MEAN
0	-.601	-.609	-.603	-.604
500	-.689	-.709	-.706	-.701
1000	-.801	-.832	-.843	-.825
1500	-.945	-.969	-.987	-.967
2000	-1.059	-1.065	-1.066	-1.063
2500	-1.111	-1.119	-1.111	-1.114
3000	-1.111	-1.119	-1.111	-1.114
3500	-1.111	-1.119	-1.111	-1.114
4000	-1.111	-1.119	-1.111	-1.114
4500	-1.111	-1.119	-1.111	-1.114
5000	-1.111	-1.119	-1.111	-1.114
5500	-1.111	-1.119	-1.111	-1.114
6000	-1.111	-1.119	-1.111	-1.114

CURRENT DENSITY: 100 MA/SQCM

TEMPERATURE : 25°C

DOUBLE LAYER CHARGING TIME: 2300 USEC

TABLE B 20 TRANSIENT STATE GALVANOSTATIC POLARISATION OF Q4 IN 5M KOH

TIME (USEC)	POTENTIAL (V)/(Hg/HgO.OH⁻) 1ST RUN	2ND RUN	3RD RUN	MEAN
0	-.665	-.689	-.711	-.688
500	-.739	-.789	-.865	-.814
1000	-.909	-.927	-.978	-.938
1500	-1.115	-1.125	-1.134	-1.125
2000	-1.165	-1.176	-1.178	-1.173
2500	-1.165	-1.176	-1.178	-1.173
3000	-1.165	-1.176	-1.178	-1.173
3500	-1.165	-1.176	-1.178	-1.173
4000	-1.165	-1.176	-1.178	-1.173
4500	-1.165	-1.176	-1.178	-1.173
5000	-1.165	-1.176	-1.178	-1.173
5500	-1.165	-1.176	-1.178	-1.173
6000	-1.165	-1.176	-1.178	-1.173

CURRENT DENSITY: 100 MA/SQCM

TEMPERATURE : 25°C

DOUBLE LAYER CHARGING TIME: 2000 USEC

TABLE B21 TRANSIENT STATE GALVANOSTATIC POLARISATION OF Zi IN 5M KOH

TIME (USEC)	POTENTIAL (V)/(Hg/HgO.OH⁻) 1ST RUN	2ND RUN	3RD RUN	MEAN
0	-.601	-.609	-.603	-.604
500	-.701	-.709	-.706	-.705
1000	-.801	-.809	-.806	-.805
1500	-.902	-.906	-.906	-.905
2000	-1.001	-1.005	-1.006	-1.004
2500	-1.011	-1.059	-1.101	-1.057
3000	-1.011	-1.059	-1.101	-1.057
3500	-1.011	-1.059	-1.101	-1.057
4000	-1.011	-1.059	-1.101	-1.057
4500	-1.011	-1.059	-1.101	-1.057
5000	-1.011	-1.059	-1.101	-1.057
5500	-1.011	-1.059	-1.101	-1.057
6000	-1.011	-1.059	-1.101	-1.057

CURRENT DENSITY: 100 MA/SQCM

TEMPERATURE : 25 °C

DOUBLE LAYER CHARGING TIME: 2100 USEC

TABLE B 22 TRANSIENT STATE GALVANOSTATIC POLARISATION OF Z2 IN 5M KOH

TIME (USEC)	POTENTIAL (V)/(Hg/HgO.OH⁻) 1ST RUN	2ND RUN	3RD RUN	MEAN
0	-.601	-.609	-.603	-.604
500	-.678	-.706	-.683	-.689
1000	-.801	-.809	-.806	-.805
1500	-.953	-.965	-.973	-.964
2000	-1.009	-1.005	-1.006	-1.007
2500	-1.109	-1.011	-1.085	-1.007
3000	-1.109	-1.011	-1.085	-1.007
3500	-1.109	-1.011	-1.085	-1.007
4000	-1.109	-1.011	-1.085	-1.007
4500	-1.109	-1.011	-1.085	-1.007
5000	-1.109	-1.011	-1.085	-1.007
5500	-1.109	-1.011	-1.085	-1.007
6000	-1.109	-1.011	-1.085	-1.007

CURRENT DENSITY: 100 MA/SQCM

TEMPERATURE : 25°C

DOUBLE LAYER CHARGING TIME: 2250 USEC

TABLE B 23 TRANSIENT STATE GALVANOSTATIC POLARISATION OF ZI IN 5M KOH

TIME (USEC)	POTENTIAL (V)/(Hg/HgO.OH⁻) 1ST RUN	2ND RUN	3RD RUN	MEAN
0	-.601	-.609	-.603	-.604
500	-.701	-.709	-.706	-.705
1000	-.826	-.834	-.832	-.831
1500	-.912	-.923	-.919	-.918
2000	-1.001	-1.001	-1.003	-1.002
2500	-1.011	-1.011	-1.011	-1.011
3000	-1.011	-1.011	-1.011	-1.011
3500	-1.011	-1.011	-1.011	-1.011
4000	-1.011	-1.011	-1.011	-1.011
4500	-1.011	-1.011	-1.011	-1.011
5000	-1.011	-1.011	-1.011	-1.011
5500	-1.011	-1.011	-1.011	-1.011
6000	-1.011	-1.011	-1.011	-1.011

CURRENT DENSITY: 100 mA/SQCM

TEMPERATURE : 25°C

DOUBLE LAYER CHARGING TIME: 2200 USEC

TABLE B 24 TRANSIENT STATE GALVANOSTATIC POLARISATION OF ZS1 IN 5M KOH

TIME (USEC)	POTENTIAL (V)/(Hg/HgO.OH⁻) 1ST RUN	2ND RUN	3RD RUN	MEAN
0	-.603	-.609	-.603	-.605
500	-.704	-.709	-.706	-.706
1000	-.873	-.883	-.869	-.877
1500	-.986	-.989	-.979	-.985
2000	-1.001	-1.003	-1.003	-1.002
2500	-1.011	-1.025	-1.011	-1.016
3000	-1.011	-1.025	-1.011	-1.016
3500	-1.011	-1.025	-1.011	-1.016
4000	-1.011	-1.025	-1.011	-1.016
4500	-1.011	-1.025	-1.011	-1.016
5000	-1.011	-1.025	-1.011	-1.016
5500	-1.011	-1.025	-1.011	-1.016
6000	-1.011	-1.025	-1.011	-1.016

CURRENT DENSITY: 100 mA/SQCM

TEMPERATURE : 25°C

DOUBLE LAYER CHARGING TIME: 2150 USEC